



ANALYSIS OF THE LONG-TERM SLOPE STABILITY OF WASTE- ROCK DUMPS

By

SUSAN JANE HENDERSON
BEng(Hons)(Civil), ME, MIEAust

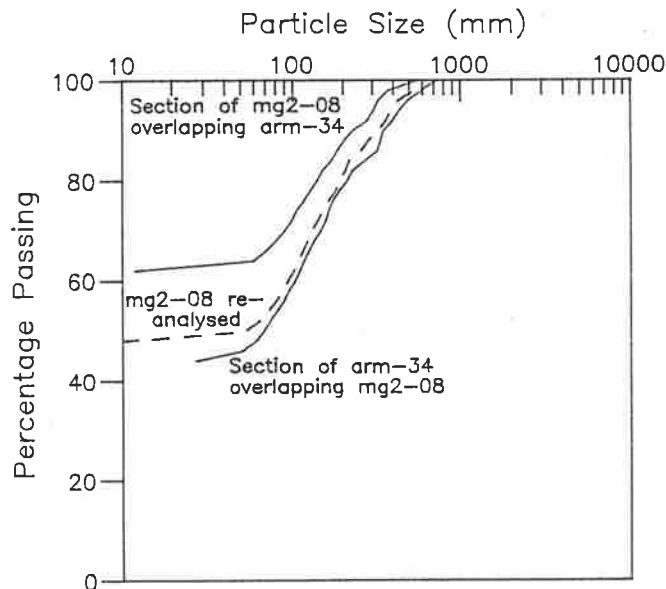
*A thesis
submitted to Department of Civil Engineering,
The University of Adelaide,
in fulfilment of the requirements
for a Doctor of Philosophy
January, 1992*

Doctor of Philosophy

1992

ERRATA

1. Page 3-2 Paragraph 1 Sentence 1 should read ".... two scale reference sticks, with one metre length marked between painted ends and a middle (half metre) mark, were placed on the slope"
2. Page 3-2 Paragraph 2 Sentence 2 should read ".... shots usually could not be taken with the lens parallel to the slope face"
3. Page 3-58 Paragraph 2 Sentence 5 should read ".... any small correlation of grading with depth will disappear."
4. Page 3-58 Paragraph 2 Sentence 6 should read ".... reasonable likelihood of valuation by area being valid for the newest"
5. Page 3-60 Figure 3-18 is incorrect in the lower right hand graph. The graph should be:



6. Page 3-72 Figure 3-26 should have (a) beside the upper graph and (b) beside the lower.
7. Page 7-13 Table 7-1 should have the description "6 yr Pegmatite" for material MG08.

ABSTRACT

One of the most visible features of a mining operation is the heaps of loosely dumped overburden and non-ore-bearing rock. Until recently, these were handled mainly on the basis of minimising operating costs, and were left as-dumped at the completion of mining. However, with growing community demand for adequate rehabilitation of mined land, a need is developing for more active design and management of such features. Based on Ranger Uranium Mine, Northern Territory, this thesis examines the analysis of structural slope stability of waste-rock dumps, including the effects of weathering on material properties.

A procedure of slope photography and computer-based image analysis was developed to measure particle size distributions for waste-rock after various periods on the dumps. Mineralogical data were obtained for corresponding subsamples collected from the dumps, and for supplementary samples, including some representative of more advanced stages of weathering. Laboratory compaction and triaxial compression tests were performed on fourteen selected materials.

The collated results showed that within the first ten years of exposure weathering of waste-rock is primarily manifest as disintegration of larger fragments, which leads to decreases in both friction angle and shear intercept. In the older mine materials production of clay minerals is pronounced and correlates with a further decrease in friction angle but an increase in shear intercept, as cohesion becomes significant.

Finite element modelling of dump slopes suggested that under sustained moisture conditions the dumps at Ranger will be stable at their current configuration throughout the intended life of the mine, and that the proposed rehabilitated landforms will be indefinitely stable against mass slippage. Batters are closest to instability in the period 5-10 years after dumping, and at all stages the critical mode of failure is sliding along a softened base.

TABLE OF CONTENTS

	Page
ABSTRACT	ii
CONTENTS	iii
LIST OF FIGURES	vi
LIST OF TABLES	ix
LIST OF PLATES	x
DECLARATION	xi
ACKNOWLEDGEMENTS	xii
1. INTRODUCTION	
1.1 Background	1-1
1.2 Scope	1-2
1.3 Research Plan	1-3
1.3.1 Concept	1-3
1.3.2 Methods	1-4
1.3.3 Thesis Format	1-7
2. WASTE-ROCK DUMPS AT RANGER URANIUM MINES	
2.1 Operational Setting	2-1
2.2 Site Observations	2-4
2.3 Weathering in the Dumps	2-11
3. PHYSICAL DESCRIPTION OF DUMP MATERIALS	
3.1 Dump Slope Photography	3-1
3.1.1 Procedure	3-1
3.1.2 Sampling Sites	3-5
3.2 Mechanical Sieving	3-7
3.3 Photo-Sieving	3-10
3.3.1 Theory	3-10
3.3.2 Procedures	3-30
3.3.3 Assessment of Method	3-58
3.4 Particle Size Distributions	3-69
4. MINERALOGICAL DESCRIPTION OF DUMP MATERIALS	
4.1 Site Geology and Mineralogy	4-1
4.2 Classification & Mineralogy of Collected Samples	4-5
4.3 Collated Sample Descriptions	4-17

	<u>Page</u>
5. MECHANICAL BEHAVIOUR OF DUMP MATERIALS	
5.1 Laboratory Test Programme	5-1
5.1.1 Sample Selection	5-1
5.1.2 Modelling of Grading Curves	5-3
5.1.3 Triaxial Test Conditions	5-5
5.2 Results and Discussion	5-10
5.2.1 Compaction Tests	5-10
5.2.2 Triaxial Compression Tests	5-12
6. CHARACTERISATION OF WEATHERING	
6.1 Grading Trends	6-1
6.1.1 Correlation with Age	6-1
6.1.2 Correlation with Shear Strength	6-9
6.2 Mineral Alteration	6-15
6.2.1 Initial Composition	6-15
6.2.2 Weathering Products	6-18
6.2.3 2:1 Layer Clay Minerals	6-24
6.3 Collated Data	6-28
7. SLOPE STABILITY	
7.1 Review of Analytical Methods	7-1
7.2 Slope Stability Model	7-5
7.2.1 The Finite Element Programme	7-5
7.2.2 Material Models	7-9
7.2.3 Geometric Details	7-16
7.3 Results and Discussions	7-21
7.3.1 General	7-21
7.3.2 Reference Analyses (<i>main</i>)	7-22
7.3.3 Analyses Incorporating Soil Layers (<i>soil</i>)	7-31
7.3.4 Analyses Incorporating Softening Under Dump (<i>base</i>)	7-34
7.3.5 Assessment of Stability over the Long-Term	7-38

	<u>Page</u>
8. SUMMARY AND CONCLUSIONS	
8.1 Techniques for Investigation	8-1
8.2 Description of Dump Materials	8-4
8.2.1 Weathering	8-4
8.2.2 Strength	8-5
8.3 Slope Stability at Ranger Uranium Mine	8-7
8.4 Further Research	8-8

APPENDICES

- A. COMPUTER SUBROUTINES FOR IMAGE ANALYSIS**
- B. DUMP SLOPE GRADING CURVES**
- C. TRIAXIAL COMPRESSION TEST RESULTS**
- D. CALIBRATIONS FOR TRIAXIAL COMPRESSION TEST EQUIPMENT**
- E. OPERATION SUMMARY OF THE FINITE ELEMENT MODEL**

REFERENCES

LIST OF FIGURES

	<u>Page</u>
1-1 Possible Strength-Weathering Relationships	1-3
1-2 Concept of Material Characteristic Interactions	1-4
2-1 Ranger Project Area	2-2
3-1 Procedure for Photographing Dump Slopes	3-2
3-2 Location Plan of Waste-Rock Dumps Sampling Sites	3-6
3-3 Batter Age versus Bulk Sample Grading (D ₁₀)	3-9
3-4 Comparison of Samples Assumed by Area and Volume based Valuations	3-13
3-5 Effect of Orientation on Particle Image	3-15
3-6 Particle Shapes Used in Monte Carlo Simulation	3-17
3-7 Distributions Generated by Random Number Algorithms	3-18
3-8 Axis Pairs Considered in Simulations	3-19
3-9 Effect of Hiding on Particle Image	3-25
3-10 Effect of Number of Particles on Standard Deviation of Estimated Mean Size	3-29
3-11 Example Particle Size Distribution	3-30
3-12 Flowchart of Programme to Calculate Total Sample Area	3-36
3-13 Flowchart of Programme to Analyse Particles in Sample	3-38
3-14 Comparison of Photo-Sieving and Mechanical Sieving for Laboratory Samples	3-43
3-15 Procedure to Assess Linearity of Longitudinal Tilt Distortion	3-47
3-16 Derivation of Tilt Correction Equations	3-50
3-17 Flowchart of Photo-Sieving Programme for Tilted Photographs	3-55
3-18 Comparative Results from Overlapping Photographs	3-60
3-19 Typical Scatter Plots for Shape Factor	3-62
3-20 Correlation of Shape Factor Regression with Vertical Tilt Ratio	3-63
3-21 Replicate Photo Analyses with Differing Rectification	3-65

	<u>Page</u>
3-22 Associations Between Grading Curve and Numbers of Particles	3-66
3-23 Confidence Ranking for Site Grading Curves	3-68
3-24 Typical Grading Curves for Dump Slopes	3-70
3-25 Comparison of Surface and Below-Surface Gradings	3-71
3-26 Typical Gradings from Upper and Lower Sections of Dump Slopes	3-72
4-1 Diffraction Patterns for Quartz and Fragment 9A Containing Quartz	4-11
5-1 Laboratory Modelling of Prototype Grading Curves	5-5
5-2 Results of 85% Standard Compaction Tests	5-10
5-3 Air Voids in Compacted Samples	5-12
5-4 Volumetric Strain During Triaxial Compression Tests	5-15
5-5 Effect of Age/Weathering on Shear Strength Parameters	5-17
5-6 Effect of Age/Weathering on Shear Strength	5-19
6-1 Variation of Particle Size Fractions with Age/Weathering	6-2
6-2 Correlation of Size Parameters with Age/Weathering	6-6
6-3 Correlation of Grading Shape Coefficients with Age/Weathering	6-8
6-4 Correlation of Shear Intercept with Site Grading	6-10
6-5 Correlation of Friction Angle with Site Grading	6-11
6-6 Correlation of Shear Strength with Site Grading	6-14
6-7 Correlations of Primary Minerals with Site Grading	6-16
6-8 Effect of Primary Minerals on Friction Angle - Grading Correlations	6-17
6-9 Variation of Clay Minerals with Age/Weathering	6-20
6-10 Correlation of Friction Angle with Clay Minerals	6-21
6-11 Correlation of Shear Intercept with Clay Minerals	6-23
6-12 Variation of 2:1 Layer Clay Minerals with Age/Weathering	6-24

	<u>Page</u>
6-13 Correlation of Strength Parameters with 2:1 Layer Clay Minerals	6-25
6-14 Relationships between Weathering Effects and Strength Parameters	6-29
7-1 Finite Element Mesh for Triaxial Compression Tests	7-10
7-2 Results of Back-Analyses of Triaxial Compression Tests	7-14
7-3 Finite Element Mesh for 1:1.5 Slope Waste-Rock Dump	7-16
7-4 Effect of Base Extension on Toe Displacement	7-18
7-5 Specification of Material Numbers for Slope Analyses	7-18
7-6 Finite Element Mesh for 1:3 Slope in Rehabilitated Landscape	7-20
7-7 Vertical Stresses for RM27A - <i>main</i> Run	7-23
7-8 Horizontal Stresses for RM27A - <i>main</i> Run	7-24
7-9 Shear Stresses for RM27A - <i>main</i> Run	7-25
7-10 Condition Flags for MG08 - <i>main</i> Run	7-27
7-11 Displacement Vectors for MG08 and RM27A - <i>main</i> Runs	7-29
7-12 Characteristic Displacements at Slope Face - <i>main</i> Runs	7-30
7-13 Condition Flags for MG08 - <i>soil</i> Run	7-32
7-14 Displacement Vectors for Frag75 - <i>soil</i> Run	7-32
7-15 Characteristic Displacements at Slope Face - <i>soil</i> Runs	7-33
7-16 Horizontal Stresses for RM27A - <i>base</i> Run	7-34
7-17 Condition Flags for Frag60 and RM27B - <i>base</i> Runs	7-35
7-18 Displacement Vectors for RM27B - <i>base</i> Run	7-36
7-19 Characteristic Displacement at Toe - <i>base</i> Runs	7-37
7-20 Correlation between Toe Displacement and Proportion of Coarse Fragments	7-38
7-21 Horizontal Stresses for RM27A - <i>1in3</i> Slope	7-40
7-22 Characteristic Displacements at Slope Face - <i>1in3</i> Slope	7-41

LIST OF TABLES

	<u>Page</u>
3-1 Details of Sampling Sites	3-5
3-2 Bulk Sample Sieving Results	3-8
3-3 Comparison of Image Length and Image Axis Parameters	3-22
3-4 Summary Statistics for Preferentially Oriented Particles	3-24
3-5 Summary Statistics for Preferentially Oriented Particles with Possible Hiding Factor Distributions	3-27
3-6 Coefficients of Variation for Measurements from Tilted Brick Photographs	3-54
3-7 Summary of Procedures in Photo-Sieving Method	3-68
4-1 Rock Fragment Composition (Estimated from Thin Sections and X-ray Diffraction)	4-12
4-2 Results of XRD Analysis on 75 micron Fractions (Estimated by Rietveld Procedure)	4-14
4-3 Results of XRD Analysis on 2.4mm Subsamples (Supplementary Samples)	4-14
4-4 Interpretation of XRD Analyses on Clay Fractions	4-16
5-1 Samples in Testing Programme	5-2
5-2 Summary of Triaxial Compression Test Results	5-13
7-1 Material Constants for Finite Element Models	7-13
7-2 Summary of Slope Analyses	7-22

LIST OF PLATES

	<u>Page</u>
2-1 Dumping of Waste-Rock	2-4
2-2 View of Waste-Rock Dumps from North (1991)	2-4
2-3 Sampling Site 18 (exposed 1.8 years)	2-8
2-4 Sampling Site 22 (freshly dumped)	2-8
2-5 Sampling Site 20 (exposed 0.4 years)	2-8
2-6 Sampling Site 2 (exposed 1.2 years)	2-9
2-7 Sampling Site 17b (exposed 2 years)	2-9
2-8 Sampling Site 16 (exposed 2.8 years)	2-10
2-9 Sampling Site 14 (exposed 6 years)	2-10
3-1 Long Distance Photograph of Dump Slope (Site 6)	3-4
3-2 Close Distance Photograph of Dump Slope (Site 6)	3-4
3-3 Set-up for Photographing Bulk Samples	3-41
3-4 Shot mg4-07 of Sample MG16 (in Heap)	3-41
3-5 Tilted Photograph of Brickwork for Distortion Analysis	3-46
4-1 Ranger Mine, looking East toward Escarpment	4-2
4-2 Ranger Pit No.1	4-2
4-3 Specimen 17Ba (Schist)	4-8
4-4 Specimen 13b (Schist)	4-8
4-5 Specimen 7Ba (Pegmatite)	4-8
4-6 Specimen 16 (Massive Chlorite Rock)	4-9
4-7 Specimen 6/ (Dolerite)	4-9
4-8 Specimen 8a (photographed under polarised light)	4-9
5-1 Triaxial Compression Test Apparatus	5-7
5-2 Test on Coarse Sample Showing Membrane Deformation	5-7
5-3 Triaxial Specimen of RM27A after Testing	5-16
5-4 Triaxial Specimen of RM26 after Testing	5-16

DECLARATION

To the author's knowledge, this thesis contains no material written or previously published by other persons, except as duly referenced in the text. No part of this thesis has been submitted for the award of any other degree or diploma.

If accepted for the award of the degree of Doctor of Philosophy, this thesis may be photocopied or loaned as determined by the Librarian of the University of Adelaide.

Susan Jane Henderson

ACKNOWLEDGEMENTS

In undertaking this research project, the author has received much support from staff at both CSIRO Division of Soils and The University of Adelaide, Department of Civil Engineering. Most importantly, she acknowledges the contributions of her supervisors, Dr Brian Richards and Prof R F Warner, both throughout the course of the research and during preparation of this thesis.

Special thanks are also owed to: Mr Martin Wright, Mr Roy Martin, and Mr Paul Peter for assistance and advice related to engineering testing; Mr Graham Riley, Dr A R Milnes, and Mr M Raven for mineralogical analyses and interpretation; Mr Cliff Hignett for assistance developing preliminary image analysis procedures; and Mr Stan McLeod and Ms Lesley Playfair for performing fine particle analyses. The finite element modelling was carried out using a computer programme developed by Dr Brian Richards, who also provided invaluable guidance on its application and interpretation.

Finally, the author wishes to thank Dr A R Milnes and personnel at Ranger Uranium Mine - in particular, Ms Corinne Unger and Ms Hazel Nisbet - for permission and assistance regarding field sampling.

CHAPTER ONE



1. INTRODUCTION

1.1 Background

Waste-rock consists of overburden and rock excavated during mining, in which the content of the object minerals is insufficient for economic recovery. Open-pit mining methods, employed in many mines throughout Australia, produce massive heaps of such spoil material. As unusable by-products of mining activity, waste-rock dumps (or spoil heaps) have traditionally been handled solely on the basis of minimising operating costs, and geotechnical design has been generally superficial. However, in response to growing community awareness of the vulnerability of natural environments, the mining industry is accepting a responsibility both to minimise environmental disturbance during mining and to leave the site in a state suitable for future alternative use. In this context there is a growing need for more rigorous design of, and active management strategies for, waste-rock dumps.

From a geotechnical engineering perspective, waste-rock dumps present certain features not generally encountered in natural slopes, cuttings, and fill embankments, which are the usual subjects of slope stability analysis. Primarily, waste-rock is a unique material, located in the uncertain area between soil and rock, and therefore difficult to classify and quantify. (For example, is it more relevant to sieve the fine particles or core the boulders?) Secondly, mechanical effects of the mining operations, together with the subsequent exposure often in severe climates, can make it susceptible to much more rapid degradation than the slow natural weathering of rock into soil. The dump structure is also different in that natural spatial variability is removed, but is not replaced with the engineered uniformity of a normal fill. Finally, dumps are now often subject to two design regimes: the immediate, strongly economic constraints of an operating mine; and the eventual, more encompassing (and so more conservative) philosophy of safety and facility to the general community. The analysis of structural slope stability of waste-rock dumps, covering the life of the mine and extending to the rehabilitated environment, forms the subject of this thesis.

1.2 Scope

The project was focussed on the waste-rock dumps at Ranger Uranium Mine, Northern Territory. As discussed in Chapter 2, the issue of dump management is particularly relevant at this mine, subject as it is to strict environmental controls protecting the surrounding Kakadu National Park and providing a combination of rock types and monsoonal climate which promotes rock weathering at a remarkable rate.

The overall aim of this research project was to investigate the effect on dump slope stability as waste-rock degrades. This may have implications for management of the dumps over the operational life of the mine (probably 20-30 years), and of the landforms of the rehabilitated site, which will be constructed largely from the waste-rock. Two components were identified within the broad objective, namely: the relationship between weathering and material strength; and the effect of changes in material strength on slope stability. The former, which is the aspect emphasised in this thesis, involved the development of procedures to quantify physical descriptions and to measure strength parameters of materials with particle size ranges beyond the scope of normal engineering methods. Existing methods of stability analysis were then briefly reviewed with regard to their applicability to waste-rock dumps and materials. On the basis of this, a finite element programme (also used by Richards, Peter, & Lucas 1986 in a previous investigation of waste-rock dumps at Ranger) was selected for analyses examining the effect of material weathering on dump slope stability in the medium to long term.

In the context of this thesis, slope stability analysis is restricted to structural stability of the dump slopes against mass sliding. Surface erosion and chemical leaching, which are included in the broad environmental understanding of dump stability, were not considered.

1.3 Research Plan

1.3.1 Concept

Investigation of the weathering-strength correlation was approached initially by posing a specific question: for a particular type of waste-rock, does strength decrease readily as weathering proceeds? Alternatively, is there a stage at which a rapid loss of strength occurs, or again (although unlikely), is there no significant change? These possibilities - three of many - are illustrated in Figure 1-1.

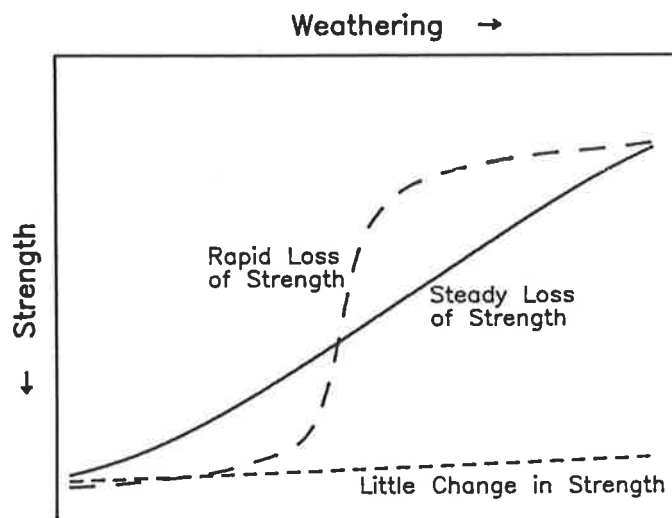


Figure 1-1 Possible Strength-Weathering Relationships

To define a relationship in this form, it is first necessary to quantify weathering. As described by Ollier (1969, p. 1), weathering consists of physical and chemical changes brought about by changes in environment. For soil and broken rock, these two aspects are typically described quantitatively by particle size distribution (grading) and mineral composition respectively. The "weathering" axis in Figure 1-1 may thus be visualised as itself a curve in the grading/composition plane, and the correlation with strength as a three-dimensional function of grading, mineral composition, and strength. If this function is imagined projected first onto the grading/strength plane and then onto the composition/strength plane, the result is two discrete (but dependent) correlations, as shown in the lower quadrants of Figure 1-2.

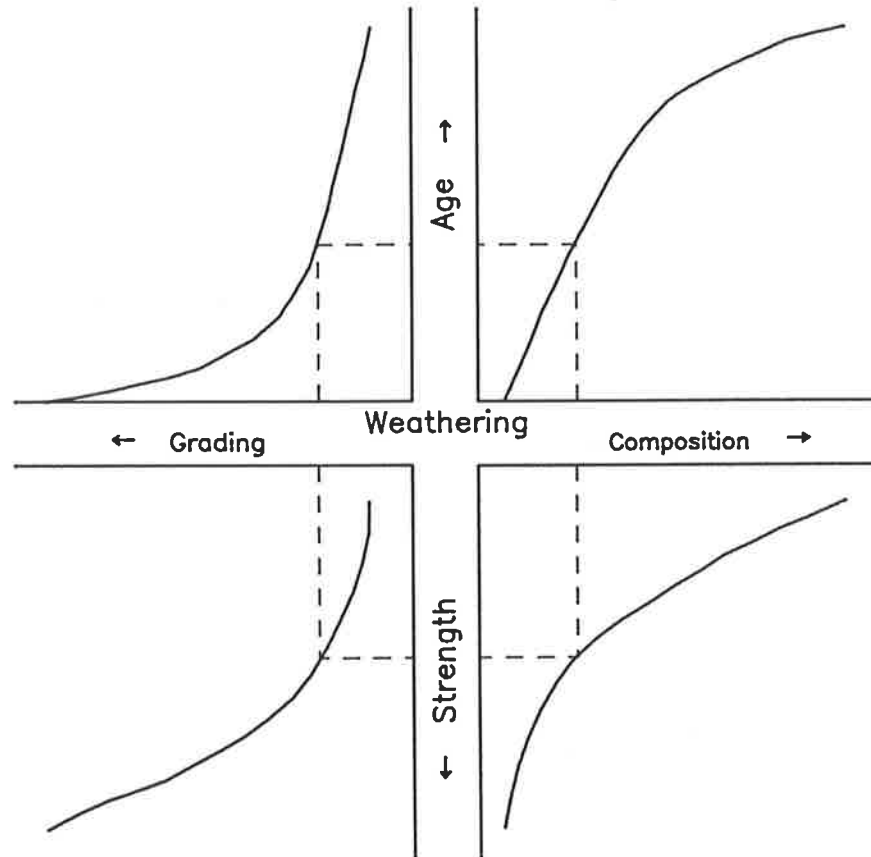


Figure 1-2 Concept of Material Characteristic Interactions

The upper half of this figure introduces links between dump age and weathering, which are relevant to applying the research to dump design and management. In 1989 (when most of the field work for the project was undertaken), the dumps at Ranger included batters ranging from new to about eight years old, which precluded comprehensive examination of these relationships within the scope of this thesis. However, it was anticipated that specific investigation of degradation in the dumps to that time, with some reference to probable later stages of weathering could provide an outline in which to frame further studies.

The diagrammatic concept of Figure 1-2 served as a basis for the methods and approaches discussed in the following section.

1.3.2 Methods

As indicated by Figure 1-2, physical characterisation of the waste-rock materials was one of the primary tasks. For soil engineering purposes the primary descriptor is the grading curve, or particle size distribution, which is obtained by sieving a representative sample of

the material through a set of sieves with serially decreasing aperture sizes. This procedure is not feasible for waste-rock because of the massive samples required to ensure representative proportions of cobbles and boulders, and because the sieves needed to grade such samples would be larger than quarry crusher screens. The option of sampling only the finer size fractions from the waste-rock was incompatible with the aim of evaluating weathering-related changes in the bulk material. This problem of scale also precluded investigation by boreholes: aside from the difficulty of achieving adequate core recovery, the information from a 100mm diameter sample is less than that which could be obtained by simply looking at the dumps.

This last observation suggested a possible solution, namely 'virtual' sampling, by photographing the dump batters. The approach of measuring particle sizes from photographs has previously been used in studies of bed characteristics of natural channels (for example, Iriondo 1972 and Adams 1979). Although the scale and unique nature of waste-rock necessitated significant adaptation of the basic philosophy, the speed and ease of sampling, and the lack of viable alternatives, led to a firm decision early in the project to pursue this method.

By nature, photographic sampling is restricted to surface material. As discussed in Section 2.3, weathering at the observed rapid rate probably occurs only in the outer few metres of the dumps. In a static structure, this would result in the surface material significantly different from that within the dumps. However, as the heaps are constructed by dumping out over existing batters, materials inside the dumps were once also at or near the surface, although for varying periods of time. Similarly, some of the faces photographed during this project have since been covered and are now "inside" the dumps. On this basis, the range of materials on the batter faces was considered representative of material throughout the dumps.

Small bulk samples (about ten kilograms mass) of material gravel-sized and finer were collected as an adjunct to the slope photography programme. These provided fragments and fines for mineralogical analyses, specifically thin section and X-ray diffraction, which were carried out by CSIRO Division of Soils Mineralogical and Geochemical Services Group. In determination of mineral composition, the omission of

oversize particles was not an issue: as established by preliminary examination, medium and coarse gravel particles in the waste-rock are mainly fragments of broken boulders, and therefore mineralogically similar. Weathering products, on the other hand, are concentrated in the silt and clay sizes. Therefore separate analysis of gravel fragments and clay fractions provided data respectively on initial composition and extent of chemical alteration.

Another consideration was achieving coverage of the range of weathering which might occur in the dumps. Mining commenced at Ranger in 1981, but despite the highly degraded appearance of some of the older batters, mineralogical analysis indicated that chemical alteration has not progressed far. Consequently additional materials, representative of more advanced stages of weathering, were sampled from other parts of the site. These could not be related to batter age, but it was possible to rank the samples with respect to extent of weathering and so obtain an appreciation of future developments in the dump materials.

The material size problem again arose with respect to the measurement of strength parameters. The largest available suitable testing equipment was a triaxial test rig for samples up to 100mm diameter, which limited maximum particle size in specimens to about 20mm. For this aspect of the study, however, a significant collection of published literature was available dealing with methods of scaling down coarse material (mainly dam rockfill) for strength testing, and their effects on resultant parameters. Although less than ideal, this approach had little practicable alternative, and in a study focussing on changes in strength, the results should remain relevant if materials which are basically similar are modified in the same manner. A full-scale test of a dump slope was of course considered, but the potential gain - detailed information about the in-situ behaviour of one of the rock types in one condition of weathering - did not justify the massive effort and expense, at least not in the context of the objectives of this research project.

Grading, mineral composition, and shear strength were brought together to establish models of dump materials at various stages of weathering. These were then used in non-linear finite element analyses of dumps constructed in lifts to 50m height. Resultant horizontal displacements

at the slope face were used to assess and compare slope stability as the dumps age and constituent waste-rocks degrade.

1.3.3 Thesis Format

The format of this thesis follows the same general lines as the conceptual research plan described in Section 1.3.1. The next chapter outlines the situation at Ranger Mine, especially with regard to environment management aspects and to the actual waste-rock dumps. Chapter 3 covers the theory and development of a procedure for photographic analysis to estimate particle size distributions of dump material. This is followed by presentation of mineralogical data. Chapter 5 describes the laboratory strength testing programme and is followed by interpretation of the correlation between weathering and material strength. The penultimate chapter deals with slope stability analysis using strength parameters derived through the study, to relate the results back to the context of mine management. The thesis concludes with a review of the outcomes of the project with respect to the stated objectives, a summary of findings specific to the waste-rock dumps at Ranger Uranium Mine, and suggestions for further research.

CHAPTER TWO

2. WASTE-ROCK DUMPS AT RANGER URANIUM MINE

2.1 Operational Setting

Ranger Uranium Mine, situated in the Alligator Rivers Region about two hours drive east from Darwin (see Figure 2-1), is one of the three uranium mines currently licensed in Australia. After discovery and confirmation of the Ranger orebodies around the early 1970s, mining was permitted subject to protection of the environment in 1977, and the mine commenced production in 1981. When Kakadu National Park was declared in 1979, the Ranger Project Area was excluded for the duration of mining, after which it will be absorbed into the park. Ranger therefore has dual responsibility to its unique world heritage environment: to avoid damaging the surrounding park by mining operations; and, after the cessation of mining, to rehabilitate the project area in a manner consistent with its inclusion in the park and providing for continued protection of the environment from the residues of mining.

The geology of Ranger Mine is summarised by Ranger Uranium Mine (1984) and Milnes, Riley & Raven (1986). Briefly, uranium occurs largely within the Cahill Formation rocks, which are assigned to "Lower Mine Series" (dominated by marbles and cherts), "Upper Mine Series" (chloritic and carbonaceous schists), and "Hanging Wall Sequence" (mica and amphibole schists). This formation is underlain by the Nanambu Complex (characterised by gneisses) to the west and a shear zone sequence to the east, and was previously overlain by Kombolgie Sandstone, which comprises the Arnhem Land escarpment. The lithology of the Cahill Formation is greatly variable due to regional metamorphism, igneous intrusions, extensive chloritisation, and alteration associated with the uranium mineralisation which occurred mainly after the lithification of the Kombolgie Formation.

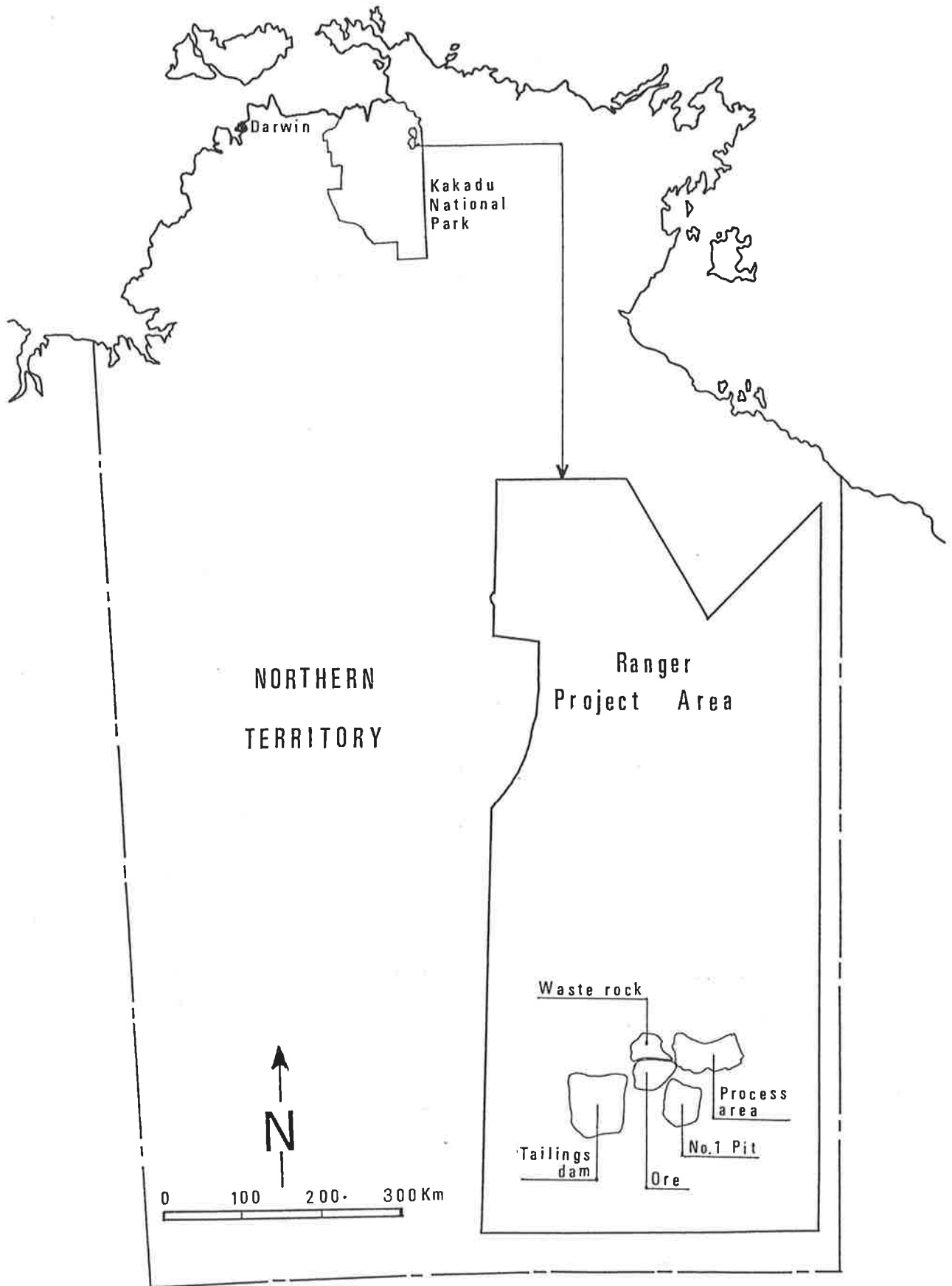


Figure 2-1 Ranger Project Area

The Ranger No.1 orebody is currently being mined by open pit methods. Rock is blasted out of benches about 7m high and loaded into 50-80 tonne dump trucks for haulage. On leaving the pit, each truck is driven under a radiometric discriminator, and based on the measured average uranium content, the load is assessed as high grade ore ($>0.075\%$ U_3O_8), low grade ore ($0.075-0.05\%$ U_3O_8), very low grade ore ($0.05-0.023\%$ U_3O_8), or waste-rock ($<0.023\%$ U_3O_8). The truck is directed to the appropriate heap, where the load is end-dumped over the existing active batter, as shown in Plate 2-1. Geotechnically, the various rock heaps are similar, except for a possible higher proportion of more degradable material in the waste-rock dumps, as a result of some of the more resistant waste-rock being stockpiled separately for construction use.

The basic construction plan for the waste-rock dumps is three lifts each of about eleven metres, within a planned raised area which will cap the tailings dam and Pit no.1 in the final rehabilitated landform, and will cover an area of about four square kilometres. However, as apparent from Plate 2-2, progressive construction of the dumps has been somewhat irregular, dependent largely on operational requirements. For example, during 1989 another dump was established near the tailings dam to facilitate subsequent rehandling of the rock to raise the dam walls. Inevitably, as the rehabilitation plan is developed and finalised over the next two decades or so of mine operation, plans for the waste-rock dumps may also change. (One issue addressed in this research project was whether the present steep slopes can be sustained as the materials degrade or whether plans will have to be amended anyway.)

During the monsoonal wet season, runoff from the primary waste-rock dumps drains into Retention Pond 4 which adjoins to the northeast. The recent dump near the tailings dam, like the ore stockpiles, is within the Restricted Release Zone. Runoff is stored within the zone, in Retention Pond 2, and subject to occasional controlled release to local waterways during periods of high flow.



Plate 2-1 Dumping of Waste-Rock



Plate 2-2 View of Waste-Rock Dumps from North (1991)

2.2 Site Observations

Considering more closely the nature of waste-rock dumps at Ranger, the following are observations made during the slope photography exercise described in Section 3.1:

a) The batter faces are loose with a high proportion of voids which are particularly apparent in the lower, coarser sections. A shallow surface layer is only marginally stable and difficult to walk on, but this does not give the impression of instability in the body of the dump. These attributes are typical of cohesionless material at its angle of repose (Campbell & Shaw 1978), since shear strength, which is proportional to normal stress, is minimal at the slope face and increases with distance into the dump. Hence there is apparently little cohesion in the near-face materials under the moisture conditions which occurred when the field work was undertaken, that is, in the middle of the dry season.

b) Sorting of fragments down-slope is observable as downward coarsening of the grading. The trend was apparent at all study locations, but was most pronounced on higher slopes not more than three years old, for example at Site 18 shown in Plate 2-3. Segregation is a normal consequence of dumping operations, as discussed by McKean (1980, p.26) and Campbell & Shaw (1978). A similar effect was referred to in natural scree slopes by Young (1972, p.128) and Statham (1972). The significance of this variation in grading was examined by photo-analysis and is discussed in Section 3.4.

c) The amount of finer particles - fine gravel size and smaller - observed among the sorted coarse fragments in the lower two-thirds of the slopes varied markedly with the age of the batter, as illustrated in the sequence of Plates 2-4 to 2-9. The newly dumped material showed moist silt and clay fines adhering to cobbles and boulders over the whole slope. This would be the condition of rock when it leaves the mine pit, having been watered after blasting to reduce dust. At locations exposed for less than a full wet season, there was less fine material in the lower sections but considerable medium and fine gravel was still present. On the year-old batters the bottom halves were generally bare of clay to sand sizes, except

in small local patches where larger fragments appear to have provided shelter, either preventing washout of fines or allowing fines washed down to accumulate. An exception was observed, where concentrated runoff from the top of the batter and degradation of already weathered pegmatite have resulted in some finer material persisting most of the way down the slope. The batters about two years old were largely deficient of smaller size fractions in the lower section. The lack of fines on these slopes of moderate age was only a surface effect: removal of the top layer of fragments at several locations revealed considerable fines within the skeleton of coarser down-slope particles, at fragment contacts and partially infilling voids. Locations on the three-year-old batter appeared to have considerable fine material down most of the slope. Close access in this section was only possible at the top of the batter, where degradation of odd larger fragments was observed, but it appeared that most of the finer material lower on the slope might have been washed down from above. This slope was high and steep, about 20 metres and 30° , and contained several erosion gullies which suggested significant sediment movement down the face. The oldest batters examined were at least six years old and showed significant proportions of finer particles down the full length of slope, much of which appeared to be due to weathering of larger fragments. They also carried sparse growth of grasses and some trees.

d) Systematic material variation was suggested by colour changes along the slope. These formed slightly wedge-shaped bands which from their width are probably related to a single truck-load. The effect was particularly noticeable on batters of moderate height. Also, there has been no significant shallowing of slopes as they are dumped onto. The implication is that when dumped, the load spreads laterally only slightly and forms a layer of approximately constant thickness as it falls over the slope.

The following tentative explanation of the changes in fines content on the batters was formulated at the time of the fieldwork:

At dumping, some sorting of the waste-rock occurs, with smaller fragments tending to stop further up the slope. Some fines, however, including those adhering to cobble and boulder-sized pieces are carried onto the lower half of the slope. During the wet season much of this

fine material is washed off the coarse, openly graded lower faces; fines washed from higher up are either not trapped or are washed in below the surface layer; and a net loss of fine matter from the surface is apparent. In keeping with the severity of tropical wets, the loss is rapid, and after about the second year, most of the batters appear bare of fines. During this time the exposed rock will have started to degrade in the presence of air, heat and moisture. However, it seems that for most of the rock-types encountered at Ranger the production of mobile fines to this stage is less than the capacity of runoff to remove it from the faces. After a couple more years, the production of fine-grained weathering products outstrips the potential for their removal, and accumulation of fines is observable on the batters. (It may be that the fines produced by weathering are also less erodible than those present initially.) The degree of accumulation is likely to depend on rock-type, aspect and hydraulic characteristics. This action will develop a weathered soil shell of some thickness over the batters.



Plate 2-3 Sampling Site 18 (exposed 1.8 years)



Plate 2-4 Sampling Site 22 (freshly dumped)



Plate 2-5 Sampling Site 20 (exposed 0.4 years)



Plate 2-6 Sampling Site 2 (exposed 1.2 years)



Plate 2-7 Sampling Site 17b (exposed 2 years)



Plate 2-8 Sampling Site 16 (exposed 2.8 years)



Plate 2-9 Sampling Site 14 (exposed 6 years)

2.3 Weathering in the Dumps

Conditions on the waste-rock dumps at Ranger are highly favourable to weathering. The mine rocks contain weatherable minerals, most notably chlorite and muscovite. Regional metamorphism and other geologic activity have induced microstructural features which can act as sites for the initiation of weathering. Another level of flawing is caused by the blasting, hauling, and dumping operations, after which the waste-rock is left in a loose, open heap with air voids and exposed surfaces permitting ingress of air and water. The tropical climate provides high temperatures (annual average daily maximum = 34°C), and a three-month monsoon season (average tri-monthly rainfall = 1050mm and average relative humidity = 70%), encouraging chemical weathering reactions and removal of the products.

It is generally accepted that chemical weathering - weathering involving alteration of mineral components (decomposition) - is the dominant process in tropical climates (Ollier 1969, pp.111-115 and Young 1972, pp.235-238). Milnes, Riley & Raven (1986) suggested that the initial weathering action in the waste-rock dumps at Ranger may be primary oxidation of pyrite. The weathering products provide an acid environment which promotes other reactions. Decomposition is apparent in the unmined rocks to depths of 20-30 metres (up to 50m in the pegmatites), but the processes are occurring at much faster rates on the waste-rock dumps.

At the tops of the dumps, the accumulation of fine particles (such as due to construction traffic) creates a low permeability layer. Combined with the lack of surface slope, this leads to short-term ponding and saturation (such as during rainstorms), which encourages the initial pyrite (sulphide) reaction (Fitzpatrick et al 1988), and dispersion of subsequent weathering products. When this system is supplemented by plant matter (naturally or deliberately seeded), the operation of soil bacteria can further assist degradation. The combined result of these effects is rapid decomposition of waste-rock on the dump terraces, such that soil layers up to about a metre thick have been observed on parts of the dumps (Fitzpatrick 1986).

On the exposed dump batters, decomposition in the early stages is localised around interfaces, microcracks, and other similar features where moisture can be trapped. The volume increase associated with the

reaction of chlorite to smectite, and to a lesser extent with other alterations, stresses the rock structure (which is already weakened by blasting and dumping), promoting further cracking. This exposes more sites for alteration, setting up a continuing cycle of physical degradation (disintegration) and decomposition, which has led to some sound boulders becoming friable mounds in less than five years.

Because of the requirements of saturation, and access for air, it is likely that the most rapid degradation is limited to relatively shallow depths, probably a few metres. Observations of runoff and outflow from batters suggest that most rainfall does not penetrate very deeply into the dumps. Also, the body of the dumps, subjected to overburden and confining lateral pressures, would have a lower amount of void space than the open unstressed surface. These restraints must slow the rate of degradation relative to the dump surfaces, although not in comparison with the undisturbed subsurface profile.

A distinctive feature of the combination of potential mechanisms operating is that while weathering, on both the terraces and batters, is essentially chemical in nature, its manifestation on the dump batters, at least in this first decade, is overridingly physical. In fact, as discussed in Section 4.2, mineralogical analyses of batter materials which have the appearance of coarse soil showed only minimal amounts of weathering products. The interplay of physical and chemical aspects is illustrated on some trial batters constructed on the dumps near Retention Pond 4 (refer Figure 3-2) to study runoff and erosion. Four slopes were prepared near the end of 1987. Two slopes were surfaced with fragments of massive chlorite rock up to 100mm maximum size and the others were similarly surfaced with schist. Massive chlorite rock has the greater potential for decomposition but little apparent internal structure whereas the schist, containing much less weatherable mineral, shows characteristic well-developed lamination. After one year, there was obvious degradation of the schist, with fragments extensively delaminated, while the massive chlorite rock appeared largely intact. This may be contrasted to expected longer term weathered materials of schist-derived soil with a mineral composition similar to that of the present, and smectite-containing soil developed from the massive chlorite rock. How strength, and therefore stability, is influenced by disintegration and decomposition is discussed in Chapter 6.

CHAPTER THREE

3. PHYSICAL DESCRIPTION OF DUMP MATERIAL

3.1 Dump Slope Photography

3.1.1 Procedure

As noted in Section 1.3.2, the dumps at Ranger Mine contain boulders of blasted rock, which are beyond the capability of mechanical sieving to grade, both with regard to apparatus available and to the mass required for representative sampling. (For example, AS 1289.A2-1977 recommends a minimum mass of 123 kg per sample for material with a nominal particle size of 150mm). Techniques for estimating particle sizes and subsequent grading distributions from photographs have previously been used for channel sediments (Adams 1979, Ibbeken & Schleyer 1986, and others), and recommend themselves by avoidance of large bulk samples, flexibility with regard to maximum particle size, and speed and simplicity of field procedures. In this application, a camera is typically held with the film plane parallel to, and within about two metres of, the target surface. Scaling is achieved either by including a rule or grid in the photograph or by calculation based on camera characteristics and its distance from the surface. The steepness of waste-rock dump batters and the size range of component materials necessitated adaptation of these field procedures.

Firstly, the full range of particle sizes could not be analysed from one photograph: even allowing for the finer fractions to be sampled and graded by normal mechanical sieving, a representative sample of the boulder fraction and image resolution of gravel-sized particles were not achievable at the one photograph scale. Consequently, a range of photographs varying from close to long distance was required for each site, from which the separate results were combined to provide an overall particle size distribution. Secondly, difficulties of access on and around the batters meant that it was often not possible to photograph with the film plane parallel to the slope surface, especially in longer distance shots. Scale reference markers were placed on the batter to permit later rectification of the resulting tilt distortion, as discussed in Section 3.3.2.3.

The field procedure thus adopted is summarised below and illustrated in Figure 3-1:

1. At each site, two scale reference sticks, with half metre and one metre length marks, were placed on the slope near the base, one across and one up the slope. Two more sticks were similarly placed further up the batter.
2. Photographs were taken, ranging from close to long distance. Close shots included at least one scale stick, and the camera was angled to minimise tilt distortion. Medium and long distance shots usually could not be taken parallel to the slope face, so one or both pairs of scale sticks were included to permit rectification of the resultant image.
3. A disturbed 'bulk' sample of material gravel-sized and finer was taken from an area included in at least one close or medium distance shot. Samples were generally about ten kilograms mass and were collected by shovel and hand.

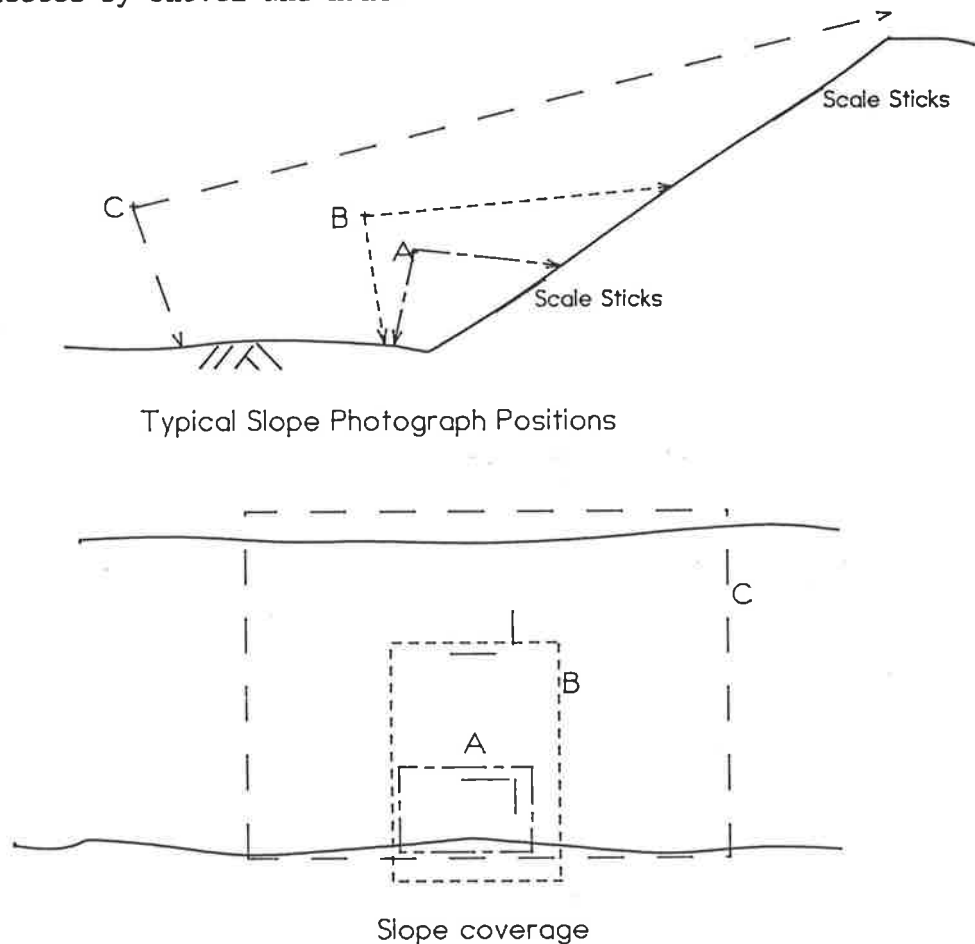


Figure 3-1 Procedure for Photographing Dump Slopes

Most of the photography was carried out using a camera with a 35mm tilt/shift lens to reduce the degree of slope/film misalignment. In some cases, a doubler attachment was added, extending the focal length to 70mm. A second camera with telephoto lens was used to provide back-up shots, and for long distance photographs of the sites edging Retention Pond 4 (refer Figure 3-2). These slopes could only be accessed from the top, so after scale sticks were placed and close distance shots were taken, each site was also photographed by the second camera, located across the retention pond on the top of another batter. At this distance the film plane could often be aligned with the target batter so that only one pair of scale sticks was required, which was an advantage on these older loose steep slopes. (In total, photographic sampling was carried out at 22 locations on the dump slopes.) Examples of slope photographs are presented as Plates 3-1 and 3-2.

As discussed in Section 2.2, some segregation of particles appears to occur during dumping, followed by subsequent changes in the fine end of particle size distributions. In order to compare the gradings obtained for waste-rock on the surfaces of the dump slopes with those of the mine rocks as excavated, photographs were also taken looking down onto loaded trucks leaving the mine pit. Two vantage points were selected on benches near the top of the western side of Pit No.1, adjacent to the rising haul road. The resultant photographs were slightly tilted, but the included truck tray of known dimensions was sufficient for rectification and scaling. As assessment of ore quality is not made until the truck has left the pit, the trucks were not necessarily destined for the waste-rock dumps. However, as noted in Section 2.1, the uranium content which differentiates between ore grades and waste-rock is not significant with regard to physical characteristics, general mineralogy, or therefore, weathering and strength behaviour.

To cover a wider range of materials than could be expected to leave the pit during a single shift, the trucks were photographed at the time of the main programme of fieldwork and again during a later site visit.



Plate 3-1 Long Distance Photograph of Dump Slope (Site 6)



Plate 3-2 Close Distance Photograph of Dump Slope (Site 6)

3.1.2 Sampling Sites

Photographic sampling of twenty-two sites around the waste-rock dumps, located on Figure 3-2 was carried out in June 1989. Sites were selected to cover the range of batter ages and rock-types. The oldest dump (>7 years) was not photographed because it was difficult to access, the batters were obscured by vegetation, and it contained predominantly pre-weathered subsoil and construction waste which was not relevant to the investigation. Further details of the sampling locations are summarised in Table 3-1.

Site	Age (yr)	Slope Height (m)	Slope Angle (°)	Aspect
1	1.2	13.2	31	N-E
2	1.2	13.2	31	N-E
3	1.2	13.2	31	N-E
4	1.2	12.8	24	E
5	0.7	8.1	30	N
6	0.7	6.8	26	N
7	3.3	7.7	26	N-W
8	6.0	6.8	34	N
9	6.5	8.2	34	N-W
10	6.5	8.2	34	N-W
11	6.5	8.0	34	N
12	6.5	7.9	35	N
13	6.5	8.0	36	N-E
14	6.0	7.9	33	N
15	3.1	20.6	30	E
16	2.8	18.9	33	E
17a	2.0	17.6	30	W
17b	2.0	17.6	30	W
18	1.8	19.6	32	W
19	1.6	19.7	34	W
20	0.4	9.5	47	S-W
21	0.1	14.2	37	S-W
22	0.0	5.2	22	W

Table 3-1 Details of Sampling Sites

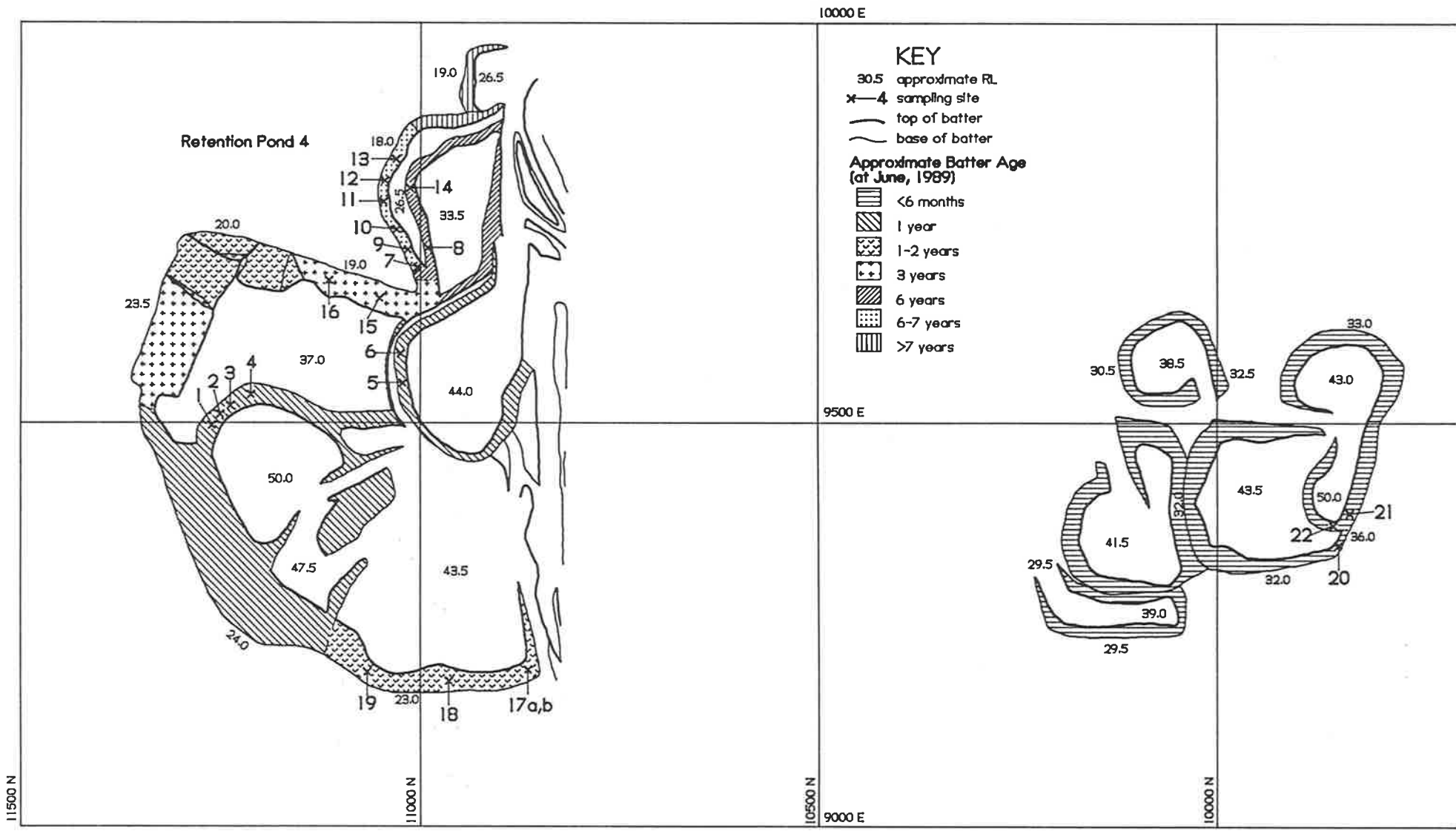


Figure 3-2 Location Plan of Waste-Rock Dumps Sampling Sites

3.2 Mechanical Sieving

Mechanical analyses were carried out on the bulk samples collected during the fieldwork programme. A 63mm square aperture sieve was used initially to remove over-size fragments, after which sieving was performed in general accordance with AS 1289.C6.2-1977, a subsidiary method, which was used because of the limited mass of each sample. It differs from the usual procedure (AS 1289.C6.1-1977) in that the 19mm-2.4mm portion is brushed clean to remove fines before dry sieving, and only the <2.4mm fraction is washed. For most of these samples, the proportion passing the 0.075mm sieve was less than 5% by weight, so detailed particle size analysis of the silt and clay fractions was not warranted. Instead, wash from the fine sieving was filtered through a Buchner funnel and the soil residue was dried and retained for later clay fraction determination.

Results, including clay percentage, are presented in Table 3-2. The main purpose of mechanical sieving of hand-collected samples was to provide the fine ends of the particle size distributions for dump slope materials, below the expected limit of resolution of the close-distance photographs. As such, the grading curves were not intended for separate interpretation. However, some specific observations are relevant:

- a) Even taking advantage of the subsidiary method, sample sizes were less than recommended in AS 1289.A2-1977 for 63mm nominal size material. The coarse ends of the sieve analyses, above about the 19mm fraction, were therefore not reliable.
- b) The samples were dry as collected, the average water content being 1%. Even sample 22, which appeared to be still moist from spraying in the mine pit (to lay dust), had a water content of only 3.7%. This was consistent with the season (dry) and the non-cohesive character of the surface observed in-situ.

SITE	SIEVE SIZE (mm)												
	63.0	37.5	26.5	19.0	9.53	4.76	2.41	1.20	0.500	0.300	0.150	0.075	0.002
PERCENTAGE PASSING													
1	Not Sampled												
2	100.0	87.4	81.6	74.1	65.9	52.0	38.6	27.2	10.6	4.8	2.0	1.1	0.2
3	Not Sampled												
4	100.0	86.2	72.1	54.0	26.4	11.6	6.7	4.2	2.7	2.2	1.5	1.1	0.2
5	100.0	59.0	40.0	27.5	12.6	6.7	4.3	2.8	1.9	1.6	1.1	0.8	0.1
6	100.0	75.0	55.9	42.6	23.3	12.9	9.1	6.7	4.6	3.8	2.8	2.1	0.4
7 (a)	100.0	87.3	77.4	69.2	56.2	37.7	22.5	11.2	4.1	2.6	1.4	0.8	0.1
7 (b)	100.0	86.5	75.1	66.5	54.3	33.5	16.5	6.9	2.3	1.4	0.7	0.4	0.0
8	100.0	89.1	84.1	78.1	68.9	54.8	39.5	26.1	13.6	9.8	6.2	4.0	0.6
9	100.0	82.7	76.7	69.0	56.2	42.0	30.8	23.2	16.2	13.0	9.2	6.6	2.1
10	100.0	84.9	81.7	75.2	66.9	55.7	46.6	40.1	30.6	25.0	17.4	11.7	2.9
11	100.0	75.7	67.8	59.1	42.2	27.5	18.5	12.1	7.3	5.6	3.8	2.5	0.7
12	100.0	84.8	74.0	66.4	52.3	39.0	27.2	18.2	9.7	7.3	5.2	3.7	0.6
13	100.0	77.6	67.0	56.5	39.4	28.1	20.7	14.9	9.4	7.2	4.9	3.4	0.1
14	100.0	88.0	80.4	70.7	58.5	45.1	33.7	23.3	13.7	10.3	6.7	4.3	0.9
15	100.0	76.3	69.5	62.5	53.4	41.2	31.3	23.2	11.2	5.7	2.8	1.7	0.1
16	100.0	89.2	80.8	70.1	49.7	21.8	7.6	4.1	2.4	1.9	1.3	0.8	0.0
17a	Not Sieved												
17b	100.0	51.6	37.7	31.5	24.0	17.2	12.6	8.7	4.6	3.2	1.8	1.0	0.1
18	Not Sieved												
19	100.0	43.3	25.7	14.9	7.7	3.1	1.3	0.4	0.1	0.0	0.0	0.0	0.0
20	100.0	72.0	58.7	50.0	33.0	23.0	17.5	12.9	8.9	7.4	5.8	4.4	0.2
21	100.0	72.0	58.7	50.0	33.0	23.0	17.5	12.9	8.9	7.4	5.8	4.4	0.3
22	100.0	87.7	71.0	62.0	47.1	35.4	28.1	23.2	18.0	15.7	12.6	9.5	2.6

Table 3-2 - Bulk Sample Sieving Results

c) Field observations of trends in the surface fines, noted in Section 2.2, are broadly reflected in the mechanical grading results. Figure 3-3 shows effective size increasing initially, (implying a relative reduction in the fine fraction), peaking at about a year, and then decreasing again as the proportion of fines increases. Considering that this figure does not differentiate between rock-types, the presence of any trend is evidence of the significance of slope age, or duration of exposure, on material characteristics.

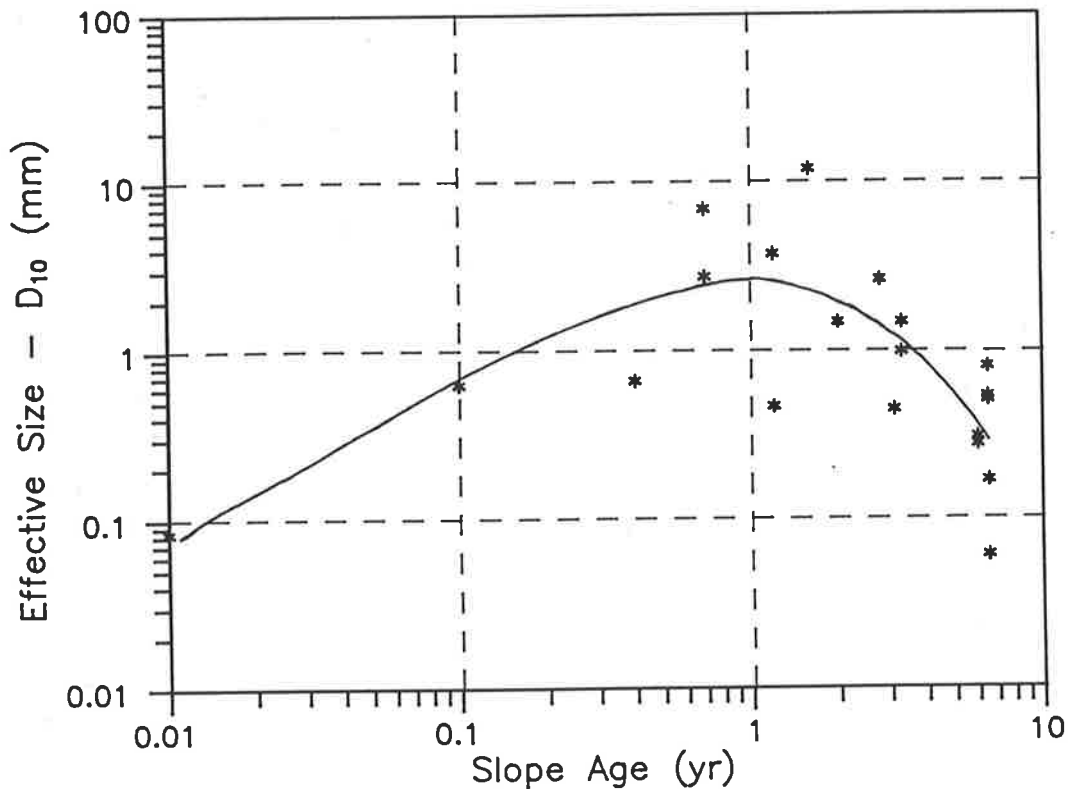


Figure 3-3 Batter Age versus Bulk Sample Grading (D_{10})

Close distance photographs were also taken of the collected bulk samples, to allow direct comparison of results produced by photo-analysis with those from the standard grading technique (mechanical sieving). This validation of preliminary photo-sieving procedures is discussed in Section 3.3.2.2.

3.3 Photo-Sieving

3.3.1 Theory

3.3.1.1 Preamble

The principle of mechanical sieving is that each particle will be retained on the largest sieve through which it cannot pass, that is, the first sieve for which the aperture dimension is larger than no more than one of three orthogonal particle axes. As a laboratory technique, there are sources of error. (For example, an elongated particle may fall with its long axis against the sieve and not pass through even though its other two axes are smaller.) However, such errors are normally considered negligible, and it is assumed that mechanical sieving produces the result for all particles that:

(sieve size on)	(length of)	(smallest sieve)
(which particle) <	(intermediate) <	(size through which)
(is retained)	(particle axis)	(particle passed)

Another relevant feature of mechanical sieving is that consecutive sieve sizes typically decrease in approximately constant ratio, rather than constant absolute decrement. For example, sizes 19mm, 9.5mm, 4.8mm, and 2.4mm are a common sequence. In this case, a particle with an intermediate axis of 10mm will be retained on the same sieve as a particle 50% larger, that is, with 15mm intermediate axis.

Mechanical sieving is the traditional method of grain-size analysis above silt size (0.06mm) so, reference to particle size material grading normally means reference to the results of this procedure. Consequently, any new technique should mimic sieving in concept, with the aim of producing equivalent results. This is the context of the following discussion.

The term photo-sieving has been borrowed from Ibbeken & Schleyer (1986), who used it for a specific procedure intended to determine "sieve-equivalents" for populations of coarse-grained channel sediments. In this thesis it refers in general to methods of analysis by photograph for which the purpose is to achieve a particle size distribution comparable to what would be obtained by mechanical grading.

The hypothesis underlying photo-analysis is that there is a definable relationship between the actual physical dimensions of a particle and a two-dimensional image of it, so that a grading curve for a set of actual particles may be deduced from certain measurements on a photograph of the set. Obviously, a close relationship must exist between an actual shape and an image of it; the uncertainty lies in its form and limits.

In essence, any particle size analysis incorporates three phases, namely:

- a) selection - the process of obtaining a sample from the total population of particles;
- b) designation - the assignment of each particle to a size class; and
- c) valuation - the determination of the significance (weighting) of each particle relative to the total sample.

With mechanical grading, selection is by representative bulk sampling of an approximate mass or volume. Each particle is designated according to the aperture size of the sieve on which it is retained, and valued by its mass as a proportion of the total mass of sample.

Kellerhals & Bray (1971) assessed the dimensional similarity of image analysis procedures to mechanical sieving. They considered two selection techniques used in photograph-based methods: grid sampling, in which a regular grid of points is established over the image and the sample comprises those particles which are under points; and areal sampling, where all particles within the photograph are included in the sample. A third technique described which might also be adapted to photographs is transect sampling, with the sample comprising all particles falling under a straight line placed randomly across the image.

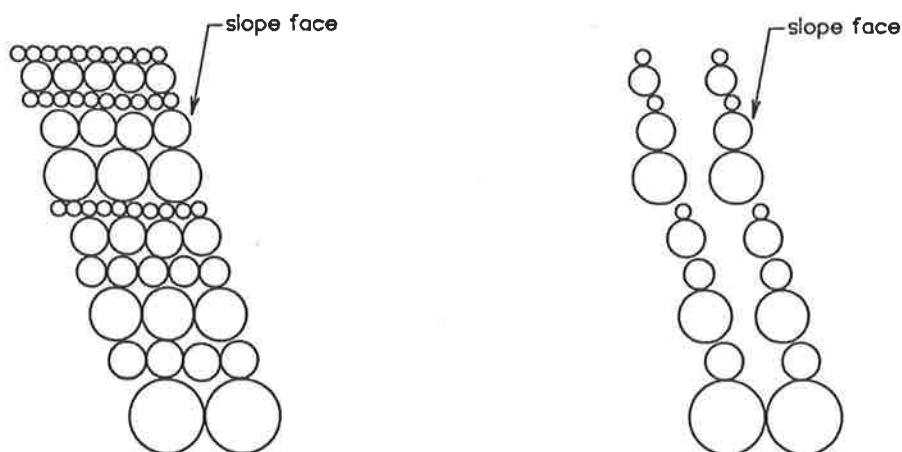
Areal sampling provides the largest sample from a given photograph, and is the option that most closely simulates bulk sampling. Grid sampling has the undesirable feature of not providing a strictly random sample, and transect sampling might be non-representative if, as suspected, particle size exhibits some spatial trend on the dump batters. One disadvantage with areal sampling is the greater analysis time associated with a much larger sample, but this is less important with computer-based procedures. Therefore, areal sampling was selected for photo-sieving of the waste-rock dumps.

Designation of size should rationally be based on some linear measure of the particle image. Selection of the measure and its relationship to the actual sieve size for the particle are crucial to the success of a photo-sieving procedure: these issues are examined in Section 3.3.1.2.

With regard to valuation, Kellerhals & Bray (1971) considered only two alternatives: by weight as a proportion of sample weight, which is the valuation used in mechanical sieving; and by number (equal weighting for each particle). Assuming constant specific gravity, the former is directly analogous to particle volume as a proportion of total sample volume, which may be applied to photographic techniques. Following the argument of Kellerhals & Bray (1971), valuation by number is non-dimensional and would require conversion by a factor of D^3 (D = particle diameter) to be equivalent to the standard valuation by weight. With regard to sample selection, volumetric sampling used for mechanical sieving allows three degrees of freedom in specifying sample size - length, breadth, and depth. Grid sampling allows no degrees of freedom (only the dimensionless number of points is specified), and it is suggested that a conversion factor of $1/D^3$ would be required to achieve equivalence. Similarly, areal sampling with two degrees of freedom would require conversion by $1/D$. From this basis Kellerhals & Bray (1971) concluded that only grid sampling combined with valuation by number (conversion factors $1/D^3$ and D^3) was naturally equivalent to the usual mechanical sieving procedure. Areal sampling with valuation by volume ($1/D$ and 1) would be dissimilar.

However, one alternative was not considered, namely areal sampling combined with valuation by area, (particle image area as a proportion of total sample area). The proposed combination meets that test of equivalence with conversion factors $1/D$ and D . The difference between material composition actually presumed in valuations by area and by volume are illustrated in Figure 3-4. Valuation by area is actually the direct expression of an assumption stated by Kellerhals & Bray (1971) as underlying their equivalence model; that the proportion of area in a photograph occupied by a given particle size is equal to the proportion of volume it contributes to the real population. Kellerhals & Bray (1971) provided no justification but supported the equivalence model, and consequently, its bases, by successfully applying it to two sets of size distribution data. The assumption will be valid if particle sizes

within the material being graded are randomly distributed with depth normal to the image plane. On the dump slopes, such a condition is likely to exist initially, as sorting occurs down the slope, not across the depth of the shallow newly dumped layer. Later movement of fine fractions may disturb the randomness, an effect which is explored in Section 3.3.3. However, for the purpose of the current theoretical discussion, and in the absence of contradictory evidence, the assumption was accepted.



Valuation by Area
(% mass = % area on surface)

Valuation by Volume
(%mass = % volume of grains on surface)

Figure 3-4 Comparison of Samples assumed by Area and Volume based Valuations

In summary, selection by areal sampling and valuation by area were adopted into the photo-sieving procedure under development, these options being judged closest in approach to mechanical sieving. It then remained to investigate the designation of size class of particles from planar images.

3.3.1.2 Parameter for Size Designation

From published literature, it appears that size designation has been most often estimated from a parameter, "minor photo axis", or "smallest visible axis". Griffiths (1967, p.121) provided early definitions of minor axis as 'the shortest intercept through the projected image', and major axis as 'the longest intercept perpendicular to the shortest'. Kellerhals & Bray (1971) and Iriondo (1972) used minor axis without further description. Adams (1979) redefined minor axis as the separation between lines which are parallel to the longest axis (major photo axis) and just touching the outline; and Ibbeken & Schleyer (1986) used the

same parameters, described diagrammatically. One exception to the use of minor photo axis was the method described by Guy (1969, pp.48-49), using the Zeiss Particle Size Analyzer, which based size designation on equivalent diameter.

The simplest assumption of the relationship between minor photo axis and actual intermediate axis (theoretical sieve size) is that of equivalence, (for example, by Iriando 1972). Some researchers have tested this premise against results of photo-sieving and corresponding mechanical sieving on the same sample and, not surprisingly, found only moderate agreement. Adams (1979) reported experiments with ten samples of river pebbles for which the minor photo axis of a pebble was on average about 6% smaller than the sieve size, and the major photo axis was about 45% larger than it. Ibbeken & Schleyer (1986) included a geometric examination of ten particle shapes oriented in seven different positions relative to the image plane. It was shown that for adverse combinations, minor photo axis could be as small as 0.3 or as large as 2.5 times the actual sieve size, (for very plated and very elongated particles respectively). Also presented were linear regression equations of photo-sieving on mechanical grading for four samples of channel surface sediments: photo-sieving based on minor photo axis predicted grading curves ranging from 10% to 40% finer than actual particle size distributions.

These reported biases warned against uncritical acceptance of minor photo axis as the parameter for size designation, as errors might be even larger for unnaturally sized and shaped waste-rock fragments. In fact, although it was favoured by subsequent authors, Griffiths (1967, p.64) admitted that there was no inherent reason why a particular axis should be the most appropriate measure. Consequently, it was decided to return to the basic relationship between the geometry of the three-dimensional particle and that of its two-dimensional image.

After size and shape, the image of any given particle in the photographed sample is compounded by two effects, namely, the orientation of the particle with respect to the photo-plane and the partial hiding of the particle by adjacent grains. These were examined in turn.

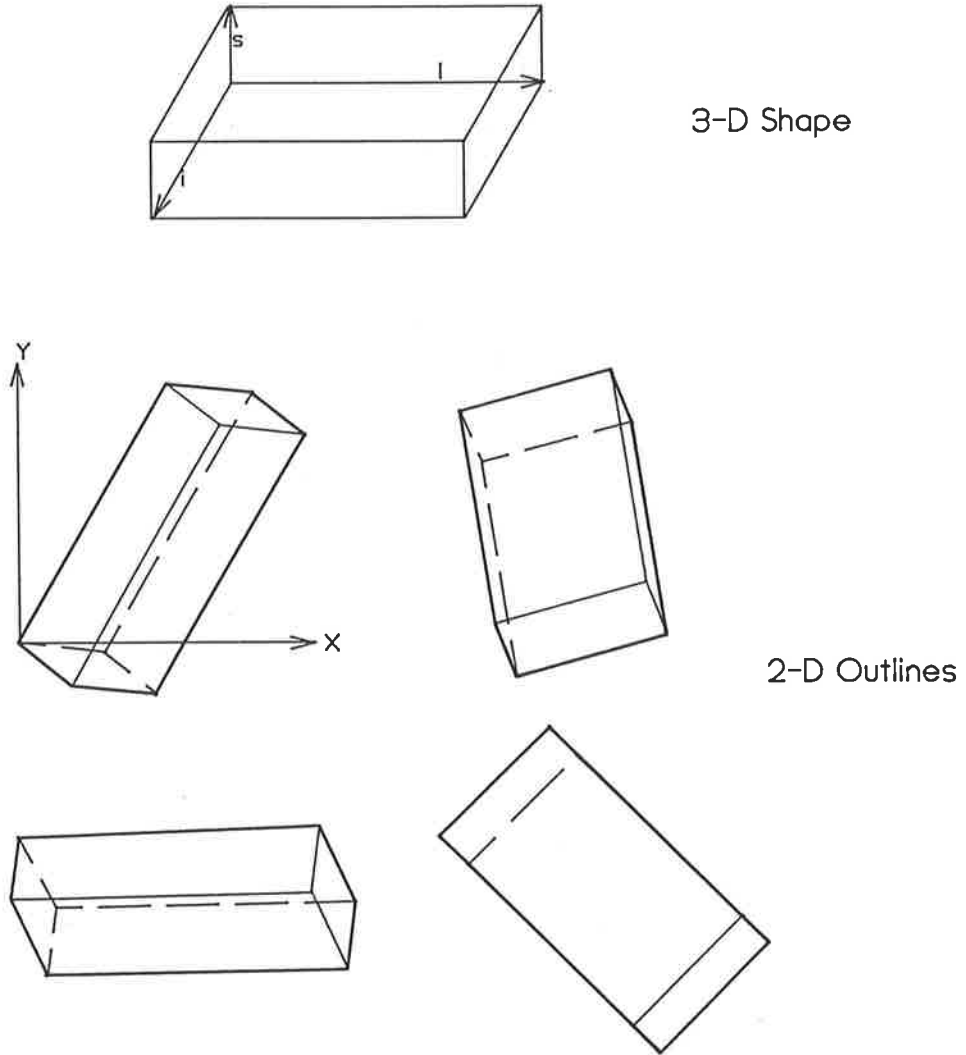


Figure 3-5 Effect of Orientation on Particle Image

Figure 3-5 illustrates the orientation effect, by which even a single simply-shaped particle can produce an infinite variety of outlines depending on its orientation relative to the image plane. The geometric relationship may be approached from a consideration of transformation of coordinates, from local particle axes - l , s , and i - to photo axes X, Y, and Z (which is normal to the photo plane and not used). A set of transformation equations, derived from Korn & Korn (1961, p.413), is:

$$\begin{bmatrix} X \\ Y \end{bmatrix} = \begin{bmatrix} \cos\alpha \cdot \cos\beta & \frac{\sin\alpha \cdot \sin\beta \cdot \cos\gamma}{- \cos\alpha \cdot \sin\gamma} & \frac{\cos\alpha \cdot \sin\beta \cdot \cos\gamma}{+ \sin\alpha \cdot \sin\gamma} \\ \cos\alpha \cdot \sin\gamma & \frac{\sin\alpha \cdot \sin\beta \cdot \sin\gamma}{+ \cos\alpha \cdot \cos\gamma} & \frac{\cos\alpha \cdot \sin\beta \cdot \sin\gamma}{- \sin\alpha \cdot \cos\gamma} \end{bmatrix} \begin{bmatrix} l \\ s \\ i \end{bmatrix}$$

where α , β , and γ are rotations about the particle axes l , s , and i respectively. Thus for a given particle shape (that is, defined initial

local coordinates), it is possible to determine the geometry of a resultant image for a particular set of relative orientations.

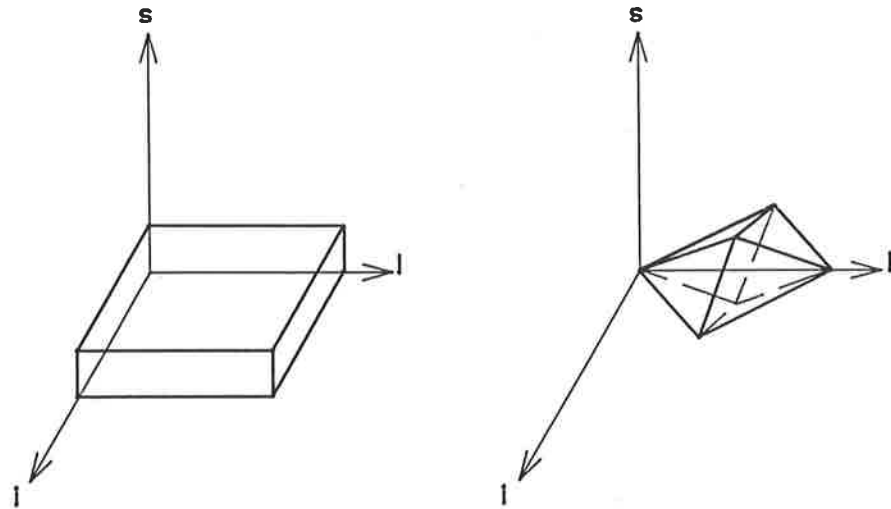
In a comparison of potential designation parameters, the important feature was the range of images (or of specific, associated linear measures) produced from the range of possible orientations. This was investigated by mathematically modelling the generation of image outlines from selected particle shapes. Just as the image geometry is defined by α , β , and γ so the probability distributions of any selected geometric parameters are constrained by the probability distributions of α , β , and γ . Hahn & Shapiro (1967) described several techniques for obtaining the probability distribution of a compound function from the distribution parameters of its components. However, the transformation formulation is complex (for example, each vertex is a discontinuity between particle edges) and involves products of periodic trigonometric functions. As a result, more elegant techniques were unsuitable or unwieldy, and direct Monte Carlo simulation was used to model probability distributions for selected geometric parameters of the image.

As explained by Hahn & Shapiro (1967), direct simulation involves generation of a random value for each component parameter - in this case, α , β , and γ - in accordance with its distribution function, which is known or assumed. The system functions are then evaluated for these specific values. (Here, the system functions are the coordinate transformation equations and calculation of any selected image parameters, such as minor photo axis.) The process is repeated many times to generate a large sample of the population of system results, the statistics of which may then be estimated.

Computer programmes were written to model the orientation effect on image measures for two basic particle shapes, shown in Figure 3-6. Long and short particle axes were specified relative to a unit intermediate axis, using shape factors $fl=l/i$ and $fs=s/i$. This allowed examination of variations of the basic shapes ranging from splintered ($fl>1$ and $fs=1$) through to platelike ($fl=1$ and $fs<1$).

A choice of three forms of distribution function was permitted for each rotation, namely uniform, normal, and bimodal normal (that is, with two peaks 180° apart). The uniform distribution, which assumes no

preferential orientation about that axis, was used in the first stage of comparison of various potential designation parameters. The bimodal form, with specifiable mean and standard deviation, was included to account for the tendency of particles to align as they roll down a steep slope. It was used in a second series of simulations to estimate the actual magnitude of bias between intermediate particle axis and preferred image parameters.



Rectangular Prismatic Particle

Octahedral Particle

Figure 3-6 Particle Shapes Used in Monte Carlo Simulation

Specific values for rotations α , β , and γ were generated pseudo-randomly using the following equations based on Priest (1989):

Input seed value, Ru^0

$Ru^i = \text{decimal part of } (37.1 Ru^{i-1})$

If $(Ru^i > Ru^{i+1})$ then $Rn^i = \sqrt{-2 \ln(Ru^i)} \times \cos(2\pi Ru^{i+1})$

otherwise $Rn^i = \sqrt{-2 \ln(Ru^i)} \times \sin(2\pi Ru^{i+1})$

If $(Ru^{i+2} < 0.5)$ then $Rbn^i = Rn^i + \pi$

otherwise $Rbn^i = Rn^i$

Random value $V^i = Ru^i \times 360^\circ$ uniform distribution

$V^i = Rn^i \times 360^\circ$ normal distribution

$V^i = Rbn^i \times 360^\circ$ bimodal normal distribution

If $(V^i > 360^\circ)$ $V^i = V^i - 360^\circ$

Trial frequency distributions produced by these equations are illustrated in Figure 3-7.

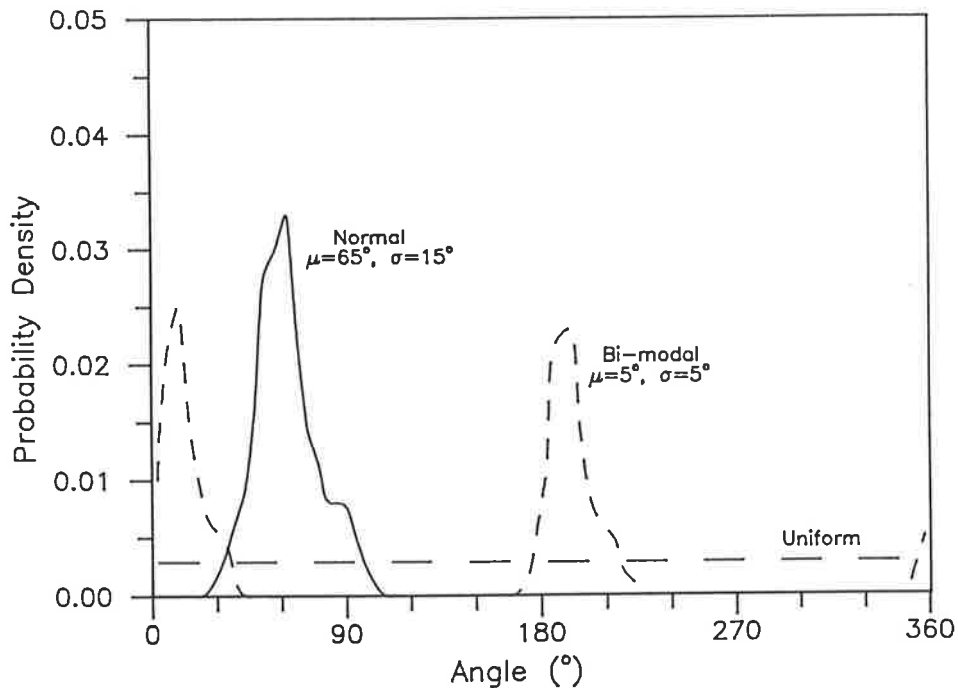


Figure 3-7 Distributions Generated by Random Number Algorithms

Initial programme runs showed no significant difference between distributions resulting from 2,000 trials, (individual calculations of system result), and 10,000. A standard of 5,000 trials was adopted as maintaining reasonable run times, of about half an hour on a Labtam V32 system minicomputer, with good repeatability of even highly irregular distributions.

Three sets of possible designation parameters were examined, based on the pairs of axes illustrated in Figure 3-8. The first were minor and major photo axes as used by Adams (1979) and others. Manual estimation is performed by a trial-and-error procedure, which was difficult to programme even for the simple regular shapes modelled. Also, as noted previously, there is no direct correspondence between minor axis, which is not even contained within the particle, and intermediate axis. However, the previous wide use of minor axis made its inclusion in the study desirable.

The second two axes were the maximum horizontal and vertical distances between points on the image outline, which will be referred to as horizontal and vertical photo lengths. Although again without obvious connection to intermediate (or any) particle axis, the advantage of

simplicity might outweigh slightly greater errors relative to another more complex parameter.

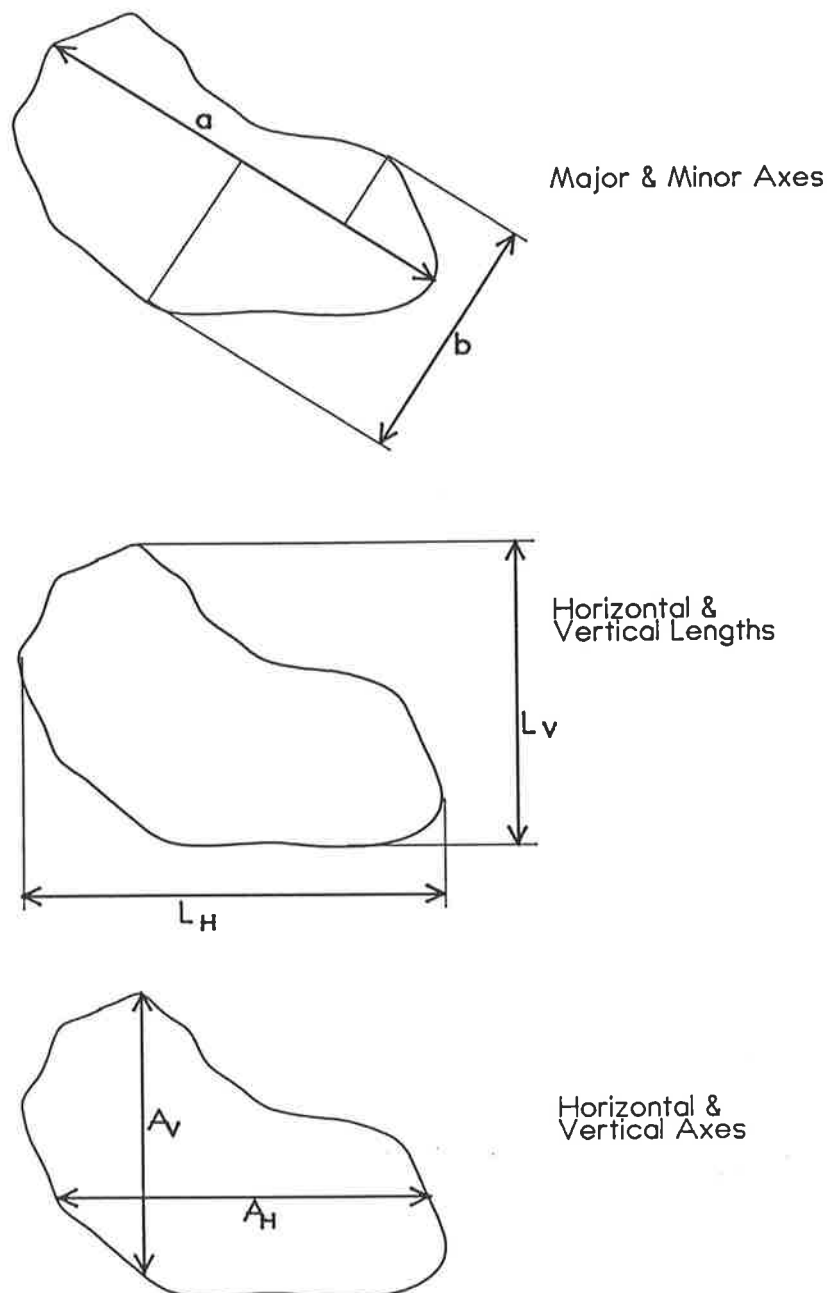


Figure 3-8 Axis Pairs Considered in Simulations

Horizontal and vertical photo axes, the third pair illustrated in Figure 3-8, were considered the most promising of those examined. The calculation of longest horizontal and vertical lengths contained wholly in the image was moderately complex to programme. However, these are at least actual linear measures within the image, and are related to the complete outline rather than just its extremities. (Intuitively, a better result would probably be obtained by removing the constraint of

Reasonable success was achieved using a simple line detection routine common to image enhancement work. Each pixel is set on or off, based on a comparison between the average grey scale value for the nine-pixel block centred on that pixel and a specifiable threshold value. Because of computer memory limits, each row of new values was written back into the digitiser memory before proceeding to the next row. As a result of light intensity variations, and imperfect pen-work, not all outlines were fully captured at the same threshold: this was overcome by optionally returning to select a new threshold. Each time, a fresh image was captured from the video, to be overwritten in memory by this *line_detect* function.

b) Measuring geometric parameters:

Once a pixel array containing an outline image of the photograph has been created, it is then necessary to extract a separate boundary trace for each particle, from which axes and area can be calculated. Manual activation of the resultant boundary routine was preferred to an automatic particle search, because this was easier to integrate with the threshold repeat option. The developed function accepts an initiating pixel coordinate pair from the mouse, searches left until an outline pixel, (that is, an 'on' pixel), is encountered, then moves clockwise around the outline until it closes back on itself. Variations of the same algorithm are used for total areas and individual particles. (The separate handling of these items is discussed in later parts of this Section.) Conditions in *boundary* were included to terminate the function if the trace goes astray - for example, if the particle outline are not closed - and to prevent the pixel storage array being overrun. It should be noted that the stored image is queried but not altered by the routine: the resulting trace appears on the monitor as 'white' pixels only to assist the operator by showing particles already analysed.

This *outline/boundary* function is capable of tracing quite complex and irregular shapes. An occasional problem was noted in that if the first pixel traced is in a one-pixel-thick section, the function will terminate when that pixel is retraced, regardless of whether the boundary is complete. This condition occurred only rarely, and could generally be avoided by selecting the initiating mouse

horizontal-vertical alignment.) However, this would greatly extend the calculation procedures (and times), and such parameters would be difficult to reconcile with procedures for the intended horizontal and vertical tilt rectification of slope photographs.

The disadvantage of horizontal-vertical alignment is that the same image can produce different results, simply due to its orientation within the image plane. Consequently, several compound parameters which reduce this effect were also investigated for the two aligned-axis pairs: namely, the shorter and longer (minimum and maximum) of the primary measures; and their arithmetic and geometric averages. Averages were also calculated for the non-aligned pair, to mitigate expected large errors associated with minor and major axes, for platelike and splintered particles respectively.

Ideally, a designation parameter should be similarly reliable for a wide range of particle shapes. However, if some variation did occur (as expected), but could be correlated with some other shape-dependent image parameter, the same purpose would be achieved. To this end, two image shape ratios, (horizontal value/vertical value) and (minimum value/maximum value) were also analysed for each axis set.

By defining the intermediate axis (the "correct" result) as unit length, all measures for the rectangular prismatic shape were automatically standardised against theoretical sieve size. For the octahedral shape the sieve size - the smallest square mesh through which the particle will pass - is actually $i/\sqrt{2}$. Values for the octahedral particle were therefore divided by $\sqrt{2}$ so that 1.0 was again the ideal, unbiased, result.

In summary, probability distributions for the following possible designation parameters were modelled:

- a) minor and major axes, the arithmetic average and geometric average of these axes, and the ratio minimum/maximum;
- b) horizontal and vertical lengths, the minimum, maximum, arithmetic average, and geometric average of these lengths, and the ratios horizontal/vertical and minimum/maximum; and
- c) horizontal and vertical axes, the minimum, maximum, arithmetic average, and geometric average of these axes, and the ratios horizontal/vertical and minimum/maximum.

Distribution parameters calculated were mean, standard deviation, third and fourth central moments, and ordinates of the cumulative frequency distribution. However, as in the following discussion, consideration of only mean and standard deviation was sufficient to select a preferred parameter by which to designate particle size.

As a preliminary stage, parallel simulations assuming random uniformly distributed orientations were performed for a range of particle shapes, in the hope that the results would indicate a clear preference for either a particular parameter or at least an axis set. Four particle shapes were specified for both rectangular prismatic and octahedral geometries, namely, equidimensional ($l:i:s = 1:1:1$), splintered ($3:1:1$), bladed ($2:1:0.5$), and platelike ($1:1:0.1$). The resulting distribution statistics are summarised in Table 3-3.

The attributes sought in the designation parameter were repeatability for any given shape (that is, small standard deviations), and mean results close to 1.0 for most particle shapes. Failing the latter, mean results should be at least close to each other, so that a constant bias could be allowed for.

Horizontal and vertical axis parameters, particularly minimum and geometric average axes, estimated closest to theoretical sieve size for all except the two platelike particles. This set also showed smallest standard deviations for the splintered and bladed shapes. Major and minor axes had significantly smaller standard deviations for the equidimensional particles only, but generally produced worse estimates of sieve size for equidimensional, splintered, and bladed shapes. Horizontal and vertical length parameters performed poorly for all shapes except the platelike particles. It is noted that these are extreme shapes, the octahedral plate being especially rare, and ones for which the assumption of uniform distributions for orientation may be too broad a simplification. Based on this first stage of examination, the set of parameters incorporating on horizontal and vertical axes showed the most potential, and further investigation was restricted to these measures.

	shape 1:1:1			shape 3:1:1			shape 2:1:0.5			shape 1:1:0.1		
	lengths	axes		lengths	axes		lengths	axes		lengths	axes	
	H & V	Maj.& Min		H & V	Maj.& Min		H & V	Maj.& Min		H & V	Maj.& Min	
RECTANGULAR PRISMATIC PARTICLE												
HORIZONTAL												
mean	1.48	1.34		2.31	1.87		1.62	1.33		0.991	0.716	
standard deviation	0.164	0.164		0.666	0.668		0.440	0.470		0.299	0.355	
VERTICAL												
mean	1.48	1.35		2.30	1.87		1.62	1.30		1.00	0.729	
standard deviation	0.161	0.161		0.667	0.662		0.447	0.460		0.299	0.355	
MINIMUM												
mean	1.41	1.27	1.52	1.93	1.39	1.78	1.36	0.997	1.30	0.801	0.565	0.725
standard deviation	0.149	0.131	0.065	0.507	0.201	0.291	0.366	0.246	0.336	0.288	0.318	0.383
MAXIMUM												
mean	1.55	1.43	1.67	2.68	2.35	2.84	1.88	1.64	1.99	1.19	0.881	1.29
standard deviation	0.146	0.151	0.080	0.592	0.617	0.568	0.355	0.411	0.350	0.140	0.317	0.124
ARITHMETIC AVERAGE												
mean	1.48	1.35	1.59	2.30	1.87	2.31	1.62	1.32	1.64	0.997	0.723	1.01
standard deviation	0.140	0.130	0.063	0.479	0.319	0.382	0.315	0.273	0.295	0.172	0.286	0.229
GEOMETRIC AVERAGE												
mean	1.48	1.34	1.59	2.25	1.79	2.23	1.59	1.26	1.60	0.959	0.687	0.936
standard deviation	0.140	0.130	0.063	0.480	0.264	0.362	0.323	0.261	0.303	0.209	0.298	0.291
OCTAHEDRAL PARTICLE												
HORIZONTAL												
mean	1.19	1.06		2.04	1.47		1.45	1.04		0.973	0.635	
standard deviation	0.141	0.125		0.949	0.536		0.605	0.394		0.331	0.354	
VERTICAL												
mean	1.20	1.06		2.03	1.47		1.42	1.04		0.972	0.640	
standard deviation	0.141	0.127		0.942	0.536		0.591	0.403		0.328	0.351	
MINIMUM												
mean	1.14	1.02	1.25	1.49	1.19	1.30	1.05	0.828	0.929	0.741	0.500	0.628
standard deviation	0.140	0.118	0.127	0.425	0.133	0.118	0.329	0.228	0.275	0.302	0.319	0.409
MAXIMUM												
mean	1.25	1.10	1.38	2.58	1.75	2.86	1.83	1.25	2.03	1.20	0.774	1.33
standard deviation	0.120	0.120	0.050	1.01	0.634	1.08	0.545	0.419	0.572	0.139	0.330	0.096
ARITHMETIC AVERAGE												
mean	1.19	1.06	1.31	2.04	1.47	2.08	1.44	1.04	1.48	0.973	0.637	0.980
standard deviation	0.121	0.113	0.079	0.600	0.337	0.526	0.364	0.287	0.355	0.157	0.301	0.216
GEOMETRIC AVERAGE												
mean	1.19	1.06	1.31	1.92	1.42	1.88	1.36	1.01	1.36	0.917	0.607	0.860
standard deviation	0.121	0.113	0.082	0.529	0.273	0.371	0.343	0.267	0.319	0.215	0.309	0.320

Table 3-3 Comparison of Image Length and Image Axis Parameters

Quite large errors were indicated by the above simulations, distribution means being of the order of a half sieve size too large for splinter shapes and about a sieve size too small for plates. (As noted in Section 3.3.1.1, a change of one sieve size represents doubling or halving the actual linear dimension.) The condition of all particle orientations having uniform probability of occurrence is, however, too general for the waste-rock dumps: movement of the dumped fragments down an existing slope face will cause some preferential orientation of extreme-shaped particles. For example, for natural scree slopes Statham (1972) found strong downslope orientation of long axis, and M^cSaveney (1972) reported preferential orientations of long axis downslope for elongated fragments; long axis downslope or across slope for bladed particles; and short axis into the slope for platy shapes. While such results are not transferable in detail to waste-rock dumps, supported by observation and visualisation of rolling and sliding, it is proposed that fragments on the dumps would lie with long axes tending parallel to the slope face.

SHAPE	1:1:1	3:1:1	2:1:0.5	1:1:0.1	1:1:1	3:1:1	2:1:0.5	1:1:0.1
ROTATION DIST'NS								
HORIZONTAL	uniform	uniform	bimodal	bimodal	uniform	uniform	bimodal	bimodal
mean, std.deviation			90,22.5	90,22.5			90,22.5	90,22.5
UPSLOPE	uniform	bimodal	bimodal	bimodal	uniform	bimodal	bimodal	bimodal
mean, std.deviation		0,22.5	0,22.5	0,22.5		0,22.5	0,22.5	0,22.5
OUT OF SLOPE	uniform	uniform	uniform	uniform	uniform	uniform	uniform	uniform
mean, std.deviation								
RECTANGULAR PRISMATIC PARTICLE					OCTAHEDRAL PARTICLE			
HORIZONTAL								
mean	1.34	2.08	1.61	1.08	1.06	1.70	1.44	1.03
standard deviation	0.164	0.759	0.437	0.142	0.125	0.702	0.406	0.171
VERTICAL								
mean	1.35	2.05	1.57	1.06	1.06	1.64	1.41	1.02
standard deviation	0.161	0.730	0.416	0.160	0.127	0.620	0.372	0.170
MINIMUM								
mean	1.27	1.43	1.20	1.02	1.02	1.24	1.19	0.973
standard deviation	0.131	0.206	0.133	0.156	0.118	0.121	0.149	0.182
MAXIMUM								
mean	1.43	2.71	1.98	1.11	1.10	2.09	1.67	1.08
standard deviation	0.151	0.499	0.215	0.132	0.120	0.710	0.409	0.137
ARITHMETIC AVERAGE								
mean	1.35	2.07	1.59	1.07	1.06	1.67	1.43	1.03
standard deviation	0.130	0.217	0.0900	0.134	0.113	0.356	0.244	0.149
GEOMETRIC AVERAGE								
mean	1.34	1.94	1.53	1.07	1.06	1.59	1.40	1.02
standard deviation	0.130	0.172	0.0808	0.136	0.113	0.265	0.220	0.152

Table 3-4 Summary Statistics for Preferentially Oriented Particles

Simulations were run for the previous eight shapes with these orientation constraints, and results are summarised in Table 3-4. As before, minimum axis and geometric average produced the closest and most

repeatable estimates of particle size. Over the range of shapes, the mean minimum axis was within a half sieve size of the theoretical value (that is, in the range 50% larger to 25% smaller). Geometric average gave about the same range except for one splinter-shaped particle which was overestimated by almost a sieve size. Standard deviations for both parameters were about 10-20% of theoretical sieve size.

A brief search was then made for relationships between the means of either minimum axis or geometric average and the calculated shape ratios, but no clear correlation was found. Although both linear and ratio parameters are dictated by particle geometry and orientation, these dependencies are apparently sufficiently complex and divergent to obscure any link between the resultant values. However, at this stage of the examination, it appeared likely that total errors for grading curves, which are essentially accumulated particle designations, would not be excessive.

3.3.1.3 Hiding Effect

As mentioned in Section 3.3.1.2, the effects of orientation on particle image are compounded by hiding, or the partial obscuring of the image by another particle closer to the camera, as illustrated in Figure 3-9. This aspect has received generally only cursory attention, with, for example, no mention made by Kellerhals & Bray (1971) and Iriondo (1972) and only a passing note made by Adams (1979). In a comparison of size designations resulting from image and mechanical methods for 550 pebbles, Ibbeken & Schleyer (1986) apparently assumed that orientation effects only occurred when size was overestimated by image analysis and that the hiding effect was only active when there was underestimation. It may well be that particle hiding has only a minor effect in the open unconsolidated stream beds on which most published work has been based. However, on structures such as the waste-rock dumps, whose steep batters derive part of their stability from the interlocking of particles, the effect of hiding, and particularly its interaction with the effects of particle orientation, might be significant.

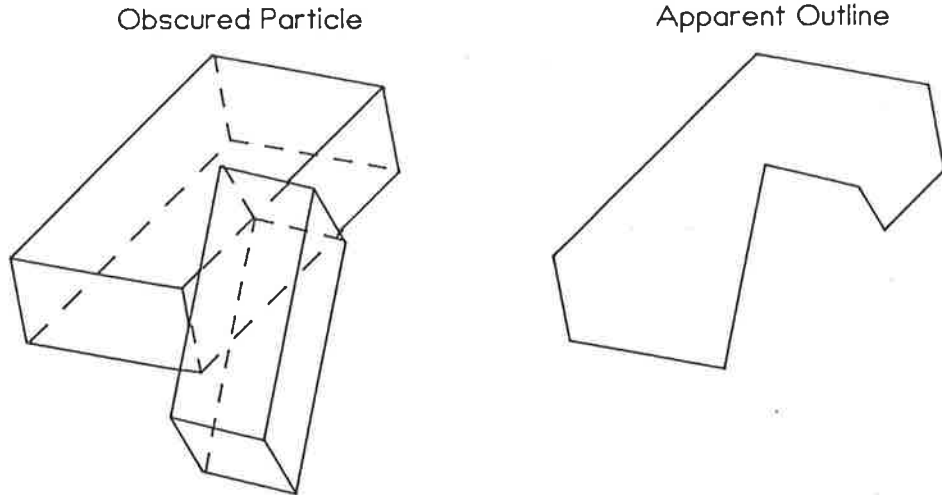


Figure 3-9 Effect of Hiding on Particle Image

The visible image is the total particle image, less that portion of the image which is hidden. The value of a linear measure of the image will be similarly reduced. This may be expressed in the form:

$$I_* = (1-h) \cdot A_*$$

where h, a hiding factor, is an independent randomly distributed variable; A_* is an axis parameter of the full particle image (in the present context, minimum axis or geometric average); and I_* is the corresponding measure in the partly obscured image. The shape of the probability function for h was not specified initially, while distributions for each A_* were those obtained from Monte Carlo simulations assuming preferential particle orientation (refer Table 3-4). These distributions were uni-modal and continuous, and in consequence it was assumed that I_* could be reasonably approximated by a Pearson distribution. This in turn permitted the use of the method of generation of system moments described by Hahn & Shapiro (1967), to obtain equations for the distribution of I_* , as follows:

$$\begin{aligned} I_* &= f(h, A_*) \\ I_* &= (1-h) \cdot A_* \\ \text{now } \frac{\partial f}{\partial h} &= -A_* \quad ; \quad \frac{\partial^2 f}{\partial h^2} = 0 \quad \text{and} \quad \frac{\partial f}{\partial A_*} = 1-h \quad ; \quad \frac{\partial^2 f}{\partial A_*^2} = 0 \end{aligned}$$

Noting that partial derivatives of second order and higher are zero, the method of generation of system moments (Hahn & Shapiro 1967) provides the following system moments:

$$\begin{aligned} \mu(I_*) &= (1-\mu(h)) \cdot \mu(A_*) \\ \partial^2(I_*) &= \left[\frac{\partial \bar{f}}{\partial h} \right]^2 \cdot \sigma^2(h) + \left[\frac{\partial \bar{f}}{\partial A_*} \right]^2 \cdot \sigma^2(A_*) \\ \partial^2(I_*) &= (-\mu(A_*))^2 \cdot \sigma^2(h) + (1-\mu(h))^2 \cdot \sigma^2(A_*) \end{aligned}$$

where $\mu()$ is the mean;
 $\sigma()$ is the standard deviation; and
 $\frac{\partial \bar{f}}{\partial}$ is the partial derivative evaluated at the mean.

Lacking real data, the distribution for h could only be guessed at. The range was known to be $0 < h < 1$. Two other constraints were that there should be a non-zero probability at $h = 0$ (since a particle image could be completely exposed), and effectively zero probability as h approaches 1 (a totally obscured particle would not be included in the image sample). Three distribution types were trialled, namely; uniform, which met the constraint at $h = 0$; normal, was more appropriate at $h = 1$; and exponential, which could meet both limit constraints. Normal and exponential distributions have theoretically infinite and semi-infinite ranges, which was overcome by selecting distribution parameters appropriate to 99% probability for $0 < h < 1$.

Means and standard deviations of the resultant I_* for various combinations of A_* and h distributions are listed in Table 3-5. For all particle shapes, minimum axis with uniformly or normally distributed hiding factor on average underestimated size by between one-half and one sieve size (that is, means ranged from about 0.5 to 0.75). With an exponentially distributed hiding factor the error in the mean was less than one-half sieve size. Geometric average axis showed similar trends but means estimated closer to 1 for uniform and normal hiding factor distributions, about half of the results being within one-half sieve size too small and the remainder within one sieve size. The exponential hiding factor distribution with geometric average axis produced mean estimates which were within one-half size either side of the ideal value.

This phase of the examination of possible designation parameters suggested a final preference for geometric average as generally the least biased size estimator. Although the distribution for hiding factor could not be specifically defined, it was apparent that its effect could be significant. Often, it could more than counteract the tendency to overestimate size due to the effect of relative particle/image orientation. If the trialled exponential distribution is a reasonable approximation for hiding factor, then it can be expected that photo-sieving will on average estimate particle size within 75% to 150% of intermediate axis, or in other words, within +/- one-half size division of theoretical sieve size.

HIDING FACTOR DISTRIBUTIONS (mean, std.deviation)	uniform (0.5,0.0833)	normal (0.5,0.194)	exponential (0.217,0.0472)	uniform (0.5,0.083)	normal (0.5,0.194)	exponential (0.217,0.0472)	
RECTANGULAR PRISMATIC PARTICLE (pref. oriented)	MINIMUM AXIS			GEOMETRIC AVERAGE AXIS			
	SHAPE 1:1:1 mean	0.635	0.635	0.994	0.670	0.670	1.049
	standard deviation	0.373	0.563	0.294	0.392	0.594	0.308
	SHAPE 3:1:1 mean	0.715	0.715	1.120	0.970	0.970	1.519
	standard deviation	0.425	0.638	0.351	0.567	0.859	0.443
	SHAPE 2:1:0.5 mean	0.600	0.600	0.940	0.765	0.765	1.198
	standard deviation	0.352	0.533	0.281	0.444	0.675	0.338
	SHAPE 1:1:0.1 mean	0.510	0.510	0.799	0.535	0.535	0.838
	standard deviation	0.305	0.456	0.253	0.316	0.476	0.256
	OCTAHEDRAL PARTICLE (pref. oriented)	MINIMUM AXIS			GEOMETRIC AVERAGE AXIS		
SHAPE 1:1:1 mean		0.510	0.510	0.799	0.530	0.530	0.830
standard deviation		0.300	0.453	0.240	0.311	0.470	0.247
SHAPE 3:1:1 mean		0.620	0.620	0.971	0.795	0.795	1.245
standard deviation		0.363	0.550	0.286	0.477	0.713	0.402
SHAPE 2:1:0.5 mean		0.595	0.595	0.932	0.700	0.700	1.096
standard deviation		0.352	0.529	0.284	0.418	0.626	0.349
SHAPE 1:1:0.1 mean		0.487	0.487	0.762	0.510	0.510	0.799
standard deviation		0.295	0.438	0.255	0.304	0.456	0.252

Table 3-5 Summary Statistics for Preferentially Oriented Particles with Possible Hiding Factor Distributions

3.3.1.4 Implication for Grading Curves

In preceding discussions, most emphasis was placed on the mean estimate of the size of one particle size, with secondary attention given to standard deviations of those estimates. This is justified by the fact that the object of photo-sieving, a particle size distribution, is a cumulative result of the designations of a very large number of particles.

For example, consider one size fraction, such as coarse gravel. This is represented as a segment of a grading curve, the midpoint of which approximates the average size of all particles comprising the fraction. If the same fraction were photo-sieved another, probably different, average size would be obtained. Because averaging is a simple additive function, the difference between these average sizes would equal the average difference between mechanical and photo sizes for each particle. In other words, the error in the average equals the average error, so that the mean biases from single particle simulations relate directly to biases in points on the grading curves.

From the Central Limit Theorem, the standard deviation for this estimated fraction mean is $1/\sqrt{n}$ times that for a single particle. As an illustration, take a grading curve which is log-linear, from 100% passing 1000mm to 10% passing 0.1mm. Based on the average size for each fraction - boulder, cobble, coarse gravel, etc. - and cube-shaped particles (and retaining the previous assumption that proportion of image area is equivalent to proportion of sample mass), a 3m x 3m area would contain a range from about 7 boulders to more than 8,000 medium gravel particles. From Table 3-5, a typical standard deviation for a single particle is about 0.5. Figure 3-10 shows the standard deviations for mean size estimates for this scenario: the range is from about 0.2 for the boulder fraction to less than 0.01 for medium gravel. For smaller fractions the standard deviation would be negligible.

The conclusion from these arguments is that, because of the large number of single estimates contributing to the grading curve, the average bias between actual and image-classed size is an important factor, but the total distribution of single particle designation results is not.

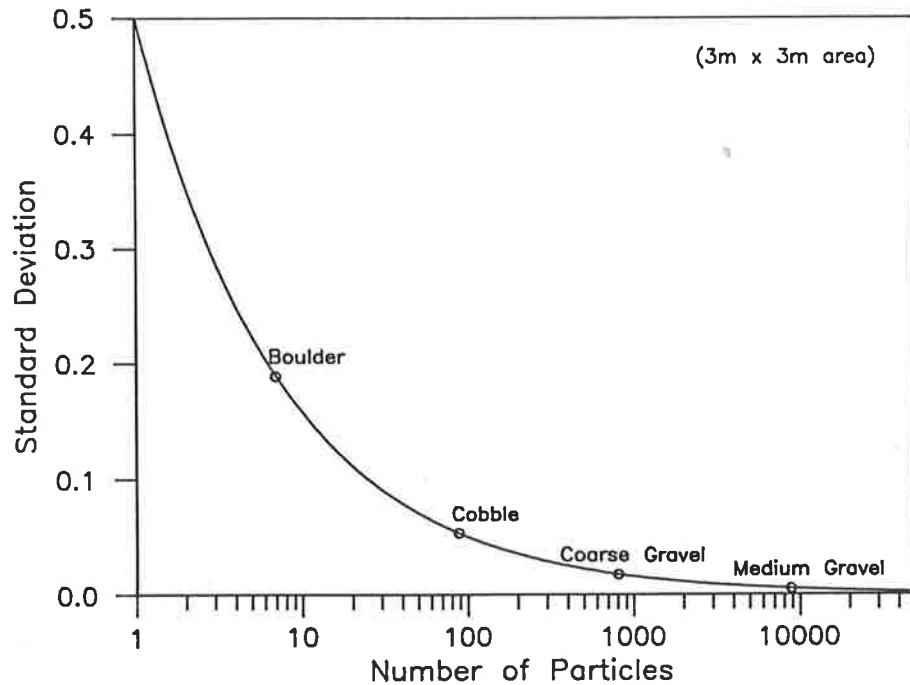


Figure 3-10 Effect of Number of Particles on Standard Deviation of Estimated Mean Size

Finally, to put this indicated error into context, the dashed lines in Figure 3-11 represent results one-half size smaller and larger than the simple grading curve assumed in the previous paragraphs. This suggested order of accuracy is within the variability often shown by replicate sampling and sieving of nominally homogeneous material. As such, it is sufficient to support the viability of a photo-sieving procedure for analysis of materials in the waste-rock dumps.

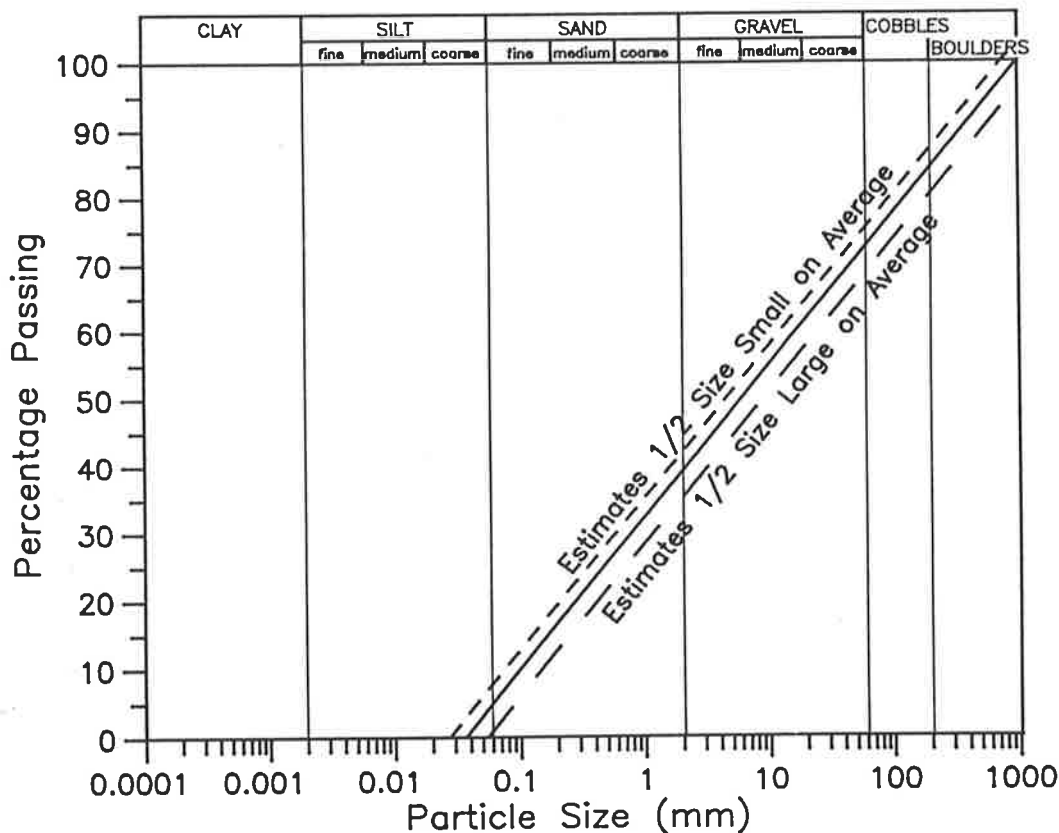


Figure 3-11 Example Particle Size Distribution

3.3.2 Procedures

3.3.2.1 Initial Programme Development

The number of photographs and the sample areas covered by some of the photographs, (typically $50-100\text{m}^2$ in a long shot), led to the use of computer-based techniques for the particle size measurement stage of the photo-sieving procedure. As discussed by Ord (1989), automated particle analysis is being researched for diverse applications, from sedimentology to quarry production. However, the unique combination of constraints to photo-sieving waste-rock batters necessitated development of a procedure specific to the purpose.

An image analysis unit was available for this work, comprising an Archimedes 305 personal computer, a Watford Electronics Archimedes Video Digitiser accepting input from an Hitachi VK-C2000E video camera, and a VGA monitor. Initially, memory included 128kbyte on the digitiser card for image storage, one 800kbyte floppy disk drive, and 1Mbyte RAM. This was upgraded during the project to 4Mbyte RAM, and a 40Mbyte hard disk

was added. The PC currently runs under the RISC operating system, which includes a "C" language library and compiler.

Initial development of techniques and programmes was based on photographs which were taken of samples collected for mechanical sieving, as described in Section 3.3.2.2. Compared to dump slope photographs, these had the advantages of uniform clarity (because of the controlled lighting), no tilt distortion, and grading curves obtained from mechanical sieving to compare photo-sieving results with.

In the context of computer-based analysis, three stages were identified, namely:

- a) entering particle outlines in a software-usable form;
- b) measuring geometric parameters from those outlines; and
- c) translating these computer-image parameters back to measures of the real particles, and subsequently producing particle size distributions for the examined sites.

The following discussions deal with the procedures developed for each of these stages. Flowcharts of relevant computer subroutines (shown *italicised*) are presented in Appendix A.

a) Entering particle outlines:

Obviously, photographs contain a lot of detail extraneous to the particle boundaries, which must be filtered out. A brief attempt was made to input directly from slide or photo through the video to computer and use published edge detection routines to highlight particle boundaries. However, this problem was beyond the capacity of these procedures. Unlike general picture enhancement, for which most such routines were written, photo-sieving requires detection of the outline of each object from a non-contrasting background of similar objects, where a specific change of colour or intensity may be neither a necessary nor a sufficient condition for a boundary.

A section of a photograph was traced manually, taking note of normally unconscious edge selection criteria, including: slight changes in colour which would be undetectable on the monitor image; recognition of shadow characteristics; and judgement of the likelihood, or plausibility of a resultant particle shape. It was quickly realised that the task of creating software which could

identify edges as competently as the operator was beyond the scope of the project. Consequently, manual outlining of particles was adopted into the developing photo-sieving procedure.

Upon this decision, two tracing options were available. A hard-copy outline image could be produced and input via the video digitiser, as had been intended for the complete photographs, or the outlines could be input directly as they were traced using a normal pad coordinate digitiser. The latter was not chosen, primarily because of limitations of the available equipment (such as the tracer being difficult to move accurately during continuous operation). Instead outlines were traced onto paper in pencil and later inked. This particle boundary image of a photograph was then transferred to the computer using the video digitiser system.

The film negatives of batter and bulk sample photographs were developed as slides. Some trial prints were made but it was difficult to consistently reproduce the clarity of the slides, because of the widely varying light conditions which had been experienced on the dump slopes. Hence it was preferred to work directly from the slides. Slides were projected onto a drafting table, set parallel to the projection plane. (An overhead projector was used, being more suitable for the anticipated extended operation than normal slide projectors.) By adjusting the separation between projector and table, images of reasonable clarity and convenient size were obtained. This equipment was used for all tracing of shots of collected bulk samples (which were used for validation of initial procedures) and also for a preliminary selection of dump slope photographs, as discussed in Section 3.3.2.3.

Images stored by the video digitiser were of 512 x 256 pixel resolution with potentially sixteen grey scales. Although the traced image was apparently two-colour (black and white), the effect of each pixel taking the average colour of the area it represents, coupled with slight variations in lighting intensity, resulted in a computer/monitor image containing several grey scales. As a first stage of programme development, it was thus necessary to devise a function to convert this input image into a simple two-value (on/off) pixel array.

Reasonable success was achieved using a simple line detection routine common to image enhancement work. Each pixel is set on or off, based on a comparison between the average grey scale value for the nine-pixel block centred on that pixel and a specifiable threshold value. Because of computer memory limits, each row of new values was written back into the digitiser memory before proceeding to the next row. As a result of light intensity variations, and imperfect pen-work, not all outlines were fully captured at the same threshold: this was overcome by optionally returning to select a new threshold. Each time, a fresh image was captured from the video, to be overwritten in memory by this *line_detect* function.

b) Measuring geometric parameters:

Once a pixel array containing an outline image of the photograph has been created, it is then necessary to extract a separate boundary trace for each particle, from which axes and area can be calculated. Manual activation of the resultant boundary routine was preferred to an automatic particle search, because this was easier to integrate with the threshold repeat option. The developed function accepts an initiating pixel coordinate pair from the mouse, searches left until an outline pixel, (that is, an 'on' pixel), is encountered, then moves clockwise around the outline until it closes back on itself. Variations of the same algorithm are used for total areas and individual particles. (The separate handling of these items is discussed in later parts of this Section.) Conditions in *boundary* were included to terminate the function if the trace goes astray - for example, if the particle outline are not closed - and to prevent the pixel storage array being overrun. It should be noted that the stored image is queried but not altered by the routine: the resulting trace appears on the monitor as 'white' pixels only to assist the operator by showing particles already analysed.

This *outline/boundary* function is capable of tracing quite complex and irregular shapes. An occasional problem was noted in that if the first pixel traced is in a one-pixel-thick section, the function will terminate when that pixel is retraced, regardless of whether the boundary is complete. This condition occurred only rarely, and could generally be avoided by selecting the initiating mouse

position appropriately, so it was considered unwarranted to complicate the function by trying to circumvent the fault completely.

For particles, *boundary* stores coordinate pairs of the pixel outline in an array. This is accessed by two more functions which calculate horizontal and vertical axes (defined in Section 3.3.1.2) and area, as detailed in the flowchart *calculate_particle_parameters* in Appendix A. Essentially, for the horizontal axis, a set of conditions is checked pixel by pixel around the outline until a leading (left) pixel is identified, then another set of conditions is checked to find the corresponding closing (right) pixel. The length between these pixels is then compared to the maximum length previously found for the particle, replacing it if larger, and it is also added to the area. Another leading pixel is then sought, and so on around the outline. Vertical axis is found by a similar procedure, with upper leading pixels and lower closing pixels. The functions were developed by trial and tested against a number of irregularly-shaped outlines. Although this did not provide verification beyond doubt, it warranted confidence that axes will be correctly measured for at least most particles.

The *outline* version of the tracing function, which was used in the measurement of total sample area, counts the number of pixels in the outline but does not store pixel coordinates. In general, *outline* is initiated from left of the area to trace around the outside of the stored sample image, again showing a white trace on the monitor. All other screen pixels are then turned off. Another adaptation of the outlining function - *infill* - then counts the screen pixels inside this outline. Querying the screen image rather than the stored image, this routine traces a green (value 15) outline inside the white (value 14) boundary. When the trace is closed, the plot colour is returned to white and the boundary colour to green, and another outline is drawn. By alternating plot and boundary colours in this way, successive outlines are traced inside each other until the shape is filled, a running count of pixels giving the area. With irregular shapes it is possible to enclose pockets of 'off' pixels (value 0), so an option was included to fill these in and add them to the total area.

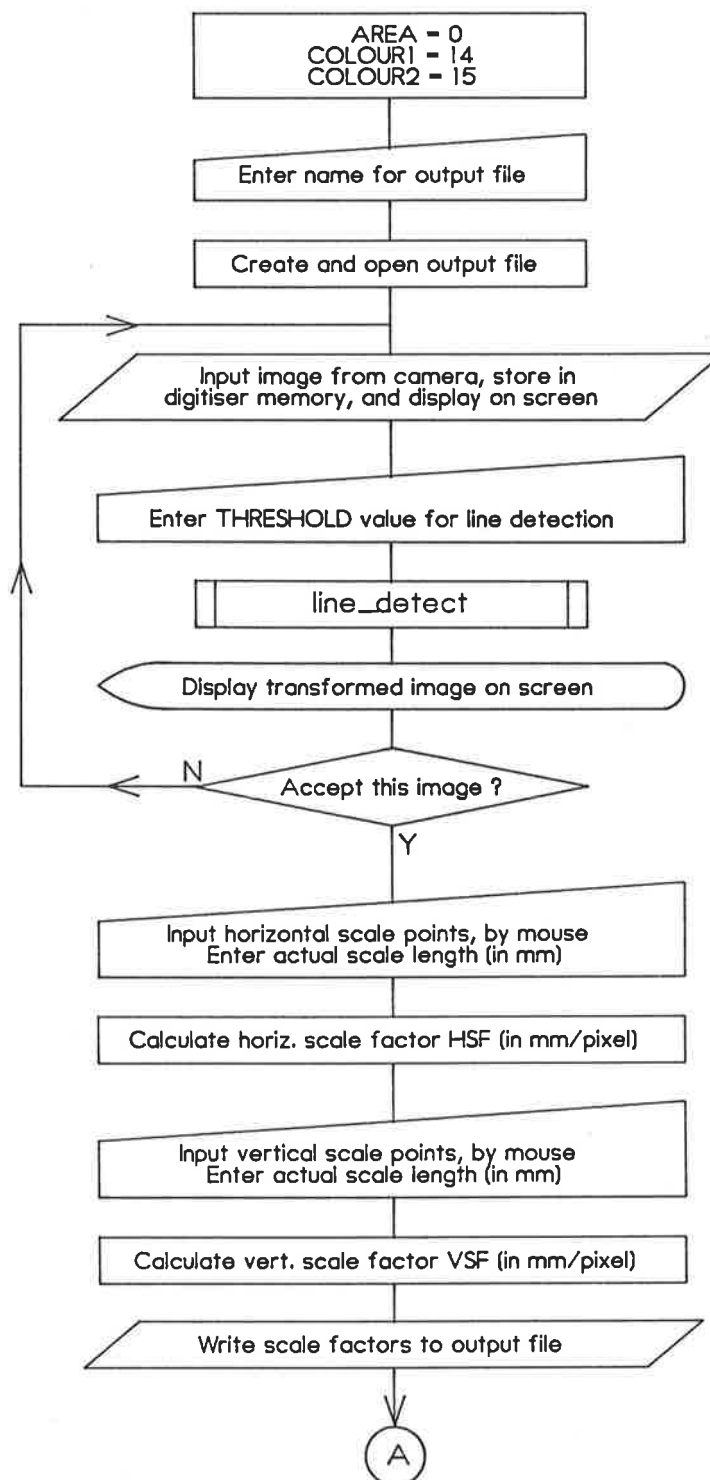
c) Translating parameters into real units, and into grading curves:

Because the photographs used during initial programme development were not tilted, conversion from pixels to millimetres was relatively simple. A scale was included in the photographs and transferred to the hand-traced outline. It is input to the programme by activating the mouse at the scale marks shown on the screen. With the system used, the digitiser and monitor operated with different coordinate sets. The screen image was compressed slightly in the horizontal direction to simplify consequent point transformation relationships, which in turn necessitated different scale factors for horizontal and vertical directions. This scaling procedure was, however, much simpler than that required for tilt-distorted photographs of the waste-rock dump slopes, as discussed in Section 3.3.2.3.

To express the results as a particle size distribution, total sample area is assigned initially to the range of arrays representing sieve sizes. For each particle the geometric average of the horizontal and vertical axes is then calculated and the particle area decremented for the sizes smaller than that value, that is, the sieve sizes through which the particle would not have passed. When all particles have been processed, the percentage passing for each size is the area remaining calculated as a percentage of the total sample area.

Initial computer memory limits (1Mbyte RAM) restricted the size of programme which could be compiled, so for this preliminary stage the procedure was separated into three programmes: the first to measure total sample area; the second to measure parameters for individual particles; and the third to calculate grading curve for the sample, as described in the previous paragraph. Flowcharts showing structures for the first two programmes are presented in Figures 3-12 and 3-13. With this system, a photograph of a laboratory sample was analysed - from entering the traced outline to producing the grading curve - in about a couple of hours.

Figure 3-12 Flowchart of Programme to Calculate Total Sample Area



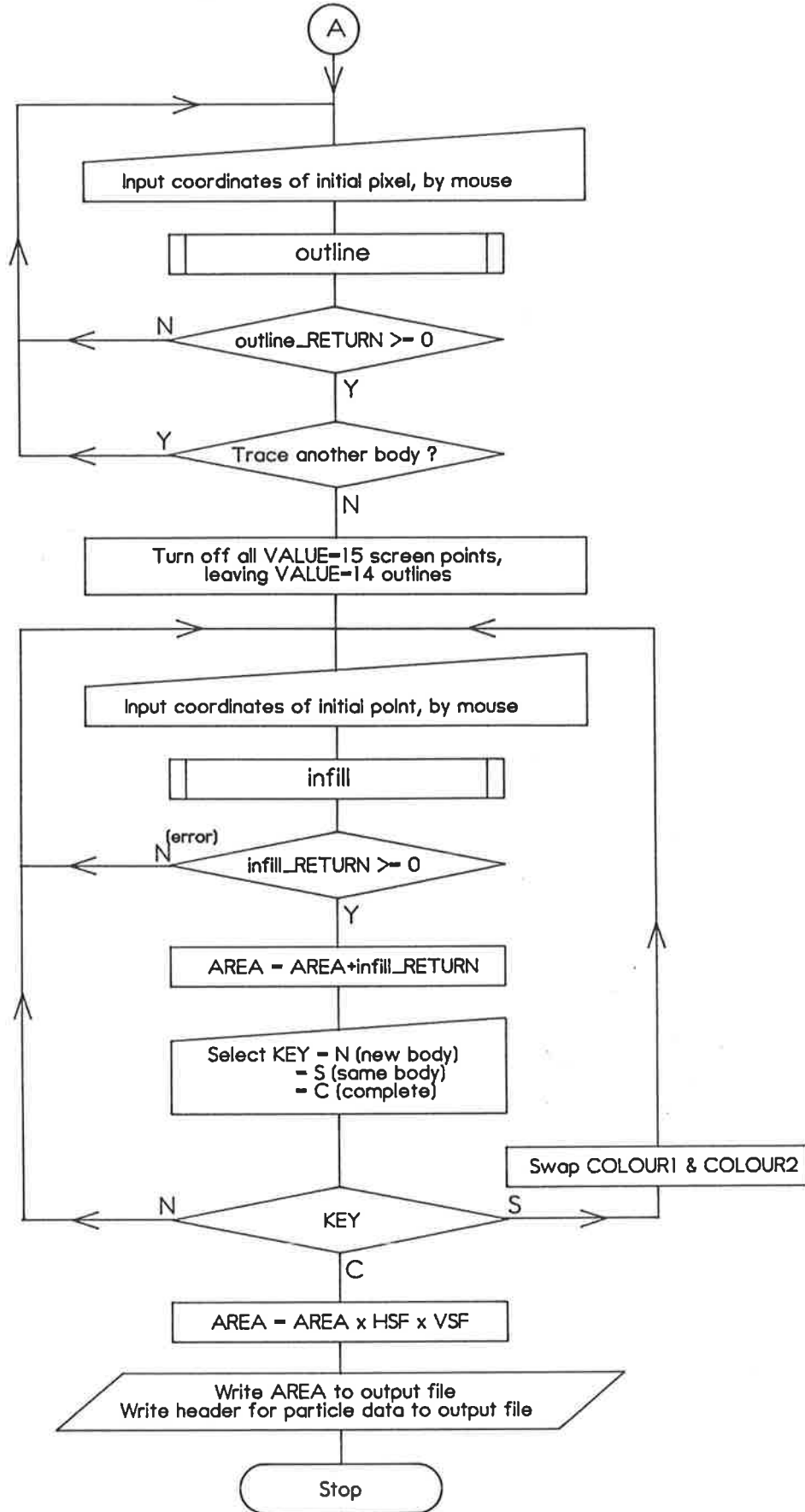
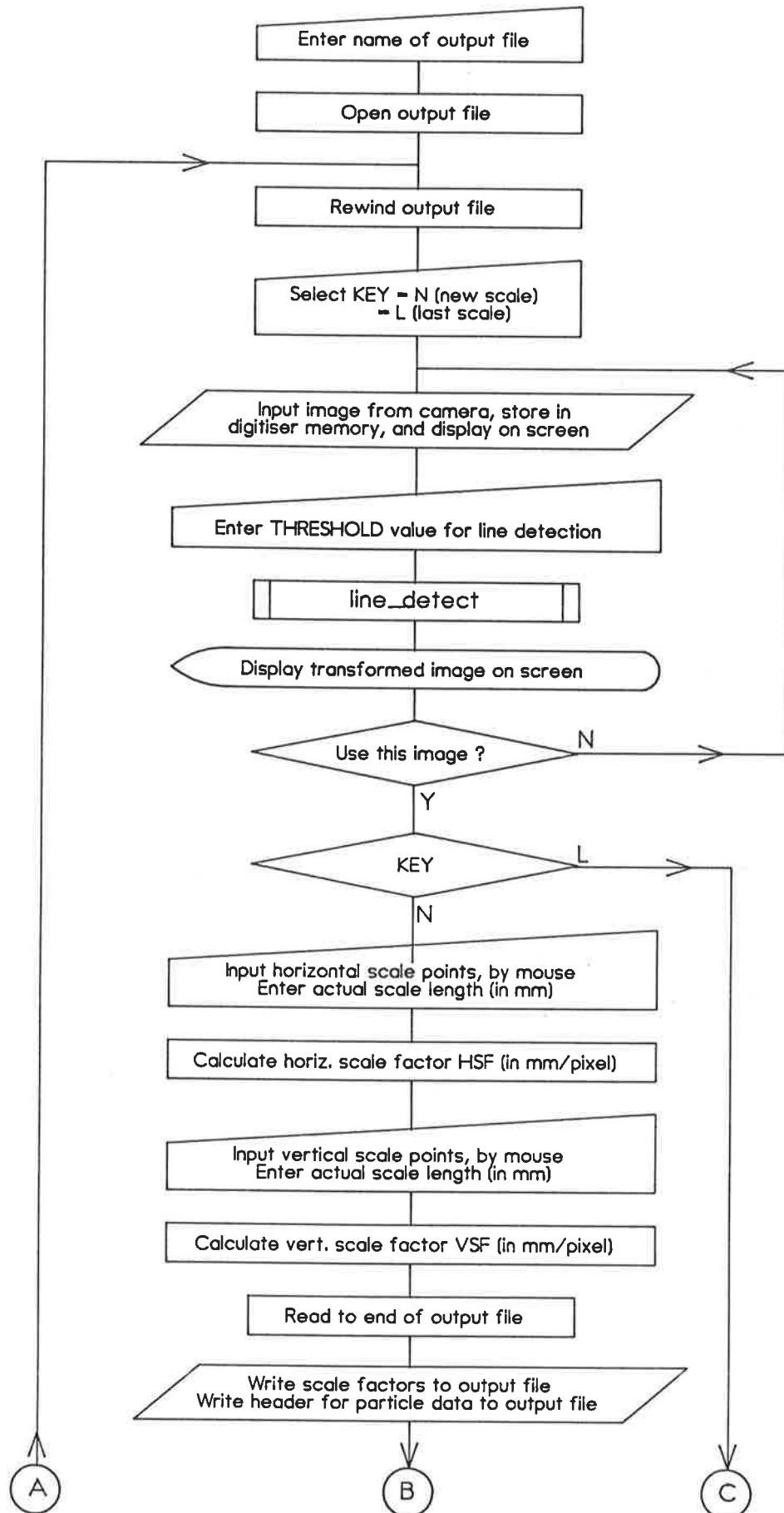


Figure 3-12 (continued)

Figure 3-13 Flowchart of Programme to Analyse Particles in Sample



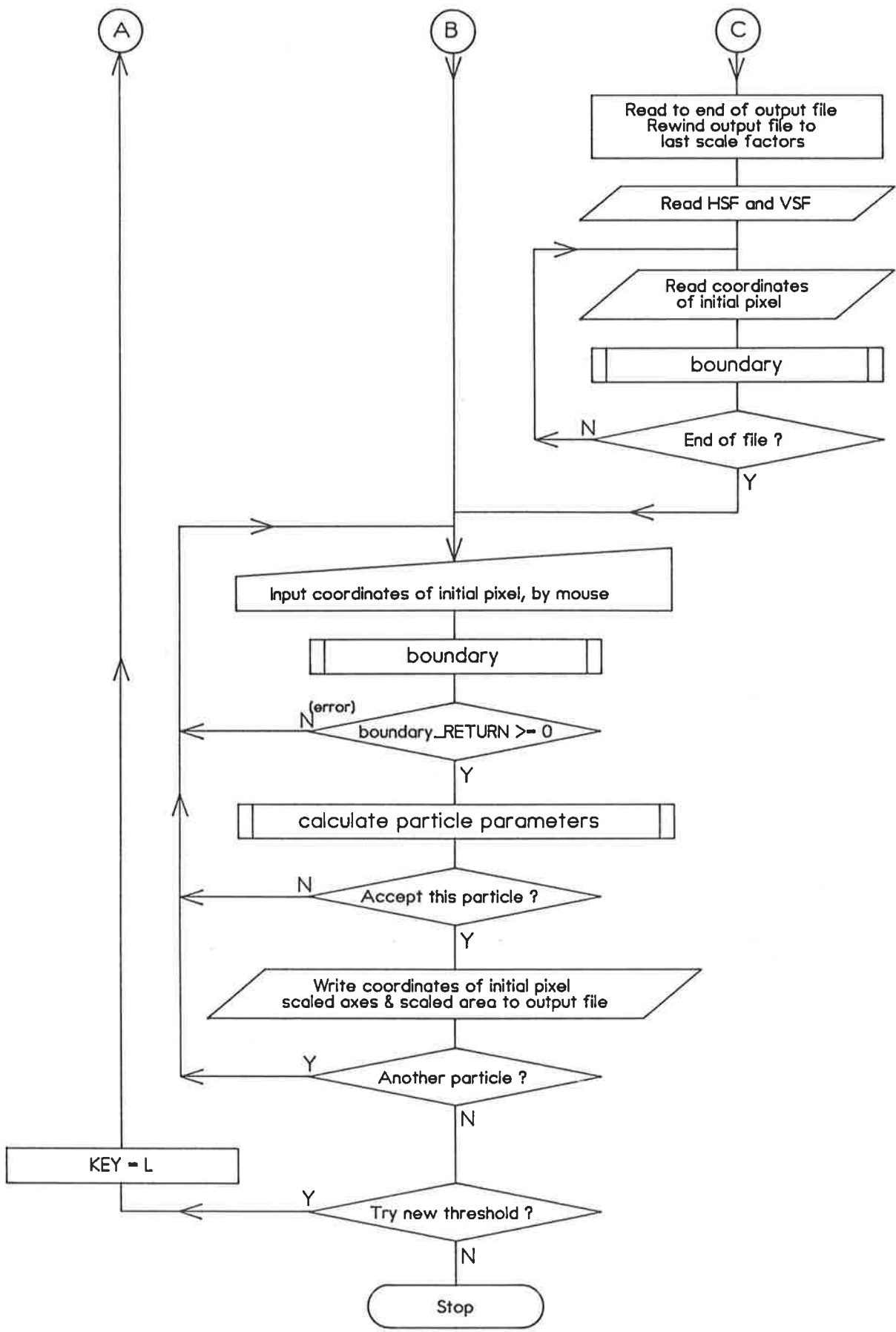


Figure 3-13 (continued)

3.3.2.2 Validation

To check the performance of procedures developed to this stage, photographs were taken of ten of the bulk samples which had been collected during the slope photography programme and graded by mechanical sieving, as described in Section 3.2. For each sample the material was emptied onto a shallow tray and photographed from about 1.5m overhead using a 50mm lens camera (refer Plates 3-3 and 3-4). Two photographs were taken of the sample, one with the material heaped up as emptied from the bag and the other with it spread out into a layer of about constant thickness. These replicate photographs were taken in an attempt to mark the previously discussed hiding effect, which was expected to be more pronounced in the shot with the sample heaped.

Results of photo-sieving for the ten samples are compared with the gradings obtained by mechanical sieving in Figure 3-14. In general, there was fair to excellent agreement with mechanical sieving over a limited size range, within which the average absolute difference at a sieve size was 5%, with a maximum difference of 12%.

The resolvable size range covered about one order of magnitude (9-60mm), and the lower limit showed clearly as a rapid flattening of the image grading curve. This observable limit of reliability was potentially a useful feature in the broader application of the procedure. The actual limiting particle size was apparently governed by the camera/sample configuration during photographing and the resultant clarity for tracing, rather than digitiser or screen resolution, since zooming the video camera into the outlined image did not significantly reduce the lower size limit.



Plate 3-3 Set-up for Photographing Bulk Samples



Plate 3-4 Shot mg4-07 of Sample MG16 (in Heap)

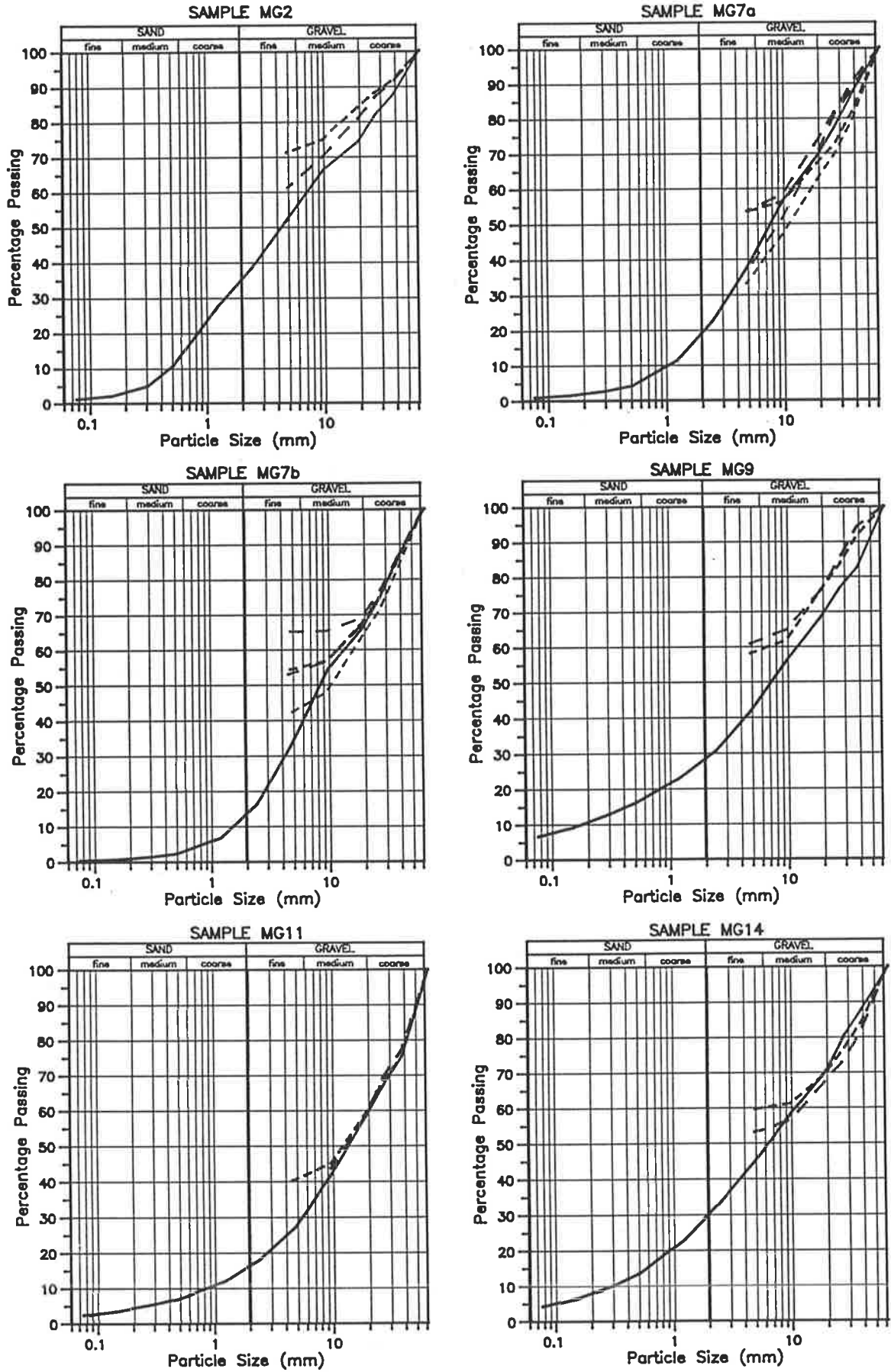
The upper size limit was fixed at 100% passing 63mm in these analyses. The few larger fragments were included in the photographed samples but were specifically excluded from the photo-sieving, as they had been from mechanical sieving. In some initial trials the oversize particles were included, and it was found that these particles were relatively so large within the sample, that a small error in determining sieve size (for example, 60mm instead of 63mm) could have a marked effect on the overall grading. It thus appeared that the reliable upper limit depended on the sample itself, rather than the photograph. Ideally, the number of particles at any size level should be such that no single particle has a significant effect. The minimum sample masses for different nominal sizes recommended in AS 1289.A1-1977 are actually intended to avoid the same problem in mechanical sieving.

As noted in Section 3.2, most samples complied with these mass recommendations for only the passing 19mm or 9.5mm fractions and smaller, so where there was significant disagreement (samples 2, 9, 15, and 16), the error could as well have been in the mechanical sieving as in the photo analysis. In fact, if curves are factored to agree at 37.5mm (instead of 63mm), the average absolute difference at a size level is reduced to 3% and the maximum difference to 8%.

There was generally little difference between results from photographs of the same sample, heaped up or spread out into a roughly even layer. While this was only a partial illustration of the hiding effect discussed in Section 3.3.1.3, it at least suggested that the influence might not be overriding.

The indication from this preliminary work on photo-analysis was thus the same as from the theoretical approach, namely that photo-sieving could produce grading curves reasonably approximating those which would be obtained by mechanical sieving if it could be carried out.

Figure 3-14 Comparison of Photo-Sieving and Mechanical Sieving for Laboratory Samples



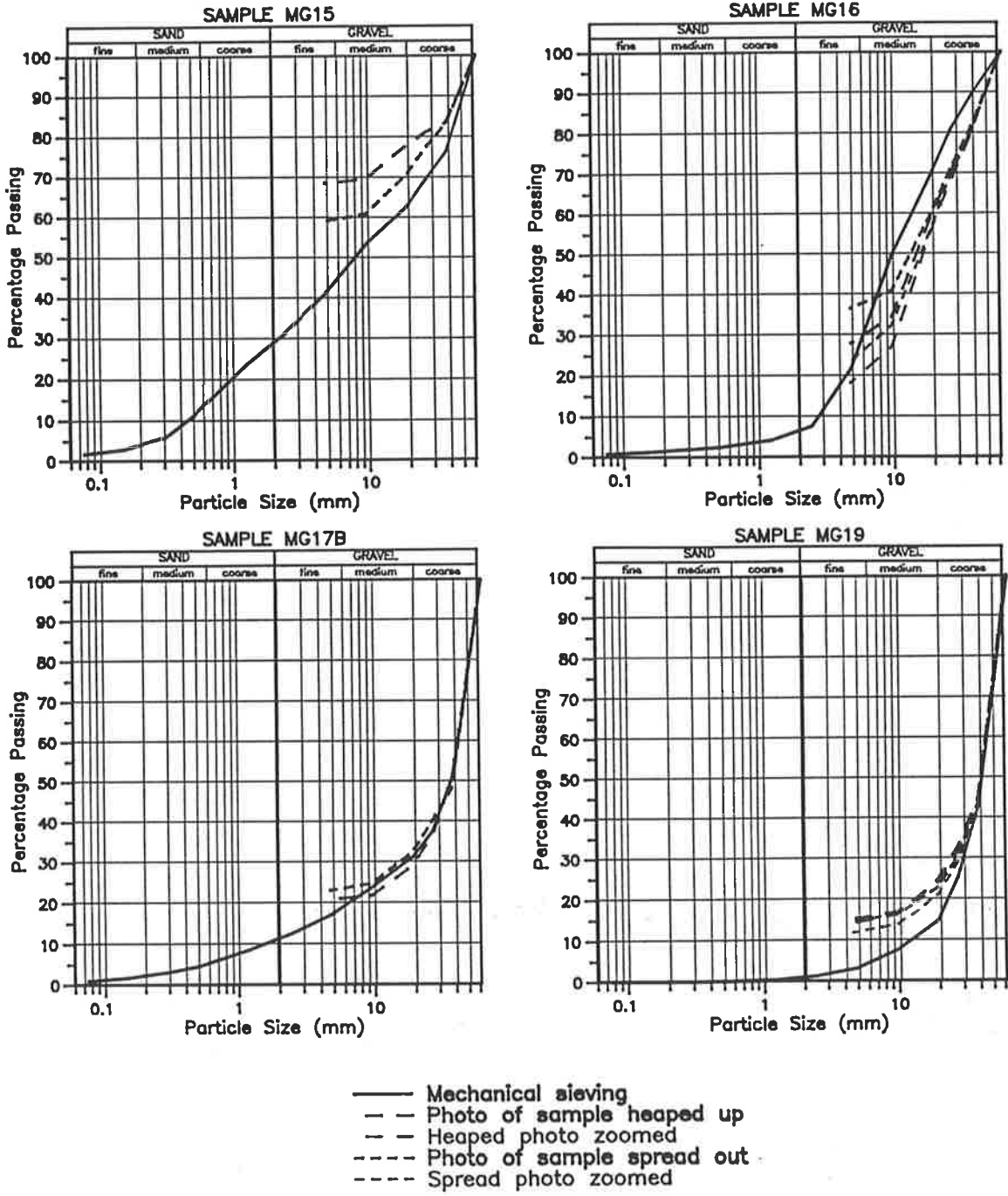


Figure 3-14 (continued)

3.3.2.3 Programmes for Slope Photos

The main task in adapting the procedures to photographs of the dump slopes was taking account of the image distortion due to distance perspective and relative tilt between the slope and film planes. Two approaches were considered for rectification: direct (analogue) correction, during boundary tracing; and indirect (algebraic) correction, after inputting the image to computer.

Using the overhead projector and drafting table set-up described in Section 3.3.2.1, and turning the table about two available axes, tilt distortion of the projected image - identified by differences in lengths of the scale mark images - was reduced. However, this was achieved at the expense of clarity, often amounting to some uneven loss of focus before full rectification was achieved, so that some algebraic correction was also required. As discussed in Section 3.3.3, loss of resolution appeared to induce more error than was retrieved by this form of rectification, so it was discontinued after an interim assessment of the procedure. In the method finally adopted, slides were traced unrectified using a stereo microscope, and algebraic correction was relied on to allow for tilt distortion.

As presented by Olsen & Altenhofen (1980), full mathematical description of the transformation between non-parallel planar coordinate sets requires the coordinates of four points in both planes, and solution of an [8x8] matrix. This would have involved the establishment of at least four surveyed points at every sampling site on the waste-rock dumps; a difficult exercise to coordinate and perform, and one implying an excessive level of accuracy in the context of the overall photo-sieving process. Instead a simpler approximation was considered.

To this end, a series of photographs of brickwork were taken at varying degrees of tilt in one direction, using the same camera and attachments as in the field work. As illustrated in Plate 3-5, the brick pattern showed up image distortion well. For example, it was apparent that the image distorts differently laterally (perpendicular to the line of tilt), and longitudinally (along the line of tilt). This is because the distortions in both directions are primarily related to position along the direction of tilt. That is, if X and Y are incremental measures

along lateral (x) and longitudinal (y) directions respectively, the distortion effects on both X and Y vary as functions of y.



Plate 3-5 Tilted Photograph of Brickwork for Distortion Analysis

Considering lateral distortion first, it was hypothesized that the tilt effect could be approximated by a linear relationship - $X/X_{(at\ y=0)} = a.Y + b$, where a and b are constants. This was an untested assumption implicit in the method for particle size analysis from tilted photographs described in Iriondo (1972). It was readily checked on the brickwork photographs by placing a straight edge against the ends of a line of mortar in the photograph and measuring the maximum deviation of the mortar line from the edge. Expressed as a percentage of the edge length along the photo, the deviation from linear was in most cases less than 2% and at worst less than 3%. This level of error was acceptable within the context of the photo-sieving exercise.

A linear hypothesis for the longitudinal direction - $Y/Y_{(at\ y=0)} = p.Y + q$ (p and q constant) - was examined by measuring brick length (l) and corresponding distance from the brick mid-point to the close-up end of the image (d), for rows of bricks along each photograph. The procedure

used for subsequent analysis is illustrated in Figure 3-15: to facilitate comparison between different shots, a curve was first drawn through the data to estimate the closer-end-intercept (l_0 , when $d=0$). Pairs of measurements were then non-dimensionalised against total image length (L) and l_0 respectively, and a linear regression was calculated passing through $(l/l_0=1, d/L=0)$. No correlation between results from different photographs was apparent at this level, so taking a simple approach, the error from each data point to its associated regression line was calculated. In the thirteen photographs checked, the maximum error for any point was less than 4% and in general the error was less than 2%. Exponential regressions were also examined but these produced greater errors. On these bases, a linear approximation for distortion correction was again accepted.

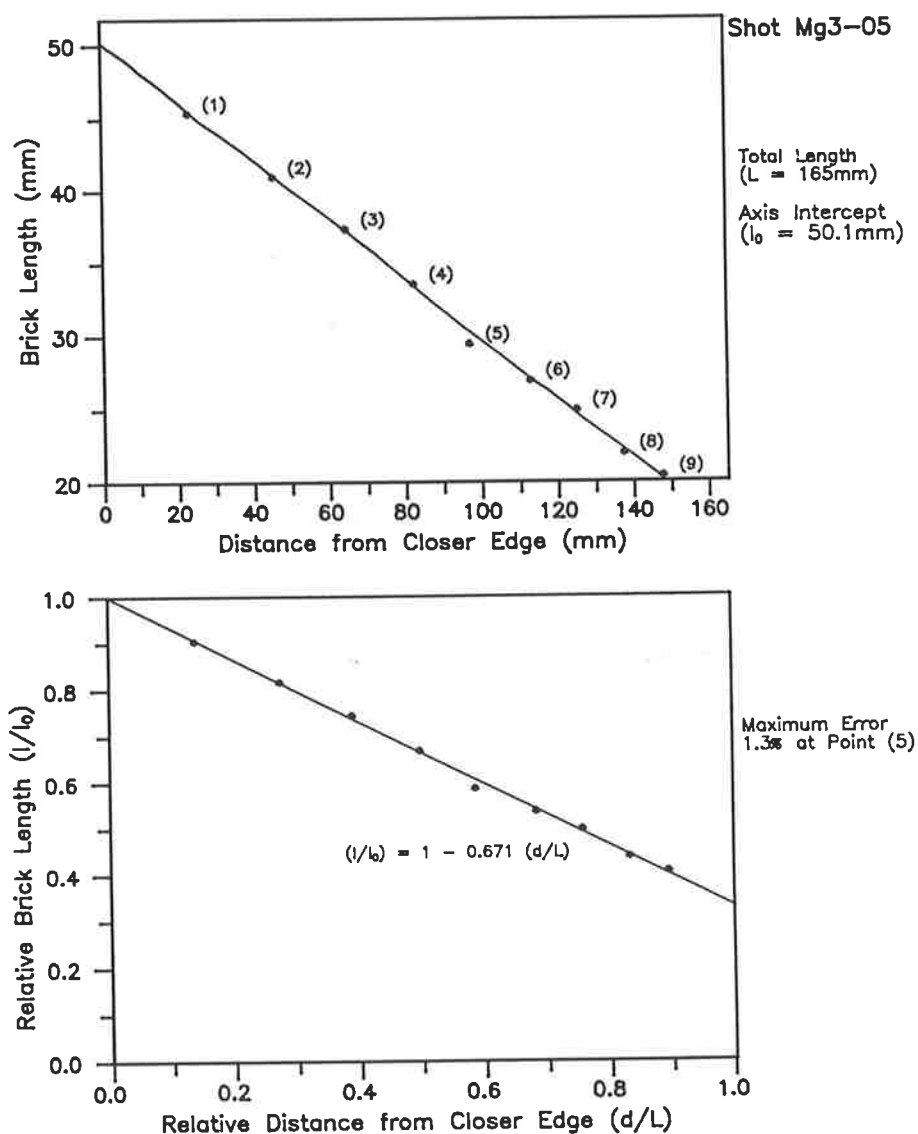


Figure 3-15 Procedure to Assess Linearity of Longitudinal Tilt Distortion

With only two constants, the equation in one direction could be defined from only two absolutely located points, or from two sets of relatively located points. The latter option was more easily provided, using scale markers painted to show points 500mm and 1000mm apart and placed on the slope as described in Section 3.1.1. Subsequent manipulation of the equations to form a basis for scaling routines is detailed in Figure 3-16. There was some concern regarding the potential for large errors if the resultant logarithmic equation for upslope rectification was extrapolated too far beyond the controlling scale stick locations. To avoid this, application of the equation was limited to the section of image centred over the scale sticks and covering a distance upslope equal to twice the separation of the scale sticks. Parts of the image falling outside this (in practice, only the top of a few photographs), were treated as not able to be reliably scaled and therefore excluded from analysis.

The scaling routines, and other adaptations from the preliminary procedures, are discussed in the remainder of this section.

a) Entering particle outlines:

In the extended computer programme, horizontal rectification is performed at an early stage. After entering the traced image and entering scale data, equations from Figure 3-16 are used to determine the vertices of the unrectified trapezoid which represents the maximum constant width strip of slope which is contained in the photograph and within the vertical scale extrapolation limit suggested above. An internal digitiser function 'stretches' this shape laterally to show on the monitor as a rectangular image, which is then written to a storage buffer (made possible by upgrading the computer memory). This is then the base image until the programme is terminated.

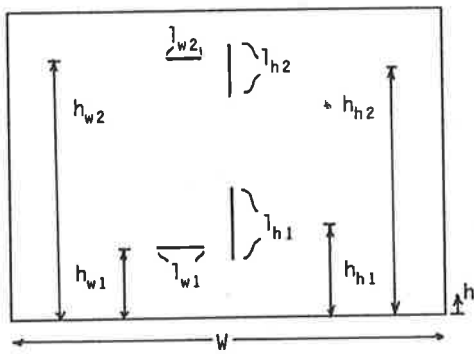
As well as the convenience of utilising an existing function, this method of handling horizontal correction eliminated a potential source of error: in a typical photograph, more of the top of the slope is included than of the lower part which is closer to the camera. Given the suspicion of particle sorting discussed in Section 2.2, photo-sieving of the total photograph could give a result favouring the upper part of the slope rather than being an average

for the whole batter. Analysis of a constant actual width rather than a constant photograph width avoided this problem.

There was, however, one disadvantage. Stretching the image tended to widen outlines as well as particles, an effect which largely persisted even after the on/off pixel image was produced by the *line_detect* function. Since the measurement routines operate inside the outlines, which are assumed to be one pixel wide, it was feared that thickening of these beyond two or three pixels might produce significant underestimation of horizontal axis and area. (Thickening also occurred in the preliminary work during zooming, but lines were thickened vertically as well as horizontally so the effect could be countered by altering the threshold value.)

In an attempt to correct this, a different edge detection function was included. Adjacent rows, and then columns, of the nine-pixel block were compared, looking for a change in intensity (grey-scale) not less than a specified threshold. The result was generally thinner outlines but these were more ragged and there was a tendency to "noise", or isolated pixels turned 'on'. Another function was attached to erase these pixels but the outlines were still not as sharp as with *line_detect*, which had been modified to give double weighting to the central pixel.

A separate line thinning function was found more effective. The function works on the two-value pixel image produced by *line_detect* to turn off isolated 'on' pixels and pixels at leading ends of rows or columns of 'on' pixels. An important feature is that the amended pixel value is immediately effective and is used in the next, adjacent, pixel block. This is in contrast to *line_detect*, where pixel values are not updated in the working buffer. One activation of *line_thin* essentially trims one excess pixel, horizontally or vertically, off outlines: A loop in the main programme allows successive trimming in both directions until a satisfactory outline image is obtained.

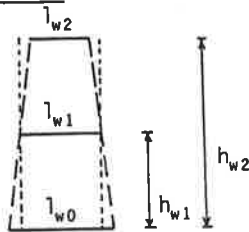


let l_{w0} and l_{h0} be the image lengths of hypothetical horizontal and vertical scale marks, respectively, at $h=0$,

and let l_w and l_h be the image lengths of hypothetical horizontal and vertical scale marks, respectively, at h .

LATERAL CORRECTION

Consider



From similar triangles,
 $l_{w0} = l_{w1} + 2 h_{w1} (l_{w1}/2 - l_{w2}/2)$

$$l_{w0} = l_{w1} + h_{w1} \frac{(l_{w1} - l_{w2})}{(h_{w2} - h_{w1})} \dots\dots(1)$$

Similarly, note that
 $l_{h0} = l_h + h(l_{w1} - l_{w2})$

Now consider



W_h is the corrected image width at h
 $\frac{W_h}{l_{w0}} = \frac{l_w}{l_{w0}}$

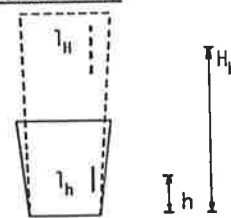
substituting for l_w

$$W_h = W \frac{l_w}{l_{w0}} = W \frac{l_w - h(l_{w1} - l_{w2})}{(h_{w2} - h_{w1})} \dots\dots(2)$$

(1) AND (2) ARE CORRECTION EQUATIONS FOR LATERAL DISTORTION DUE TO LONGITUDINAL TILT.

LONGITUDINAL CORRECTION

Consider



H_h is the corrected image height for h , and l_h is the corrected scale mark length at h .

Assuming a linear relationship,

$$l_h = m \cdot h + c \text{ where } m \text{ and } c \text{ are constants}$$

at $h = 0$, $l_h = l_{h0} \Rightarrow c = l_{h0}$
 $\Rightarrow l_h = m \cdot h + l_{h0}$

substituting l_{h1} & h_{h1} $l_{h1} = m \cdot h_{h1} + l_{h0}$
 substituting l_{h2} & h_{h2} $l_{h2} = m \cdot h_{h2} + l_{h0}$
 subtracting $l_{h1} - l_{h2} = m(h_{h1} - h_{h2})$

$$m = \frac{(l_{h1} - l_{h2})}{(h_{h1} - h_{h2})} \dots\dots(3)$$

Substituting back
 $l_{h1} = \frac{(l_{h1} - l_{h2})}{(h_{h1} - h_{h2})} h_{h1} + l_{h0}$

$$l_{h0} = \frac{(l_{h2} h_{h1} - l_{h1} h_{h2})}{(h_{h1} - h_{h2})} \dots\dots(4)$$

A correction equation is required to make scale mark length constant, that is, $l_H = l_{w0}$

let $l_H = f(h) l_h = l_{w0}$
 then $f(h) (m \cdot h + l_{h0}) = l_{w0}$
 $f(h) = \frac{l_{w0}}{(m \cdot h + l_{h0})}$

so $l_H = \frac{(m \cdot h + l_{h0})}{l_{w0}} l_h$
 $l_H = \frac{(m \cdot h + l_{h0})}{(m \cdot h + l_{h0})} l_h$

Now, observing that l_h is a discrete increment of h , and that l_H is a discrete increment H_h ,

let $l_h = \Delta h$ and $l_H = \Delta H_h$
 then $\Delta H_h = \frac{\Delta h}{l_{w0}} \Delta h$

$$\Delta H_h = \frac{(m \cdot h + l_{h0})}{l_{w0}} \Delta h$$

taking the limit, $\frac{dH_h}{dh} = \frac{l_{w0}}{(m \cdot h + l_{h0})}$

$$H_h = \int_0^h \frac{l_{w0}}{(m \cdot h + l_{h0})} dh$$

$$H_h = \frac{l_{w0}}{m} \ln(m \cdot h + 1) \dots\dots(5)$$

(3), (4) AND (5) ARE CORRECTION EQUATIONS FOR LONGITUDINAL DISTORTION DUE TO LONGITUDINAL TILT.

SCALING OF CORRECTED IMAGE

multiply all linear measurements by

(actual length of scale marks)

$$l_{w0}$$

Figure 3-16 Derivation of Tilt Correction Equations

b) Measuring geometric parameters:

For tracing particles, *boundary* was used, with the minor modification of an increase in the storage array from 500 to 600 pixels. This was done, again taking advantage of extra memory, to increase the range of particle sizes which can be analysed at one magnification (zoom), which was particularly useful where the batter included a few large particles embedded amongst smaller ones.

In the preliminary programmes total area was calculated in a separate operation because this suited the three-programme structure (enforced by initial memory constraints), and because it was a simple matter to adapt the basic *boundary* algorithm. In the case of slope photos (particularly long distance shots), resolution is much poorer when working with the total shot, so separate calculation of total sample area was not desirable. (In fact, the complete image is usually only entered initially, to record scale and rectification data.) Therefore, in the slope analysis programme, total area is calculated by summing the areas of individual particles and the areas of fine material where the particles are too small to be separately traced. These latter 'lumped' areas necessitated the development of a new function, *lump*.

In essence the function fills an outline with columns of counted pixels, proceeding up and down from left to right. The routine is simple, and terminates prematurely under not infrequent conditions (such as when a filling column runs down along the left side of a vertical section of outline), and unfilled pockets are sometimes left in complex shapes. This was countered by including in the main programme the option to reactivate *lump* in the same area, adding to the previous pixel count. In fact equivalent rather than actual pixels are counted: the vertical tilt equation calculates 'rectified' coordinates for the ends of filled columns, and the difference is the number of pixels in the column if the image had not been distorted. This conversion within *lump* was necessary to avoid summing dissimilar entities, in the form of non-equal pixels.

While the repeat option device is a little clumsy, 'lumped' areas comprise only a small part of most analyses, so the development of a more comprehensive and complex function was considered unnecessary.

Note also that, although used predominantly to measure areas of fine material, *lump* is generally applicable to any shape within the image for which area is the only parameter required. In particular, it has been used to extract shadows and other unclear sections of photograph where separate particles could not be identified.

The functions to calculate particle axes and area were modified versions of those initially developed: they are now physically separated from the main programme; instead of measuring X0 (the x-coordinate of the horizontal axis), Y0 (the y-coordinate of the mid-point of the vertical axis) is determined; and, as in *lump*, area is calculated as the sum of columns of equivalent rectified pixels.

c) Translating parameters into real units and grading curves:

Analysis of tilted photographs requires, at the outset, sufficient data to specify the equations of Figure 3-16, which deal with the removal of tilt distortion and conversion of the resultant rectified pixel counts into real lengths. At the first run of the programme for a particular photograph, image lengths and locations of the two horizontal and two vertical scale markers are entered by mouse, as pixels; or by keyboard, as millimetres on the hard copy traced image; along with the actual length of the scale markers (usually 1000mm). Also, the width and height of the hard copy image are input as both pixels and millimetres. These pairs of corresponding values are required firstly to convert keyboard-entered scale data (if used) to pixels, and later to recalculate the scale equation parameters when a part of the image is zoomed into.

As previously mentioned, whole photographs generally do not give a pixel image of sufficient resolution to proceed with particle analysis. Instead, the video camera is sequentially zoomed into sections of the hard copy trace for detailed work. In addition to the initial scale data (already stored in the output file for that shot), two more reference points are required: the first located by mouse and horizontal and vertical offsets in millimetres from the photograph origin; and the second located by mouse and horizontal offset from the first. This is sufficient to calculate new scale equation parameters, and also translation parameters relative to the

whole shot image, which are needed to perform the horizontal rectification and vertical truncation discussed previously.

Except for the partial conversion of area within the subroutines *lump* and *calculate_particle_parameters*, geometric parameters are scaled from pixels to millimetres in the main programme, just prior to being written to the output file. Horizontal axis and area are simply multiplied by a scale factor; because of the logarithmic relationship, vertical axis is calculated as the difference between the scaled heights of the axis end points; and height (Y0) is similarly calculated. (A small complication was the inclusion of the zoomed-image vertical shift in calculations of vertical axis and height).

In contrast to the preliminary programmes developed, particle size distributions for slope photographs are calculated by accumulation from the finest fractions upwards (for example, starting from 'lumped' areas of fines). This is carried out using commercial spreadsheet software. Normally, size levels at which percentage passing is calculated range from 10-2000mm but this can be altered as necessary for close-up photographs. The grading curve ordinates thus obtained for separate shots of a site are then overlaid, with the corresponding mechanical sieving results. Working from coarsest to finest, successive curves are factored down manually to fit together into a single particle size distribution for the site.

Advantage was taken of the increased computer power to compile all the image analysis procedures into one programme, summarised in Figure 3-17. As noted above, interpretation of the results into grading curves is then performed via spreadsheets, which were preferred because of the flexible combination of operator control and automatic functions (for example, sort routines and screen graphics). The software used was installed on an IBM-compatible personal computer, so a small Archimedes-based programme was written to convert the data into a more convenient form for transmission to IBM format and subsequent direct importation into the spreadsheet.

A typical medium distance shot required about a day to produce the hard-copy outline, half to one day to analyse the 2000-3000 particles, and a couple of hours to extract grading curves for the shot and for the

complete site. If it was intended to use photo-sieving as a routine procedure, further development of hardware and software could greatly reduce processing time. For the purposes of this research project, however, it was sufficient to establish a workable, if tedious, method.

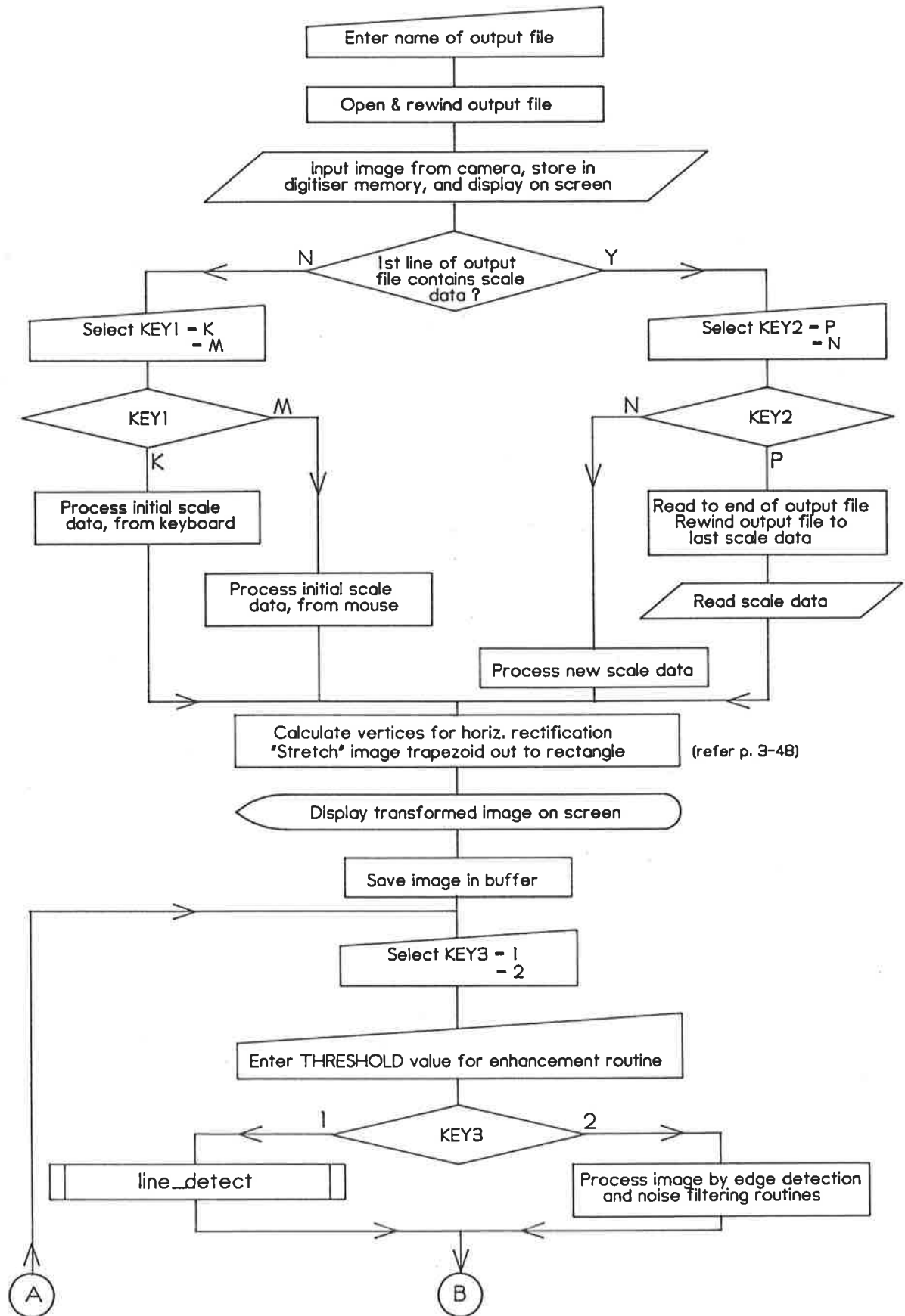
Since the purpose of developing photo-sieving techniques for dump batters was the impracticability of alternatives, the method could not be validated by direct comparison with mechanical sieving. However, isolated routines and functions were checked using trial shapes, and two of the tilted photographs of brickwork were repeatedly analysed, using various combinations of the programme options. Mean results per analysis gave the ranges: brick width = 73-78mm; and brick length = 228-236mm. These compare well with the approximate actual dimensions of 76x230mm. Table 3-6 summarises coefficients of variation (standard deviation/mean) for a range of analyses, which suggested preferences for entering scale data by keyboard; the *line_detect* image function; and zooming to closer scale. The trials were run before development of the *line_thin* enhancement routine, which would have improved the results. Despite this, the results showed a mean accuracy of +/-5% and a repeatability of better than 3%, which was considered adequate for particle size distribution.

SCALE DATA ENTRY	OUTLINING ROUTINE	IMAGE MAGNIF'N	PHOTO MG3-07 AXES		PHOTO MG3-02 AXES	
			Horiz.	Vert.	Horiz.	Vert.
Mouse	Line_det.	Normal	0.022	0.012	0.067	0.045
		Zoomed	0.022	0.017	0.030	0.035
	Edge_det.	Normal	0.027	0.014	0.044	0.049
		Zoomed	-	-	-	-
Keyboard	Line_det.	Normal	0.036	0.019	0.057	0.042
		Zoomed	0.021	0.013	0.029	0.039
	Edge_det.	Normal	0.023	0.017	0.067	0.074
		Zoomed	-	-	0.024	0.056

Table 3-6 Coefficients of Variation for Measurements from Tilted Brick Photographs

Programme operation was also assessed during its use to characterise dump slope materials, both specifically, based on a preliminary group of shots, and by continual observation. This is discussed in Section 3.3.3.

Figure 3-17 Flowchart of Photo-Sieving Programme for Tilted Photographs



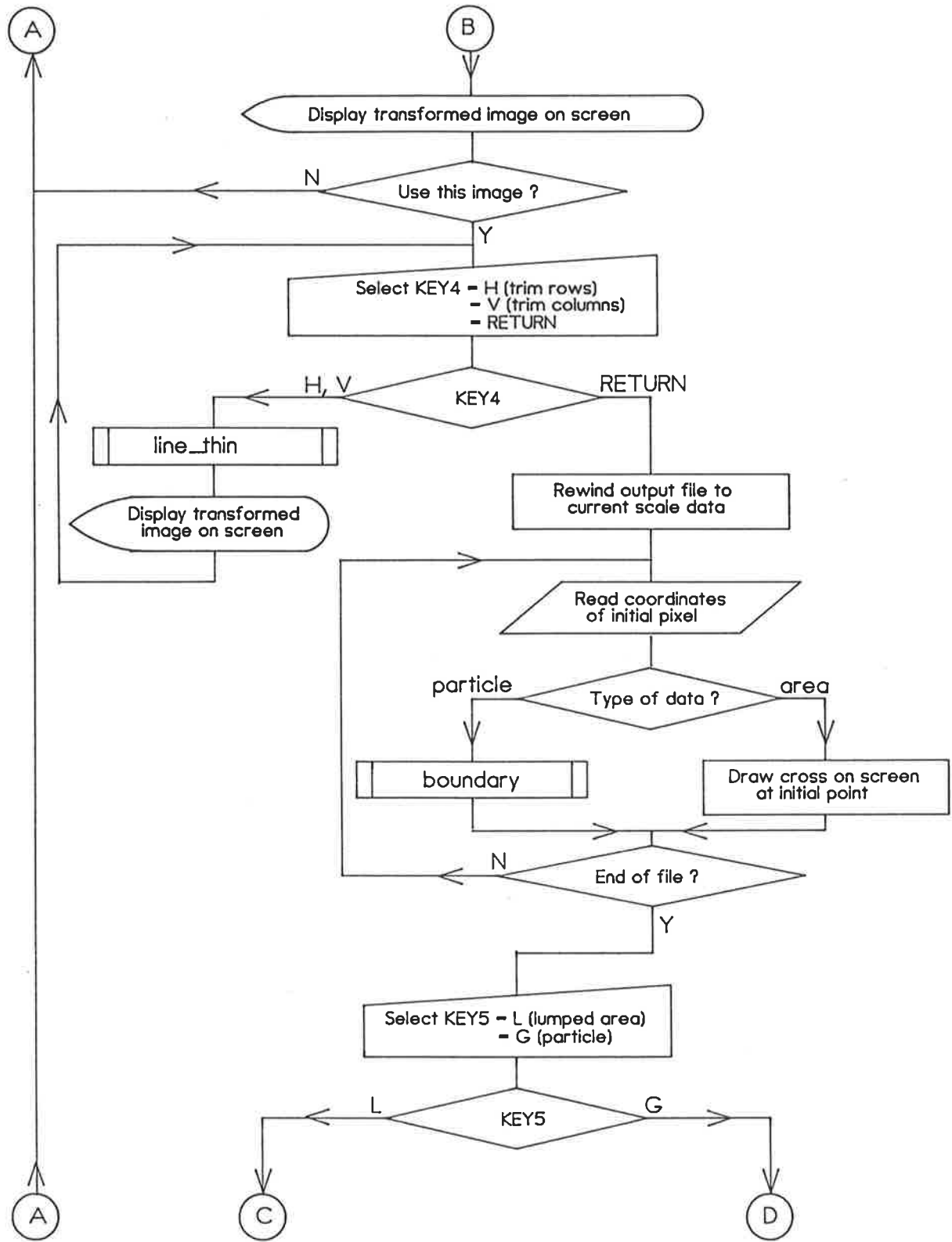


Figure 3-17 (continued)

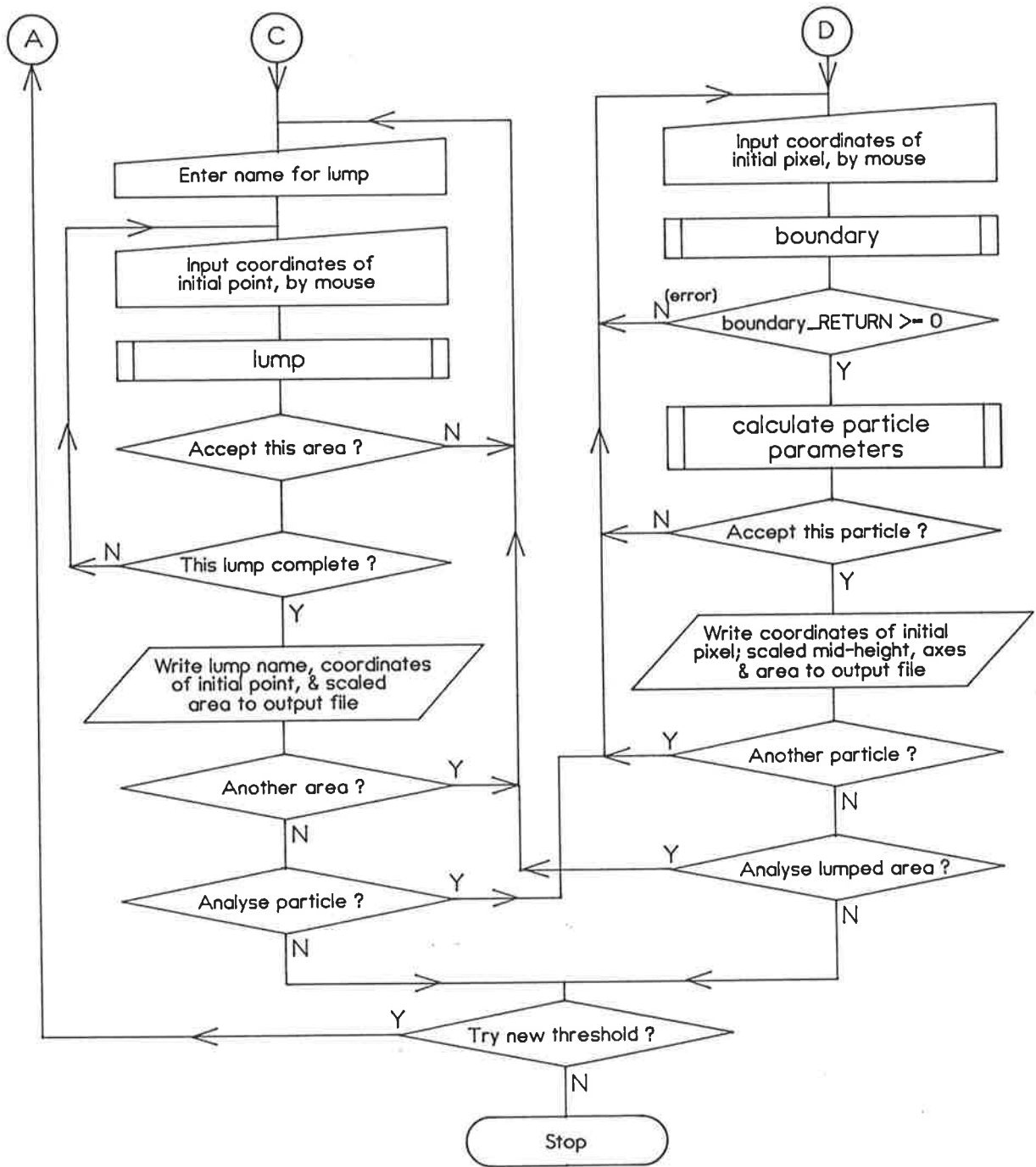


Figure 3-17 (continued)

3.3.3 Assessment of Method

The theoretical justification of photo-sieving presented in Section 3.3.1 rested on three conditions: a) that valuation by area of a planar image is equivalent to valuation by mass of a bulk sample; b) that geometric average axis of the particle image gives a reasonable approximation of sieve size; and c) that the effect of partial hiding of particles does not invalidate the previous condition. The second relates to the particle in isolation, and its general acceptance was validated by the parallel photo-analysis and mechanical sieving of laboratory samples, as discussed in Section 3.3.2.2. However, the other two conditions relate to the spatial arrangement of material on the dump batters, and were only indirectly supported by the laboratory comparison.

Regarding valuation by area, the issue is whether the grading obtained at the slope surface is representative of the whole of that material layer at that site. When it is considered that a material layer typically consists of a few truck-loads of the same rock type dumped over strips of slope about 4 metres wide and 10 metres high, it is apparent that at most such layers will be only a couple of metres thick. Over this small depth, it is likely that particle size variation will be initially random, as there is no reason to expect sorting normal to the slope when the rock is dumped. Subsequent transport of smaller size fractions, as discussed in Section 2.3, might induce some depth-dependent variation in the fine tail of the particle size distribution, although the grading of the coarse skeleton should be essentially unchanged. As the waste-rock weathers, and fines fill up the larger voids below, any small correlation with depth will disappear. In summary, it was felt that there is reasonable likelihood of valuation by area being valid for the newest, and the older, dumped material, although photo-sieved gradings for slopes in the range of one to two years old may be biased by lack of surface fines. However, any significant variation of particle size distribution with depth would also present problems in sampling for mechanical sieving, and interpretation of its results.

The stipulation relating to hiding effect is more difficult to argue. A definite test of its significance really requires corresponding photo-

sieving and mechanical grading of an actual slope face but, as observed in previous sections, mechanical sieving of the total waste-rock material is not feasible. It might be possible to approximate sieving by measuring particles in-situ on the slope - essentially taking the aperture to the particle instead of putting the particle through the aperture - but an exercise of that scale was not justifiable in the context of the development of photo-sieving procedures being a subordinate aim of the research. A laboratory model of a dump slope was briefly considered but discounted because it repeats the original problem of validation of a model against the actual slopes.

In the absence of a practicable decisive test, some inference on hiding effect was drawn from comparative analyses, using pairs of photographs of the same site. The degree of hiding of each particle must change as the angle of the camera relative to the slope face, (that is, tilt), changes. Therefore, significant differences in gradings obtained from photographs of the same area taken at different angles should relate to differences in overall hiding effect, and give some indication of the significance of this factor on results of photo-sieving for dump slopes. A preliminary assessment of the method was made after fifteen photographs had been analysed, in which gradings were calculated for the common portions of four pairs of overlapping shots. As seen from Figure 3-18, three pairs gave reasonable agreement, with notable deviation occurring only at the fine tail of the grading curves, due to finer resolution in the closer distance shots. Photographs mg2-08 and arm-34 showed more disparity. However, mg2-08 had been indistinct and difficult to trace from the partially rectified image projected onto the drafting table (refer Section 3.3.2.1), and it was suspected that the sections which had been designated as too fine to analyse contained larger fragments which were blurred into the surrounding material. Consequently, mg2-08 was retraced using the stereo-microscope and analysed again. Shown dashed in Figure 3-18(d), the new grading curve agreed well with that of arm-34. Although they are not conclusive, these comparisons suggest that, since different conditions of particle hiding do not produce marked differences in the resultant grading curves, hiding effect might not be a major source of error in photo-sieving of the waste-rock dump slopes.

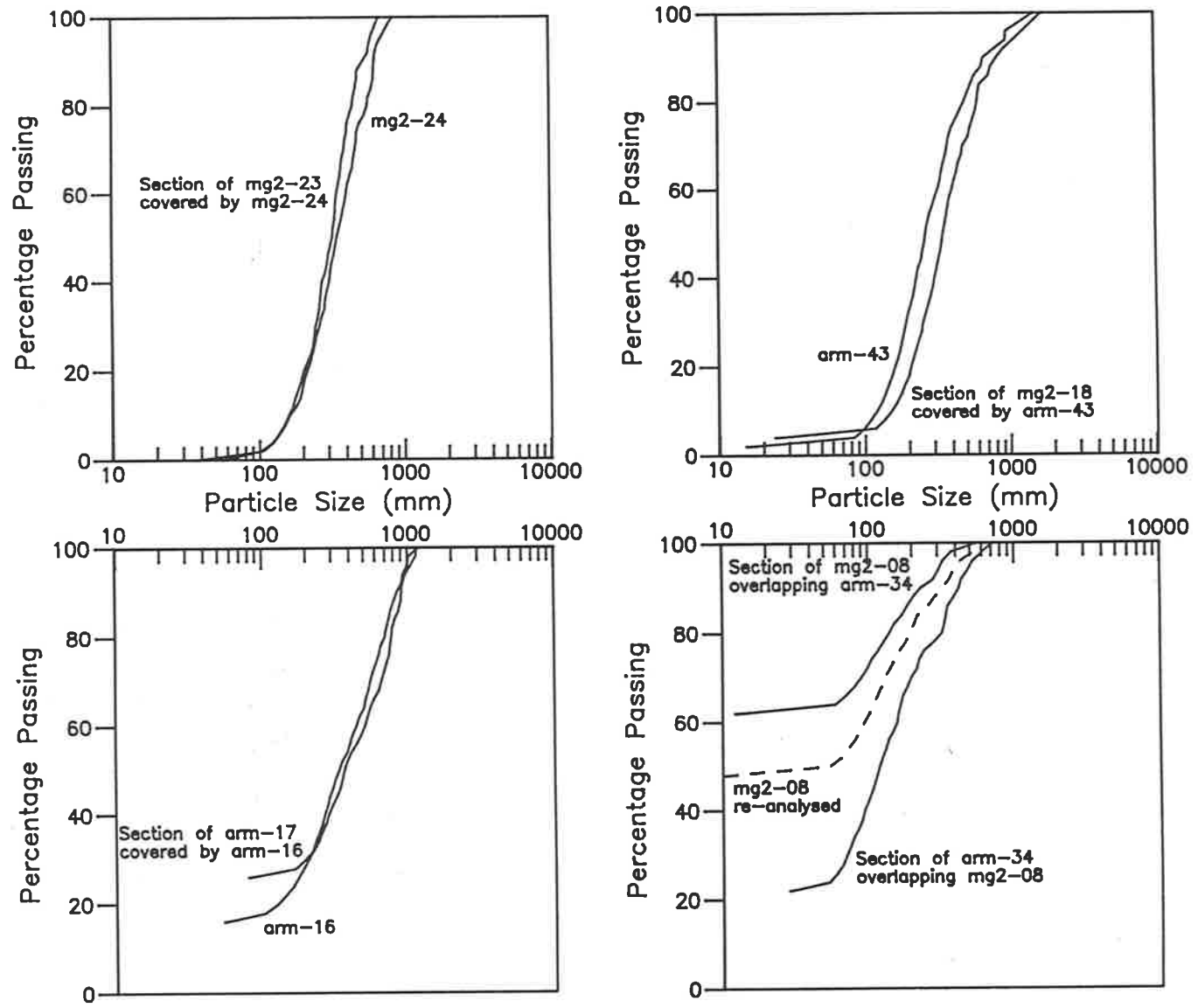


Figure 3-18 Comparative Results from Overlapping Photographs

It was also observed from these preliminary analyses that a shape factor (horizontal axis ÷ vertical axis) was predominantly less than unity. While this bias could have reflected real preferential particle orientation, no trend had been noticed during the field work, and so closer examination was warranted. Scatter plots for each photograph suggested no correlation between shape factor and particle size, but most showed shape factor decreasing, amidst a broad scatter, with increasing distance from the base of the image, as illustrated in Figure 3-19. The correlation was steeper for images with greater algebraically corrected tilt distortion. An initial thought was that thickening of particle outlines due to the horizontal rectification, procedure (refer Section 3.3.2.3), might have caused underestimation of the horizontal axis, which is measured between outline pixels. Such an error would be greater the greater horizontal rectification and so would increase with both tilt and distance up-slope. The enhancement routine *line_thin* was written to correct outline thickening, but although it improved programme operation there was little effect on the results. Therefore associations were investigated between shape factor and three parameters relevant to the algebraic rectification routines, namely: horizontal tilt ratio $(l_{w1}-l_{w2})/(h_{w2}-h_{w1})$; vertical tilt ratio $(l_{h1}-l_{h2})/(h_{h2}-h_{h1})$; and scale fraction $(h_{w1}-h_{w2})/h_{total}$ (refer Figure 3-16 for symbol definitions).

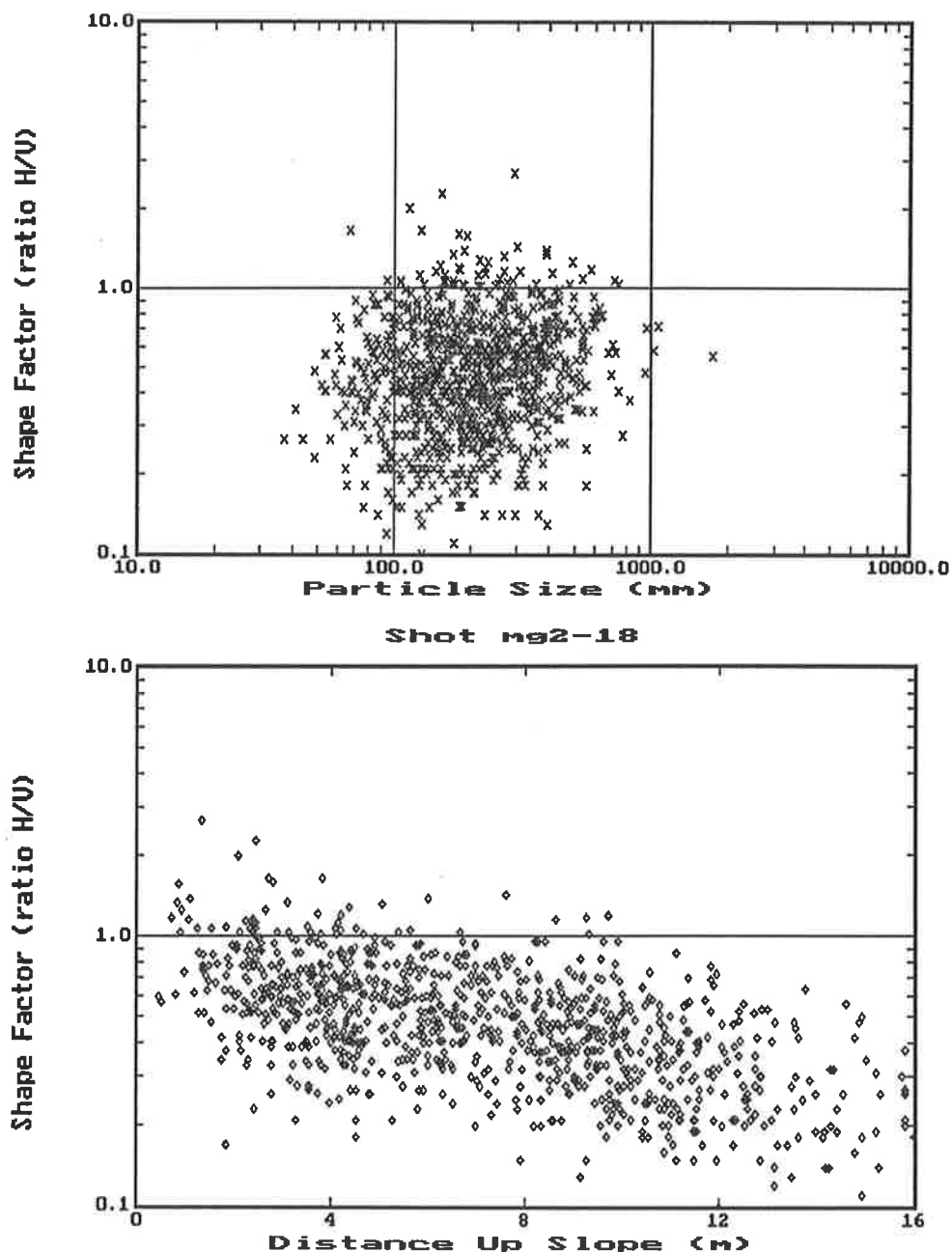


Figure 3-19 Typical Scatter Plots for Shape Factor

The logarithmic mean shape factor showed no correlation with any of these measures, contrary to the expectation if the noted bias was due only to the tilt rectification procedures. Finally, log-linear regressions were calculated for each image for shape factor against distance, and the slope of the regression showed correlation especially with vertical tilt ratio, as shown in Figure 3-20. However, if the trend was produced solely by the approximate equation used for vertical tilt rectification, there should be two points of inflexion, or zero error, corresponding to the locations of the vertical scale sticks from which

the algorithm was specified. The linearity observed from the scatter plots did not conform to this expectation.

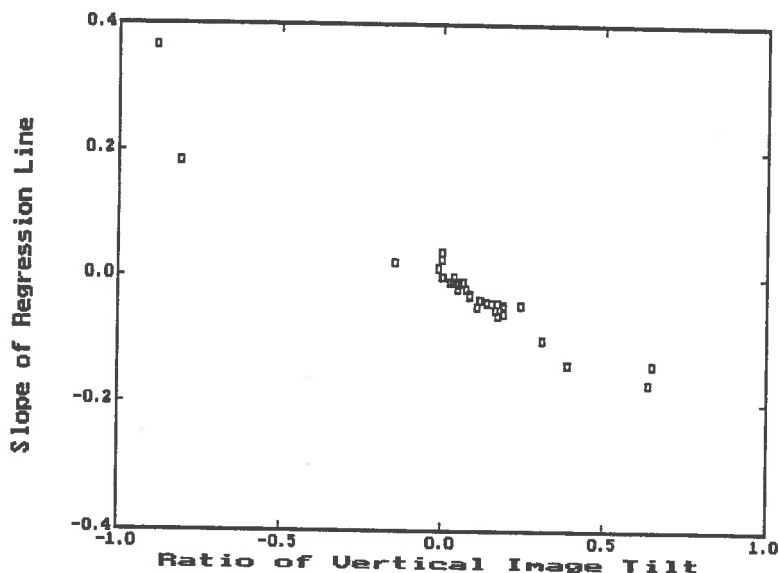


Figure 3-20 Correlation of Shape Factor Regression with Vertical Tilt Ratio

The other point in the tilt correction procedure where a systematic error might have been introduced was in the actual placement of the scale sticks on the slope. Derivation of the rectification equations assumed that the sticks lie parallel to the average slope of the batter face (as do the bricks in the photographs used to validate the algebraic routines, as discussed in Section 3.3.2.3). Admittedly this was not always kept in mind during the fieldwork, such as when balancing on boulders five metres up the loose face of a high batter. However, for scale stick misalignment to have produced the observed effect, it would have been necessary to consistently lay the upper stick at a shallower angle than the lower stick, so that vertical axis would be overestimated for the higher particles. This proposition might be credited on convex slopes, since the sticks might be laid to the local slope angle, but the batters at Ranger are generally planar to slightly concave, and it is difficult to accept that the sticks were consistently mis-placed in the required manner.

In summary, results of image analysis showed a bias towards vertical axis being on average greater than horizontal axis, and a tendency for this inequality to increase with distance up from the close end of the photograph. The magnitude of the latter trend was greater the more

severe the vertical tilt of the input image. The behaviour is not clearly attributable to either actual preferential orientation of particles, a systematic error in the field procedure, or the tilt rectification algorithms, and there is evidence against each of these three as the sole cause. At this stage, since the development of a photo-sieving method was not the primary objective of the project, it was decided to assess the impact on derived particle size distributions before pursuing this problem.

In general, the more tilted photographs were close distance shots, so that although the shape factor/slope distance correlation was steep, the resultant range in shape factor was relatively small. Solving the regression equations at the top and base of each image, the worst variation was in shot arm-47 (vertical tilt ratio = 0.12; slope of regression = -0.037; distance up slope = 14.3m), which gave a best-fit shape factor of 0.23 at the top of the image compared to a mean of 0.47. In terms of geometric average axis, this translates to only a 44% underestimate, that is, less than one sieve size. The typical difference in geometric average axis calculated at the extremities of the regression line was about 20%. Thus, even if the trend was a completely artificial effect, most particles would still be assigned to the correct size class.

For direct illustration of the impact on particle size distribution, two photographs were analysed in replicate, once with partial analogue rectification prior to analysis and once with outlines traced unrectified. The results, presented in Figure 3-21, showed minimal disagreement for the differing degrees of tilt rectification applied algebraically during computer analysis. The concurrence of grading curves from overlapping shots (Figure 3-18) confirms the low significance of this shape factor effect for even greater differences in severity of scale correction - shots mg2-23 and mg2-24, for example had vertical tilt ratios of 0.164 and 0.001 respectively.

To conclude, the logarithmic mean shape factor (horizontal axis/vertical axis) was more often less than unity for photographs from the waste-rock dump slopes, an effect which could not be attributed to the image analysis procedure. However, there was also a noticeable correlation between shape factor and distance up-slope, the slope of which in turn

correlated strongly with the vertical tilt of the image input to computer. It could not be established that vertical tilt or the method for its rectification caused the trend, and it is possible that both are dependent on some other property. Regardless of its source, this shape factor behaviour has no significant effect on the grading curves obtained by photo-sieving.

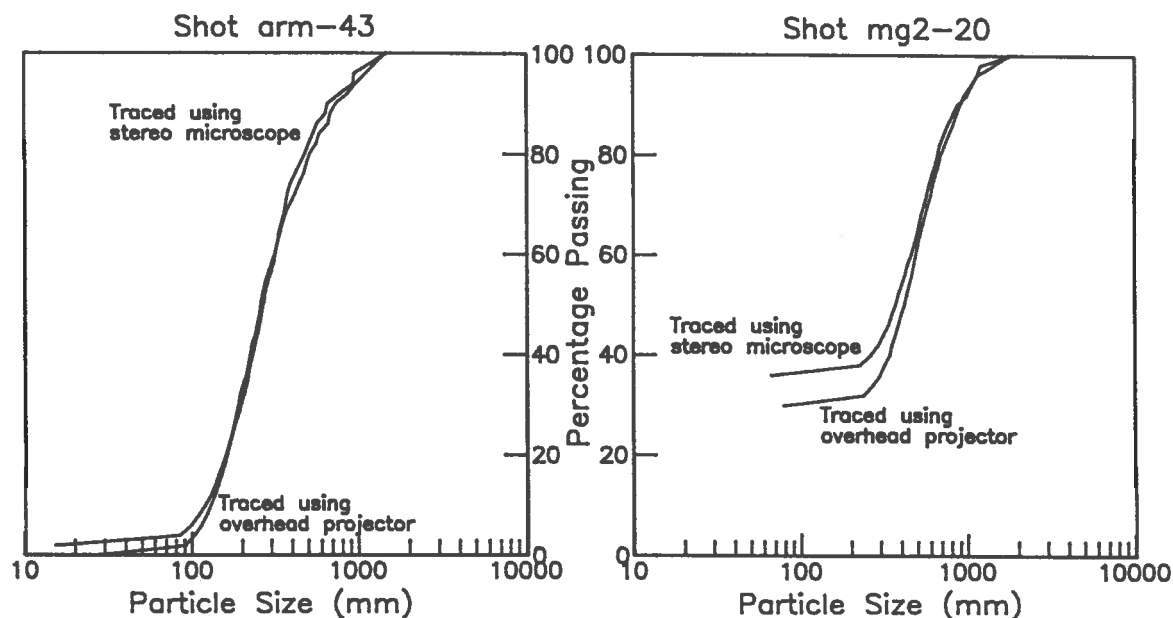


Figure 3-21 Replicate Photo-Analyses with Differing Rectification

As with photo-sieving of the collected bulk samples, discussed in Section 3.3.2.2, gradings curves for slope photographs showed rapid levelling at the fine end. That this was again related to smallest identifiable particle size was suggested by the comparisons in Figure 3-18, where the medium distance shots continued to a smaller particle size than long shots before starting to flatten. Histograms of numbers of particles were overlaid on the grading curves for several of the initially analysed shots, as those shown in Figure 3-22. All showed a rapid decrease in particle numbers as the grading curve turned over. A value of 100 particles per 0.15 log cycle particle size, (that is, per bar of the histograms in Figure 3-22), was taken as a tentative limit to the reliable size range for particle size distributions from individual photographs. These limits were then used as guides in fitting together the site grading curves.

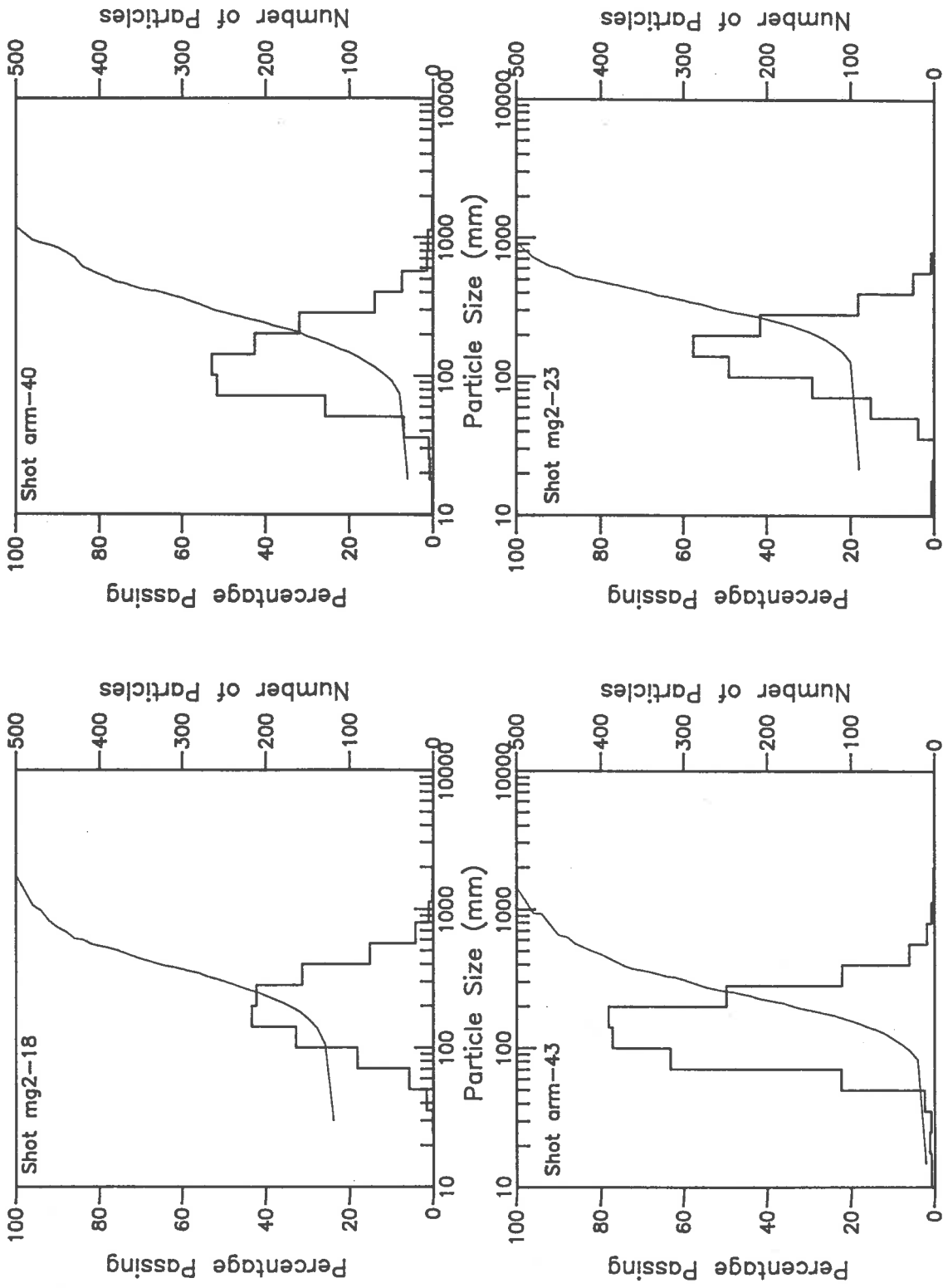


Figure 3-22 Associations Between Grading Curve and Numbers of Particles

This resolution limit was generally at 200-300mm for long distance shots and about 100mm for medium distance shots. The complete particle size range for close photographs was typically 20mm to 80mm. As noted in Section 3.2, mechanical sieving results were considered reliable below 10-20mm. Thus at times the contributing particle size distributions left gaps within the range of the overall site grading, which necessitated some extrapolation to complete the curve. In this project, slope photography preceded development of the photo-analysis routines, so this difficulty could not be remedied. However, careful planning of photograph location and scale could improve coverage in any future work.

During the preliminary assessment, it was also observed that individual shot distributions were noticeably jagged when the total number of particles was less than about 500. This is probably the level at which individual particles have a noticeable impact on the cumulative distribution, in the same manner as discussed in Section 3.3.2.2 for oversize fragments in the collected bulk samples. Curves calculated from greater than 1,000 particles were consistently smooth throughout most of their range.

The retracing of photograph mg2-08, discussed earlier in this section, highlighted the importance of image clarity even at the penalty of more severe tilt. The main reason appears to be reduced error due to mistakenly including poorly imaged larger fragments in lumped areas of fines. Transfer to use of the stereo microscope for outline tracing, with care taken to designate occasional poorly focussed areas as "unclear" rather than as "fines", minimised this potential source of error.

The "unclear" designation was also applied to obscured parts of the image, for example, those in deep shadow or underneath the scale sticks. Such sections were excluded from the total sample area on which grading curves were based, so in general no adverse impact was expected unless the remaining area contained insufficient particles. However, if a large proportion of the image was thus excluded there could be some doubt whether the remaining sections were representative of the whole image area. For this reason, analyses were considered more reliable when the obscured areas totalled less than 20% of the photo-sieved area.

Aspects of the photo-sieving method considered in the preceding discussion were identified from the preliminary assessment of results from fifteen individual photographs. The insights and arguments were extended through subsequent analyses, including the compilation of site grading curves. In awareness of the lack of more definitive validation, a confidence ranking was devised for the site gradings, shown in Figure 3-23, which incorporated most of the above factors. Weightings were assigned for vertical tilt, number of particles, and fraction unclear, for each contributing image, and also for coverage of the whole size range and for the general ease of fitting the separate distributions into a single curve. According to this table, site gradings were ranked almost exclusively as "fair" and "good".

CONFIDENCE IN GRADING CURVE				
Shot	?????	?????	?????	average
Sample size (>500=0.5, >1000=1.0)	()
VTilt Ratio (<0.1=0.5, <0.05=1.0)	()
% Unclear (<20%=1.0)	()
Size Range Coverage (no.overlaps / no.curves.....)				()
Ease of Combination (rate 0 to 1)			
				Confidence Value () Ranking { }
				{ 0 to 2 = POOR; 2 to 4 = FAIR; 4 to 6 = GOOD; 6 = V.GOOD}

Figure 3-23 Confidence Ranking for Site Grading Curves

A final summary of the procedures for photo-sieving used in this research project, and anticipated improvements, is provided in Table 3-7:

ITEM	ADOPTED PROCEDURE	POSSIBLE IMPROVEMENTS
Field Photography	As described in Section 3.1.1	Take care that scale sticks are aligned with slope face Run a trial site analysis to help plan shot distance for complete size range coverage
Particle Outline Digitising	Trace hard copy from stereo microscope and input to computer via video digitiser	Input direct to computer while tracing (e.g. with a stylus and sensitized pad digitiser) Develop software to show image on screen as traced and to permit on-line editing
Scaling and Rectification	Corrected algebraically, using approximate algorithms discussed in Section 3.3.2.3	Use hardware capable of better analogue rectification Improve algorithms for algebraic rectification (this should not be at the expense of facility of the field procedure)
Particle Analysis	Computation routine activated manually for each particle	Partly automate particle search (e.g. use manual interrupts instead of manual activation)
Site Grading	Compiled by operator, using spreadsheets	No modification suggested

Table 3-7 Summary of Procedures in Photo-Sieving Method

3.4 Dump Site Grading Curves

The resultant grading curves for sites on the waste-rock dump slopes, with their contributing bulk sample and photograph particle size distributions, are presented in Appendix B. Gradings for eighteen sites were compiled and two distributions were also analysed from photographs of trucks leaving the mine pit (refer Section 3.1.1). A grading for Site 13 could not be produced because the tilt was not simply horizontally/vertically aligned and so could not be handled by the programmes developed. Sites 1, 2, and 3 were not analysed because representative samples for mechanical sieving had not been collected, and there were several other sites of similar age. The gradings showed no discernible correlation with rock type, but a trend with slope age was apparent.

Selected results illustrating the range of slope ages sampled are also included in Figure 3-24. These concur with site observations discussed in Section 2.2 regarding the loss of smaller particles during the first couple of years, and their subsequent replacement as the waste-rock weathers. As noted in Section 1.3.2, the measured grading curves strictly only relate to the slope surfaces. While arguments were advanced against initial grading variation with depth, the overall impression is that the subsequent depletion of finer fractions may occur within a shallower layer than that occupied by a given rock type.

Assume, for the sake of this discussion, that the material lost according to the difference between the gradings for Site 21 and Site 17b, (refer Figure 3-24), is washed from the surface metre into the metre below. The fractions moved may be calculated by subtraction of percentages retained in the two gradings, and added to the initial distribution, (Site 21), to obtain the grading for the lower metre after 2 years. This hypothetical result, illustrated in Figure 3-25, suggests that the grading at depth may be slightly finer than that which initially exists throughout the material. The generation of fine fragments by weathering, which proceeds most rapidly at the exposed surface soon predominates over such increases due to early particle movement, as illustrated by the grading after 3 years (Site 15).

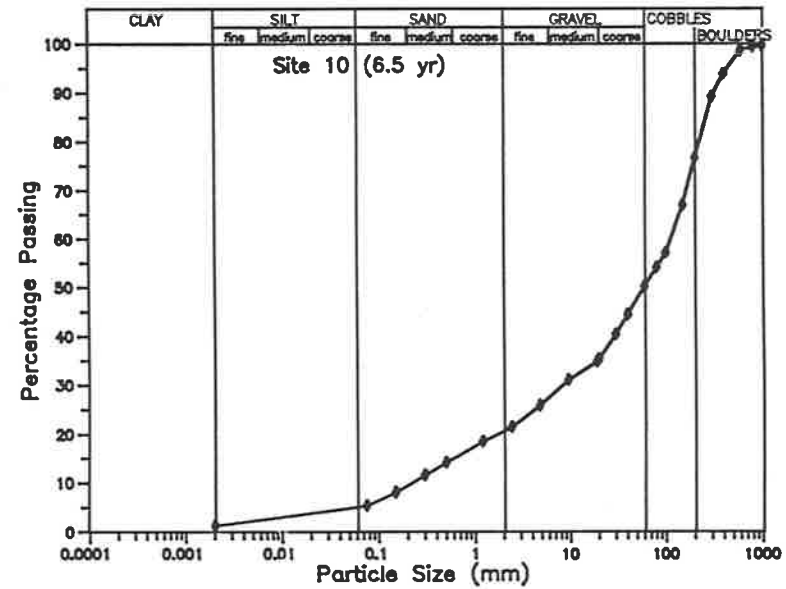
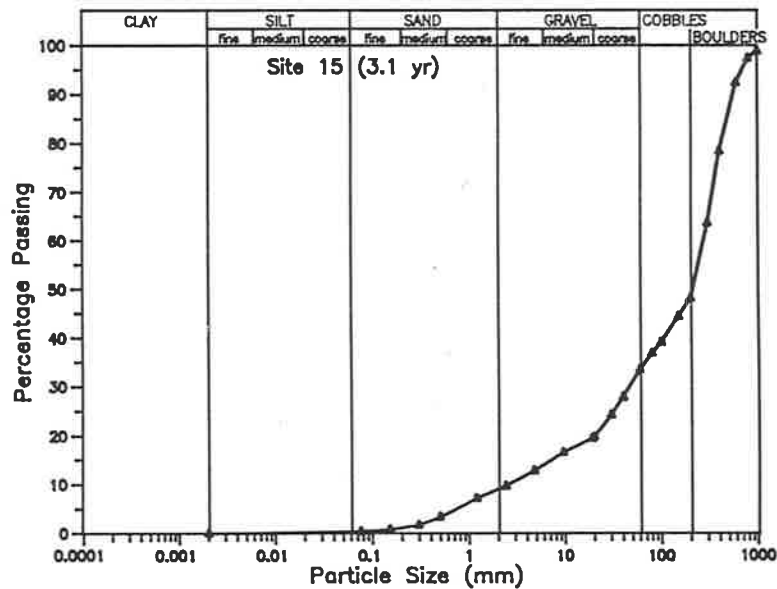
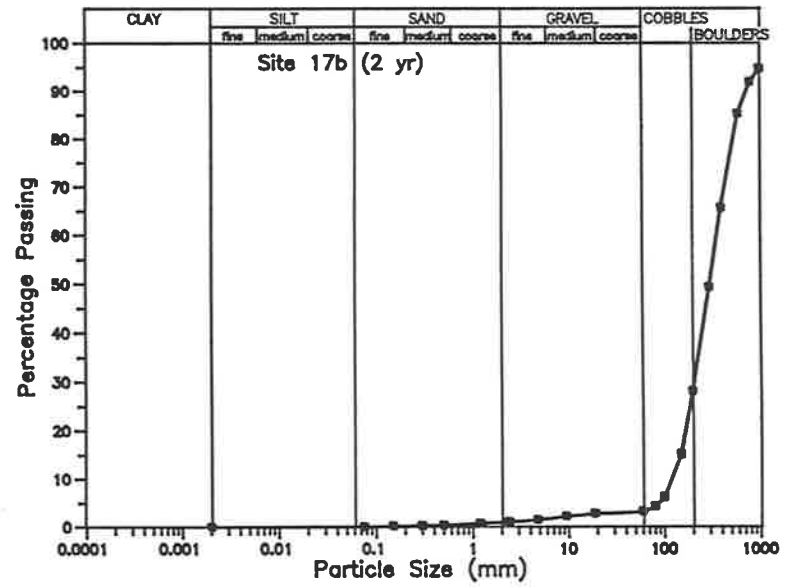
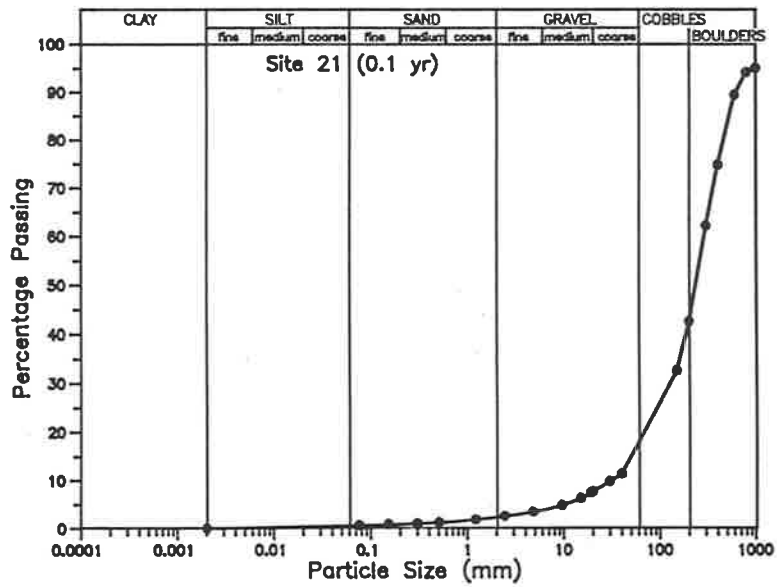


Figure 3-24 Typical Grading Curves for Dump Slopes

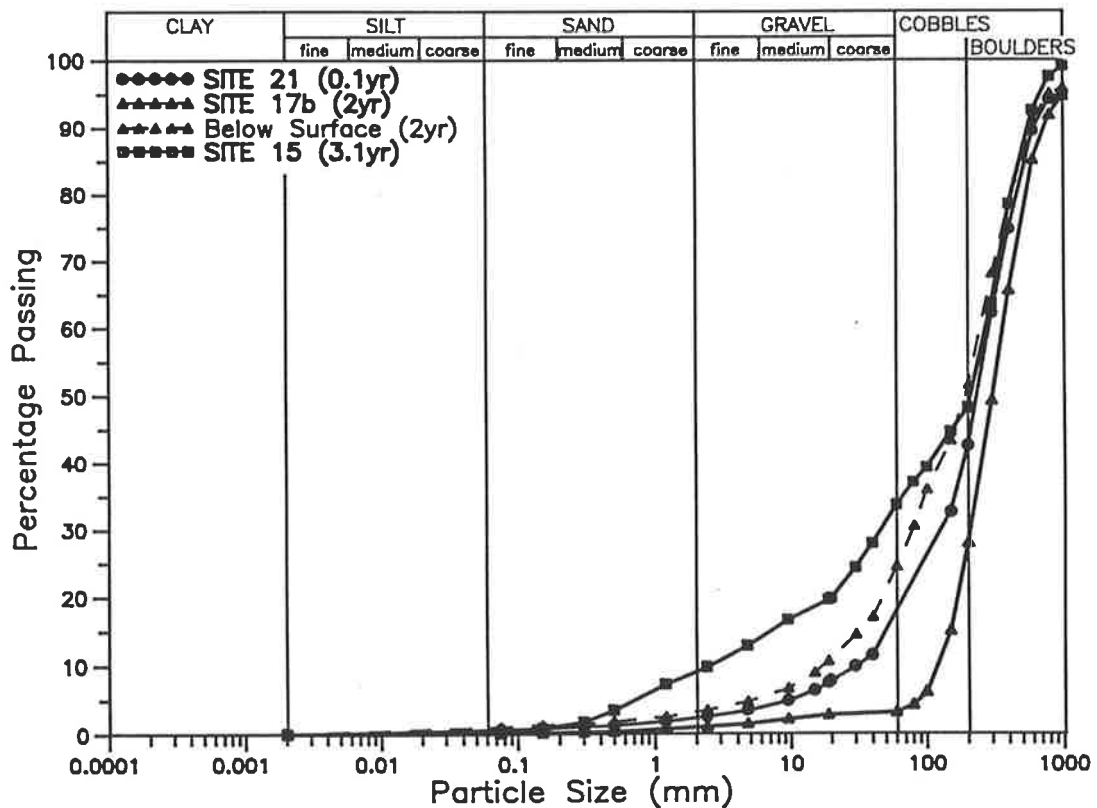


Figure 3-25 Comparison of Surface and Below-Surface Gradings

Regarding the significance of this temporary effect on strength characteristics of the waste-rock materials, current slope angles, such as those given in Table 3-1, show no trend over six years, and certainly no obvious loss of stability. The age period of 1 to 2 years over which the surface depletion is observable was therefore not considered critical to the association between weathering and strength in the constituent materials of the waste-rock dumps, and it was not examined in the laboratory strength testing programme, discussed in Chapter 5.

Another observation made during the field work related to apparent sorting of particle sizes down the slopes (refer Section 2.2). This aspect was explored by re-analysing long distance photographs with upper and lower segments of the slope treated as separate samples. As apparent from the example in Figure 3-26(a), smaller proportions of "lumped" areas of fines occurred in the lower halves, for which the minimum reliable size was also slightly lower. These features became significant when the up-slope length was more than about 12 metres. In other regards, the general shapes of pairs of grading curves were usually similar: this initially suggested that any sorting effect might be

restricted to variation of the finer material within a coarse skeleton which remained essentially constant over the height of the slope. To test this, the grading curves were recalculated excluding particles of less than 100mm geometric average axis.

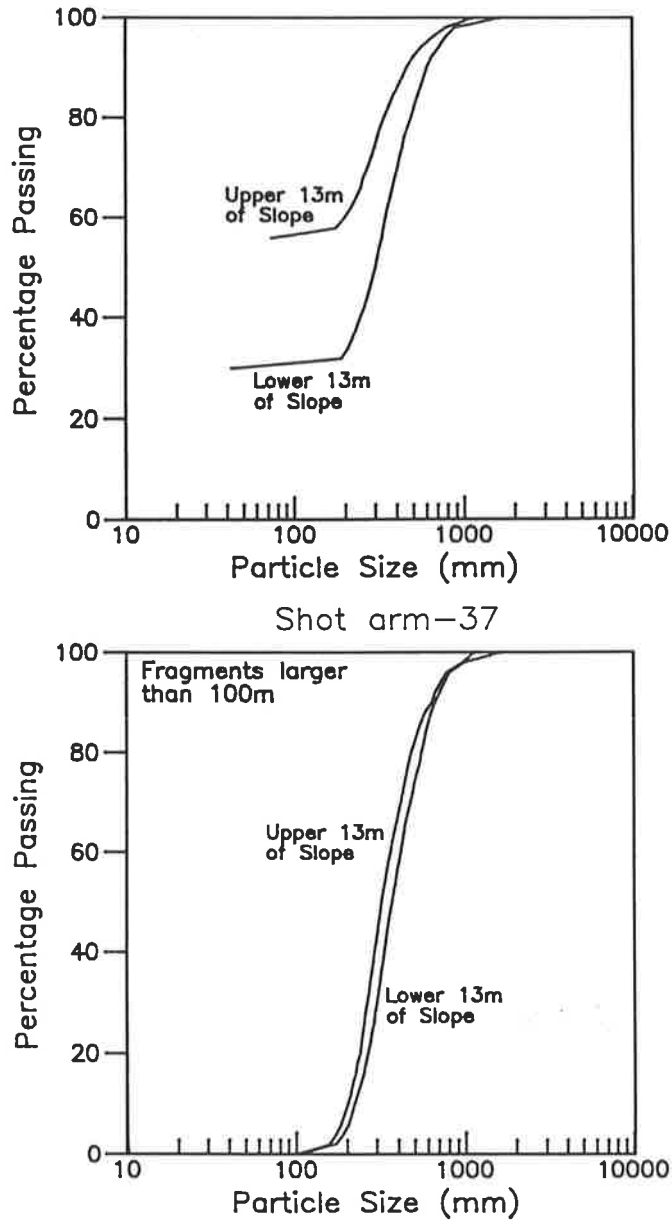


Figure 3-26 Typical Gradings from Upper and Lower Sections of Dump Slope

At the stage of the preliminary assessment of method, results, such as in Figure 3-26(b), supported the hypothesis. However, the impression gained during field work had been of a downward increase in large fragments, in addition to a surplus of smaller particles near the top of

the slope, so further analyses were carried out as site gradings were compiled. The results showed no consistent trend but there was generally not a large difference between upper and lower slopes. However, the reliability of such gradings was considered doubtful - those for upper slope segments, in particular, were possibly affected by the smaller numbers of traceable particles and occasional very large boulders lodged at the top of the batter. Therefore it was concluded that the long distance photographs were only suitable for a broad consideration of down-slope sorting. Dashed curves in Appendix B, representing particle size distributions compiled using the two part-slope analyses of long shots, suggest the range of grading variation related to sorting. For the purpose of an investigation into the effect of weathering condition on material strength, only overall site gradings were used.

As discussed in Section 5.5.1, additional disturbed samples of specific mine materials were collected in June 1991. Several of these were representative of current batter materials, for which total (site) gradings were estimated from the results for photo-sieved batters of similar age. Five samples were of more weathered material ($\approx 100\%$ passing 63mm) for which mechanical sieving results were equivalent to the total material grading. Because of the greater proportion of silt and clay, these materials were washed at the $<19\text{mm}$ subsample before intermediate and fine sieving, in accordance with AS 1289.C6.1-1977 (refer Section 3.2 for comparison), and more detailed analyses were also obtained for the $<0.075\text{mm}$ fractions. Particle size distributions for these materials are included in Appendix B.

CHAPTER FOUR

4. MINERALOGICAL DESCRIPTION OF DUMP MATERIAL

4.1 Site Geology and Mineralogy

As described by Needham (1982), the basement geological formation of the area is the Nanambu Complex, more than 2200 million years old, which consists of mainly granites and gneisses. Overlying this is the Cahill Formation, deposited between 2200 and 1900 million years ago, and comprising metasediments including a carbonate unit, schist and microgneiss, and coarse schist. About 1650 million years ago these were covered by sediments which became Kombolgie sandstone.

About 1870-1800 million years ago, prior to deposition of the Kombolgie Sandstone, the Cahill Formation was intruded by pegmatite dykes, widely deformed and metamorphosed, and eroded to a low relief surface. Uranium mineralisation, which was generally confined to the Cahill Formation, occurred around 1600 million years ago, and non-mineralised basic dykes were intruded around the same time. Chloritisation was associated with both the major regional metamorphism and the later mineralisation. The Kombolgie Sandstone has since retreated to form the Arnhem Land escarpment, overlooking the wetlands (see Plate 4-1). These are now surfaced by weathered Nanambu Complex and Cahill Formation rocks, and alluvium washed down from the escarpment country.

Within the Ranger Project Area there are two major orebodies, No.1 and No.3, the former of which is currently being mined. Nanambu Complex rocks, locally termed "Footwall Sequence", crop out at the western side of Pit No.1 and dip moderately steeply to the east. The overlying "Lower Mine Series", (within the Cahill Formation), is mainly chert and massive chlorite rock within the pit outline, with carbonate-rich rocks beyond the planned eastern limit. The orebody, which extends to about 170 metres depth, is contained within the chert/massive chlorite rock and the "Upper Mine Series" schists and pegmatites above. The western side of orebody No.3 is bounded by a fault, dropping the basement complex which again becomes even deeper towards the east. On current information, the "Lower Mine Series" here is largely comprised of carbonate-rich rocks, and the orebody occurs essentially within the "Upper Mine Series" schists. In Pit No.1, shown in Plate 4-2, weathering is evident to depths of 20 to 30 metres below original

ground surface generally, and to greater than 50 metres depth in the pegmatite dykes.



Plate 4-1 Ranger Mine, looking East toward Escarpment



Plate 4-2 Ranger Pit No.1

Presently mined rocks are thus predominantly schists (muscovitic and chloritic), chert, massive chlorite rock, and pegmatite, with small amounts of dolerite, carbonate rocks, and gneiss. However, chert, in particular, is often diverted for construction use and so occurs less frequently in the waste-rock dumps. It will also be only a minor rock type in Pit No.3.

Rock types encountered at Ranger are differentiated primarily by rock structure, or fabric. Apart from the limited carbonate rocks, all rocks as-mined are comprised of the same group of minerals, albeit in various proportions. These primary minerals are quartz, muscovite (white mica), and chlorite, with generally only minor hematite. Some of the current muscovite and chlorite is altered feldspar, the result of metamorphic events and weathering which also produced the hematite. With regard to chemical weathering in the waste-rock dumps, quartz is expected to remain essentially unaltered; chlorite will probably weather to vermiculite, smectite and ultimately kaolinite; muscovite will eventually become kaolinite, possibly after illite; and hematite will, under certain circumstances weather to goethite (Milnes, Riley & Raven 1986).

Unlike most other mines in the region, primary sulphide minerals like pyrite are present in relatively low concentrations in the rocks at Ranger. Where they are present, oxidation of sulphides is one of the first weathering reactions to proceed, creating an acid environment favourable to other alteration reactions. Even with the small amount present at Ranger, weathering of occasional sulphide-rich zones is thought to have been responsible for sulphuric acid generation at the base of one of the ore stockpiles (Milnes & Fazey, 1988). This has not been observed to any significant extent on the dump batters (Milnes et al 1991), although the reaction was recognised in soils forming on the dump terraces (Fitzpatrick 1986).

In the absence of some such propellant reaction, decomposition on the dump batters is proceeding in a very localised manner around structural anomalies such as grain boundaries and internal flaws. The volume increase which is associated with the production of smectite and, to a lesser extent, of illite causes stresses at these sites which tend to push the rock fragments apart from within. Weaknesses induced by the

mining activities and laminations inherent in the dominant schists have assisted this mechanism, with the result that marked disintegration has occurred on the waste-rock dumps in the first decade, with relatively little generation or transformation of clay minerals.

The breakdown of larger particles exposes more sites for weathering, which is thus expected to accelerate, at least until the material approaches a soil-like texture. Chlorite and muscovite are both based on the typical 2:1 clay structural unit (an octahedral atomic sheet between two tetrahedral sheets), as are their transitional weathering products, vermiculite and smectite, and illite. Ultimate weathering to kaolinite requires alteration to a 1:1 structural unit, which is thus likely to proceed at a slower rate than the previous stages.

4.2 Classification and Mineralogy of Collected Samples

Mineralogical descriptions of the waste-rock samples collected within the slope photography programme (refer Section 3.1), were required for assessments of weathering potential and extent of weathering, and also to assist in selection of samples for laboratory strength testing. Several methods were utilised, commencing with general description and classification of all samples based on visual inspection. During this stage, coarse gravel fragments, some representative of the range of rock types and some of rocks which were difficult to identify, were selected for preparation of thin sections. In addition to refining visual descriptions, some thin sections were used in conjunction with X-ray diffraction (XRD) analysis to obtain quantitative estimates of mineral composition of the most prevalent rock types. XRD analyses were also carried out on fractions retained on the 75 micron sieve and on clay subsamples, to provide data relevant to the progress of chemical weathering.

As discussed in Section 5.1.1, extra samples were collected in 1991, to provide specific materials for laboratory strength testing, including some which were more weathered than any waste-rock currently found on the dump batters. These were broadly classified in the field according to rock type, and XRD analyses were carried out on <2.4mm subsamples for characteristic mineral composition as sampled. For the five more weathered samples, detailed XRD and chemical analyses of the clay fractions were also performed.

All XRD analyses were carried out by CSIRO Division of Soils Mineralogical and Geochemical Services Group, principally by Mr M.D.Raven and Mr G.G.Riley. Individual thin sections and XRD patterns were described and interpreted by Dr A.R.Milnes and Mr G.G.Riley.

Final sample descriptions are included in Section 4.3, but some general observations made during visual examination are noted here:

- a) Most bulk samples included more than one rock type, for example, 'muscovite schist with some massive chlorite rock'. Although such mixing is a real feature of the dumps, in this study it was preferred to investigate the strength-weathering behaviour of individual rock types, since these represent bounds between which

mixed samples should fall. Consequently, of the samples collected during the slope photography programme, only those comprised of predominantly one rock type were considered for strength testing.

- b) In any sample, fragments throughout the cobble and gravel size range, with the same general rock description, showed no observable trend in degree of alteration. Weak pieces could be broken along existing planes, such as laminations in a schist, and inspection of the resultant surfaces revealed only minor production of clay minerals. Thin sections confirmed that as yet there was little chemical weathering proceeding within the fragments. Consequently mineral compositions obtained for rock pieces are indicative of the in-situ mine rocks.
- c) As dolerite and chert are particularly fine grained, the characteristics of coarse gravel persisted to the fine sand level. With the coarser grained rocks, particles in the coarse sand range and smaller tended to consist of single minerals.

Thin sections are fine slices of rock prepared for viewing and analysis using an optical microscope. First, the selected fragment is sliced at the desired location with a diamond saw, and then ground to a very flat surface. This face is fixed to a glass slide after which the rock is cut again, about a millimetre back from the slide. The resultant wafer of rock is then ground away until about a 20 micron thickness remains on the slide. Finally, the thin section is either finely polished using a variety of diamond pastes (as were those prepared for this project), or topped with a cover slip.

These slides show constituent minerals, and their arrangement within the rock fragment, in greater detail than is possible through hand-specimen examination. For example, a specimen from sample MG9 appeared on visual inspection to be chlorite-mica schist. However, in thin section it was apparent that prior mica had altered during a metamorphic event so that the fragment actually contained chlorite, and chlorite in the shape of mica. (Such occurrence of chlorite, and sometimes mica, in more than one form, was frequently observed.)

Thin sections also display rock structure more vividly, so that variations within a classification become apparent. Plates 4-3 and 4-4

are both mica schists, but while 17Ba shows characteristic preferential grain orientation, in specimen 13b there is also significant lamination, or segregation of constituents into bands. Such a distinction could markedly affect rate of weathering, with the laminated schist likely to degrade more rapidly in the early stages. Plate 4-5 shows a typical pegmatite, with very coarse grains embedded in a finer matrix. Plates 4-6 and 4-7 are respectively massive chlorite rock and dolerite, both massive in structure - randomly arranged grains of similar size - but quite distinct in detail.

Because of the degree of variation, even within a sample, it was most useful to describe structure only broadly, as laminated schistose, schistose, pegmatitic, and massive. Where there was some disparity, classification based on thin sections was preferred to visual inspection in compiling the sample descriptions presented in Section 4.3.

Most of the thin sections showed previous alteration, predominantly chloritisation of the original minerals, but current weathering was also identified in a few cases. As illustrated in Plate 4-8, such weathering is highly localised around a few grain boundaries and involves only a small area in the total section. This is further evidence of the slight mineral decomposition associated to date with the extensive disintegration occurring on the waste-rock batters.

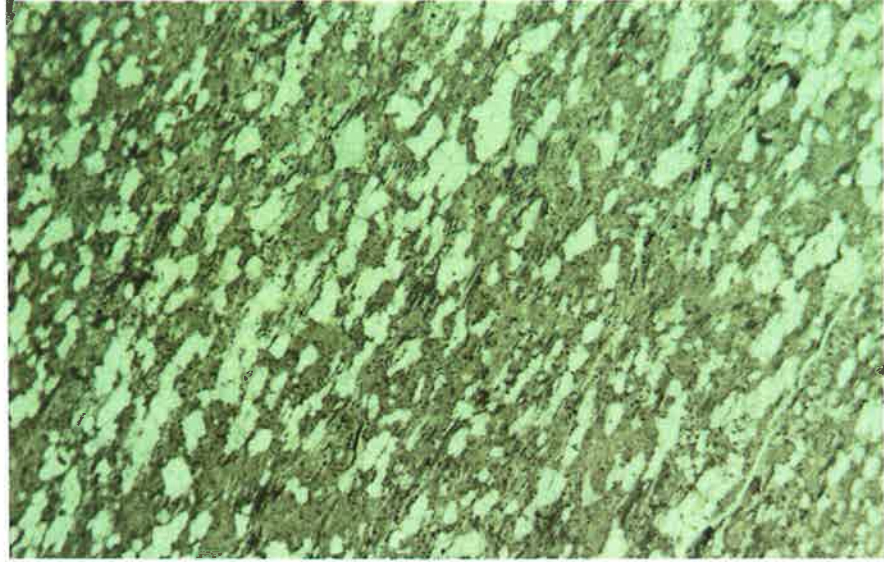


Plate 4-3 Specimen 17Ba (Schist)

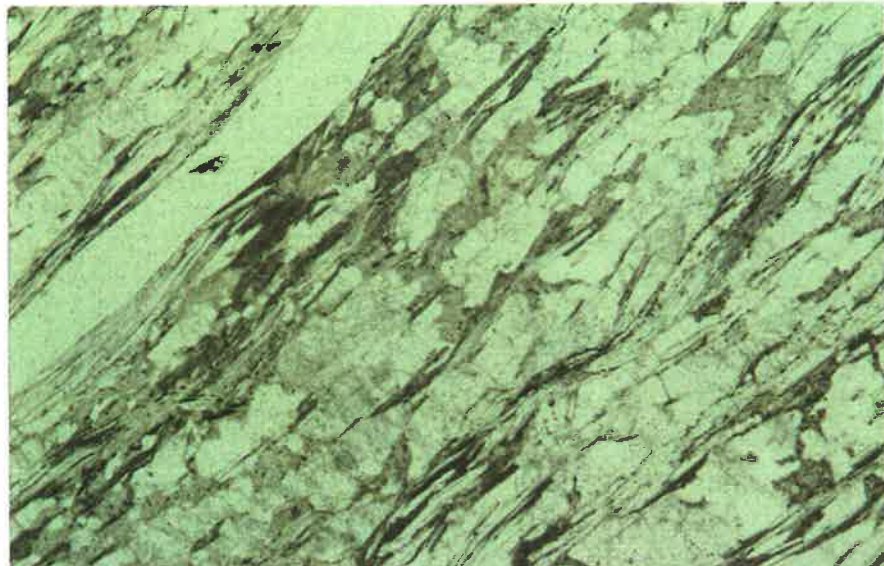


Plate 4-4 Specimen 13b (Schist)

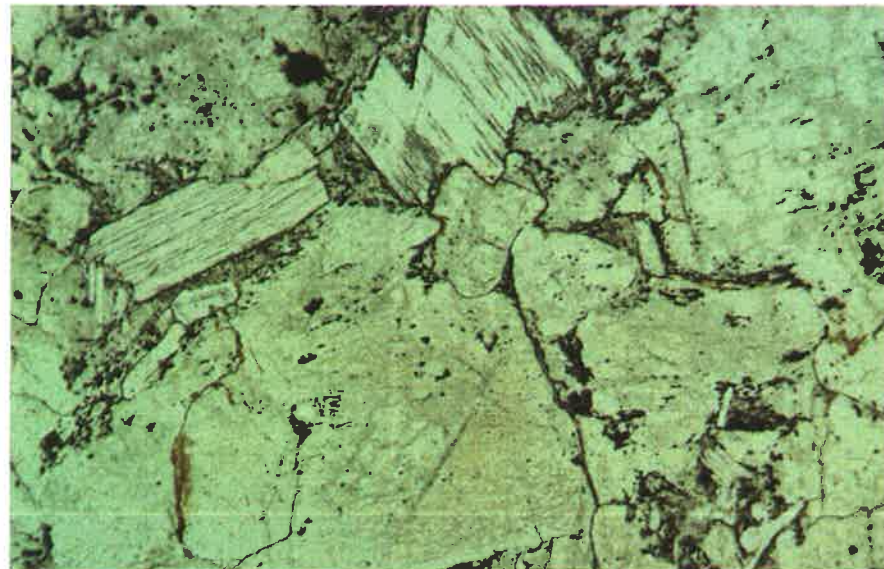


Plate 4-5 Specimen 7Ba (Pegmatite)

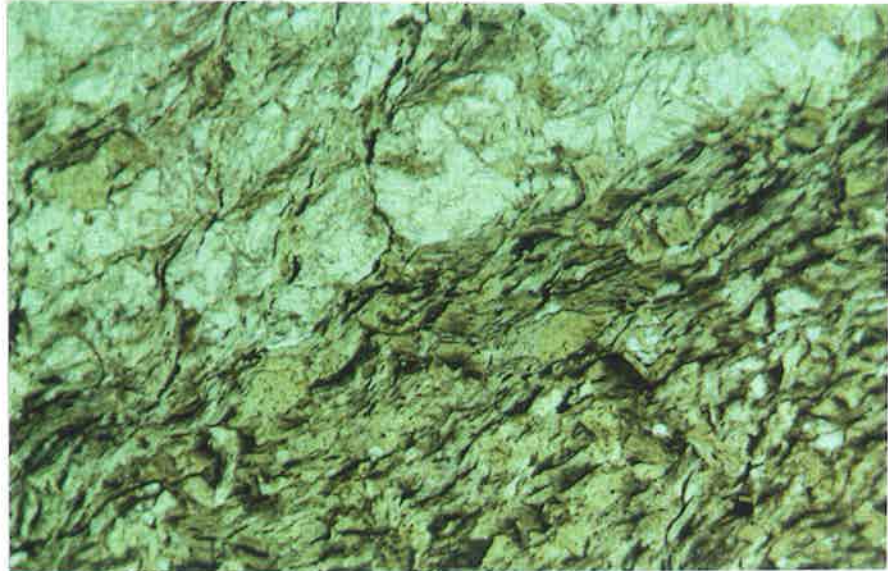


Plate 4-6 Specimen 16 (Massive Chlorite Rock)

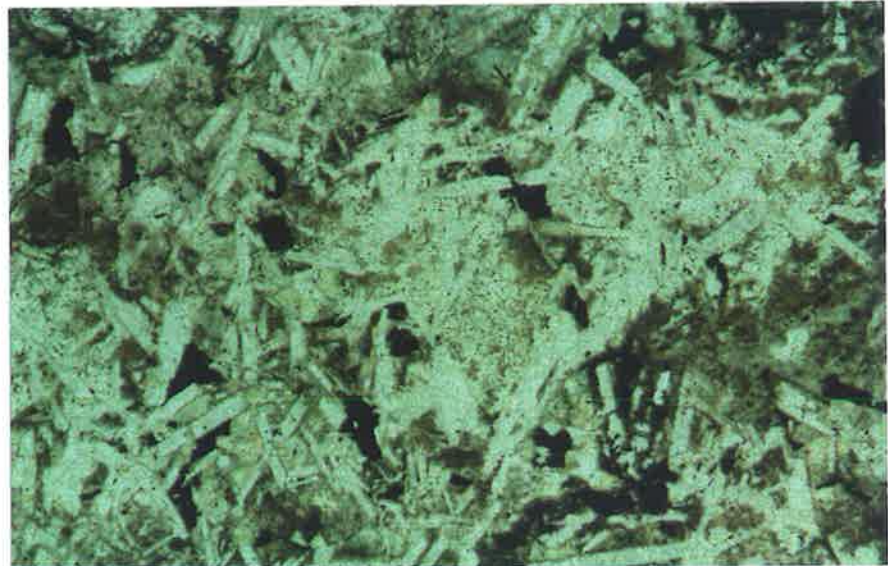


Plate 4-7 Specimen 61 (Dolerite)

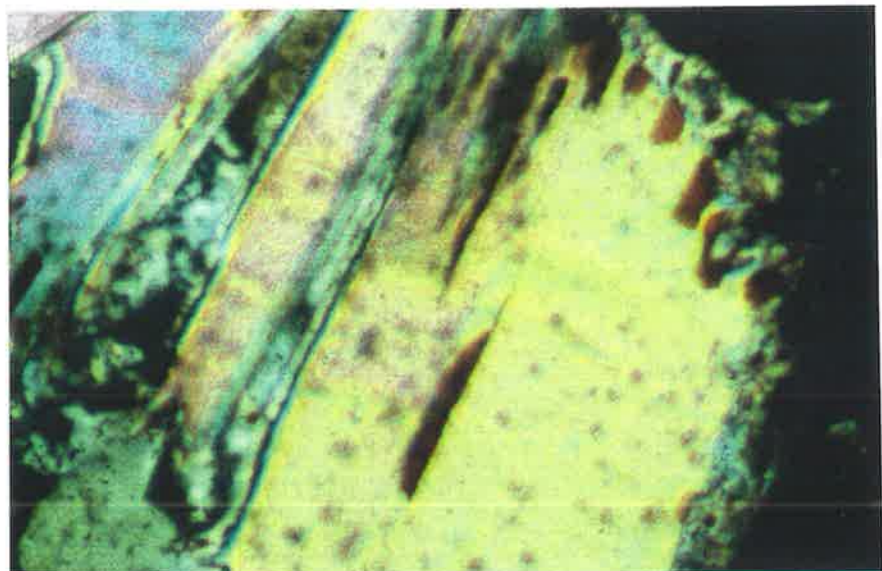


Plate 4-8 Specimen 8a (photographed under polarised light)

As described by Zussman (1967), X-ray diffraction analysis uses the characteristic of an X-ray striking a mineral plane at angle θ to be partly transmitted, and partly diffracted at angle $(\pi - \theta)$. Minerals are composed of regular arrangements of atomic layers, and when the angle of incidence is such that $\sin \theta = \lambda/2d$, (λ = wavelength, d = layer spacing), diffractions from successive layers are in phase and superimpose to maximise the intensity, producing a diffraction peak at angle $(\pi - \theta)$. A second set of layers with different spacing and orientation will produce another peak at a different angle. In a diffractometer, the specimen and a detector are rotated in combination to increment θ , and the pattern of intensity of diffracted rays is recorded. Standard diffraction patterns for pure minerals have been established so that by comparing these to the pattern obtained for a material, as in Figure 4-1, the component minerals can be identified.

As discussed in Section 5.1.1, three rock types were targeted for strength testing, namely schist, pegmatite, and massive chlorite rock. Subsamples of the fragments of these rocks for which thin sections had been prepared were very finely ground, and the resultant powders were pressed into aluminium sample holders. Because of the random orientation of innumerable fine particles thus achieved, fragments of each component in which atomic plates were aligned parallel to the holder base, and which thus contributed to the diffraction pattern, were in proportion to their abundance in the subsample. A specimen of pure quartz was also analysed, and the relative strength of the critical quartz peak in each pattern was used to calculate the percentages of quartz in the ground samples. Because of their fine-grained nature, for schist and massive chlorite rock the percentage was assumed typical of the whole rock fragment, so that referring back to the thin sections, proportions of other major component minerals were then estimated. With the pegmatites, the size of individual grains is such that the subsamples taken randomly for XRD analysis might not be representative of the total fragment. For these four fragments, thin section descriptions were relied on to estimate mineral proportions and XRD patterns were referred to for confirmation of mineral identification.

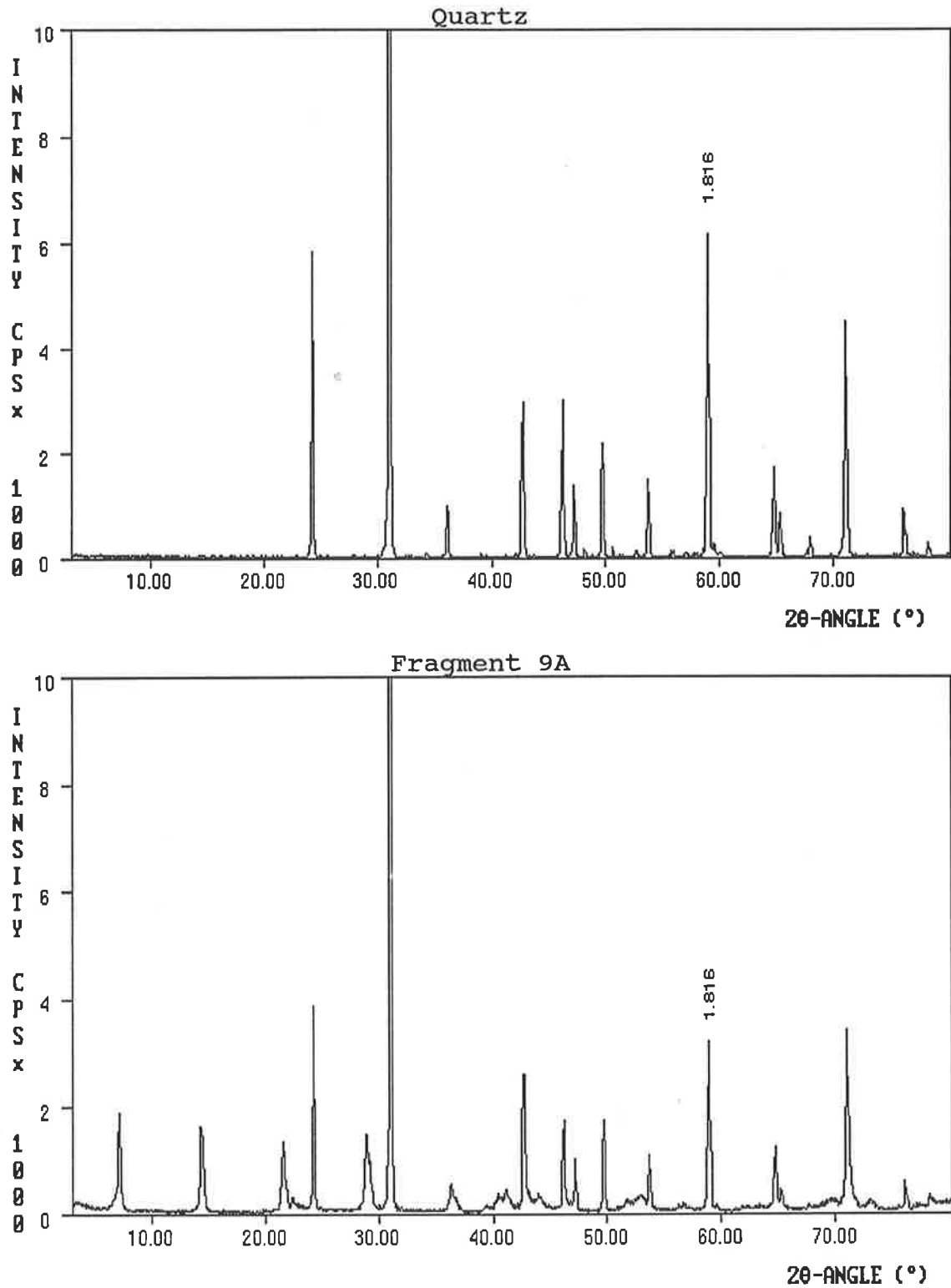


Figure 4-1 Diffraction Patterns for Quartz and Fragment 9A Containing Quartz

Although fragments were not chosen primarily to be representative of the various rock types, the results presented in Table 4-1 show clear trends. For example, the composition of massive chlorite rock fragments is generally consistent at about 14% quartz and 86% chlorite. Schists

clustered loosely around the composition 40% quartz, 25% muscovite, and 35% chlorite. Odd samples with a much lower proportion of muscovite may represent a further degree of alteration than the former - in the thin sections of 9b and 10b chloritised mica was observed with its lath-like mica shape intact. However, the range in quartz content cannot be attributed to alteration and indicates broad variation in both initial and present composition. The four specimens of pegmatite have in common high proportions of chlorite, which comprises the groundmass, or matrix. Considering its manner of formation, no other strong trend in the composition of pegmatite.

ROCK TYPE	FRAGMENT	Estimated Mineral Proportions				
		QUARTZ	MUSCOVITE	CHLORITE	OTHER	
Schist	8a	26	20	54		
	9a	53	≈17	≈30		
	9b	22	≈26	≈52		
	10b	41		59		
	13a	51	30	19		
	13b	56	30	14		
	17Ba	27	23	50		
	19b	45	20	35		
	20	39	30	31		
	21b	53		47		
	JAB200a [#]	38	minor	major		
	JAB200b [#]	31	minor	major	trace [*]	
	JAB200c [#]	61	minor	major	trace [*]	
	JAB200d [#]	22	major	minor	trace [*]	
Massive Chlorite Rock	16	14		86		
	17Aa	11		45	46 ⁺	
	19a	13	1	86	1 [*]	
	21a	14		86		
	JAB201a [#]	trace	minor	dominant	trace [*]	
	JAB201b [#]	45		dominant	trace [*]	
	JAB201c [#]	trace	trace	dominant		
	JAB201d [#]	49	trace	major		
	Pegmatite	7Ab	20	minor	dominant	trace [*]
		7Ba		major	major	trace [*]
8b		trace	trace	90	trace [*]	
12b		40	trace	50	trace ⁻	

(NOTE: dominant=>50%, major=20-50%, minor=5-20%, trace=<5%)

[#] Samples taken from experimental batters (refer Section 5.1.1)

⁺ apatite

^{*} hematite

⁻ tourmaline

Table 4-1 Rock Fragment Composition
(Estimated from Thin Sections and X-ray Diffraction)

CHAPTER FIVE

5. MECHANICAL BEHAVIOUR OF DUMP MATERIALS

5.1 Laboratory Test Programme

5.1.1 Sample Selection

Consideration of the mechanical behaviour of dump material was based around triaxial compression tests on three of the most common rock types in the waste-rock dumps. Although most of the samples collected in June 1989 comprised mixed material (as noted in Section 4.2) it was thought that differentiating between rock types would help in interpretation of the relationships between weathering processes and strength changes. With regard to stability analysis, for a mixed sample, the value of a design parameter such as shear strength should lie between the values for the separate component rocks. Thus the mechanical behaviour of individual rock types provides bounds for the collective dump material.

The three rock types investigated were schist, pegmatite and massive chlorite rock. Based on recent mine cross-sections, it was estimated that of the total material intended to be excavated from Pit No.1, there will be about 40% schist, 25% undifferentiated near-surface weathered material (saprolite), 10% of each chert and massive chlorite rock, and 10% other rock types. As previously noted, chert is frequently directed away from the waste-rock dumps and to the construction stockpiles. Schist, pegmatite and massive chlorite rock are thus the three dominant rock types in the waste-rock dumps. They also cover the ranges of fabric types and mineral compositions significant in the mine rocks. (The Supervising Scientist for the Adelaide Rivers Region selected schist and massive chlorite as typical dump rocks for the experimental batters mentioned in Section 2.3.)

It was observed in Section 3.4 that the dump slopes to date show no tendency to instability or shallowing with age, a sign which would indicate loss of material strength. Further, as discussed in Section 6.1.1, there is little significant change in particle size distribution over the first few years, other than a loss of fines from the surface. Between 3 and 6 years exposure there is obvious breakdown of gravel and larger particles, but even after more than 6 years the production of chemical weathering products is small (refer to Section 4.2). Within this setting, it was decided that three ages were adequate to cover the grades of weathering currently present in the dumps, but that it was

also desirable to obtain material representative of more advanced weathering.

Of the samples already collected, only four met the criteria of predominantly consisting of one of the targeted rock types and of being one of the selected ages. Samples MG15 and MG8 provided pegmatite from 3 and 6 year old slopes respectively, while MG13 and MG9 were both schist exposed for about 6 years. It was initially hoped to combine these schists to increase the mass of sample, but a preliminary check based on compaction tests showed the materials to be quite different in mechanical behaviour, as discussed in Section 5.2.1. Consequently only MG13 was used for a triaxial compression test.

Bulk samples collected from the experimental batters in 1988 provided suitable fresh schist and fresh massive chlorite rock. Additional sampling was carried out in June 1991 to obtain other materials for the test programme. Most were found readily, either on the dumps or elsewhere on site (for example, extremely weathered schist and pegmatite were taken from the upper benches of Pit No.1). The exception was massive chlorite rock, for which the most weathered example discovered was a small zone dumped about 4 years ago, at the top of the batter near Site 19. In addition, two surface soils were sampled, one from the top of an older dump, near Site 8, and the other a heavily leached natural residual soil weathered from Nanambu Complex rock (probably granite). The samples thus used for laboratory strength testing are summarised in Table 5-1.

	Fresh	Exposed 3 years	Exposed 6 years	Extremely Weathered	Soil
Schist	JAB200	JAB200z	MG13 MG9*	RM26	JAB202z (dump)
Pegmatite	RM23	MG15	MG8	RM27A RM27B	RM25 (natural)
Massive Chlorite Rock	JAB201	JAB201z	RM24 [#]		

* compaction test only

[#] exposed about 4 years

Table 5-1 Samples in Testing Programme

5.1.2 Modelling of Grading Curves

A major difficulty in measuring the mechanical behaviour of the dump materials was the large discrepancy between the size of the largest fragments (boulders) and the maximum specimen size for the available triaxial rig. There exist a few large triaxial machines (Marsal et al 1965 and Fumagalli 1969) for testing rockfill specimens containing particles up to about 250mm, but even this is an order of magnitude smaller than the prototype materials. In this project the equipment to hand, and the impracticality of transporting masses of waste-rock from Jabiru to any large test facility, restricted specimen size to 100mm diameter. Maximum particle size was correspondingly limited to 20mm.

As inferred by Marachi, Chan & Seed (1972), experimental investigations into the effect of maximum particle size on measured strength have been inconclusive. In general, it has been found that friction angle is either unchanged or slightly increased with decreasing particle size. However, in most studies maximum particle size was varied through relatively narrow ranges, and diverse approaches were taken to scaling the remainder of the grading curve, so extrapolation to prototype rockfill, much less to boulder fill in general, is uncertain. The problem may be more fundamental than modelling a sample for triaxial testing, and rest in the validity of treating very coarse materials as continua. Unfortunately, as observed by Mitchell (1976, p.135), particulate mechanics has not developed to a stage of practical use for geologic materials, so continuum theories are almost universally accepted. In the project which is the subject of this thesis, the primary interest was in the relative strength of various materials. In this context, it was considered that if the prototype gradings were modelled rationally, with regard to the nature of contributions of various fractions to overall mechanical behaviour, the results would be relevant.

An approach taken by Zeller & Wulliman (1957), was to simply exclude the oversized particles, so that relative proportions of the remaining size fractions were maintained. Alternatively, Lowe (1964) modelled dam embankment material with a laboratory grading curve parallel to that of the prototype (that is, with particles scaled to one-eighth size). Marachi, Chan & Seed (1972), preferred the latter approach, which maintains the shape of the particle size distribution. These studies all

involved rockfills in which the shape and mineralogy of particles, by nature or selection, did not vary greatly with particle size, and which contained minimal proportions of silt and clay.

Neither of these models is suitable when there are significant proportions of the finer fractions - 10% fine silt or clay in a model would not behave like 10% fine sand in the prototype. This was recognised by Gonano, Kirkby & Dight (1978), in an investigation of cemented rockfill, the strength of which was dominated by the fine material. They varied the method of Zeller & Wulliman (1957) by increasing the proportions of sand and gravel to compensate for the excluded coarser fractions, and so keeping the ratio of fines to granular material the same as in the prototype. One reported effect of this was that in-situ void ratios were more easily reproduced in the test specimens. This approach was taken a step further for the dump materials.

As discussed in Section 4.2, in the waste-rock samples, particles throughout the cobble and gravel size range had similar visual and mineralogical characteristics (essentially those of the parent rock), while the sand fractions tended towards single mineral particles. Dump materials were thus considered as comprising three discrete components - gravel and coarser fragments; sand and coarse silt; and fine silt and clay - each with distinct impacts on mechanical behaviour. To maintain the relative contributions of each class, the excluded coarse fractions were replaced in the same class, that is, by fine and medium gravel. Figure 5-1 compares this approach to the three discussed above. In practice, use of this model meant that laboratory specimens were prepared with the same percent passing 2.4mm as the prototype and the proportions of gravel fractions (2.4-4.8mm; 4.8-9.5mm; 9.5-19mm) calculated as follows:

$$M_x = (P_x - P_{2.4}) \cdot (100 - P_{2.4}) \div (P_{19} - P_{2.4}) + P_{2.4}$$

where x = sieve size

M_x = percent retained on sieve x in model

P_x = percent retained on sieve x in prototype

The pit/soil materials consisted of only gravel sized and smaller particles, so prototype gradings were provided by mechanical sieving of the samples as-collected. For the supplementary waste-rock samples, prototype site gradings were inferred for the appropriate ages from the

collated slope particle size distributions (refer Section 3.4). Gradings for the test specimens are included with the triaxial compression results in Appendix C.

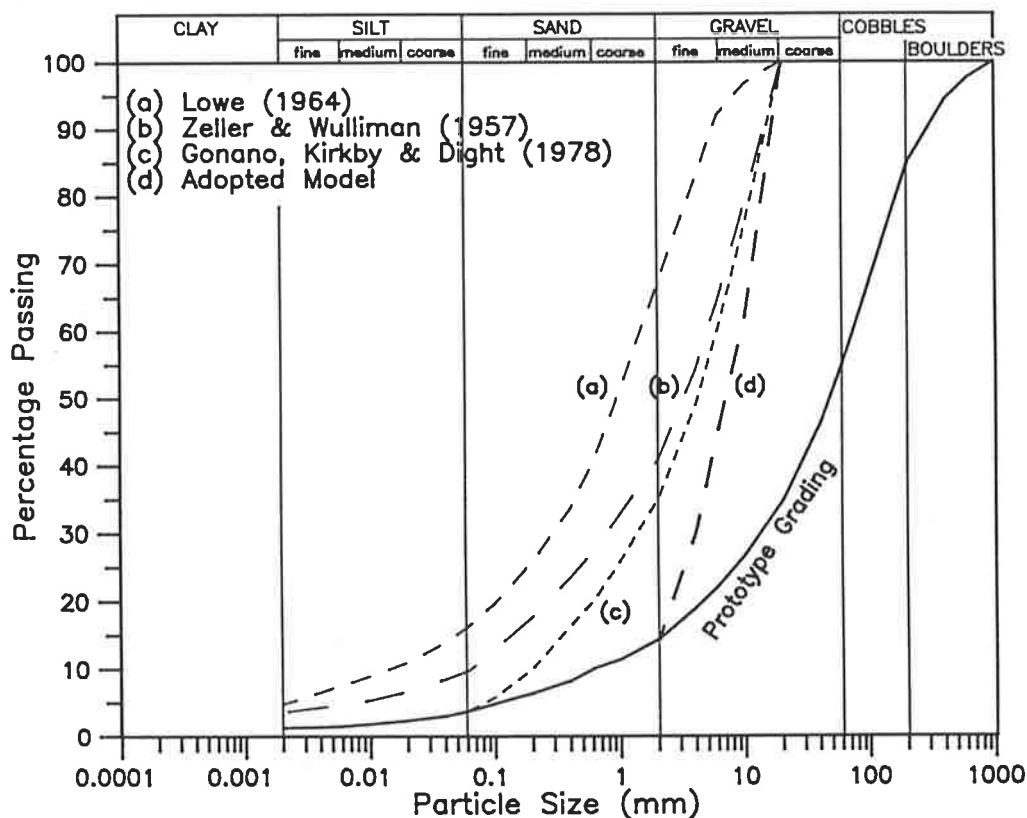


Figure 5-1 Laboratory Modelling of Prototype Grading Curves

5.1.3 Triaxial Test Conditions

Strength tests were carried using a Farnell Triaxial Compression Apparatus (10 ton capacity), with a 1700kPa working pressure cell taking 100mm diameter specimens (refer Plate 5-1). The main test programme consisted of unsaturated undrained triaxial compression tests for which cell pressure, axial load, vertical displacement, and volume change were monitored. Cell pressure was controlled by a pressure regulator and measured using an electronic pressure transducer. Axial load was measured with an electronic linear displacement transducer and a back-up mechanical displacement gauge on the proving ring, and axial displacement with a mechanical displacement gauge only. Sample volume change was determined by monitoring the compensating change in cell fluid volume via a direct volume displacement gauge in the fluid feed system. Initially, a mercury-filled annular meter was used but sudden large fluid inflows twice spilled mercury into the system. The meter was subsequently replaced with a straight gauge utilising dyed kerosene as the indicator fluid (Bishop & Henkel 1962, pp.207-209). Calibrations of

the transducers, proving ring, and cell volume change were carried out before commencement of testing and the resultant calibration curves are included in Appendix D.

As the samples were in a loose cohesionless state, it was necessary to establish consistent procedures and conditions for preparation of the triaxial specimens. In a preliminary investigation of stability of the waste-rock dumps (Richards, Peter & Lucas 1986), a kneading compactor operating at 200kPa pneumatic pressure was used to compact samples of <6mm fractions into a direct shear box for testing. This standard was not suitable for the coarse materials in the current testing programme as the compactor foot was only 17mm square, smaller than the largest included particles. Consequently, it was decided to compact dynamically using a standard 2.7kg rammer. The degraded nature of gravel fragments in the older samples led to concern regarding particle breakage during compaction, and a standard compaction test on a trial sample of waste-rock (containing reasonably sound gravel) produced an increase of about 2% passing each sieve size. After some discussion, a compactive effort of 85% standard (AS 1289.E1.1-1977) was selected, obtained with a rammer drop of 100mm, 5 layers and 38 blows/layer.

A dry density/moisture content curve was produced for each sample (using the model grading) to obtain an optimum moisture content at which to prepare the triaxial specimen. About 3.5 kg of dry material was then wet up and cured for three days before compaction into the 100mm diameter x 200mm high split mould (using 8 layers and 37 blows per layer to achieve 85% standard compaction). The assembled specimen, cell and piston weighed about 20kg and required two people to lift it onto the rig pedestal, and it was found that specimens of the coarse batter material could not be installed without risk of damage. Placing the specimen under a suction to impart temporary apparent cohesion would have been difficult in view of the unsaturated state and the high proportion of free-draining voids. Instead, the specimen, still in the mould, was placed in a freezer overnight, then installed and thawed in the cell under a small lateral pressure for at least twelve hours before the test was commenced. This procedure was in fact carried out for all materials, to buffer the specimen against damage during stripping of the mould and positioning of the cell in the loading apparatus. Because of the open fabric of most of the materials and the generally low water contents

(<15%), there was no observable expansion of the specimens during freezing, and the treatment was not thought to have affected mechanical behaviour during testing.

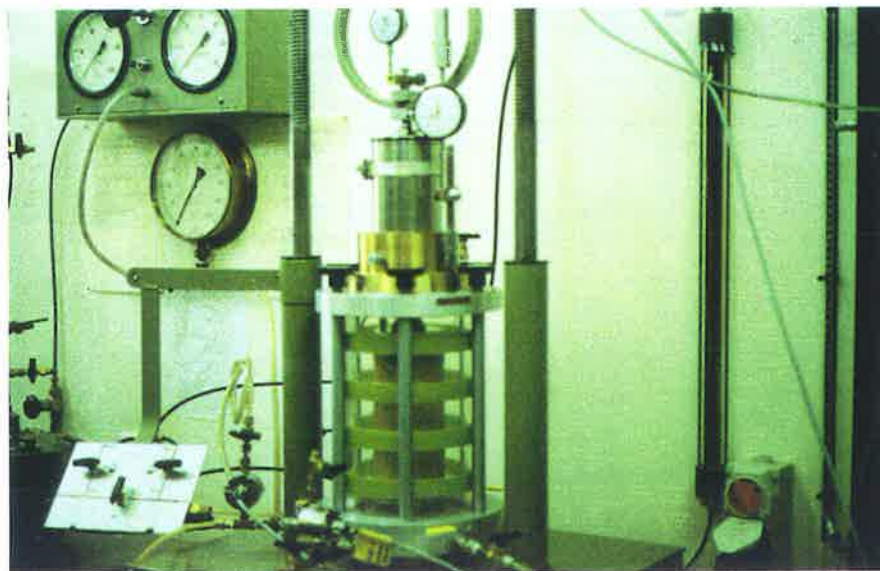


Plate 5-1 Triaxial Compression Test Apparatus

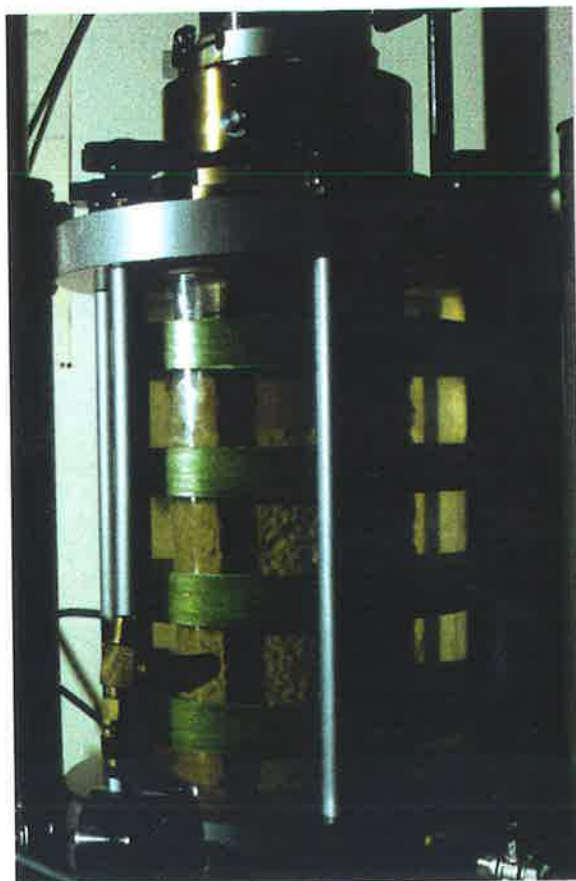


Plate 5-2 Test on Coarse Sample Showing Membrane Deformation

After initial compression for at least 12 hours under 50kPa global cell pressure, an undrained triaxial compression test was performed. A strain rate of 0.11mm/min was selected to achieve failure within a reasonable time (1-2 hours per stage), while providing sufficient time to take readings and to back off the load at failure before the specimen collapsed. Tests were staged by applying constant cell pressure and then straining the specimen axially. When maximum principal stress was obtained (or was imminent), axial load was reduced and cell pressure incremented to commence the next stage.

Based on analysis carried out for a preliminary investigation in 1986, horizontal stresses up to the order of the overburden pressure are anticipated in the middle of the waste-rock dumps, with stresses decreasing somewhat towards the batter faces (Richards 1986). For a final dump height of 30m, this corresponds to a maximum of about 500kPa total stress in horizontal and vertical directions. Within this range, cell pressures of 50, 100, 200, and 400kPa were initially selected for the four test stages. However, problems were experienced with the coarser graded samples, with the membrane being pushed into surface voids as cell pressure was increased, as apparent in Plate 5-2. After two membranes were punctured on the fourth stage (causing the sudden volume changes and mercury spills mentioned above), tests on batter specimens were altered to three stages up to 300kPa cell pressure.

During a test, transducers were read at generally three minute intervals. Data was entered immediately into a computer spreadsheet which calculated corrected area (taking account of both axial and volume strains) and displayed a progressive stress-strain plot. This was sufficient to decide when to terminate a stage and back off the axial load, thus keeping the sample intact for the next stage. The system would not be satisfactory for sensitive or strain-softening materials, but all specimens in this programme were robust with regard to limited straining beyond failure, and did not exhibit rapid changes in behaviour.

The density and moisture standard described above was selected as representative of long term conditions in the bulk of the waste-rock dumps. It is foreseeable that for short durations or in limited areas, the dumps could become significantly wetter (for example, during a

severe wet season). Such occurrences are not relevant with respect to weathering and long term strength but they may affect short term stability, and so are applicable in detailed dump and landform design. In recognition of this, Richards, Peter & Lucas (1986) performed a series of direct shear tests on saturated samples. A similar procedure for undrained triaxial compression testing was adopted in the current project for two illustrative samples (MG15 and JAB202z). Specimens were prepared and installed in the rig as previously described. After thawing under 10kPa cell pressure (with no applied pore pressure), cell pressure and pore pressure were increased concurrently up to 100kPa and 90kPa respectively, and then later (after one day for MG15 and four days for JAB202z) to 300kPa and 250kPa. Pore pressure was applied at the base of the specimen, using de-aired water, and a drainage outlet at the top was opened intermittently to release undissolved air. After a further 3-4 days no further air was expelled and cell and pore pressures were reduced to 100kPa and 50kPa respectively, to commence the first load stage of the test.

At the commencement of each stage, pore pressure was brought to 50kPa and cell pressure to a value selected to correspond with the stages used in the unsaturated tests (100, 170, and 350kPa for MG15 and 100, 150, 250, and 450kPa for JAB202z). The pore pressure valve was then locked off and the stage was performed under constant total lateral stress (pore pressure), with pore pressure monitored throughout. Specimen MG15 was loaded at an axial strain rate of 0.05mm/min, while for JAB202z, which was a finer material but still reasonably permeable, the rate was reduced to 0.028mm/min.

5.2 Results and Discussion

5.2.1 Compaction Tests

Although conducted primarily to establish conditions for triaxial compression testing, the compaction test results provided a first indication of the change in mechanical behaviour as mine-rocks weather. Figure 5-2 summarises maximum dry density and optimum moisture content for the fifteen samples. The scatter in results for materials up to 4 years old is largely testing error due to the difficulty in working and trimming samples with such high proportions of medium gravel. Despite this it is clear that, whereas maximum dry density shows little trend with age, optimum moisture content increases markedly. This increase is actually a secondary correlation. Optimum moisture content is affected most directly by changes in grading (in particular, in percentage clay), and these are the specific result of the weathering process. There was no obvious differentiation between rock types, although with a limited number of samples the apparent homogeneity was not conclusive.

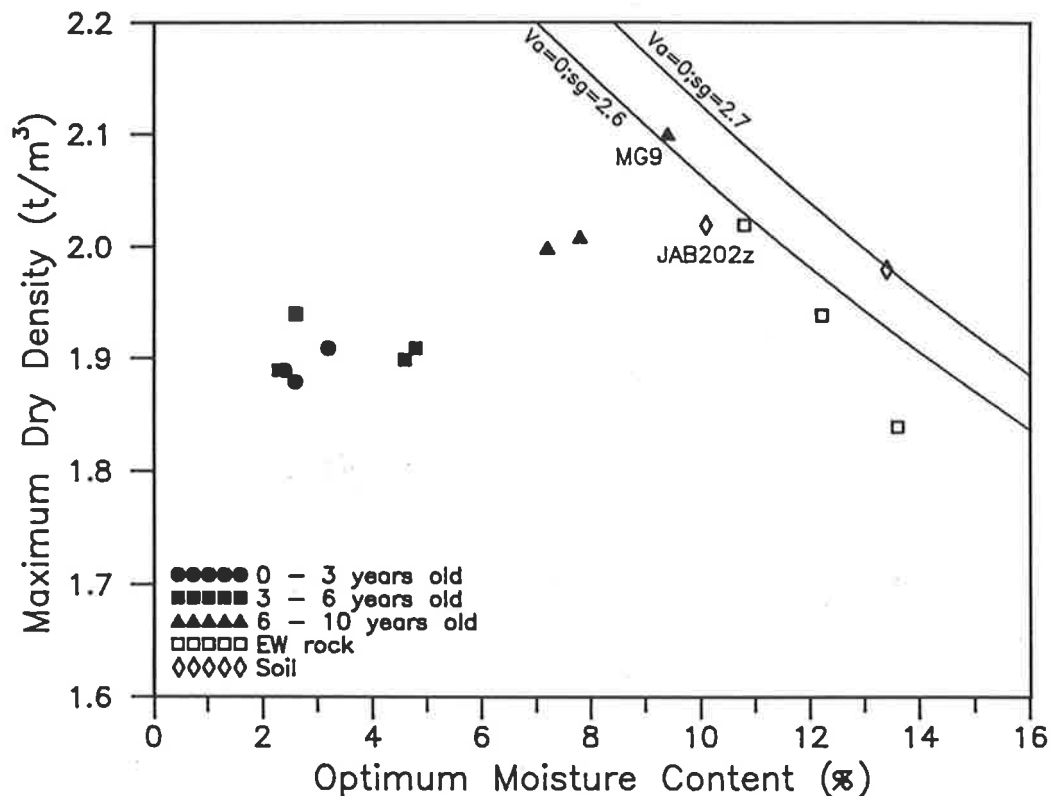


Figure 5-2 Results of 85% Standard Compaction Tests

Samples MG13 and MG9 were both schists about 6 years old, but which gave quite different results. The optimum moisture content for MG9 was about 2 percent higher than for the other batter samples (closer to the

pit/soil samples), and the maximum dry density was markedly higher than any other result. As noted in Section 4.3, rock fragments in MG9 had an unusual fabric indicative of extensive deformation and also contained an unspecified heavy mineral. Although the particle size distribution for Site 9 (refer Appendix B) was reasonably consistent with others of similar age, it was apparent that sample MG9 was not a typical waste-rock and, as there was insufficient sample to test separately, it was not included in the triaxial compression test programme.

The result for dump soil is also notable. Sample JAB202z was collected in 1991 from the top of a dump lift which was then about 8 years old. With an optimum moisture of 10%, it is closer in behaviour to the naturally weathered pit samples (RM26, RM27A, and RM27B), than the 6 to 7 year-old dump slope samples which were collected nearby. As outlined in Section 2.3, soil is formed on top of the dumps more rapidly than on the slopes. It follows that age of a dump terrace soil is not directly comparable to period of exposure on the slope faces (which is the time scale generally used in this thesis).

Another point of interest is the absolute location of the younger samples (less than 4 years) on Figure 5-2, and the implication with respect to specimen structure. For natural and engineered soils, maximum dry density is usually achieved with about 5% air by volume, calculated from the equation:

$$V_a = 100 [1 - \rho_d (1/\rho_s + w/100)] \quad (\text{AS 1289.A1-1983})$$

where V_a = percentage air by volume
 ρ_d = dry density
 ρ_s = soil particle density
 w = water content

From the data in Figure 5-2 it was inferred that the younger waste-rocks either compact to a much higher voids volume than is common, or have a soil particle density less than 2.2t/m^3 . Subsequently, soil particle density (or specific gravity) was determined for each material and, with the exceptions of RM27B ($\rho_s = 2.69\text{t/m}^3$) and RM25 ($\rho_s = 2.85\text{t/m}^3$ due to inclusion of ironstone gravel), values ranged from 2.7 to 2.8t/m^3 . These results were subsequently used to calculate volume of air at maximum dry density, which is plotted against slope age and weathering in Figure 5-3.

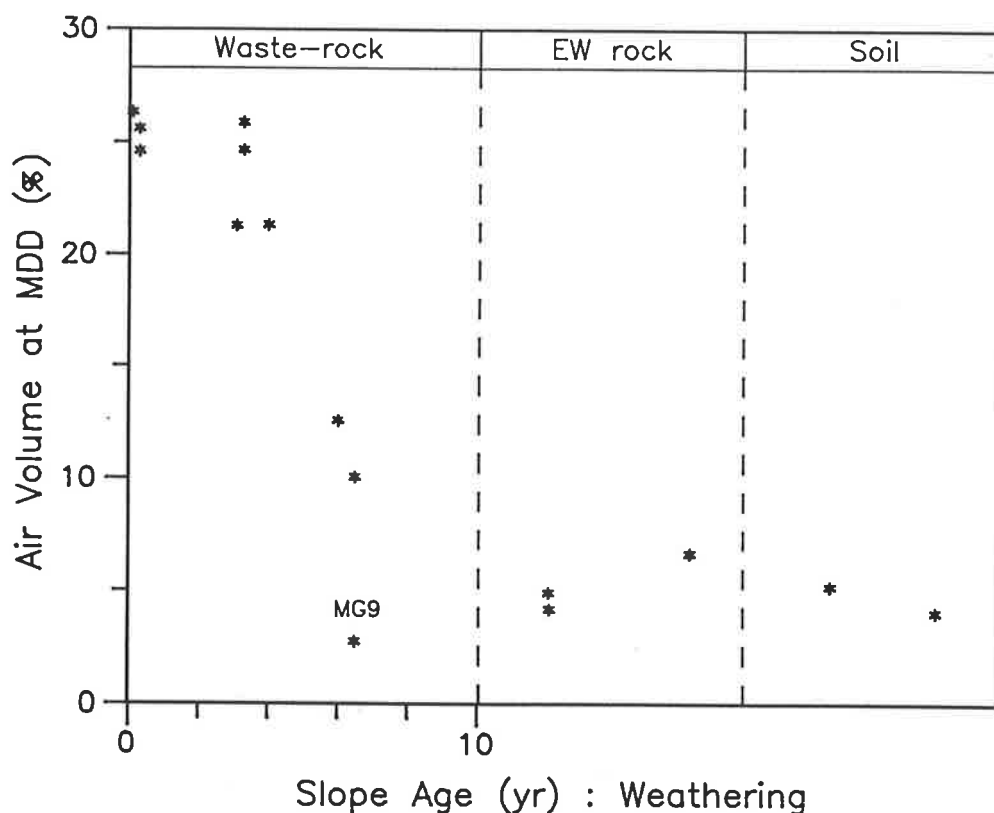


Figure 5-3 Air Voids in Compacted Samples

The volume of air is very high in the younger batter samples, and only reduces to "typical" levels for the extremely weathered rocks and mine soils. (Sample MG9 is again anomalous, with less than 3% air at optimum moisture content.) As with optimum moisture content, this correlation with age is again secondary, with void volume being more directly related to the shape of the grading curve: in the waste-rock samples there is simply insufficient fine material to fill the spaces between the coarser gravel fragments. Although no data have been collected for the waste-rock dumps at Ranger Mines, air voids volumes of the order of 30% have been reported for modelled rockfill (Zeller & Wulliman 1957 and Marsal et al 1965). Thus the selected standard for compaction of triaxial samples produced a material structure which is reasonable in the context of the waste-rock dumps.

5.2.2 Triaxial Compression Tests

Shear strength parameters obtained from the unsaturated undrained triaxial compression tests are summarised in Table 5-2, and stress-strain and Mohr circle plots are included in Appendix C. A striking feature of the data is that all tests gave non-zero shear axis intercept (normally termed cohesion), even those on cohesionless fresh gravels

such as RM23 and JAB200. This effect has previously been noted for rockfill, for example by Zeller & Wulliman (1957), who suggested that it was probably due to particle interlock. Several other researchers, including Becker, Chan & Seed (1972), Leps (1970), and Marachi, Chan & Seed (1972), preferred to maintain cohesion intercept as zero and to accept friction angle as variable (that is, ϕ equal to the slope of the line passing through the origin and tangential to the particular Mohr circle, rather than equal to the slope of the line enclosing all the Mohr circles). That approach was not used in the current project because there was no obvious advantage in replacing the usual shear strength equation, $\tau = c + \sigma \tan \phi$ where c and ϕ are constant, by two equations, $\phi = f(\sigma)$; $\tau = \sigma \tan \phi$. Also, the more weathered samples such as RM25 and RM26 display cohesion in the normal sense, and in a comparative study it is logical to maintain consistent shear strength parameters.

SAMPLE	AGE (yr)	PEAK		POST-FAILURE		Elastic Modulus E (kPa 10^3)
		Shear Intercept c (kPa)	Friction Angle ϕ ($^\circ$)	Shear Intercept c_r (kPa)	Friction Angle ϕ_r ($^\circ$)	
MG8	6.0	39	27.8	33	25.1	79 - 134
MG13	6.5	43	33.2	35	28.7	133 - 173
MG15	3.1	39	30.3	31	27.1	72 - 154
JAB200	0.3	58	31.6	43	28.4	163 - 175
JAB201	0.3	59	29.8	49	26.6	220 - 233
JAB200z	3.3	70	34.8	54	29.9	199 - 236
JAB201z	3.3	51	31.4	41	27.7	145 - 223
RM23	0.0	64	31.3	51	27.7	191 - 393
RM24	4.0	65	32.2	51	28.3	193 - 196
RM26	EW Rock	59	22.1	53	20.8	37 - 110
RM27A	EW Rock	74	22.4	65	21.2	48 - 160
RM27B	EW Rock	103	11.9	99	11.9	20 - 89
JAB202z	Dump Soil	84	19.0	77	18.3	76 - 127
RM25	Mine Soil	85	26.4	72	24.3	121 - 190

Table 5-2 Summary of Triaxial Compression Test Results

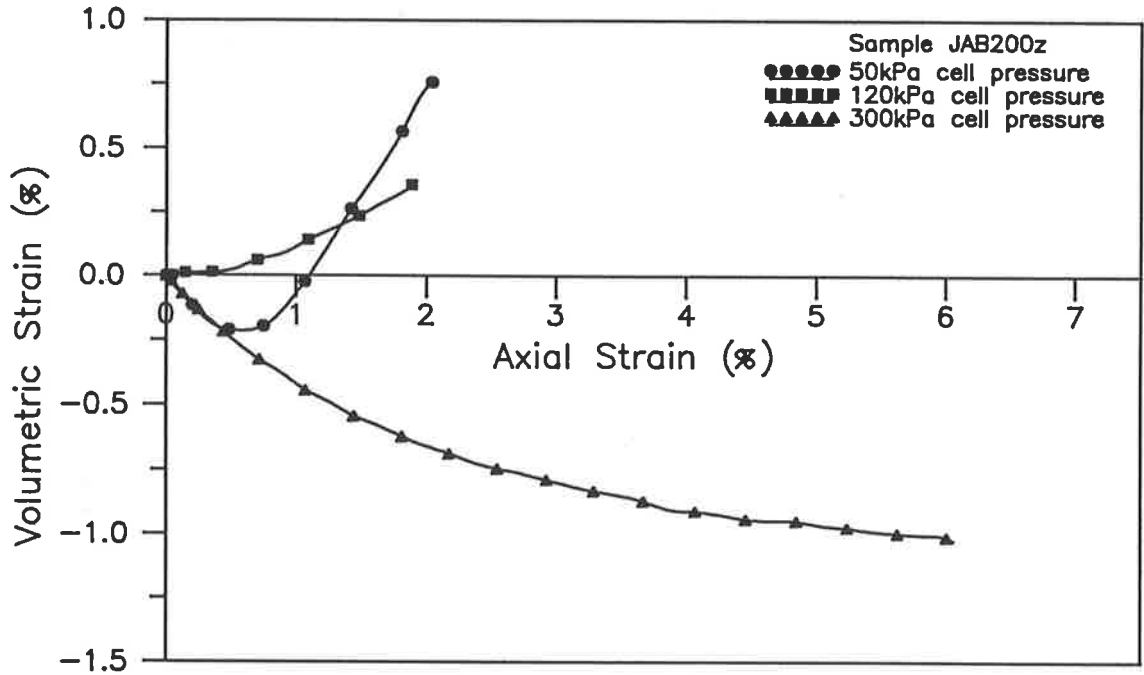
The post-failure values, c_r and ϕ_r , listed in Table 5-2 were estimated according to a non-associated flow rule (Davis 1968) for the line through the points of maximum shear stress on the Mohr circles. This is in contrast to the usual method of measuring residual strength obtained at large strain, since in a staged test only the final stage can be continued very far past peak strength conditions. These parameters have been included primarily because they were used to model post peak load-deformation behaviour in finite element analysis of slope stability, described in Chapter 7.

In the previous study of slope stability, Richards, Peter & Lucas (1986), obtained values of $c = 60\text{kPa}$; $\phi = 29.5^\circ$ from direct shear tests on a sample prepared to similar moisture and density conditions. Considering that that material, although exposed for only about 3 years, was taken from a dump platform and that particles larger than 6mm were removed (both of which produce an increase in the proportion of fines relative to a material of the same age on a batter face), the agreement between results is excellent. Because of the different parameterisation of shear strength mentioned above, many of the published values of friction angle for rockfill are not directly comparable with the current results. However, calculating back from stress-ratio/strain plots provided by Marachi, Chan and Seed (1972), original Mohr circles were estimated, which gave failure envelopes described by $c = 280\text{kPa}$; $\phi = 34.5^\circ$ for Pyramid Dam rockfill (blasted argillite), and $c = 260\text{kPa}$; $\phi = 37.8^\circ$ for Oroville Dam fill (rounded meta-volcanic cobble). Zeller & Wulliman (1957) reported $c = 50\text{kPa}$; $\phi = 38^\circ$ for natural scree. In view of the softer, more weatherable (and more weathered) nature of the Ranger Mines dump materials, the results obtained are in reasonable accord with published data.

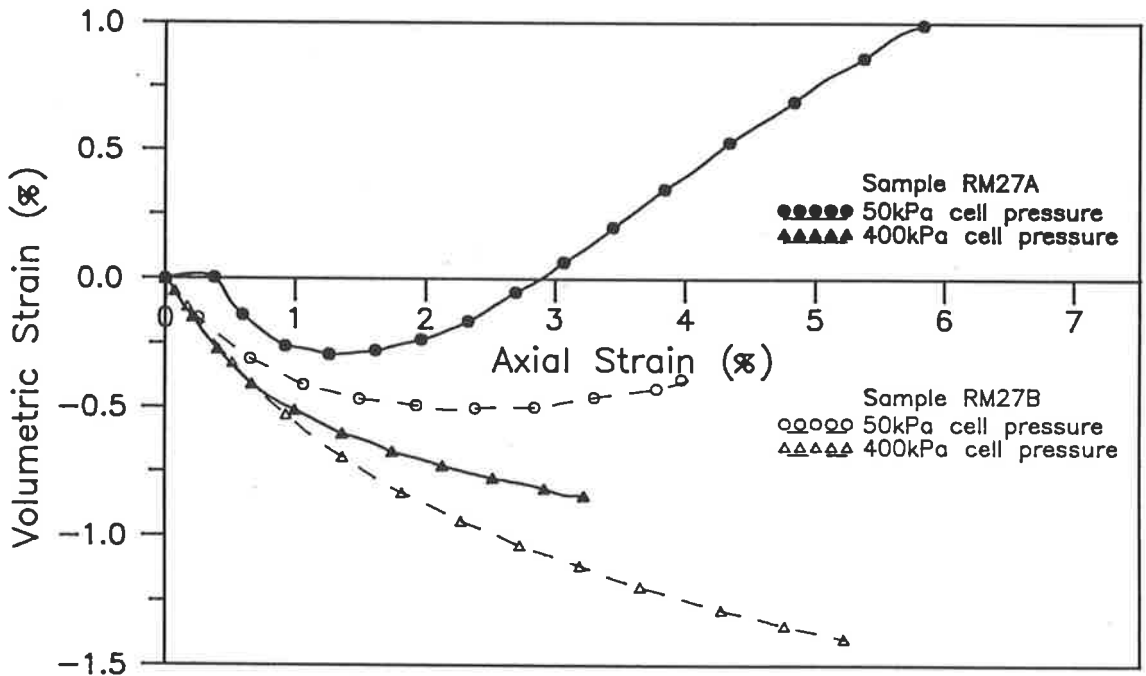
Values for elastic modulus given in Table 5-2 were estimated from readings which bracketed the previous maximum load, for the second and final stages respectively. The first stage was omitted, as the typical slower build up of axial load was thought to reflect the top platen bedding in, rather than legitimate load-deformation behaviour. (Note in Appendix C the stiffer first stage response of MG13 which was restarted after rig breakdown.) The range of E for each sample was relatively small, generally less than a factor of 3, indicating that parameters for normal (as opposed to shear) deformation are not strongly stress-dependent. Viewing the results together, there is a marked tendency for stiffness to decrease with age and weathering.

Volumetric strain was calculated in the test spreadsheet primarily to determine corrected loaded area. As illustrated in Figure 5-4(a), specimens of fresher material, in particular, experienced dilation at failure under low cell pressures and compression at higher pressures, replicating typical results on modelled rockfill (eg. Marachi, Chan, & Seed 1972; Zeller & Wulliman 1957). The behaviour is similar to that for other cohesionless soils which dilate or compress when in dense or loose

states respectively (Mitchell 1976, p.290). Dilation is also characteristic of overconsolidated clays (Lambe & Whitman 1969, pp.301-302). Dilation was displayed to some extent by even the weathered samples, (for examples, see Figure 5-4(b)), although in RM27B it was only a slight trend at the end of the first test stage.



(a)



(b)

Figure 5-4 Volumetric Strain During Triaxial Compression Tests



Plate 5-3 Triaxial Specimen of RM27A after Testing



Plate 5-4 Triaxial Specimen of RM26 after Testing

Axial stress-strain behaviour followed a concurrent trend, as seen in the plots in Appendix C. With the coarsely graded materials, at low cell pressures, peak axial load tended to be reached rapidly and then begin to reduce (at which point unloading was commenced). At other stages, and for the more weathered samples, failure was noticeably plastic, with axial load continuing to increase slowly up to significant strain. The non-cohesive samples could not be removed from the cell intact, but Plates 5-3 and 5-4 of extremely weathered rock are good examples of the final stage failures, showing the barrelled shaped and lack of strongly developed shear planes. In Plate 5-4, some of the compaction layers can

also be detected, but these had no apparent effect on specimen behaviour.

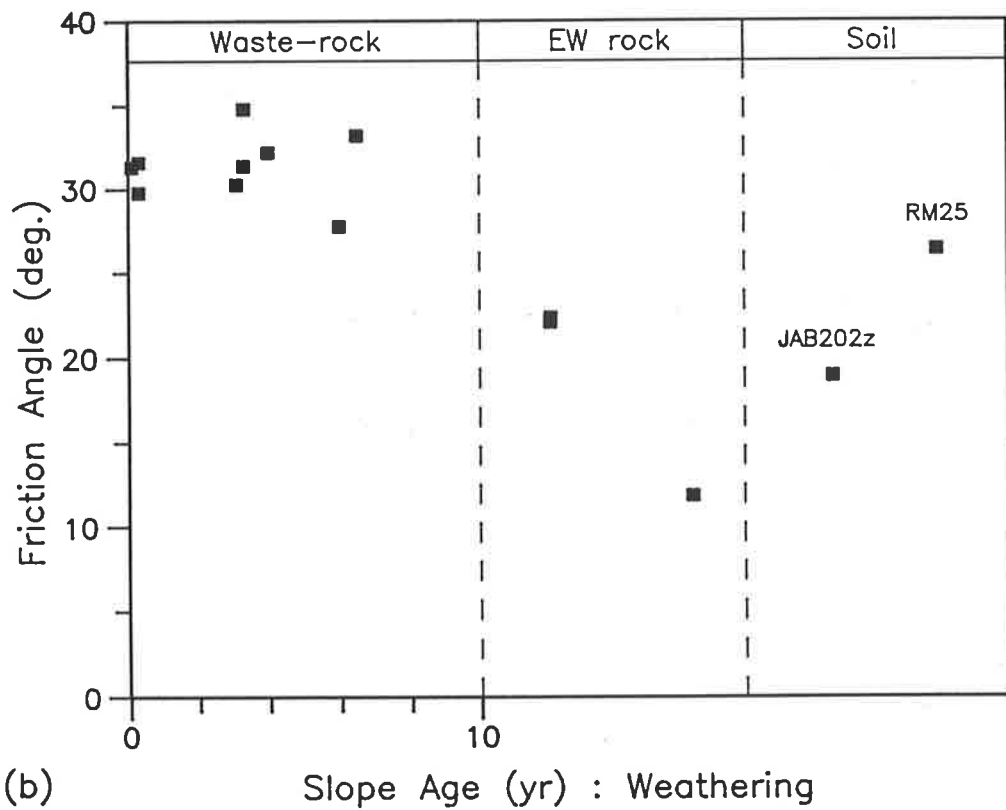
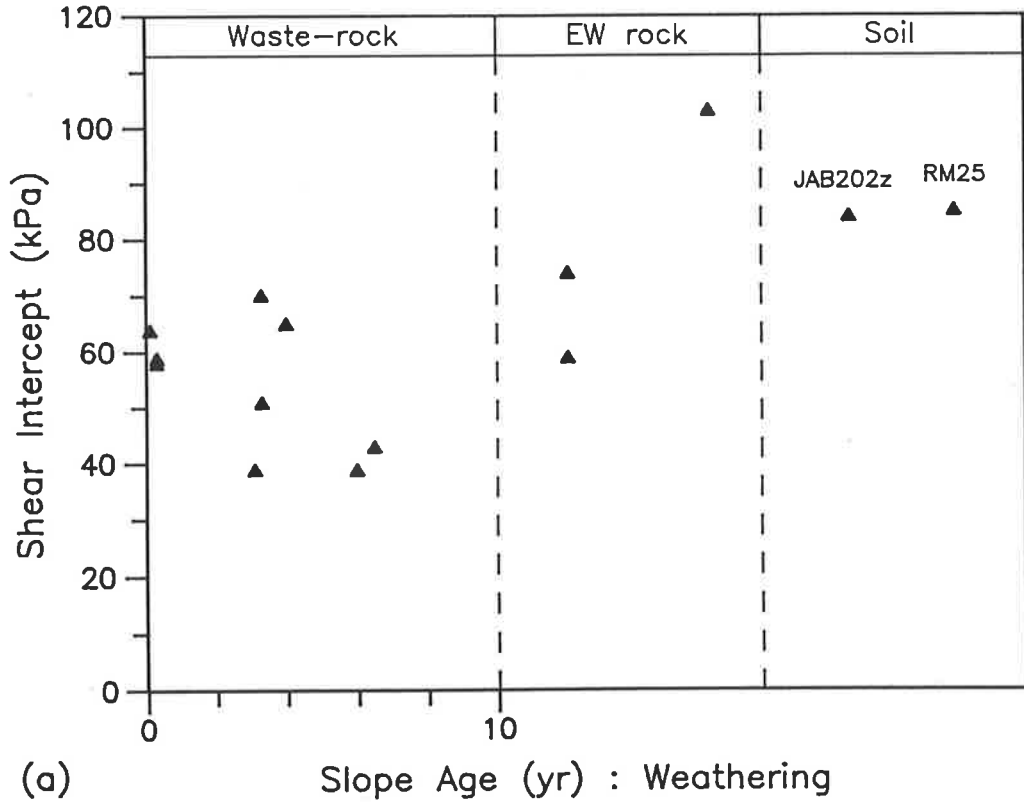


Figure 5-5 Effect of Age/Weathering on Shear Strength Parameters

To preview the relationship between strength and weathering, Figure 5-5(a) & (b) present, respectively, c and ϕ against slope age. Within a broad scatter, shear strength intercept increases somewhat with age. The corresponding reduction in ϕ is more clearly defined (Figure 5-5(b)), but although the values fall in a tighter band, in high stress fields small variations in ϕ imply large differences in strength.

Because the conflicting trends in the components of shear strength confuse the effect of age on strength, the net value of shear strength at a moderate normal stress ($\tau_{300} = c + 300 \tan \phi$), was also examined. From Figure 5-6, it is obvious that for much of the stress range expected in the waste-rock dumps, the gain in cohesion as the materials degrade and weather does not compensate for the loss in frictional strength. (Note that RM27B, the weakest specimen, had the highest value of cohesion). The scatter in results makes any trend inconclusive for less than 4 years exposure - there may be either a small loss or gain in strength over this period - but by 6 years exposure shear strength is clearly decreasing. In these results, there is no apparent distinction between rock types. This may be because, during the early stages of weathering, natural variation has obscured any trends within the limited number of tests, or because the effect of fractures and stress concentrations imposed by mining operations overrides natural material differences.

The two soil samples are also interesting. As previously noted, the dump soil was developed on a terrace level and had been exposed for about 8 years when sampled. From Figure 5-6, the mechanical behaviour of JAB202z is closer to that of the extremely weathered rock sampled from the mine pit than of the material from the 6 to 7 year old dump slopes. RM25, as a natural near-surface minesoil, had been exposed longer than any other material sampled, but its shear strength was greater than any of the pit/soil samples. From Figure 5-5, its cohesion intercept was slightly higher, and its friction angle slightly lower, than the 6-7 year old dump samples. The apparently anomalous behaviour of the two soil samples indicated that duration of exposure is not a sufficiently discriminating parameter with which to measure degree of weathering. Attempts to define more suitable descriptors are discussed in the following chapter. It may be noted in passing that, if RM25 is typical of soils surfacing the natural landscape within Ranger Project Area, the present angle of

stable natural slopes may not be a good basis for the design of rehabilitated landforms constructed from possibly weaker dump material.

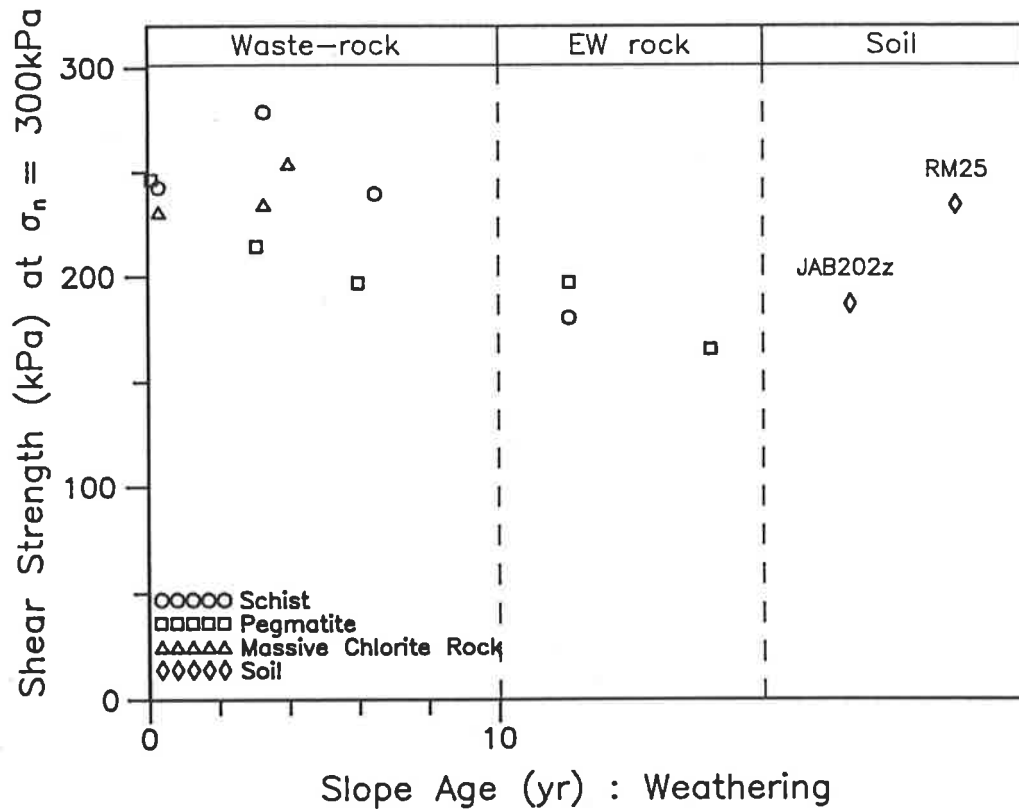


Figure 5-6 Effect of Age/Weathering on Shear Strength

Results from the two saturated triaxial compression tests are also included in Appendix C. Resultant effective stress parameters were $\phi' = 29.6^\circ$, $c' = 70\text{kPa}$ for MG15 and $\phi' = 26.6^\circ$, $c' = 27\text{kPa}$ for JAB202z. These two tests were carried out only to illustrate the magnitude of strength parameters for saturated dump materials. Any saturation in the waste-rock dumps would be transient, and so unrelated to weathering or general long-term stability. Even in the short term it is unlikely that a dump could become fully saturated, and to assume so would be an unrealistically harsh design condition. Such detailed design is beyond the scope of this thesis.

CHAPTER SIX

6. CHARACTERISATION OF WEATHERING

6.1 Grading Trends

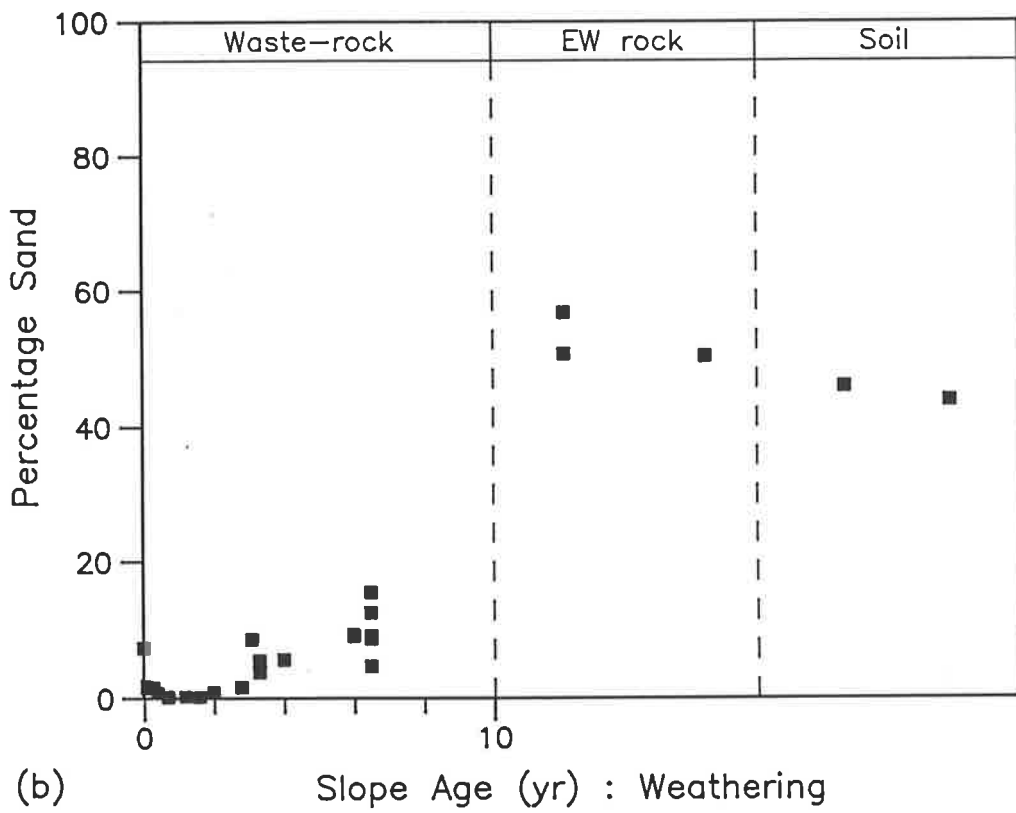
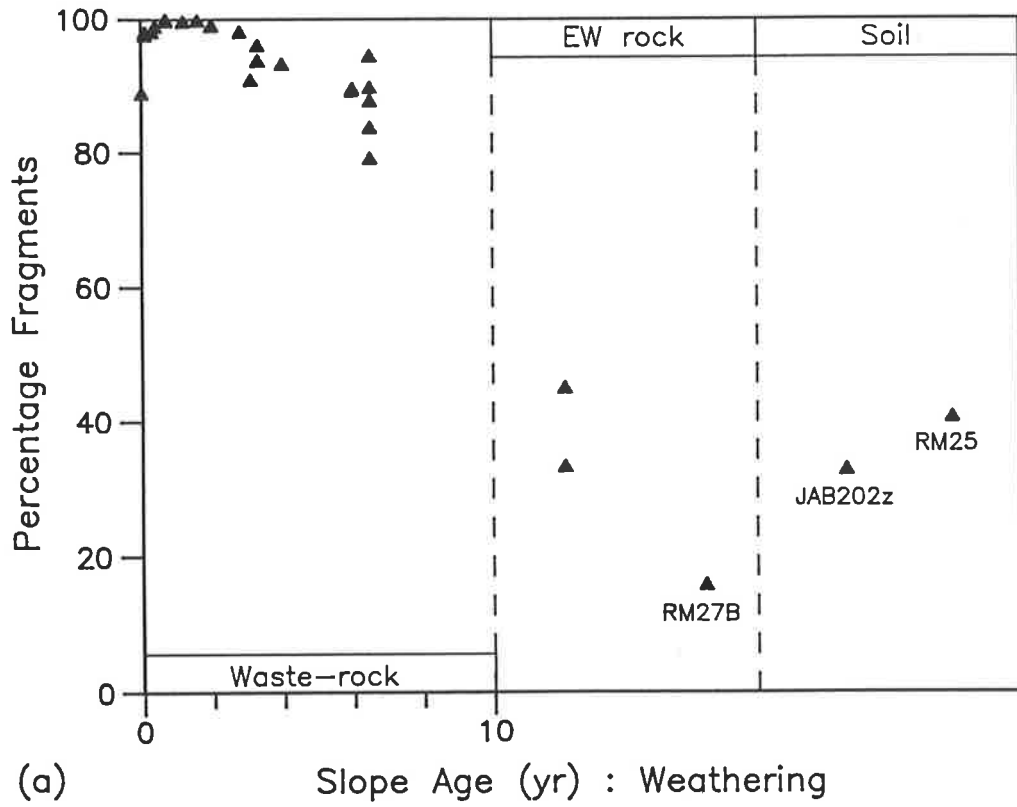
6.1.1 Correlation with Age

It was observed in Section 5.2.2 that although various aspects of mechanical behaviour showed broad trends with slope age, the correlations were indirect and some were not well-defined (for example, Figure 5-4(a)). In addition, slope age is not applicable as a quantitative measure for the pit/soil samples. It was repeatedly observed throughout the project that, to date, weathering in the waste-rock samples is manifest predominantly as disintegration. In spite of the active processes being those of chemical weathering, decomposition was barely detectable except in the oldest batter samples. (Of course, decomposition was significant in the pit/soil materials.) Consequently, physical descriptions of the collected samples were now re-examined in the context of material strength.

In Figure 6-1, site grading data (detailed in Appendix B) are expressed as proportions of the major particle size classifications. With regard to the dump batter materials, those up to 2 years old were composed almost entirely of coarse fragments (boulders, cobbles, and gravel) after which there was a general decrease in coarse fragments with age. Sand content shows a reverse trend, with the initial small proportion quickly depleted and beginning to re-accumulate after about 2 years. There is significant scatter in the age trends for both fractions but strong correlation between the fractions. Silt follows a similar trend to the sand fraction on a diminished scale: production of silt from weathering was not apparent until after about 3 years and at 6.5 years the proportion was still less than 5%. Clay content was minimal until after 5 years exposure on the dump batters.

Taking the batter samples in overview, it may be inferred that disintegration occurs predominantly as the breaking down of coarse fragments into smaller fragments and sand-sized particles. Generation of silt and, in particular, clay follows the increase in sand content which suggests that particles in these size ranges result primarily from disintegration and decomposition of the sand fraction.

Figure 6-1 Variation of Particle Size Fractions with Age/Weathering



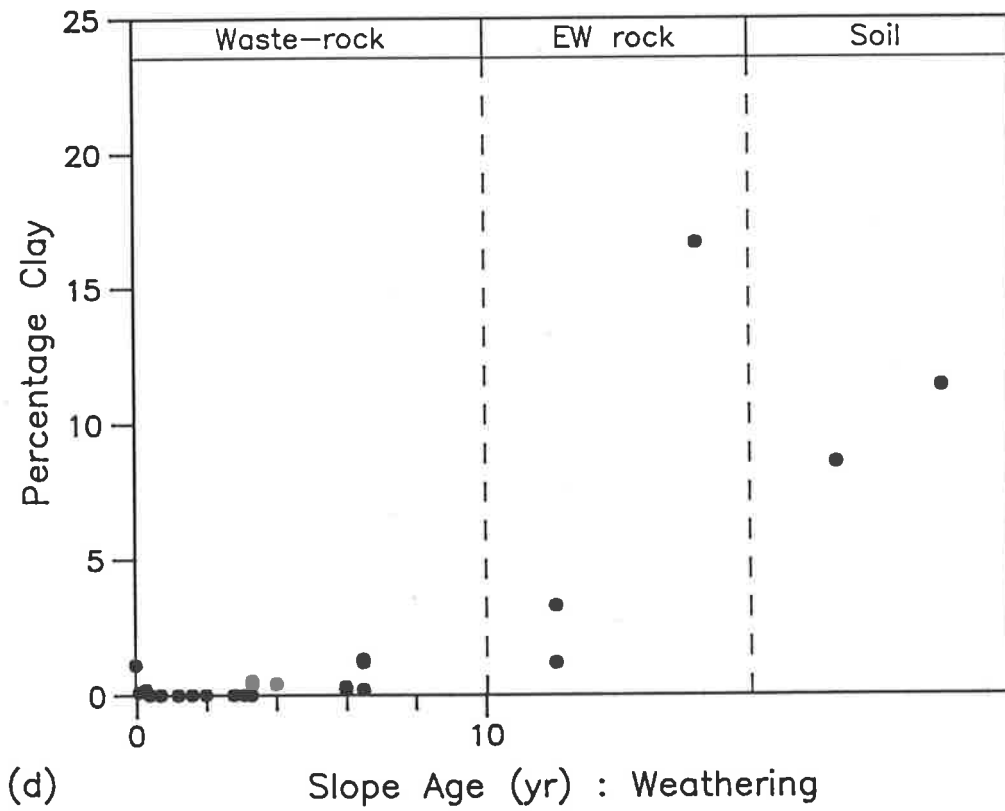
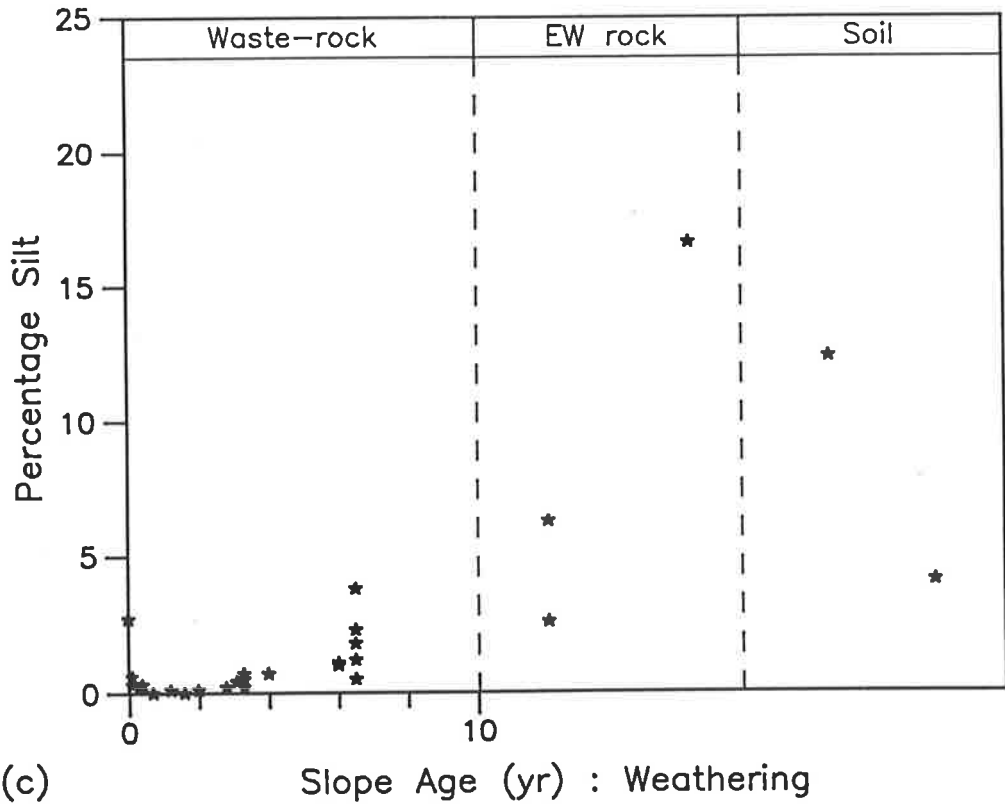


Figure 6-1 (continued)

Regarding the pit/soil samples, it is observed that RM27B (subsoil pegmatite), which was the weakest material tested, contained markedly less gravel, and more silt and clay, than the other samples. All of these more weathered materials contained about 50% sand (compared with less than 20% in the batter samples), with slightly less in the soils than in the extremely weathered rocks. This decrease suggests that in the soils, decomposition has become predominant over disintegration of fragments to sand, although it may also be that under in-situ conditions disintegration is less pronounced than it is in the initial stages of weathering on the waste-rock dumps. The sample of soil formed on a dump lift (JAB202z) contained more silt and less clay than the natural granitic mine-soil (RM25), which is consistent with a lesser degree of weathering.

This examination of the separate grading fractions helped distinguish the mechanisms involved in weathering of the waste-rock at Ranger. In terms of a parameter to characterise weathering, the proportion of coarse fragments (or its complement, the total proportion of sand, silt, and clay) is directly related to the disintegration aspect of weathering and shows an encouraging trend in Figure 6-1(a). Although sand fraction is similarly related and contains slightly less scatter in its correlation with age/weathering, there is an anomaly apparent in sample RM27B, which had a sand content typical of the weathered materials but showed much lower shear strength in the triaxial compression tests. Neither silt nor clay are present in sufficient proportions to be rationally correlated with mechanical behaviour for batter materials less than 10 years old. Coarse fraction was therefore considered the most promising quantifier for degree of weathering. However, it was also thought that a better measure might be derived from the complete grading curve rather than from a limited fraction.

Scott (1980, p.12), lists three parameters commonly used in the description of particle size distributions of soils, namely:

effective size D_{10} ;

uniformity coefficient $C_u = D_{60}/D_{10}$; and

coefficient of curvature $C_c = D_{30}^2 / (D_{60} \cdot D_{10})$;

where D_x is the particle size at which there is x% passing (by weight). Low values of C_u , approaching unity, indicate uniform particle size. Large values of C_c , approaching C_u , result from strongly concave

grading curves while very small values suggest convexity. (This coefficient might be difficult to interpret, however, if the grading curve contains contraflexure, such as by being convex in the coarse portion and concave at the fine end.) Effective size relates essentially to the location of the grading curve, whereas the two coefficients relate to curve shape.

With respect to dump batters, effective size might increase slightly in the first 2 years due to removal of the original fines but should then decrease continuously as disintegration proceeds and decomposition commences. A limitation on its use in characterising weathering is that the value of effective size becomes uncertain when materials contain more than 10% clay. Also, as D_{10} is calculated from the tail of the distribution, it may be susceptible to errors in sampling and analysis sufficient to confuse any correlation with weathering. For these reasons, D_{30} , which remains plainly determinate up to 30% clay content and is less affected by variations at the extremity of the grading curve, was also considered as a weathering parameter.

Trends in the shape coefficients are much more difficult to anticipate. Both D_{10} and D_{60} will decrease initially due to disintegration of boulders, cobbles, and gravel: the relative change is probably greater in D_{10} so C_u could be expected to increase. As decomposition becomes significant and D_{10} decreases towards clay size, if D_{60} is greater than sand size it might remain almost constant in which case C_u will continue to increase. However, if more than 60% of the material becomes finer than sand, D_{10} and D_{60} may decrease independently and the resultant effect on uniformity coefficient is unpredictable. Because coefficient of curvature is a function of three size measures it was impossible to postulate trends. The parameter was considered for completeness but it was suspected from the outset that the interplay of weathering mechanisms required a more absolute measure than degree of curvature of the particle size distribution.

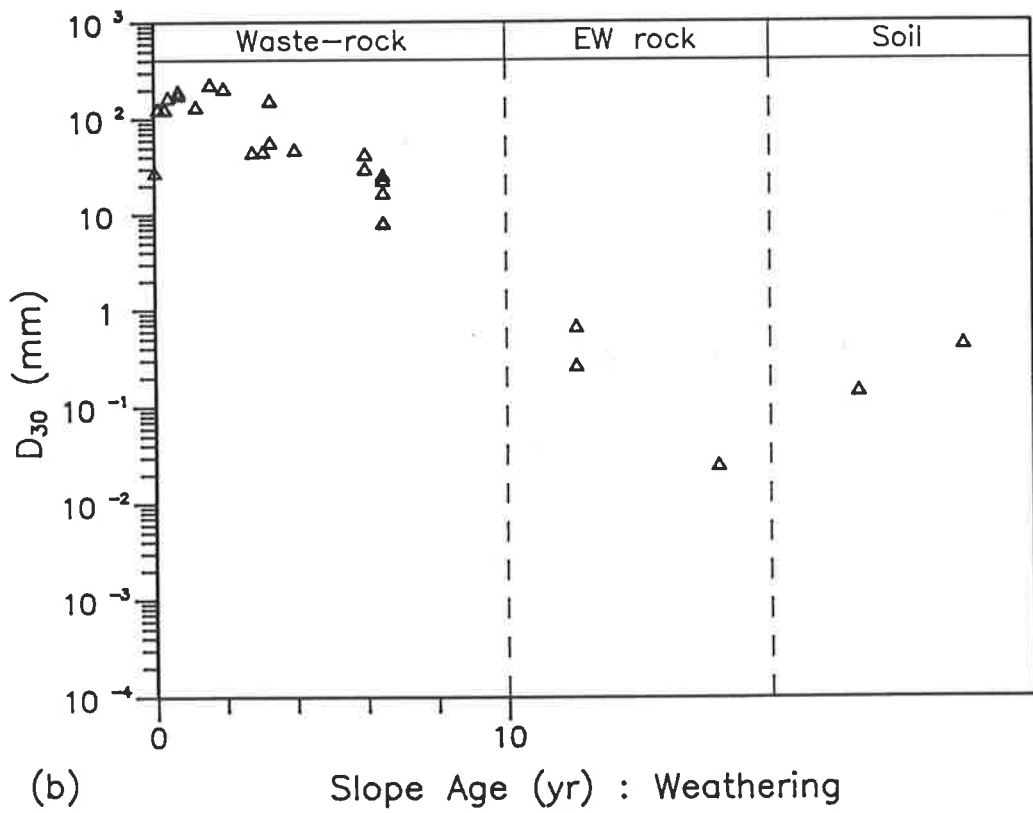
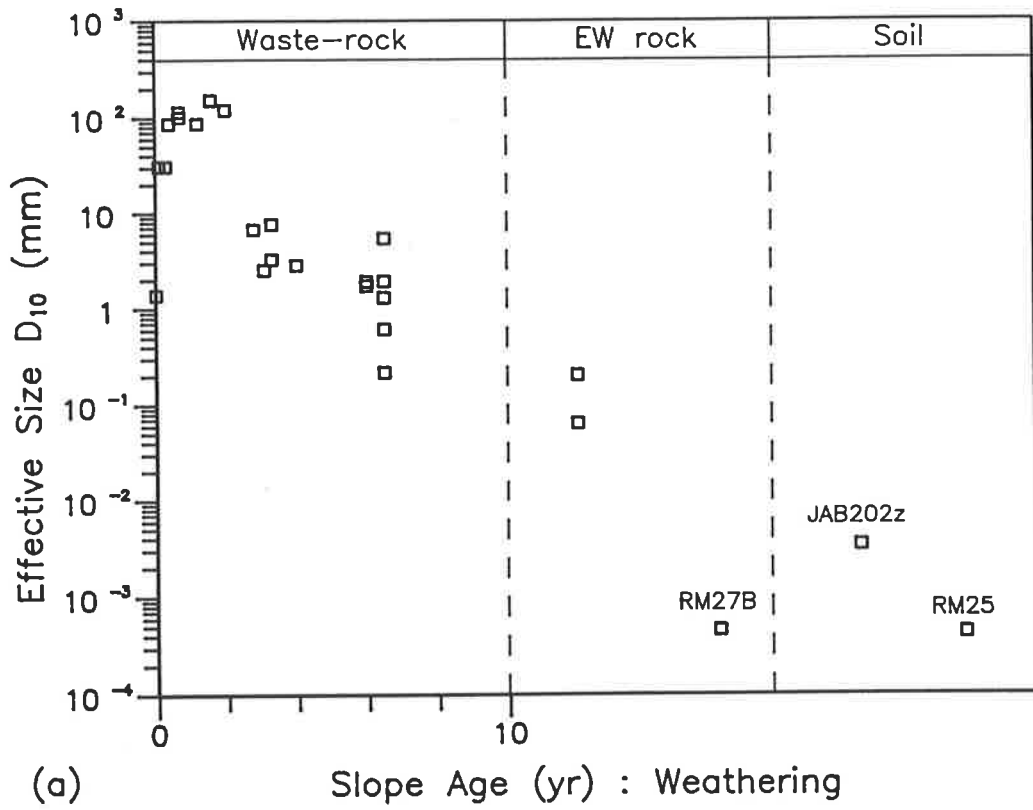


Figure 6-2 Correlation of Size Parameters with Age/Weathering

The actual correlations of the size parameters with age/weathering are presented in Figure 6-2. Effective size, D_{10} , and D_{30} both show recognisable trends of D_x decreasing with age, for the better sites. However, the band of scatter for D_{30} is much narrower, such that even the slight initial increase due to depletion of surface fines is apparent. With D_{10} , the decreasing trend continues through extremely weathered rock and soil, although values for the latter were extrapolated from percentages passing 2 micron and 6 micron (both soils containing more than 10% clay) and are thus suspect. By contrast, D_{30} is of the same order for the soils as for the stronger weathered rocks, RM26 and RM27A, which is consistent with trends in individual size fractions (refer Figure 6-1).

The grading curve shape coefficients, C_u and C_c , are shown in Figure 6-3. Amid a broad scatter, uniformity coefficient increases with slope age and weathering, as predicted. Referring to Figure 6-2(a) and the variability of D_{10} , which is the denominator in C_u , the large scatter is not surprising. As anticipated, coefficient of curvature has no apparent correlation with weathering.

Based on the foregoing examination of particle size distribution parameters, percentage coarse fragments (Figure 6-1(a)) and D_{30} (Figure 6-2(b)) were selected as the best-correlated measures of, in particular, the physical changes occurring during weathering of the waste-rock at Ranger Mine.

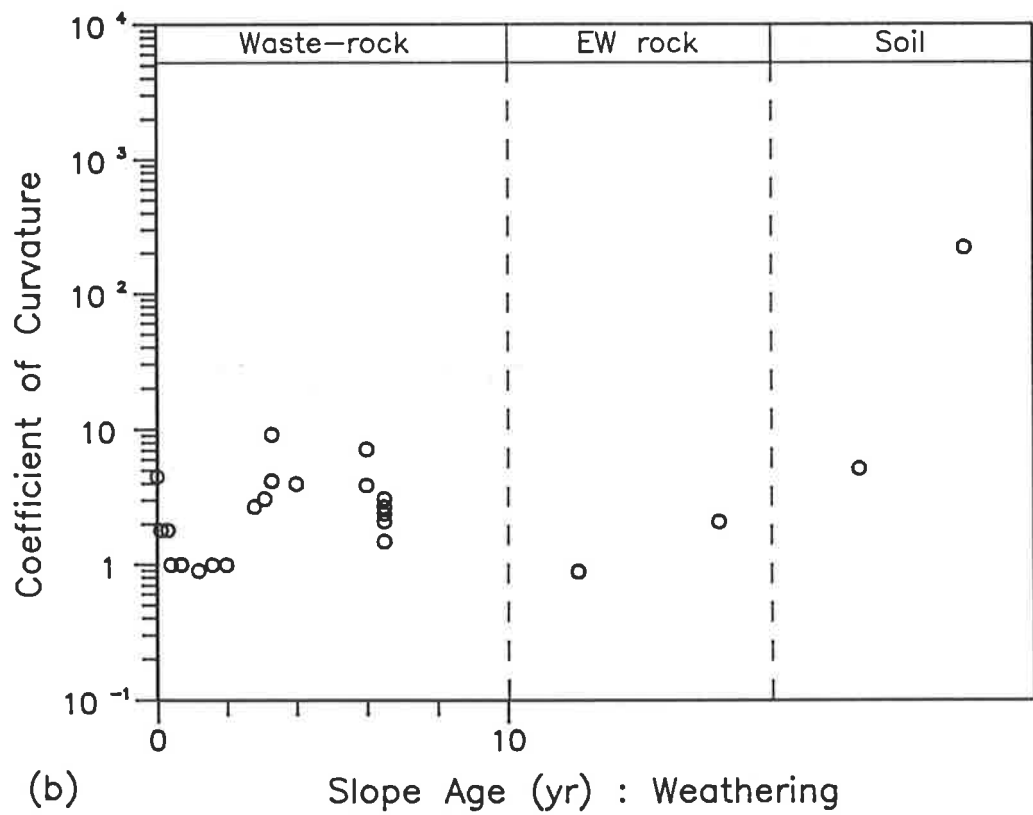
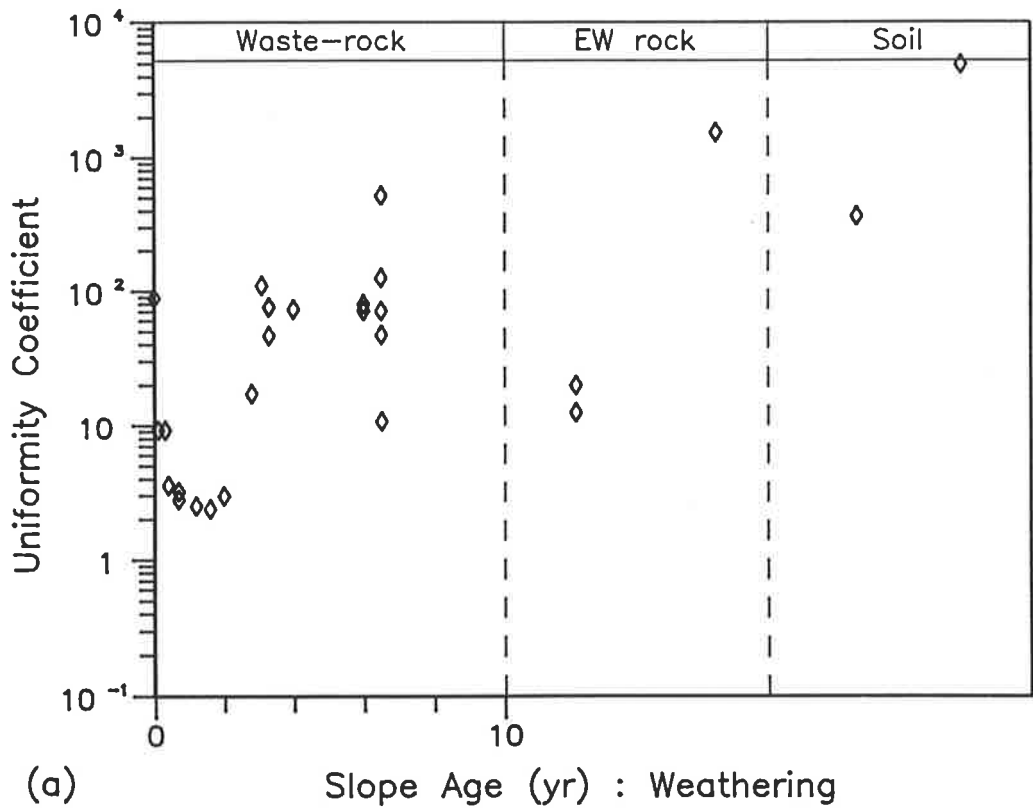


Figure 6-3 Correlation of Grading Shape Coefficients with Age/Weathering

6.1.2 Correlation with Shear Strength

The shear strength parameters adopted in Chapter 5 - c , ϕ , and τ_{300} - are shown versus *%Fragments* and D_{30} in Figures 6-4, 6-5, and 6-6 respectively. Trends are almost identical for both grading measures (*%Fragments* on a linear scale and D_{30} on a logarithmic scale), so the following discussion, while framed around *%Fragments*, applies similarly to D_{30} .

On brief inspection, shear intercept appeared to increase in a broad trend with decreasing percentage coarse fragments. However, as noted in Section 5.2.2, the non-zero intercept for the batter samples was due to particle interlock (or a similar effect) rather than to clay cohesion which is effective in the more decomposed samples. In the context of these separate mechanisms, Figure 6-4 suggests two narrower trends. The first is shear intercept decreasing with *%Fragments* in the batter samples (that is, on the right side of the graph). By extrapolating the trend, it is estimated that the effect of particles interlocking is minimal below about 80% fragments. This suggests that essentially direct fragment to fragment contact is required, and that the mechanism becomes ineffective when the proportion of fine particles is sufficient to form a matrix. Because there were no samples in the range of 50-85% coarse fragments, the 80% limit is somewhat speculative, but it can at least be stated that the contribution of fragment interference is readily lost as the exposed waste-rock degrades.

The second trend of the correlation is shear intercept, as cohesion, increasing with decreasing *%Fragments* (or conversely, with increasing percentage fines). This aspect is apparent from the five pit/soil data points, and although extrapolation was not attempted, the indication is that the two effects are jointly active over at most a small range of gradings. This is understandable, since cohesion requires a continuous matrix of fines whereas interference apparently depends on almost direct contact between fragments.

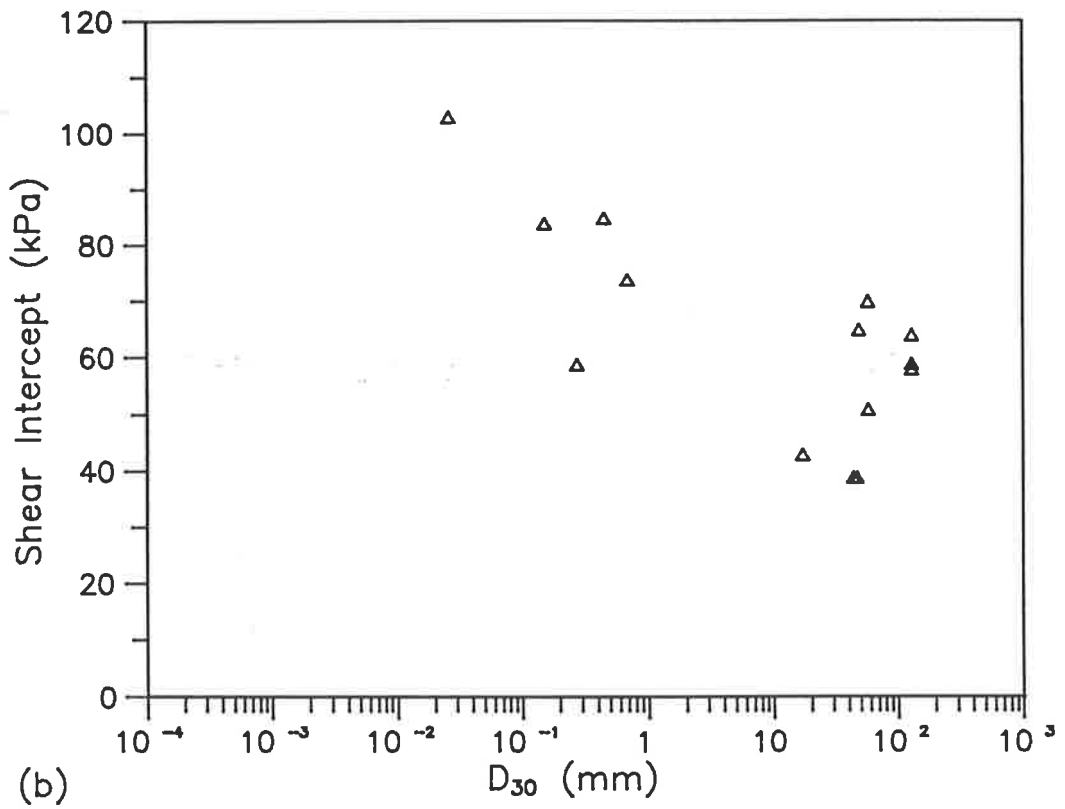
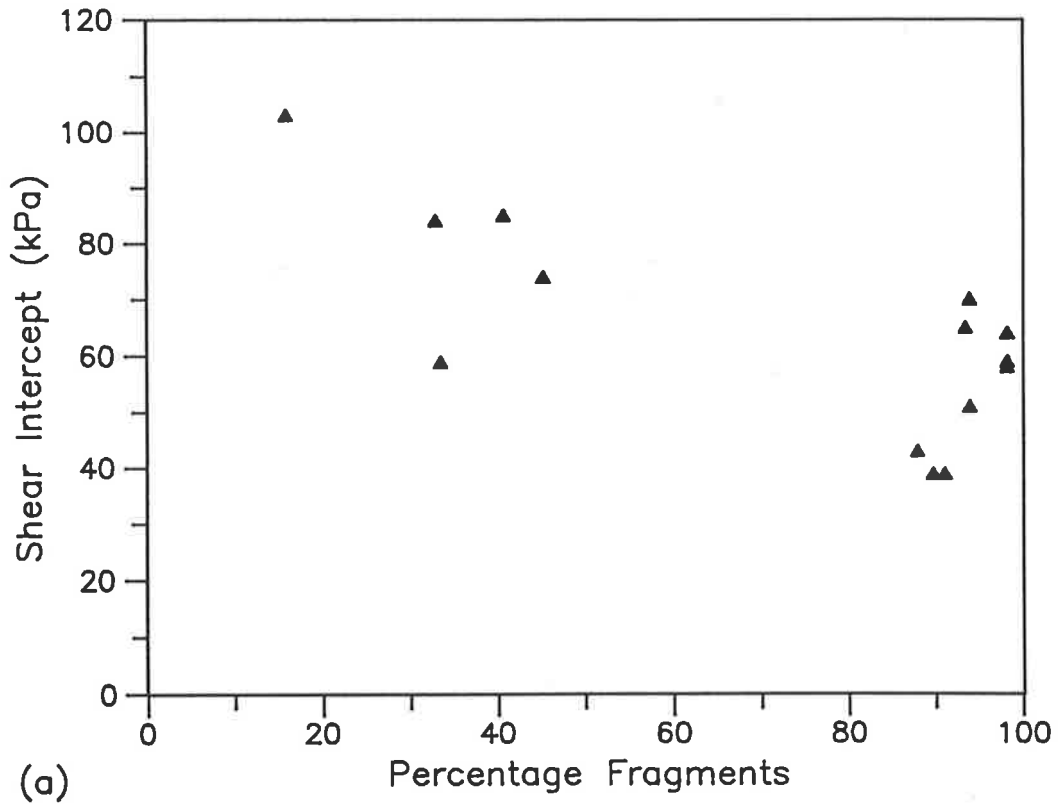


Figure 6-4 Correlation of Shear Intercept with Site Grading

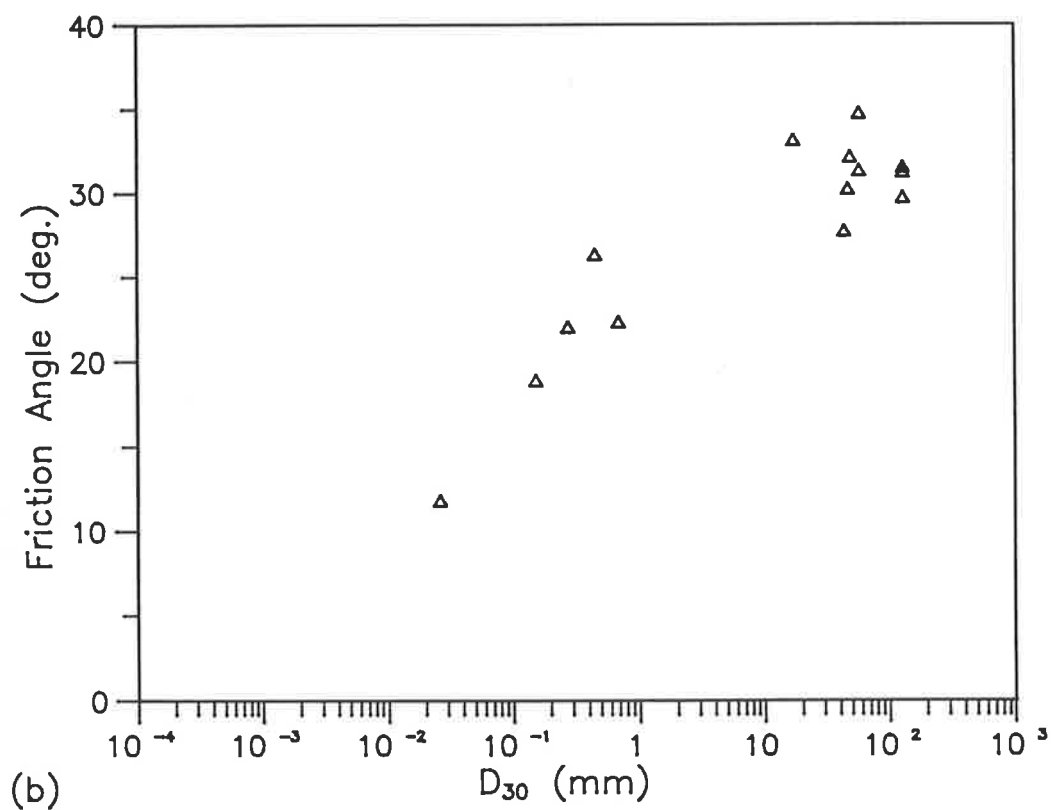
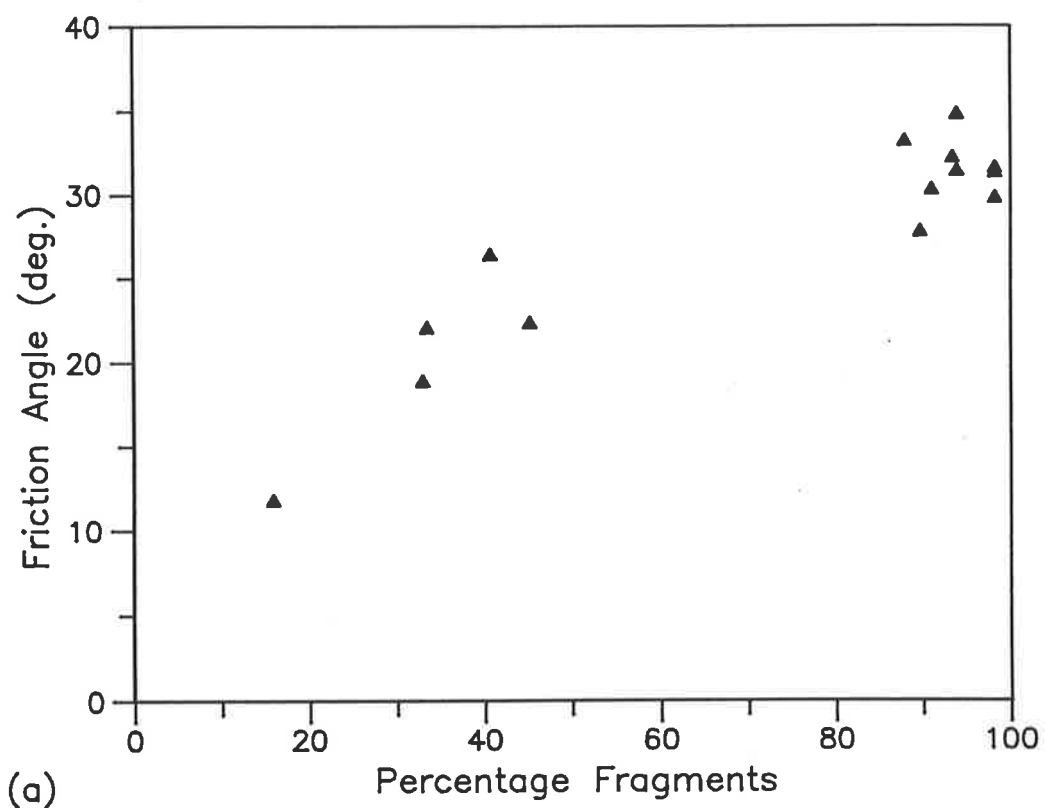


Figure 6-5 Correlation of Friction Angle with Site Grading

Figure 6-5 shows a broad but consistent trend of friction angle decreasing with decreasing %Fragments. It is noted that the soil samples which appeared anomalous in the preliminary correlation of Figure 5-5(b), are here consistent with the other materials. Despite the gap in data between the batter and pit/soil samples, it is clear that the correlation is not linear, with the reduction in friction angle accelerating below 60-50% coarse fragments. If further sampling is carried out as the dumps age it might be possible to establish whether this effect is related to the transition from disintegration to decomposition as the dominant weathering mechanism.

Mitchell (1976, pp.310, 315) quoted internal friction angle as 12° for saturated chlorite and effective residual friction angle ranging from 4° to 10° for montmorillonite (smectite). The value of $\phi=12^\circ$ (obtained for sample RM27B) is therefore probably approaching a lower limit for weathered waste-rock and residual mine-soil at Ranger Mine.

As with the age/weathering correlation in Figure 5-6, τ_{300} which combines contributions from shear intercept and friction angle, shows in Figure 6-6 a net loss of shear strength (at 300kPa normal stress) as waste-rock degrades and the proportion of coarse fragments declines. Specifically, there is a reduction in shear strength of about 40% for the change in coarse fraction from 100% to 20%. As with previous correlations, there is no apparent distinction between rock types. It might be said that the pegmatite samples fall generally on the low side of the band of scatter, and that schists tend towards the high side, but there are exceptions to both. There may in fact be differences in the average mechanical properties, but it appears that such distinctions are not as significant as random variability within each rock type.

Although the sample of natural residual soil fell within the band of scatter in Figures 6-4 and 6-5, both c and ϕ were above the average trend, with the result that RM25 is again an apparent outlier in Figure 6-6. The material is unique among those tested in having weathered from Nanambu Complex rock, whereas the schist, massive chlorite rock and pegmatite are all Cahill Formation. As discussed in Section 6.2.2, it was inferred from examination of further strength/mineralogy correlations that the singular behaviour of this sample is due to

critical compositional differences. The dump soil sample, JAB202z, conforms with general trends in the grading-based correlations presented in this section. In this context, it is only anomalous in the sense of having reached a condition typical of extremely weathered rock after a comparatively short period of exposure. As discussed in Section 2.3, this is attributable to the highly aggressive weathering environment which is rapidly established at lift terraces on the waste-rock dumps.

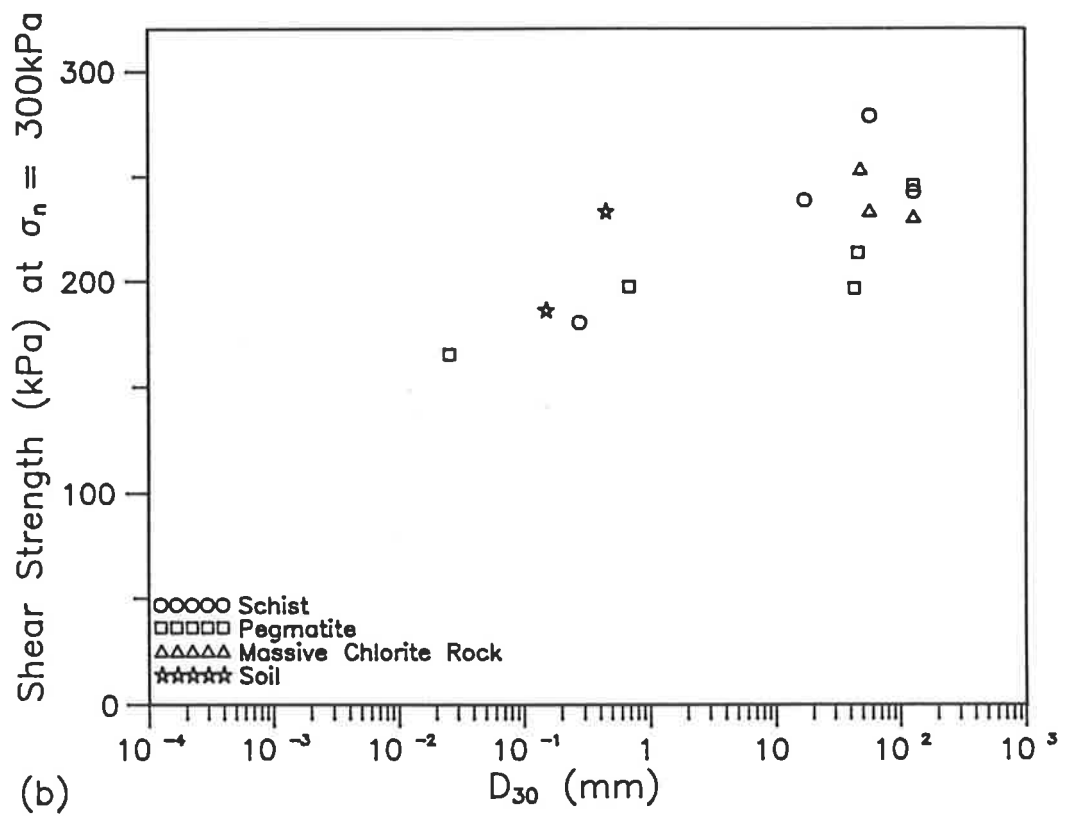
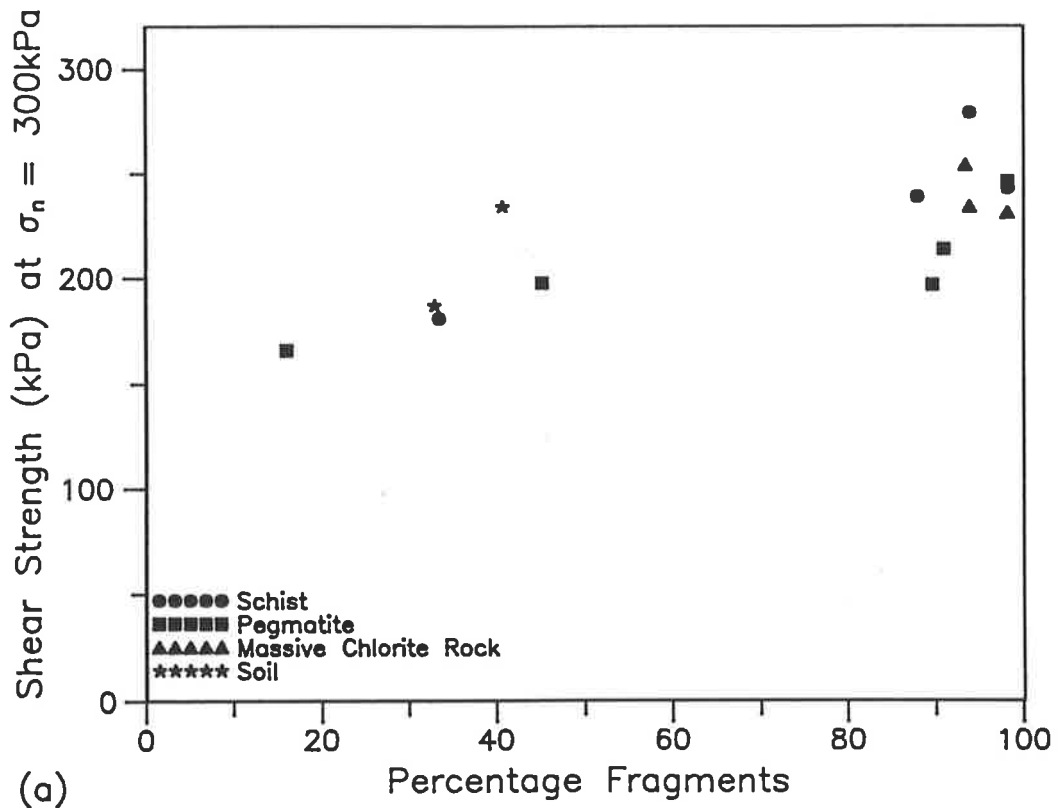


Figure 6-6 Correlation of Shear Strength with Site Grading

6.2 Mineral Alteration

6.2.1 Initial Composition

The amount of variation observed in particle grading correlations supported the presumption that other factors also contribute to changes in mechanical behaviour. Attempts to differentiate on the basis of rock type (for example, in Figure 6-6) were not particularly successful. As noted in Section 4-1, Ranger mine-rocks, especially those of the Cahill Formation, are composed of a common set of minerals, such that rock type may be largely a classification of natural rock fabric rather than of mineral content. The differences in fabric are more apparent, but it was reasonable to suspect that at least in the longer term, the development of weathering (and thus its effect on strength), is more sensitive to the proportions of primary minerals. This aspect was therefore examined separately.

Within the context of this thesis, "primary minerals" refers to components of unweathered mine-rocks, rather than to original minerals at lithification. (For example, chlorite is a reactant in dump weathering processes and so is here considered a primary mineral, although it was itself a product of earlier metamorphism.) Quartz and chlorite, as respectively the most resistant and most weatherable primary components, were selected for correlation with strength. For the samples collected during the dump photography exercise (prefixed MG), which had shown little mineral decomposition, proportions were estimated from Rietveld analyses of the 75 micron fractions and corresponding thin section analyses (refer Section 4.2). For the later supplementary samples (prefixed RM and JAB), estimates were based on XRD analyses of <2.4mm subsamples. Several of these samples contained significant proportions of weathering products, and initial compositions were inferred from the likely weathering paths discussed in Section 4.1. (For example, smectite was assumed to have been produced from primary chlorite).

Figure 6-7 shows correlations of quartz and chlorite with friction angle, with slope age overlaid. There is a general tendency in both the <5yr and 5-10yr samples for friction angle to be less for samples with less initial quartz and more chlorite, but it seems that friction angle for the pit/soil materials is not strongly dependent on initial

composition. This is in accord with the observation by Mitchell (1976, p.52) that parent material dictates the early stages of weathering but that ultimately other influences, such as climate, govern the nature of residual soil formed.

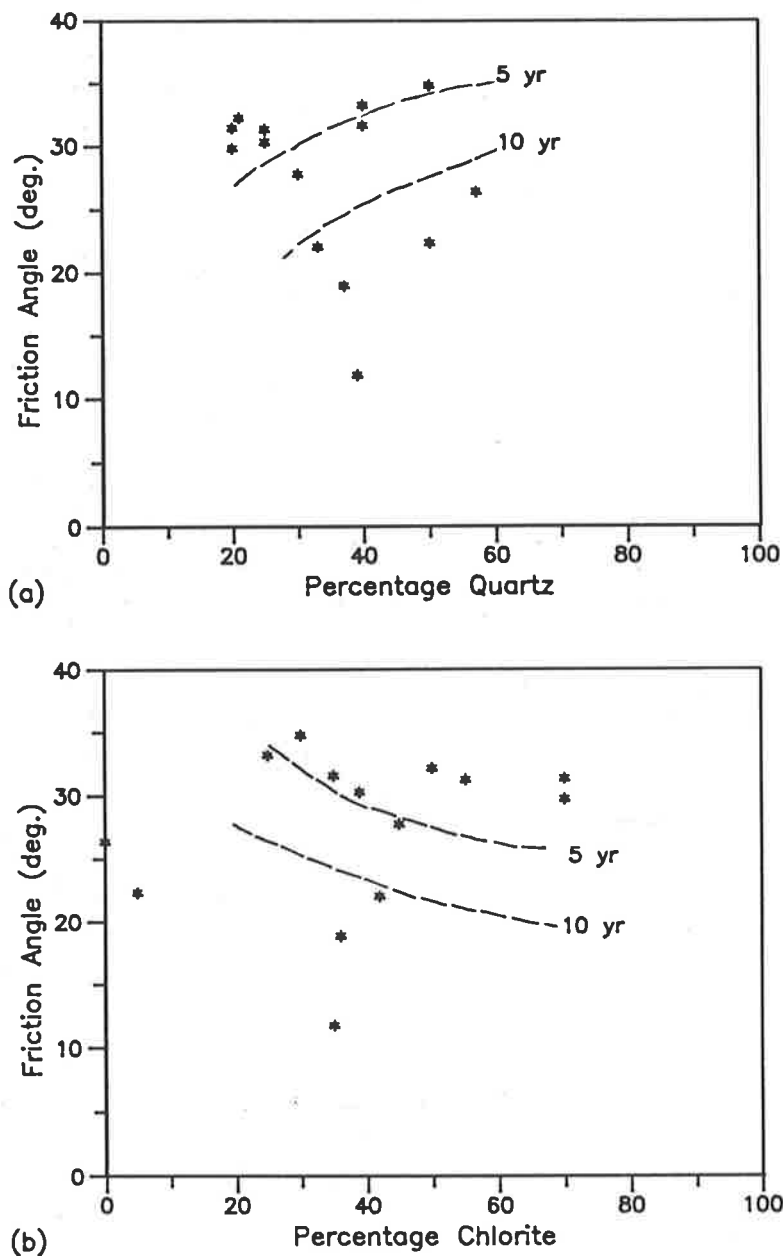


Figure 6-7 Correlations of Primary Minerals with Friction Angle

Alternatively, replicates of Figures 6-5(a) with quartz and chlorite contents differentiated are shown in Figure 6-8. From these it is suggested that the trends discussed above, while clearer than similar previous trials based on rock type, are by no means conclusive. However, initial compositions of the samples tested and of the range of

mine-rocks they represent, fall within a relatively narrow range (typically 20-60% of each quartz, muscovite, and chlorite). Consequently, the lack of a marked correlation with shear strength is perhaps not surprising. It is noted that sample RM25, whose contrasting mechanical properties were apparent in several previous correlations, has the one exceptional mineral composition (no chlorite).

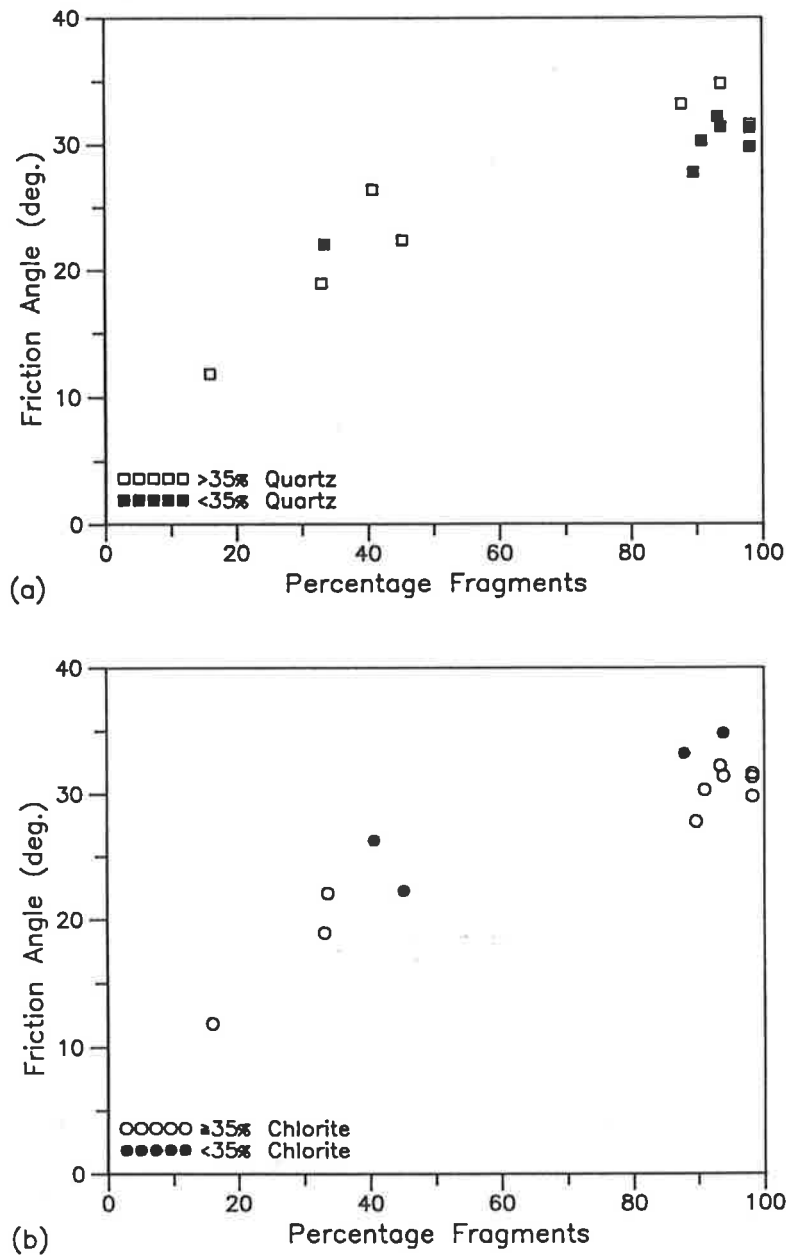


Figure 6-8 Effect of Primary Minerals on Friction Angle-Grading Correlations

6.2.2 Weathering Products

Mineral composition was thus of limited use in eliciting narrower trends within the broad strength-grading correlations obtained for Ranger mine-rocks. However, mineralogical descriptors still warranted investigation as potential measures of weathering, in the same sense as the grading parameters D_{30} and *%Fragments*. Although these physical descriptors correlated reasonably well with both dump slope age and shear strength, they are limited in that they primarily reflect disintegration which is not the dominant weathering process in the long term.

As discussed in Section 4.1, the key decomposition reactions were expected to be chlorite → vermiculite → smectite → kaolinite and muscovite → illite → kaolinite. Clay fraction analyses on batter and pit/soil samples, summarised in Table 4-3, did not detect vermiculite: this mineral was suspected, but not separately identified, in a previous investigation of Ranger dump and mine soils (Fitzpatrick et al 1989), and it may be that the vermiculite stage is at most transitory. Thus the significant mineral products of weathering found at the Ranger minesite were illite, smectite, and kaolinite. The presence of all three minerals in four of the five pit/soil samples (RM25 contained no chlorite and so predictably no smectite), indicates that the reactions are proceeding concurrently. It was conjectured that the result is probably a complex relationship between weathering and strength, unless the effect of one of these products is dominant. This was the first possibility examined.

Repeating a previous approach, Figure 6-9 shows illite, smectite, and kaolinite separately (as proportions of the whole material) against slope age/weathering. Since negligible weathering product was detected in most of the batter samples, indicators of chemical alteration are not relevant to these. However, for comparative purposes, the data points are included, along the *% clay mineral* axis, in this and subsequent figures. Referring to Figure 6-1 (showing particle size fractions), illite gives a similar-shaped plot to silt (or to a reflection of *%Fragments*), with a peak value occurring at RM27B, and the dump soil being higher than the natural surface soil. The result for smectite is essentially the same correlation exaggerated. Kaolinite diverges only

for RM25, which contained no smectite and only a small amount of illite, but had the greatest proportion of kaolinite. The resultant continuous increase in kaolinite with weathering is at variance with obtained strength results (refer Figure 5-5) which showed RM25 as significantly stronger than some less weathered materials. Thus it was foreshadowed that while percentage kaolinite may be a fair measure of the degree of general decomposition, it does not relate directly to the specific aspects of weathering which are critical to mechanical behaviour.

Considering Figure 6-9 in total, it is apparent that regardless of its appearance and location, the dump soil is effectively more weathered than RM26 and RM27A (in-situ weathered schist and pegmatite) but less weathered than RM27B (subsoil pegmatite). The high kaolinite content confirms the natural near-surface soil as the most extensively decomposed sample collected and, in context, its low proportion of illite is indicative not of less weathering of muscovite but rather of more alteration of illite to kaolinite.

It is also noted that, with about 10% total secondary minerals in the most weathered sample (from >40% weatherable primary minerals), even the soils and subsoils are relatively "young" in terms of total potential alteration. Although weathering is occurring in the waste-rock dumps at an accelerated rate, as degradation proceeds the factors promoting rapid weathering (such as free ingress of fluids) will decline. Hence it is expected that the dump material might approach, but will not exceed, the degree of weathering in-situ. The impact of weathering on mass stability of dumps and subsequent landforms is related to this segment of the potential complete degradation sequence.

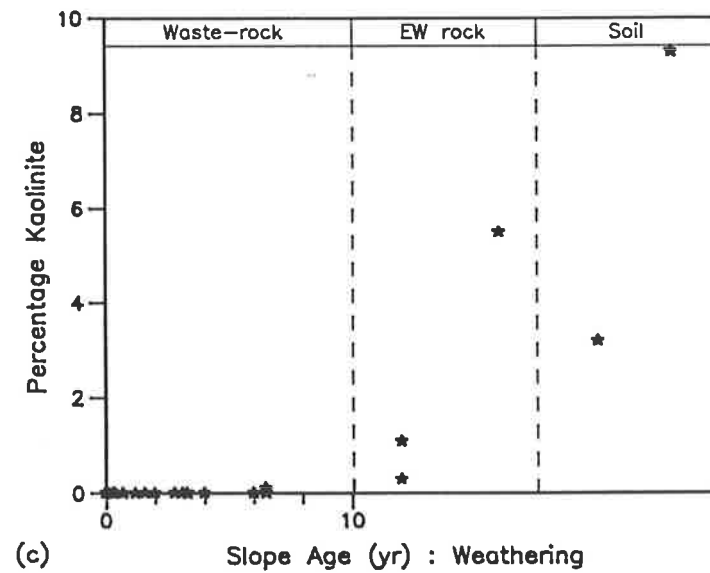
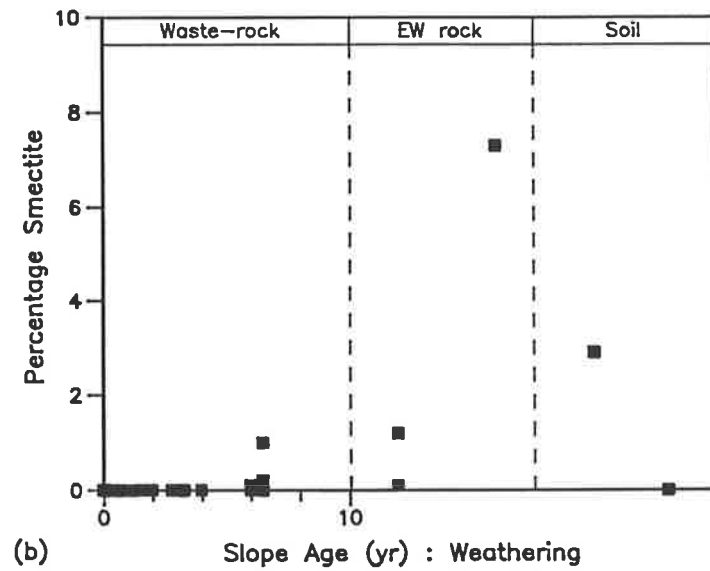
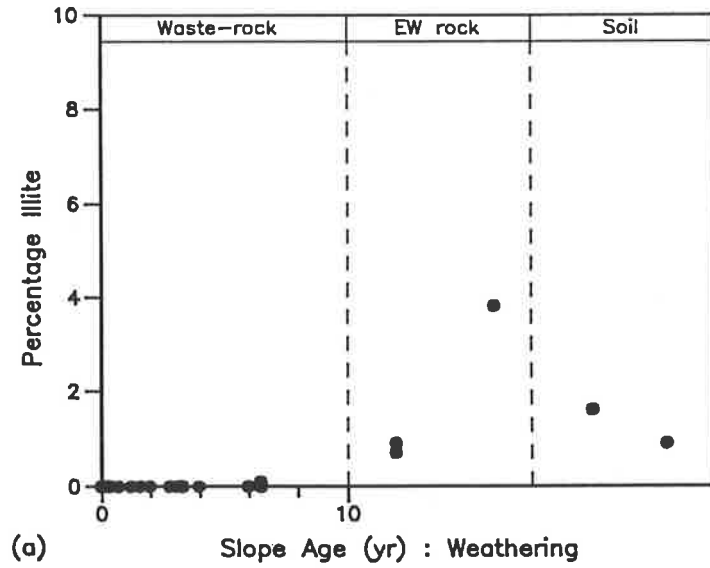


Figure 6-9 Variation of Clay Minerals with Age/Weathering

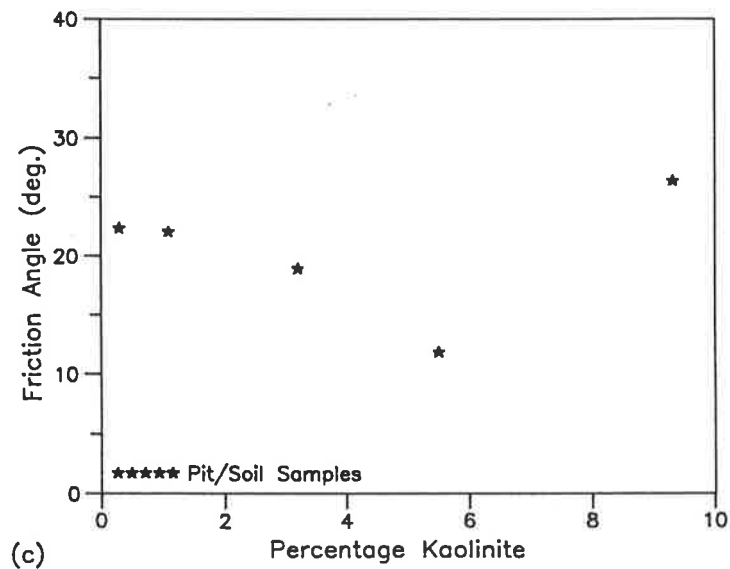
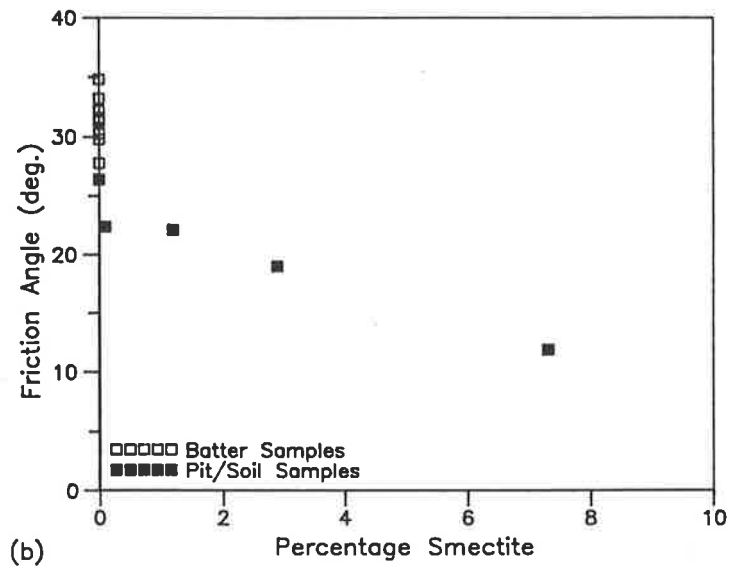
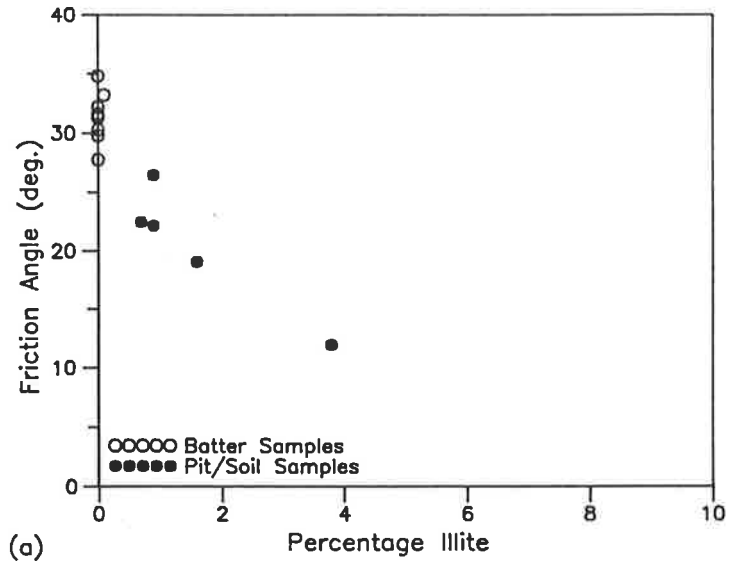


Figure 6-10 Correlation of Friction Angle with Clay Minerals

Figure 6-10 presents correlations of illite, smectite, and kaolinite with friction angle for the materials tested. Despite the limited number of pit/soil samples, there is a clear trend of ϕ decreasing as illite increases from 0% to 4%, with which the waste-rock samples (along the axis) appear consistent. Smectite has an even stronger, almost linear, correlation in the same direction. However, this mineral also shows a clear discontinuity between the trend in the five pit/soil materials (projected back to $\phi=25^\circ$ at zero smectite) and the results for the undecomposed batter samples ($\phi\approx 28^\circ-35^\circ$). In section 6.1.2 it was observed that the shear intercept can be produced by two different mechanisms, namely particle interference and true clay cohesion. Although a similar distinction was not also interpreted from the friction angle - grading correlation (Figure 6-5), that trend was noted as bilinear.

The parameter friction angle was originally derived from consideration of two surfaces sliding against each other (Lambe & Whitman 1969, pp.61-62) which in a continuum translates directly to the shear plane. In a discontinuous mass such as jointed rock, the local interfaces on which sliding takes place may be significantly misaligned from the global direction of shearing, and ϕ is increased because of the need to ride over, or shear through, such asperities (McAnally & Boyce 1980, p.246). In the essentially fragmentary waste-rocks a similar mechanism can be envisaged, with interlock not as rigid but asperities much larger. Re-interpreting Figure 6-5, it appears that this particle interference effect dissipates at about 60% fragments, slightly lower than the level estimated for shear intercept.

As anticipated, the correlation with kaolinite shows RM25 as non-conforming (Figure 6-10(c)). However, as with smectite, a sharp distinction between pit/soil samples and batter material is obvious.

Correlations of the weathering products with shear intercept are shown in Figure 6-11. In all, cohesion increases generally with increasing proportion of the particular clay mineral, although the trends are not as clearly defined as those for friction angle. The trend with kaolinite flattens out (or possibly reverses) after about 4%, which was further evidence that mechanical behaviour is more strongly influenced by some other factor.

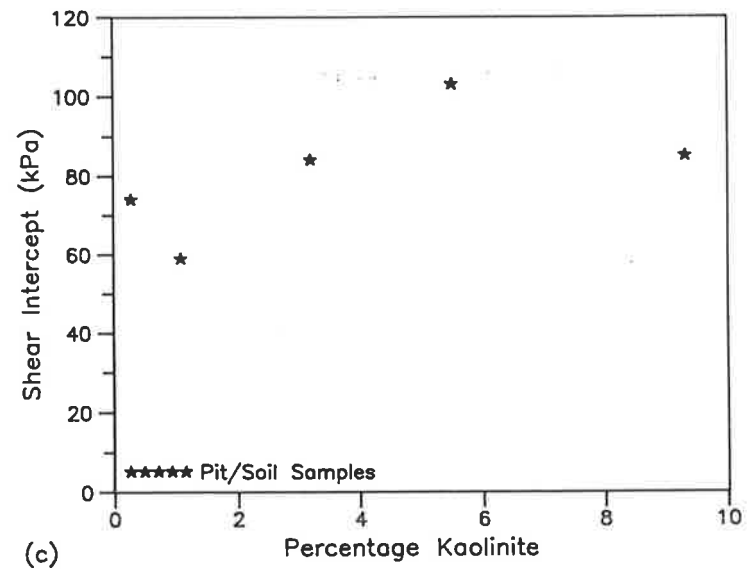
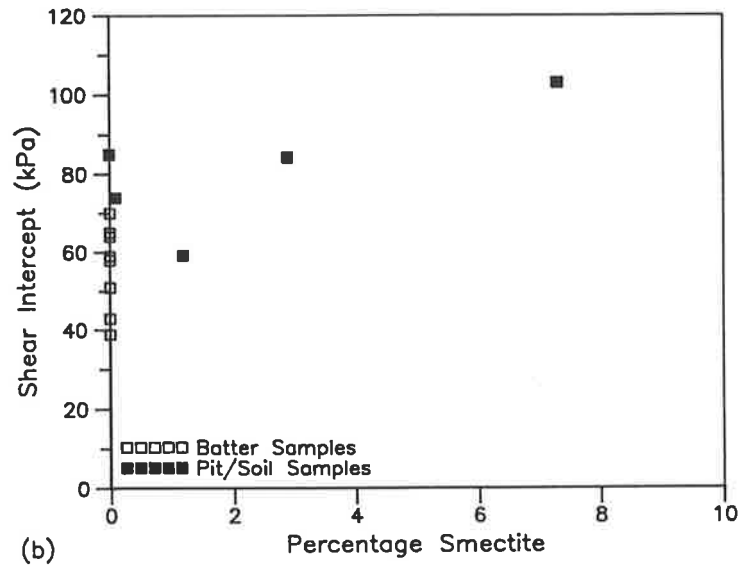
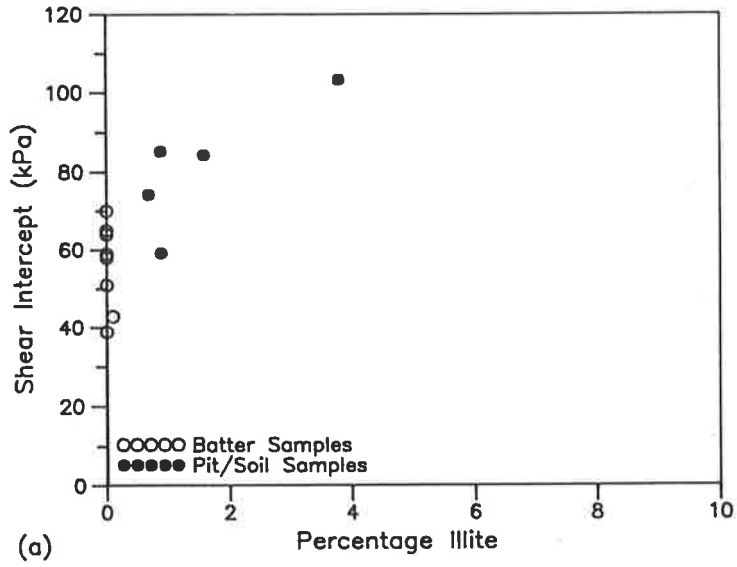


Figure 6-11 Correlation of Shear Intercept with Clay Minerals

6.2.3 2:1 Layer Clay Minerals

Some incompatibility was perceived between the number of strength results for weathered materials and the precision implied in attempting correlations with small proportions of specific clay minerals. The total percentage of weathering products was considered, but taking the clay fraction - age/weathering data in Figure 6-1(d) as an approximation, it was clear that this parameter could again not account for the natural soil sample. The measures which best included RM25 within the general trend for both c and ϕ were percentage illite and percentage smectite, although the latter may have been coincidental as the material contained no smectite. Both minerals are intermediate products of weathering and have 2:1 layer structures, and both derive from plate-like primary minerals (muscovite and chlorite). Thus illite and smectite are likely to have similar effects on mechanical behaviour. By contrast kaolinite is a product of further weathering (including leaching), has a more stable 1:1 clay layer structure, and tends to aggregate into small compact particles.

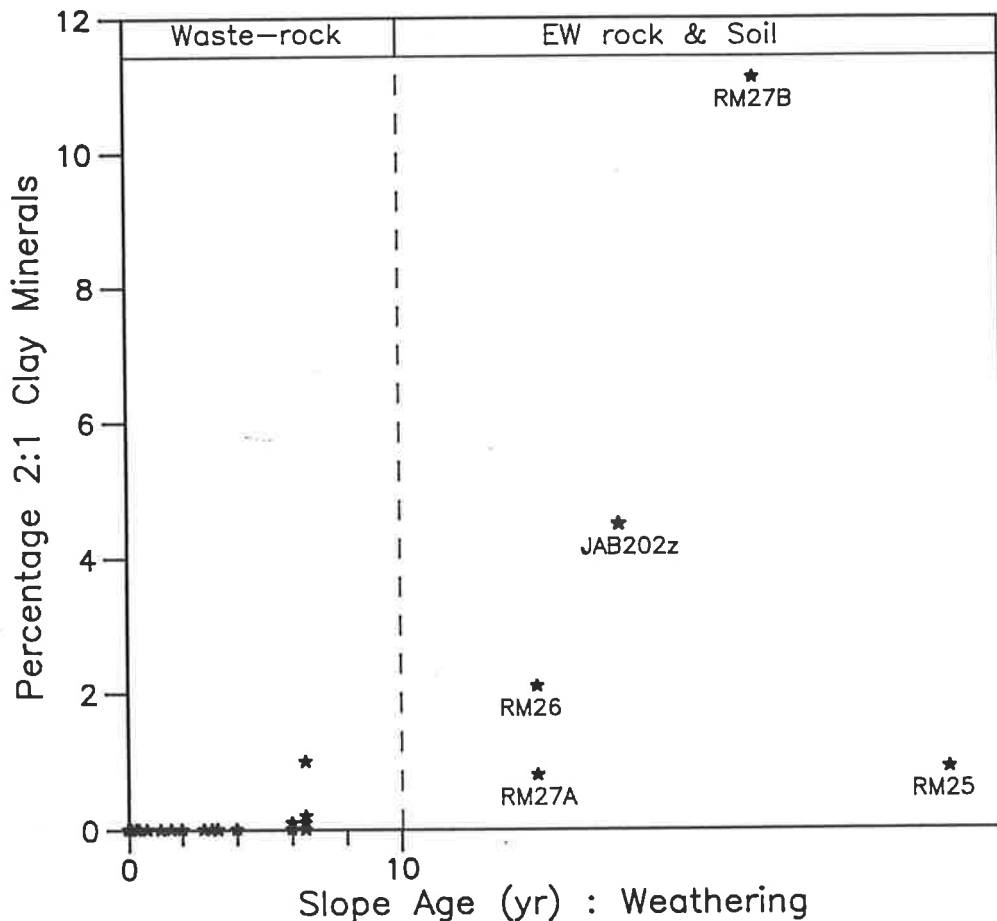


Figure 6-12 Variation of 2:1 Layer Clay Minerals with Age/Weathering

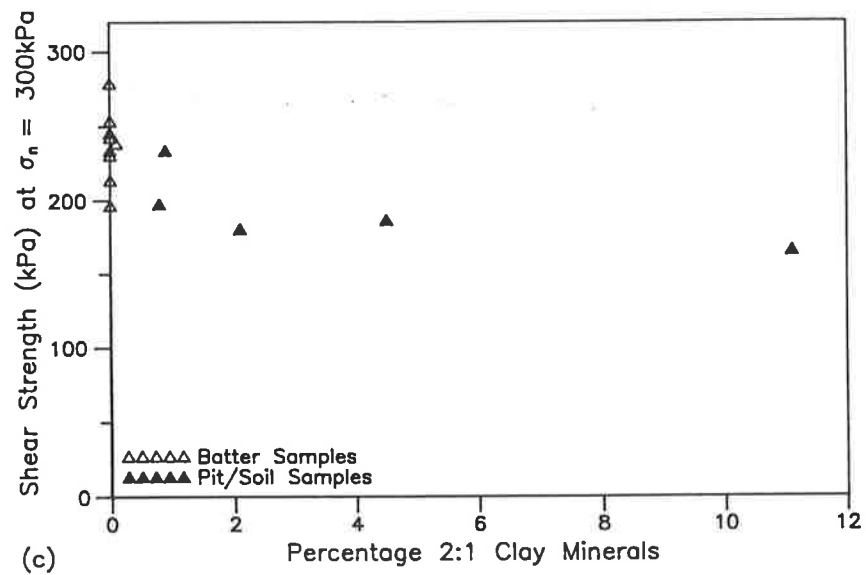
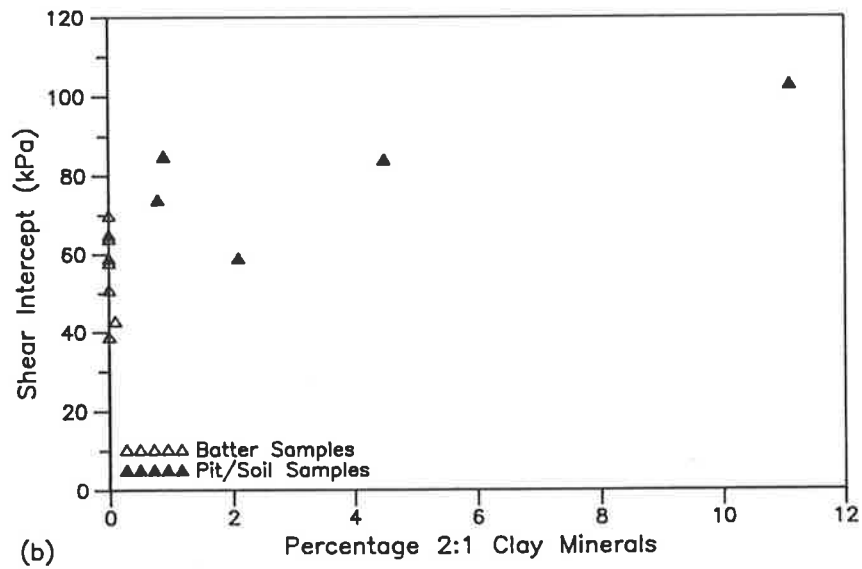
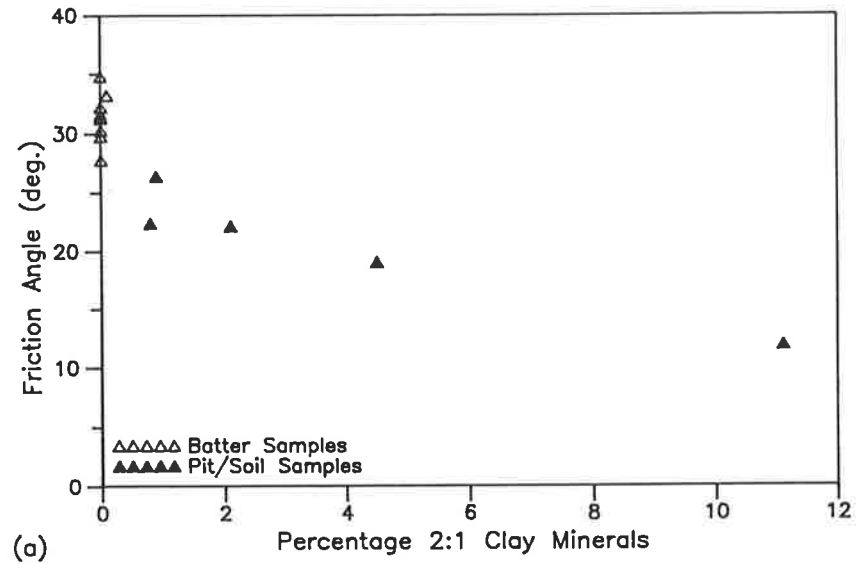


Figure 6-13 Correlation of Strength Parameters with 2:1 Layer Clay Minerals

In Figure 6-12 the grouped 2:1 layer clay minerals are correlated with age/weathering. The ranking of dump soil between extremely weathered rock and subsoil pegmatite on the weathering axis was accepted earlier in this section, as was the decrease from RM27B to RM25 in intermediate weathering products, because of the subsequent reaction to kaolinite. With respect to strength, Figure 6-13(a) shows a clear trend for friction angle and the discontinuity between pit/soil materials and batter samples. As with previous correlations, the trend in cohesion has a broader scatter (Figure 6-13(b)), and the net effect of changes in friction angle and shear intercept is a slight decrease in shear strength (at 300kPa normal stress) with increasing proportions of 2:1 clay minerals, as demonstrated in Figure 6-13(c).

The fact that previously anomalous materials fall within consistent trends in Figure 6-13 supports a strong relationship between the proportion of 2:1 clay minerals and shear strength. However it is unlikely that such small amounts of illite plus smectite affect cohesion and friction angle so markedly. The strength of correlations may rather be due to the fact that the percentage of 2:1 layer clays is also an indirect measure of influential aspects of particles further up the grading curve, such as in the fine sand and silt fractions. Both muscovite and chlorite form angular platelike particles in these fractions whereas the other primary component, quartz, tends to a cubic or nodular shape throughout the size range. The sand content ranged from 40-60% in the pit/soil samples and silt from 2-20%, so it is reasonable to expect that the difference in the nature of these fractions is important to mechanical behaviour of the bulk material.

From this basis, the results obtained for sample RM25 may now be explained. The bulk analysis for this natural residual soil showed dominant quartz and minor goethite, with only minor muscovite and no chlorite. Consistent with this, no smectite was detected in the clay fraction. Therefore, more than any other non-batter sample, the fine sand and silt fraction was dominated by hard nodular quartz particles and the clay fraction by stable 1:1 layer kaolinite. By contrast RM27B, which was the weakest material tested, contained more than 10% 2:1 clay minerals and about 40-45% muscovite plus chlorite.

A final inference is that the weathering reactions of 2:1 minerals into kaolinite tend to increase strength. Because of its different mineral composition, the strength of RM25 would probably be higher than average at any stage of weathering, but the difference between 2:1 and 1:1 clays is a more general effect. None of the other samples yet contain sufficient kaolinite to dominate, but it can be foreseen that if weathering continues friction angle could reach a minimum and then start to increase as the platy minerals and less stable clays are depleted and replaced by kaolinite. However, since even the most weathered material sampled contained only 10% kaolinite the reversal of trend is probably beyond that range of weathering relevant to the waste-rock dumps and subsequent constructed landforms.

6.3 Collated Data

The clearest correlations of physical and mineralogical parameters with slope age and material strength are summarised in Figure 6-14. For characterisation of particle grading, %Fragments (boulders, cobbles, and gravel) was preferred to D_{30} because of its linear rather than logarithmic scale. Both fundamental shear strength parameters (c and ϕ) are included but τ_{300} has been omitted. As shear strength evaluated at 300kPa normal stress, τ_{300} was useful in discussion to demonstrate the net effect of weathering-related changes on material strength at a typical stress level. However, because trends in c and ϕ are similar in magnitude but opposite in direction, the interactions are easier to appreciate with these strength components separated. The shadings on Figure 6-14 are intended to mark the trends and effects of various mechanisms, not to define quantitative bounds. Many more data points would be required - to fill in from 50-80% Fragments and to define the transverse correlation with initial mineral composition - before specific mathematical limits could be justified.

The most valuable outcome of this study of weathering characteristics was exposition of the various mechanisms through which material weathering affects mechanical behaviour, and how they interact. It was not attempted to further condense the data into the format suggested by Figure 1-1 or to extract a single parameter as a measure of degree of weathering. Not only was the latter unwarranted by the limited data set, there are specific attributes of the dumps and materials at Ranger (such as similarity of composition, apparent dominance of mining-induced fabric, and the pattern of high concentrated rainfall), such that the observed sequence of weathering may be unusual. Therefore a single parameter designed to suit Ranger is unlikely to be generally applicable. Figure 6-14 is thus submitted as the most useful compilation of the effects of material weathering on shear strength in the Ranger waste-rock dumps. The next stage of the research project was to include this understanding in stability analysis of the long term dump batters and rehabilitated landform slopes.

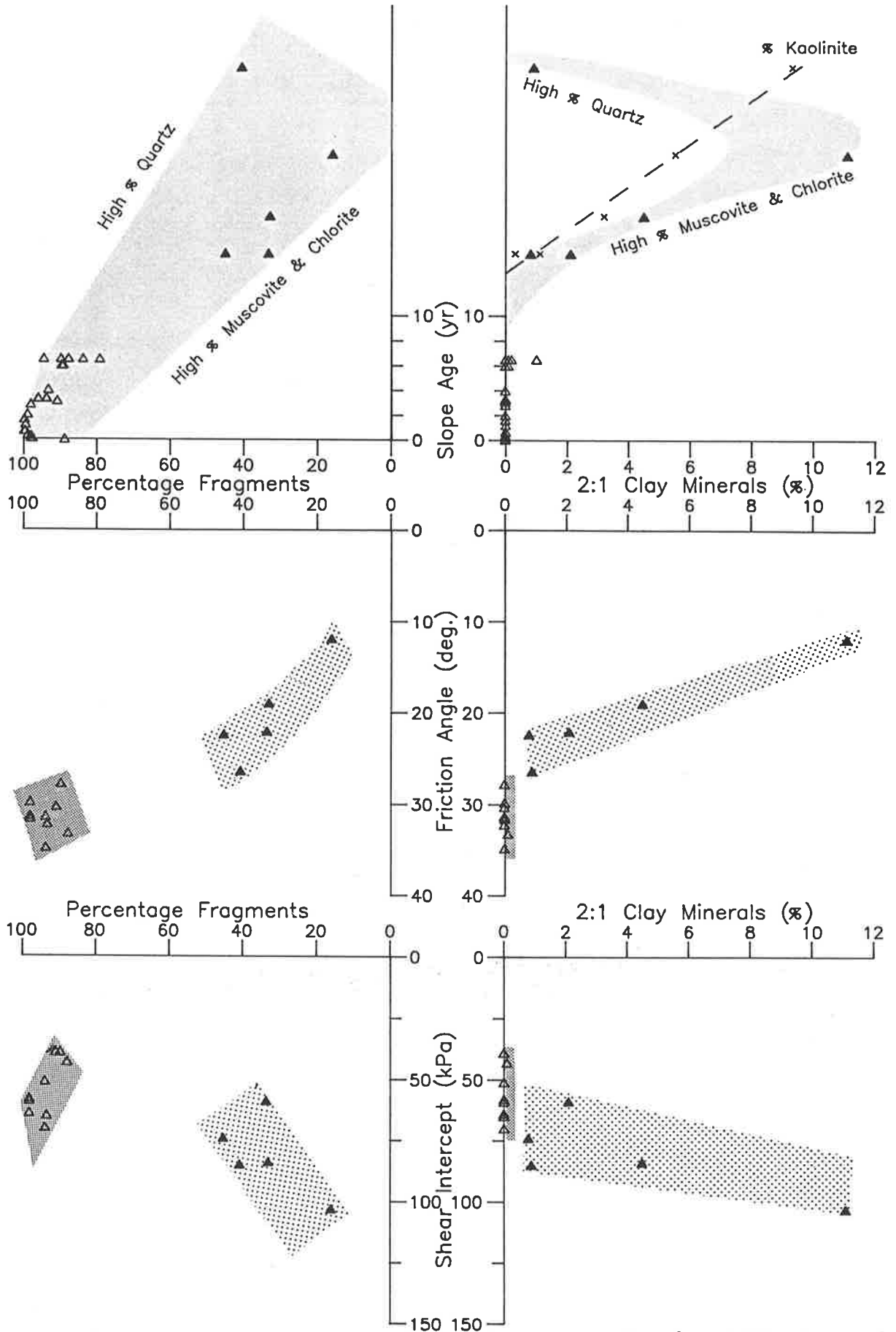


Figure 6-14 Relationships between Weathering Effects and Strength Parameters

CHAPTER SEVEN

7. DUMP STABILITY ANALYSIS

7.1 Review of Analytical Methods

In the actual dumps, each lift is constructed of essentially fresh waste-rock. There may then be some period, during which degradation commences on the batters and lift terrace, before the next lift of fresh material is dumped. After completion (typically within ten years), the heap is likely to remain as dumped for two decades or more - while weathering proceeds - before the area is reshaped into the rehabilitated landform. Two problems were identified with regard to closely modelling this sequence in slope stability analysis, namely:

- a) the pauses between construction of successive lifts has to date been quite variable, such that a "typical" duration is hard to rationalise; and
- b) as asserted in Section 6.3, it was not appropriate to mathematically formalise the weathering-strength relationship, which would have been more convenient for integrated analysis.

As a result, it was proposed to devise series of analyses which, while not replicating the history of the physical dumps, would illustrate changes in dump slope stability as waste-rock weathers. Specifically, it was planned to perform sets of analyses for slopes, each comprised of a single material (representing a discrete degree of weathering) and built up lift by lift assuming no change in material properties between lifts.

Throughout this research project, it was repeatedly observed that waste-rock does not fit easily into normal geotechnical engineering practices. From sampling to classification to laboratory testing, the established framework of procedures required modification to accommodate, in particular, the unique size and age-dependent aspects of spoil material from Ranger Mine. As it was anticipated that this difficulty might extend to slope stability analysis, a preliminary review was made of the bases and development of the various analytical methods, in order to select one reasonably appropriate to the problem at hand.

Central to any geomechanical theory is the type of mathematical model assumed for the material itself. As Jaeger (1971) pointed out, soil and rock mechanics diverge at this rudimentary level, with soils approached

involve postulating a shape for the slip surface and then searching for a location for this surface which minimises the ratio of global forces resisting slip to global forces promoting it. (This ratio is termed the factor of safety against slope failure.) In some respects, the soil model is thus transformed to resemble the rock mechanics concept of a mass dominated by discontinuity. However, in a soil slope the joint (slip) is not pre-existing, and remains hypothetical unless failure actually occurs.

The various limit equilibrium theories are differentiated by the shape of the postulated failure surface and by the assumptions invoked to make the force equilibrium equations determinate. The first aspect implies that a specific mode of failure is anticipated: Caldwell and Moss (1985) listed seven possible modes for mine-waste embankments, ranging from edge slip to foundation failure. For each mode of instability there may be several analytical methods, representing various degrees of rigorousness in the solution of limit equilibrium. (For example, Fredlund and Krahn 1977, reported about a dozen methods just based on a circular failure surface with the slope considered as a series of vertical slices).

The validity of a particular result thus depends firstly on correct prediction of the critical failure mode. Often it can be confidently anticipated, because of a particular geometry of soil strata, or from investigations of previous slips under similar conditions. For example, Blight (1969 and 1985) back-analysed a number of slips in dumps on the Witwatersrand gold fields, and subsequently proposed a wedge method of stability analysis for rockfill on weak foundations. In the context of a design tool, the major benefit of limit equilibrium methods is that, because of extensive use, factor of safety gives a well accepted and comprehended measure of the margin against failure. A lurking weakness in the global limiting equilibrium approach is the assumption that peak strength can be achieved simultaneously along the whole of the potential slip surface. The implications of this for strain-softening materials (which show a reduction in strength after yield) has been highlighted in the classic papers by Skempton (1964) and Bjerrum (1967) on progressive failure of clay slopes.

A smaller but developing group of models uses finite element procedures to analyse the distributions of stress and strain throughout the whole soil continuum. With appropriate constitutive laws to describe stress-strain behaviour, this technique can be used to investigate slope stability from the basics of load equilibrium and strain compatibility, so that the critical mode of failure is determined by the analysis, rather than being required as input. Some disadvantages are that the level of sophistication is often incompatible with the quality of the available soil data, and that finite element models require experienced specification and interpretation to produce reliable results. Also, because of the relative newness of the method and the amount of data produced, there is as yet no widely acknowledged measure of the margin against failure implied by the results of a finite element analysis. However, the insight provided into the mechanisms and development of instability may be of more assistance to engineering judgement than the prevalent, but sometimes deceptive, single factor of safety.

A finite element procedure was selected for the current investigation into long-term slope stability of waste-rock dumps, primarily because of the undesirability of presuming one mode of failure for the diverse range of materials. For example, the triaxial testing indicated that the fresher waste-rock has significantly greater shear strength than residual minesoil sampled near the dumps, which is probably similar to that on which the dumps were constructed. Consequently, in a fresh dump it is anticipated that failure could be instigated in the weaker foundation. The natural soil however was stronger than both the dump soil and the sampled extremely weathered rock, so it is less likely that a slip in a more degraded dump would extend into the natural base. In addition, finite element analysis uses more of the information available from laboratory strength tests (limit equilibrium methods use only cohesion and friction angle) and produces more detailed results which can assist the assessment of slope stability even if, for a particular analysis, the modelled slope does not fail. Finally, a finite element model was used in the preliminary investigation of dump stability at Ranger Mine (Richards, Peter, and Lucas 1986), and it was expedient to continue with the same programme. The conceptual model and associated computer routines are discussed in Section 7.2.1.

There is a final level of differentiation in analytical techniques in geotechnical engineering, namely whether the model is formulated in a deterministic or probabilistic manner. The former is the traditional option, with representative values (typically mean or lower bound) judged for each material parameter and occasional replicate analyses carried out using optimistic and pessimistic estimates to check the sensitivity of results. In concept, the probabilistic technique replaces each single value parameter with the probability distribution for that parameter (or with repeated estimates generated from the probability distribution), in order to obtain a probability density function for the result. The technique has occasionally been overlaid on limit equilibrium slope stability models (for example, McMahon 1982) which is intriguing considering the degree of determinism involved in predicting the failure mode and in formulating a determinate force equilibrium equation. To the author's knowledge, the probabilistic approach has not been used with finite element modelling in geomechanics. The likely reason for this is the multiplying effect on an already complex and computation-intensive procedure. A limit equilibrium model may have several layers, each described by two strength parameters, whereas a finite element model often contains several hundred elements with perhaps a dozen material parameters. Recalling that the Monte Carlo simulation described in Chapter 3 involved 5000 repetitions to obtain probability distributions for one-dimensional geometric measures, it is apparent that probabilistic finite element modelling is not yet a feasible alternative. In view of the present rapid development of computers, and if quantitative data on the distribution functions of soil parameters are also collated at a consistent rate, the combination of finite elements and probability may hold promise. At present, however, the deterministic approach is an accepted feature of the finite element model used to analyse dump slopes composed of waste-rock at various stages of weathering.

7.2 Slope Stability Model

7.2.1 The Finite Element Programme

Since its formulation in about the late 1950's, the finite element method has been the subject of many texts (for example, Zienkiewicz 1971 and Rockey et al 1983), and so it will not be detailed in this thesis. It is briefly noted that the technique was developed for the analysis of two and three dimensional continuous structures and involves dividing the structure into a number of connected segments (elements). Load equilibrium and displacement compatibility constraints are satisfied, at points of connection between elements (nodes), to determine stresses and strains throughout the structure. Specifically, finite element analysis involves assembling the structural stiffness matrix, $[K]$, from stiffness contributions of the individual elements. Nodal displacements, δ , are then calculated from $\{\delta\} = [K]^{-1} \{F\}$, where F consists of nodal forces equivalent to applied loads and internal stresses. Finally, elemental stresses and strains are determined from the displacements.

The computer programme used in this study was the load-deformation-swell module of a programme developed by Dr B.G.Richards to analyse interactive loading and fluid flow in soils. Some of its features include non-linear material stiffness parameters; potential to change material properties within the analysis; mesh geometry updated according to cumulative displacements; and a facility to add to, or remove from, the mesh during the analysis. Again, the concepts and procedures are described more fully elsewhere (for example, Richards 1984 and 1992), and the following discussion is restricted to specific aspects of the programme relevant to the analyses undertaken.

In its current form, the model uses three-node triangular plane strain elements. An optional subroutine is included to generate a simple mesh on a rectangular grid, from which other shapes may be obtained by "turning off" sections of the mesh. This approach is inefficient for sloping structures, since large portions of the programme arrays are wasted on dummy elements filling out the rectangle. Consequently, a separate more flexible generation programme was used, and the resultant

node geometry and element associations were included directly in the finite element input file. One function of this generation programme was to optimise node numbering for minimum bandwidth: this caused some conflict with minor sections of the model which assume that numbering proceeded in rows from the top left. To overcome this, a simple sort routine was added which produces arrays mapping actual node and element numbers to equivalent positions within a rectangular mesh.

The construction sequence for the dumps was modelled using a separate material specification for each lift, and at each increment declaring materials above the current lift to be ineffective. The technique was previously employed in the analysis of dragline-placed spoil piles (Richards, Coulthard & Toh 1981), and also in preliminary modelling of dump slope at Ranger Mine (Richards, Peter & Lucas 1986). In practice the "turning off" is achieved by dividing stiffness contributions from ineffective elements by 1000. Resultant small stresses in these elements are reset after each increment and have not been found significant.

During the analysis, the mesh geometry is updated after each increment to take account of nodal displacements. Because of the compatibility constraint at lift interfaces, upper parts of the mesh are distorted by displacements accumulated in the underlying lifts before those top lifts are "turned on". In addition, the first increment in which a lift becomes effective includes small settlements in the lift due to self-weight. Both of these sets of displacements are inappropriate to the movement which would be observed or measured on an actual dump, as the finished level at any stage is largely independent of prior surface depressions or compaction of the current lift during placement. Because of the programme structure, with element and node arrays fully assembled before entering the analysis subroutines (and because of the necessity of displacement compatibility between adjacent elements), the anomaly cannot be easily amended within the programme. Instead, output displacements were approximately corrected by subtracting the corresponding displacement at the top of the underlying lift in the increment before the new lift was applied. Self-weight settlements were estimated by analysing a single 10m lift built up row by row, and these were also subtracted. (Displacements discussed and illustrated in the remainder of this chapter have been adjusted in this manner.)

Non-linear load-deformation behaviour is modelled using the incremental elasticity approach. That is, stiffness parameters are expressed as functions of stress. At each iteration they are evaluated based on current stresses, and assumed constant in the stiffness matrix assembled to solve nodal displacements for loads applied in the present increment. New current stresses are calculated from these displacements and used to recalculate stiffness parameters for the next iteration. After the specified number of iterations, a new increment is commenced, based on the latest current stresses and a new set of nodal loads. Equations for the stiffness parameters, specifically, bulk modulus and shear modulus, are described in Section 7.2.2.

Also at each iteration, current shear stress for each element is compared to its yield stress, which for the slope stability analysis was calculated from the Mohr-Coulomb equation. If yield stress is exceeded new equations for bulk and shear modulus are invoked. If overstressing continues, the initial shear strength parameters, c and ϕ , are replaced by c_r and ϕ_r and another formulation of the element stiffness matrix, applicable to shear elements, becomes effective. (Richards 1980a, reported better success modelling post-yield behaviour with such automatically converted shear elements than with conventional plasticity theories.) Elements are also checked against tensile failure, and excess shear and tensile stresses are redistributed to neighbouring elements via nodal loads.

The programme writes selected data (for example, failure flags, stresses, and displacements) to an ASCII output file for direct printing. This subroutine was edited to utilise the sorted mode and element lists in setting up print rows resembling the shape of the mesh, to facilitate preliminary inspection of results. A binary file of all output data is also optionally written, which was previously read by a hardware specific plotting programme. This programme, however, cannot handle incremental and irregularly numbered meshes and, as the source code was not available for editing, another small programme was written to selectively extract data for transfer to IBM format. Final stress and displacement plots were then produced using commercial spreadsheet and graphics software. A summary of the operation sequence of the finite element programme, as accessed by dump slope stability analysis, is provided in Appendix E.

7.2.2 Material Models

One of the major conclusions stressed by Richards (1990) was the need for consistency of theory between the analysis of laboratory tests to obtain soil parameters and the modelling of field problems using those parameters. For example, in the interpretation of triaxial compression tests it is normally assumed that axial and lateral stresses are uniform throughout the sample, and that the sample maintains a cylindrical shape as it deforms (that is, the sides remain straight and vertical). In practice barrelling is more common as the sample approaches failure (as in Plate 5-3), which also implies non-uniform stresses. Classical limit equilibrium theories do not explicitly consider deformation, and the simplifications in laboratory interpretation and problem analysis are in reasonable accord. However, it would be inappropriate in an analysis of field load-deformation behaviour to use strength parameters whose theory contradicts the actual deformations observed in the laboratory test.

Material properties for the dump slope analyses were obtained using the approach described by Richards (1978, 1980a, & 1991), in which the laboratory tests are themselves back-analysed using the finite element programme. Working from first estimates based on simple theory and previous data sets, trial-and-error adjustment is carried out on the soil parameters until reasonable correspondence with the measured data is achieved. Those parameters then constitute the material models used in analyses of the dump slopes.

The mesh used to model triaxial compression tests on dump material and weathered mine-rocks is shown in Figure 7-1. Thin joint elements interfacing the soil and top platen, and also at the base of the sample, were included to permit modelling of finite lateral restraint at the ends of the sample (Richards 1978). As may be observed on Plates 5-3 and 5-4 of weathered rock samples, there was typically minimal lateral deformation beneath the top platen and only slightly more movement at the base, such that the setting of these joint elements was not critical. However, they were also found to improve the stress distributions, particularly along the base, and thus prevent minor numerical instability from instigating artificial failure in the model.

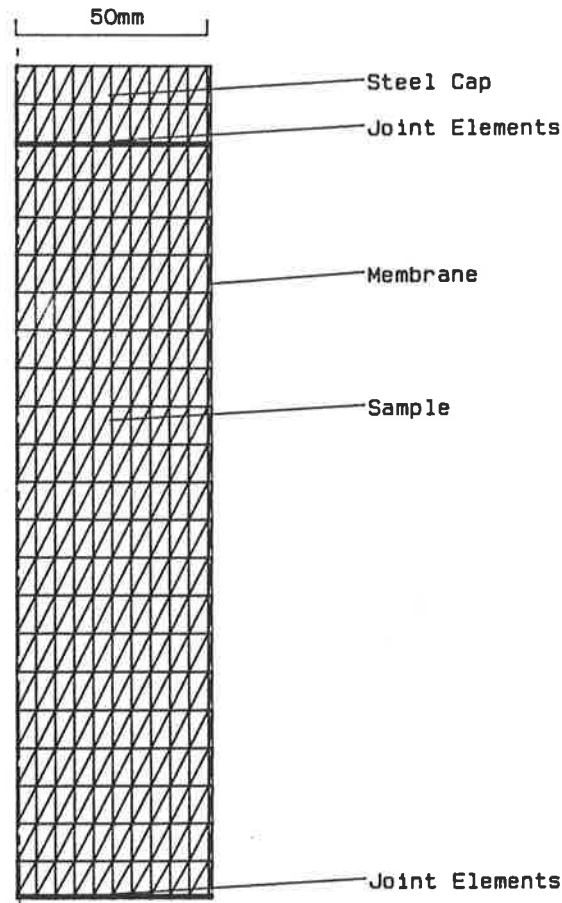


Figure 7-1 Finite Element Mesh for Triaxial Compression Tests

As discussed later in this section, when the shear strength of an element is exceeded, its failure is flagged and different equations are invoked to evaluate element stiffness parameters. Once an element has failed, it cannot revert to the pre-failure equations, even if the stresses change such that it is no longer yielding. (Unloading is modelled using parameters evaluated at maximum previous shear stress.) Consequently, it was not possible to model a multiple-stage triaxial compression test in a single analysis. Instead, each stage was considered separately, with initial vertical and horizontal stresses specified respectively as the maximum vertical stress in the previous stage and the current cell pressure.

Strain-controlled loading was simulated by applying increments of vertical displacement, typically 0.2mm, to the top nodes of the loading platen. As occurs in actual triaxial samples, in the finite element analyses large portions of the mesh often reached failure simultaneously. This sometimes produced an apparent small jump in

average vertical stress, which was actually related to difficulty handling the sudden large changes in the stiffness matrix. The problem was generally overcome by repeating the analysis using smaller increments of displacement near the commencement of failure.

The basic constitutive model used in the programme is a composite of the Modified Variable Moduli Model (Richards 1978), which defines material stiffness parameters up to yield, the Mohr-Coulomb shear strength equation based on an associated flow rule (Davis 1968) up to yield and non-associated flow post-yield, and shear element stiffness formulation (Richards 1980a) after yield. Specifically the equations as used in the triaxial test and dump slope models were:

- (a) Bulk modulus, $K = k_o$ prior to yield and
 $K = k_r$ at yield and post-yield.
 (k_o and k_r are constants.)

The assumption of constant values for bulk modulus before and after yield is a great simplification of the hyperbolic equations available in the programme. It is justified by extensive modelling of a range of materials (Richards 1978, 1980b, & 1982) which has suggested that, except for initial loading of loose silts and sands, load-deformation behaviour is not sensitive to changes in bulk modulus. The selected value should, however, be reasonable in the context of its relations to other stiffness parameters (Young's modulus, Poisson's ratio, and shear modulus).

- (b) Shear modulus, $G = (1 - \tau/\tau_f^q) \cdot g_1 + g_o$ prior to yield and
 $G = g_r$ at yield and post-yield.
 (q , g_1 , g_o , and g_r are constants;
 τ is maximum shear stress; and
 τ_f is shear stress at yield.)

The option exists to include in the unyielded modulus a term relating to normal stress. However, based on the modelling experience referred to above, it was anticipated that reasonable modelling of the waste-rock and weathered rock samples could be achieved with the simpler version. This was in fact the case and, considering the limited extent of the laboratory test programme, greater elaboration was considered unwarranted. Again consistent with previous modelling, shear modulus was found to be the critical stiffness parameter.

- (c) Shear strength, $\tau_f = c + \sigma_n \cdot \tan \phi$ prior to yield and
 $\tau_f = c_r + \sigma_n \cdot \tan \phi_r$ at yield and post-yield.
 (c, c_r , ϕ , and ϕ_r are constants; and
 σ_n is normal stress.)

This specification represents two different strength criteria: the initiation of yield is judged according to the normal Mohr-Coulomb equation for maximum shear stress, but once yield has occurred strength is evaluated along the slip plane (that is, in the direction of maximum shear strain). Davis (1968) demonstrated the relationships between these conditions as $c_r = c \cdot \cos \phi$, and $\phi_r = \tan^{-1} \sin \phi$, although for strain-softening materials c_r and ϕ_r are better approximated by the actual residual shear strength parameters. The approach correlates with the shear element stiffness matrix formulation invoked for post-yield behaviour (Richards 1980a), which essentially involves preventing further normal stress parallel to the calculated slip plane. Any excess shear stress in these yielded elements may be redistributed in the next iteration via nodal loads.

For stability analysis materials ranging from fresh waste-rock to soil were selected from the lower bound of laboratory strength test results shown in Figure 6-6(a). In order of decreasing percentage coarse fragments, they were JAB201, MG08, RM27A, JAB202z, and RM27B. Because of the gap between MG08 and RM27A, two hypothetical materials were added (named Frag75 and Frag60) with stiffness and strength parameters intermediate between the two sampled materials. RM25 was also included to represent the natural surface material over which the dumps are constructed.

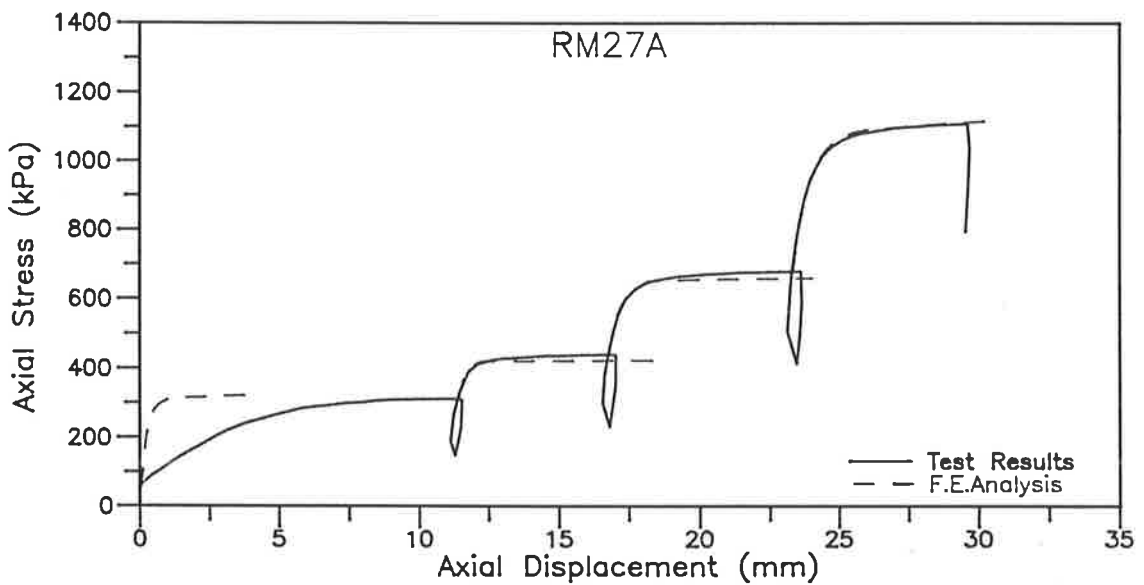
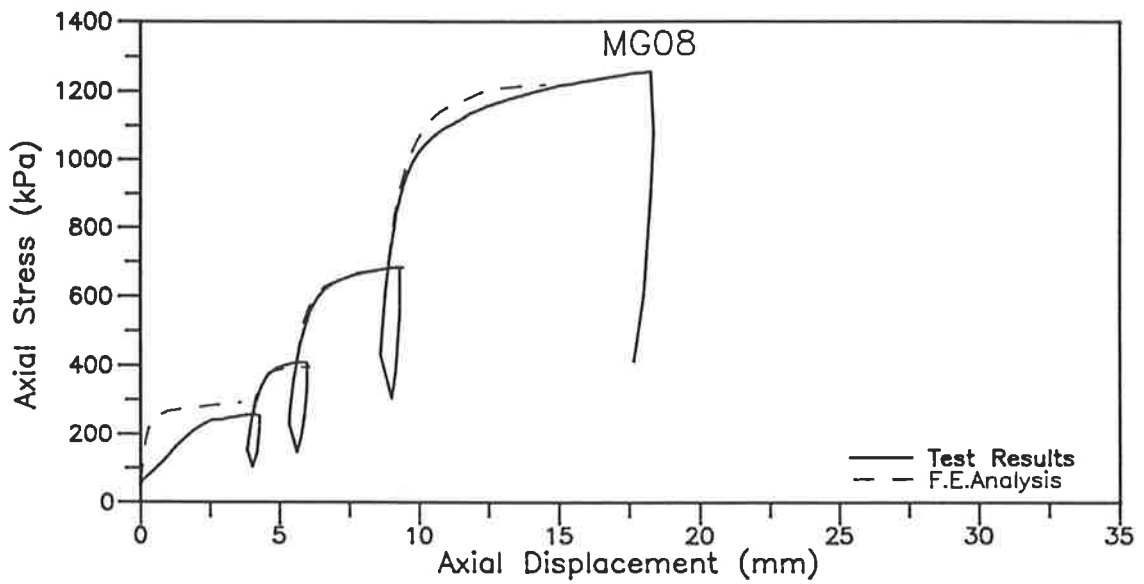
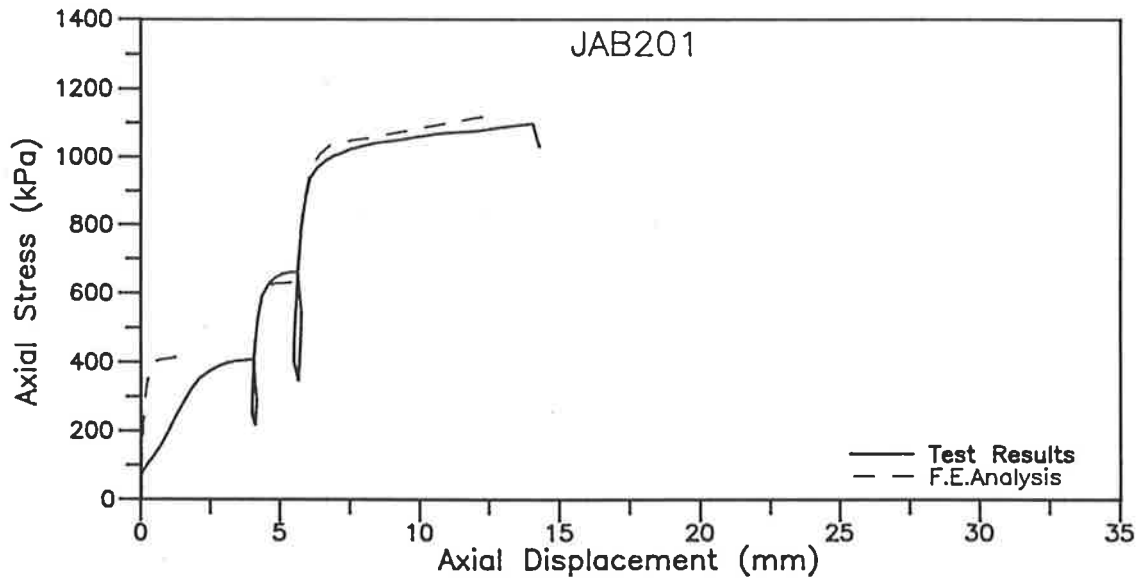
Table 5-2 provided initial estimates for shear strength constants. For the first laboratory test modelled, trial values for bulk and shear moduli were calculated from the early increments of each load stage. However, volume strain measurements in particular were not sufficiently precise in these ranges, and first-run values for other materials were adapted from the amended previous analyses. For each triaxial test, constants were altered by trial-and-error until reasonable fit was obtained with peak strength for the first load stage, and with the complete axial stress-deformation curves for later stages. (As noted in Section 5.2.2, bedding-in was suspected in the first stage, so its load-deformation behaviour was not modelled.) Figure 7-2 presents

results of the final models, and Table 7-1 summarises the contributing constants. These material models were then incorporated into the finite element analysis of dump slope stability.

MATERIAL	DESCRIPTION	BULK MODULUS		SHEAR MODULUS			SHEAR STRENGTH				
		k MPa	k MPa	q	g ₁ MPa	g ₂ , g _r MPa	c kPa	φ _o	c kPa	φ _r	
JAB201	Fresh M.Chlorite 6yr Schist	800	50	0.70	350	1.5	57	28.0	55	25.5	
MG08		800	50	0.35	250	0.5	40	25.6	35	23.0	
Frag75		800	50	0.35	250	0.5	48	24.4	43	22.3	
Frag60	EW Pegmatite	800	50	0.35	250	1.0	57	23.2	52	21.5	
RM27A		800	50	0.35	250	1.0	65	22.0	60	20.8	
JAB202z		Dump Soil	800	50	0.40	200	0.5	80	18.0	72	17.2
RM27B		EW Pegmatite	800	50	0.25	150	1.0	96	11.3	94	11.3
RM25		Mine-soil	800	50	0.60	250	0.3	66	27.0	50	24.0

Table 7-1 Material Constants for Finite Element Models

Figure 7-2 Results of Back-Analyses of Triaxial Compression Tests



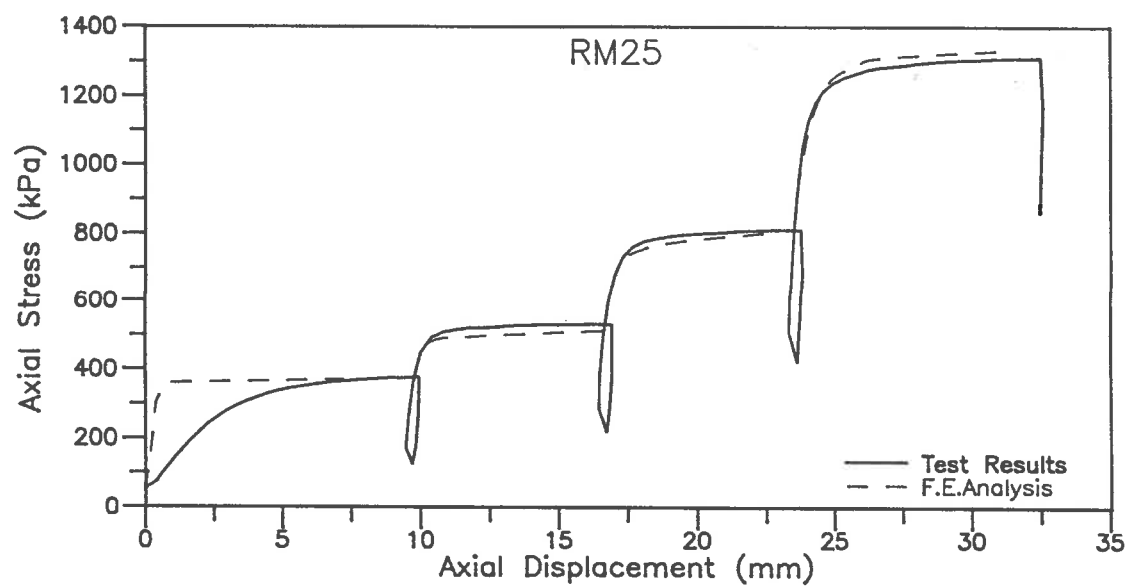
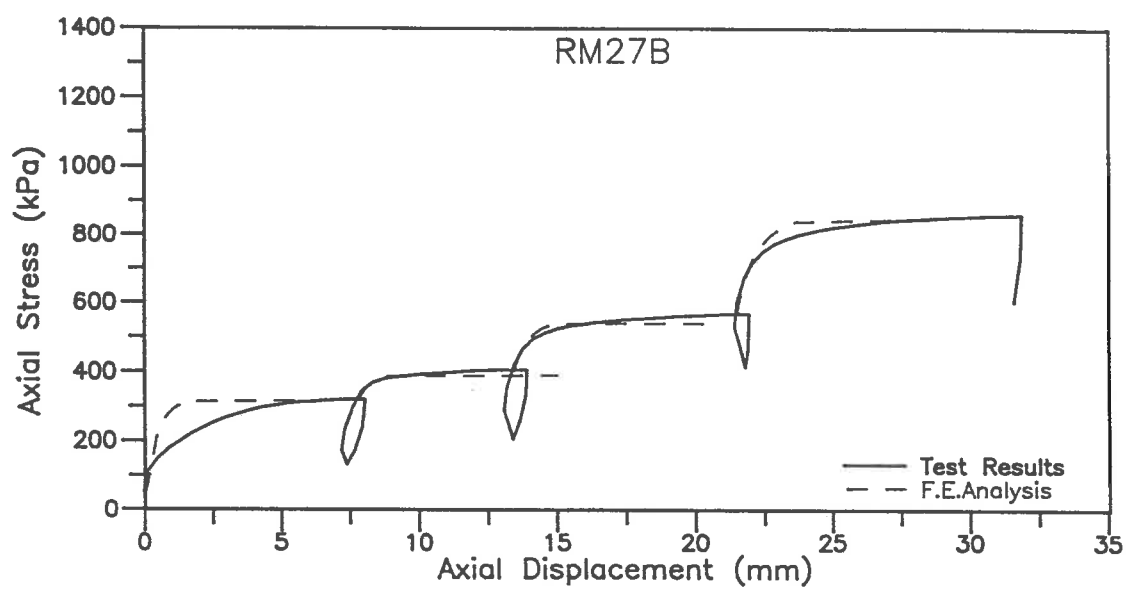
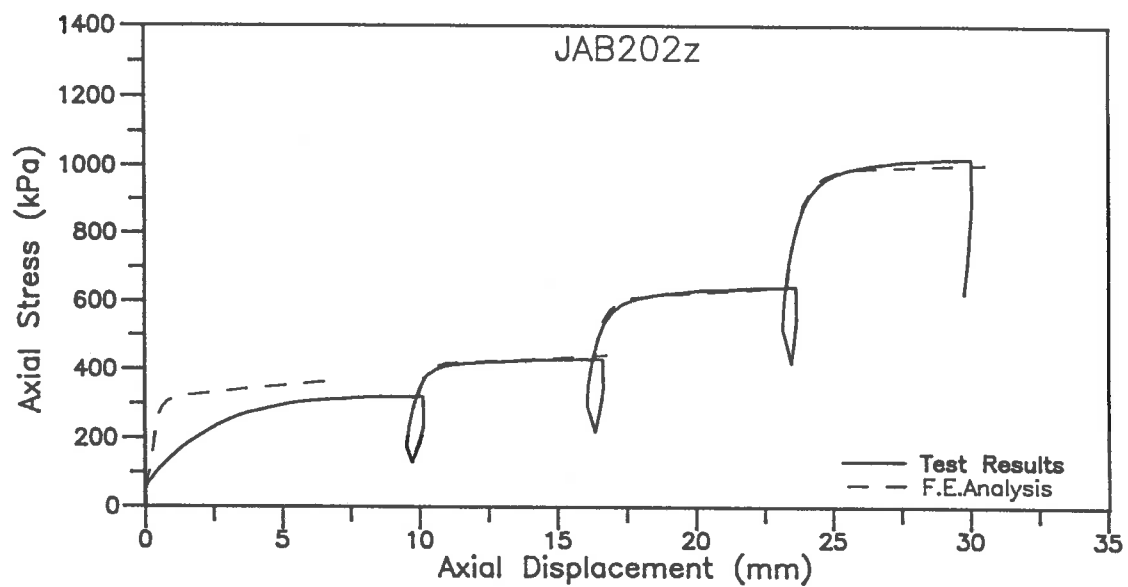


Figure 7-2 (continued)

7.2.3 Geometric Details

Table 3-1 included slope angles for the dump sampling and photography sites, which were estimated from mine contour plans. Values ranged from 22° to 47° , with a tangent mean of 32° . Richards, Peter, & Lucas (1986) adopted 36° (1:1.4) as a typical angle of repose in the earlier preliminary investigation of the waste-rock dumps. However, for the analyses carried out within the present project, a slope angle of 33.7° (1:1.5) was selected to simplify the mesh geometry while remaining within the range of typical dump batter slopes.

According to Richards, Peter & Lucas (1986), the general plan for construction of the dumps was three lifts of 11m height: perusal of mine survey plans from 1981 to 1989 indicated that actual lift heights have ranged from about 6m to 11m and that the time lapse between completion of one lift and commencement of the next has varied from less than one year to several years. A model lift height of 10m was selected, again from consideration of geometric simplicity of the mesh. Although primary interest was in dump stability up to three lifts, as the planned configuration, analyses were continued for two extra lifts to a total dump height of 50m. The main purpose of this was to assist understanding of the mechanisms failure for dump slopes, but analysis of higher dumps could also prove useful with regard to planning future dump extensions and constructions.

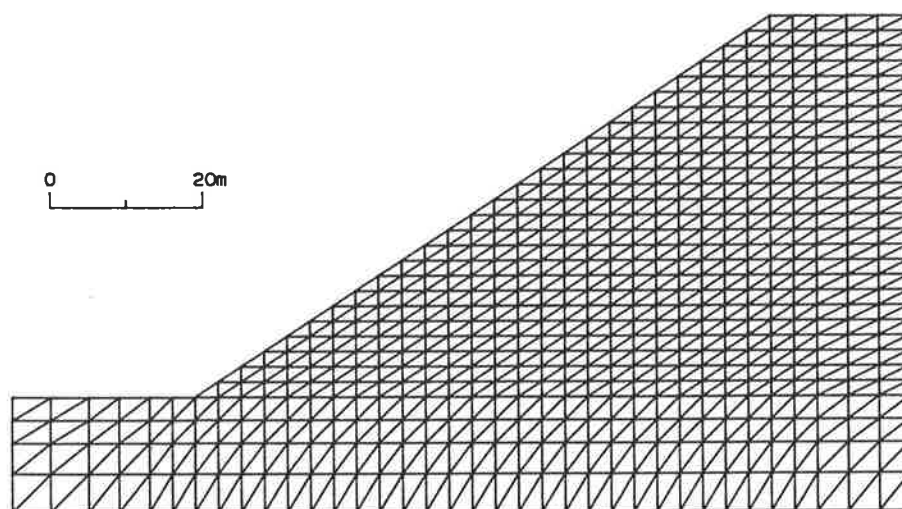


Figure 7-3 Finite Element Mesh for 1:1.5 Slope Waste-Rock Dump

The consequent finite element mesh, modelling a 1:1.5 slope built up in 10m high lifts to 50m, is illustrated in Figure 7-3. Locations of the mesh boundaries, ideally distant from the slope face, were constrained by programme array limitations (700 nodes and 1200 elements) and the undesirability of highly elongated elements. The vertical boundary through the dump and natural subsurface base was further than 40m behind the slope face over the first three lifts. Although at the final model height the top of the slope was 14m from this boundary, only horizontal restraint was imposed. As displacement at the top of a slope is predominantly vertical, particularly at the onset of failure, significant interference was not expected. (As discussed in Section 7.3, the proximity of the boundary did appear to intersect slip surfaces, but only at the upper two lifts.)

Nodes along the bottom of the mesh were pinned in both horizontal and vertical directions. Partial horizontal restraint could have been modelled using specially defined joint elements but in view of the competent nature of the undisturbed subsurface, the simpler option of full restraint was a reasonable approximation. To minimise any chance of disturbance to stress distributions in the proximity of the slope, the boundary was located 15m below the original land surface, compared to 8m as used by Richards, Peter, & Lucas (1986).

The short vertical boundary beyond the toe was restrained against horizontal displacement only. Some concern was held that fixity in this region might artificially support the toe (by providing horizontal reaction) and thus inhibit failure in the model. Consequently, a series of runs was made varying the extension of the mesh beyond the toe. As shown in Figure 7-4, for boundaries closer than about 20m the toe displacement was significantly reduced, but for wider meshes the further change was small. Consequently, a base extension of 24m beyond the toe of the slope was specified for the mesh modelling the 1:1.5 batter.

Staged construction of the waste-rock dumps was modelled by specifying each lift with different material numbers (although not necessarily with different material properties), as shown in Figure 7-5. For each increment a maximum effective material number corresponding to the top of the current lift was also specified. To emphasise any relationship

between weathering and stability it was decided to focus on slopes modelled as comprising homogeneous material. However, a series of runs was also performed which considered soil formation at the top of the first three lifts. The material numbering in Figure 7-5 permitted both options, as material numbers 3, 5, and 7 could be assigned the properties of either the current bulk material or the dump soil (JAB202z).

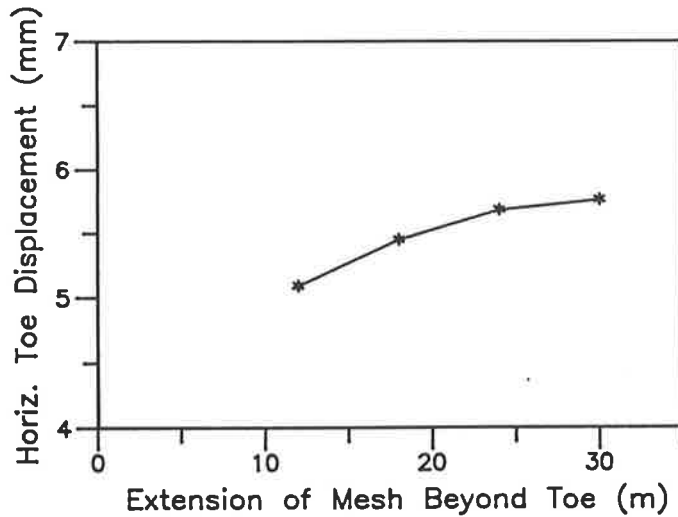


Figure 7-4 Effect of Base Extension on Toe Displacement

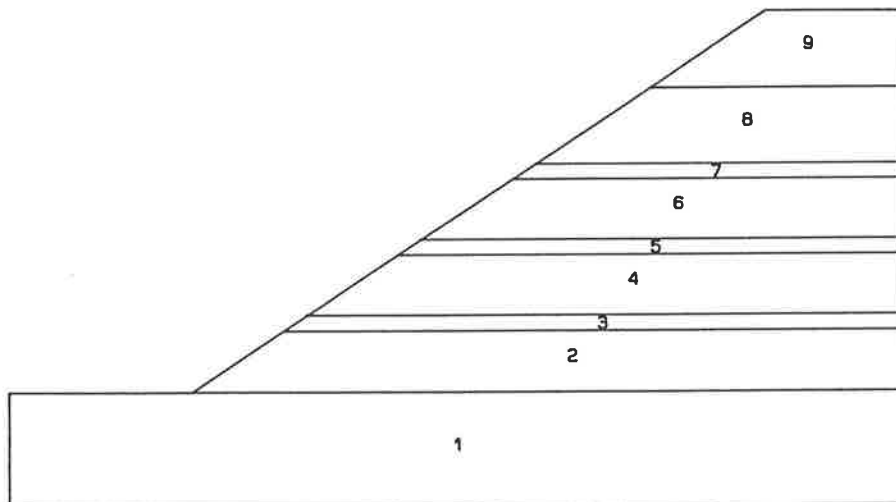


Figure 7-5 Specification of Material Numbers for Slope Analyses

Failure through the natural base is one of the common modes of dump instability (Caldwell & Moss 1985). It is normally anticipated when the foundation is weak or saturated, conditions which a dump can itself induce in otherwise sound material. The weight of waste-rock creates a bowl-shaped deformation in the underlying surface. In fact, Richards

(1987) predicted more than 1m differential vertical compression under dumps at Ranger Mine. In the common case of the dump being much more permeable than the base, water (seepage and runoff) can drain into this depression and gradually wet up the material under the dump. Therefore, another set of analyses was carried out in which the row of base elements immediately below the dump were assigned different material properties after the second lift was applied. Since the focus of this research was strength-weathering relationships in waste-rock, natural surface mine-soil was considered mainly in a comparative sense and was not widely sampled or tested. The constants selected to model softened base represent reasonable possible strength values ($c=c_r=15\text{kPa}$; $\phi=18^\circ$; $\phi_r=12^\circ$). The intention of these analyses was simply to test the potential for foundation failure, and whether separate detailed investigation might be warranted.

Slopes in the final rehabilitated landform will be much flatter than the present waste-rock dumps, with the current proposal based on 1:5 (11.3°) grades. Consequently, it was intended to undertake finite element analyses using two other meshes, modelling 1:3 and 1:5 slopes, to investigate mass stability, in particular of the more weathered materials, within longer term landscape geometries. However, based on results for the 1:3 mesh, discussed in Section 7.3, the flatter series was considered unnecessary. The mesh for the 1:3 slope is given in Figure 7-6.

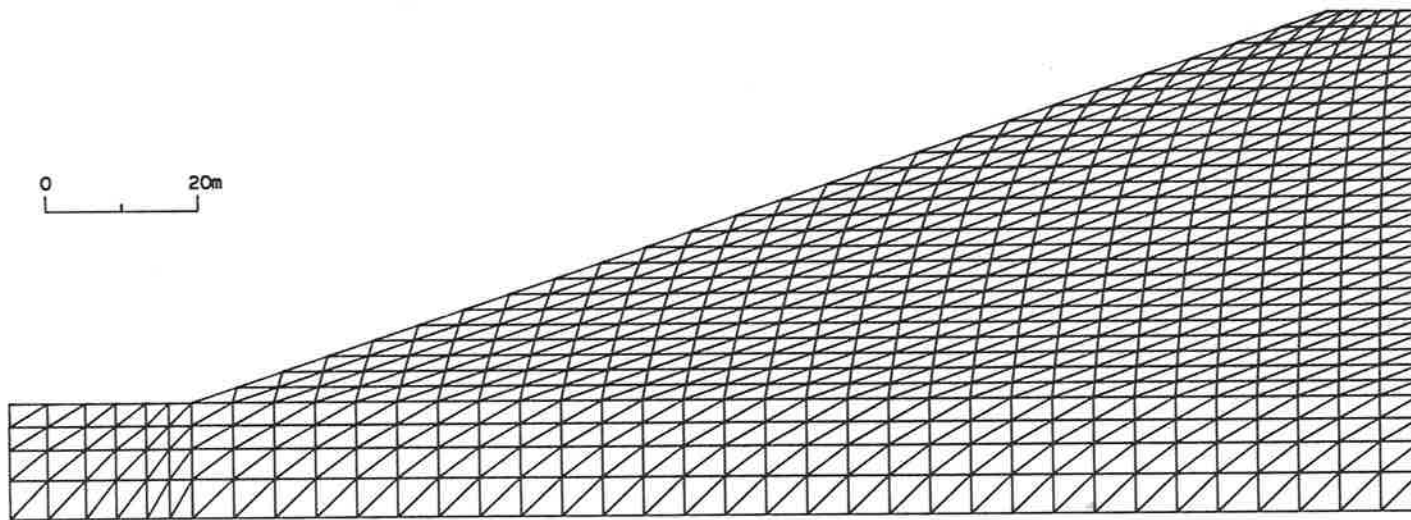


Figure 7-6 Finite Element Mesh for 1:3 Slope in Rehabilitated Landscape

7.3 Results and Discussions

7.3.1 General

A summary of the finite analyses carried out is provided in Table 7-2. Regarding general interpretation of the results, it was found that stress contours provided a check on the behaviour of the model and some appreciation of the mechanisms by which a slip could develop. However, yield is dictated by the ratio of stress to strength, rather than by stress in an absolute sense, and so these contours were inadequate to positively identify progression towards slope failure. Furthermore, at the onset of failure there was a tendency to numerical instability which rapidly invalidated stress contours throughout much of the mesh. A condition flag indicating the state of failure was included in the output for each element. This flag is specified such that it is not very sensitive prior to failure, but unlike stress contours it remains meaningful when slope instability occurs (refer to the legend in Figure 7-10). Condition flags were thus valuable in illustrating the shape of any slip which occurred in the model.

Nodal displacement vectors gave a better perception of the accumulating deformation leading up to slope instability. As failure occurred, numerical instability usually affected displacements at the top of the model, but the lower portion and most of the batter face continued to produce interpretable results. Vector plots also provided some indication of the locations of slip surfaces, but generally not as clearly as the condition flags. To allow direct comparison of different analyses, two single-value parameters were extracted, namely, H_{toe} (horizontal displacement of the first node above the toe on the slope face) and H_{max} (maximum horizontal displacement along the slope face, excluding any numerically unstable parts of the mesh). The former is more neatly defined, being at a fixed location, but it was thought that H_{max} might be more appropriate if slip failures occurred which daylighted above the toe. In fact, displacements were often greatest some distance up the face, but H_{toe} and H_{max} provided consistent comparisons between model runs.

In following discussions of the separate series of runs, a general assessment of slope stresses is presented first, taking material RM27A as reference. This is followed by descriptions of any slope instability

observed, including inference of the modes of failure. The characteristic displacements at increasing dump heights are then compared for the different materials and related to a level of stability (or otherwise) of waste-rock dumps at Ranger Mine.

SERIES	DESCRIPTION	MATERIAL	COMMENTS
main	1:1.5 slope; dump comprised of a single material; 5 x 10m lifts.	JAB201 MG08 Frag75 Frag60 RM27A JAB202z RM27B	Massive slope failure Approaching failure Large deformation
soil	1:1.5 slope; dump comprised of a predominant material with 2m thick soil layers (JAB202z) at the top of the first 3 lifts; 5 x 10m lifts.	JAB201 MG08 Frag75 Frag60 RM27A	Slope failing Approaching failure
base	1:1.5 slope; dump comprised of a single material; the row of elements immediately below the dump modelled as softening after the second lift is placed; 5 x 10m lifts.	JAB201 MG08 Frag75 Frag60 RM27A JAB202z RM27B	Overstressed regions Massive slope failure Massive slope failure Slope failing Slope failing Slope failing Commencing failure
lin3	1:3 slope; dump comprised of a single material; the row of elements immediately below the dump modelled as softening after the second lift is placed; 5 x 10m lifts.	JAB201 MG08 Frag75 Frag60 RM27A JAB202z RM27B	

Table 7-2 Summary of Slope Analyses

7.3.2 Reference Analyses (*main*)

The *main* series of programme runs modelled a dump consisting of homogeneous material with 1:1.5 batter slopes, and constructed on a base of natural minesoil with the properties of sample RM25. Stress contours, from the analysis for RM27A are presented in Figures 7-7, 7-8, and 7-9. Vertical stress distributions were typical of gravity loading, with parallel contours following the slope of the surface. This characteristic showed no variation related to the level of slope stability or otherwise but was a useful check on the status of the model with respect to numerical stability.

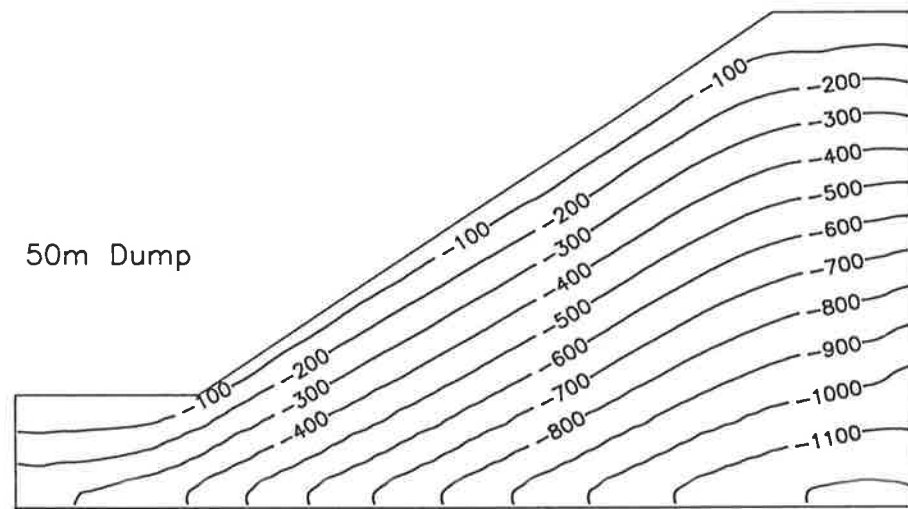
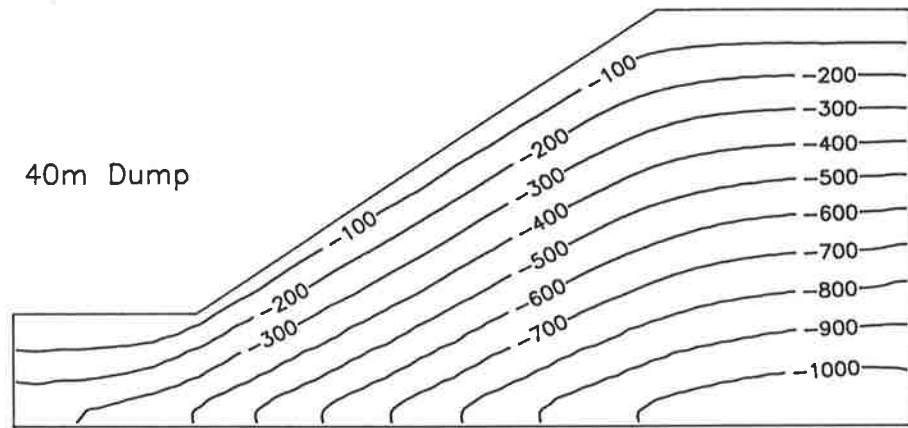
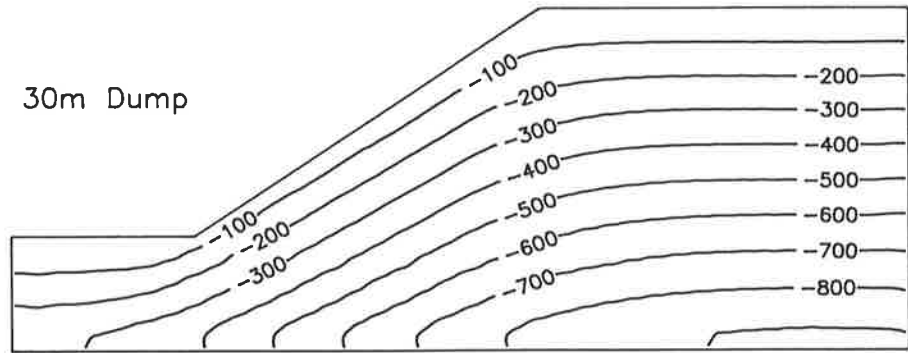
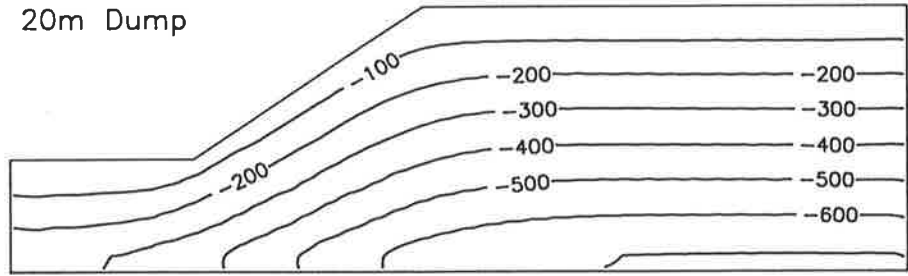


Figure 7-7 Vertical Stresses for RM27A - main Run

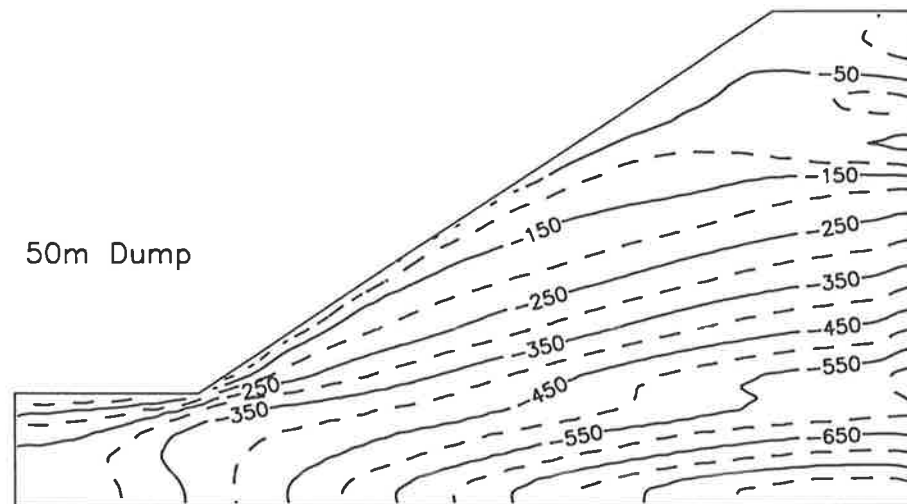
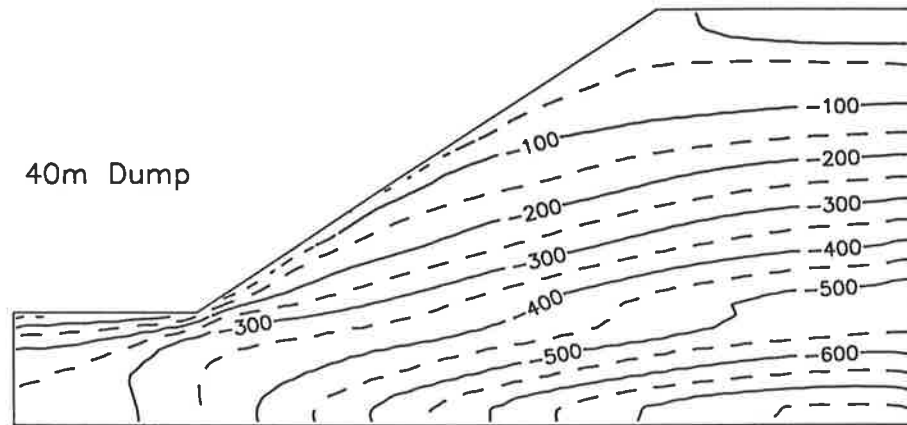
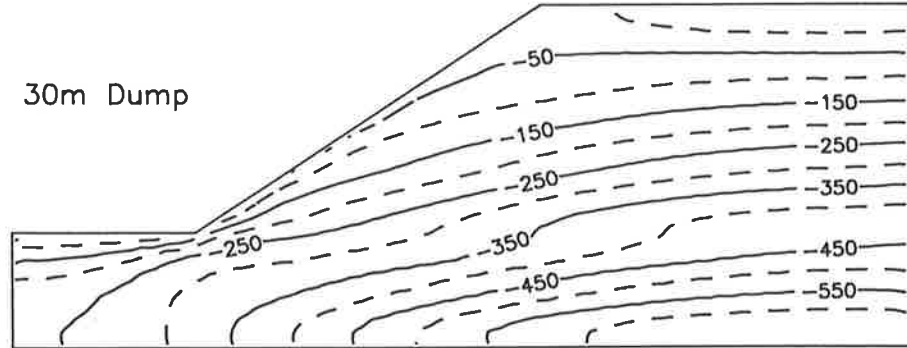
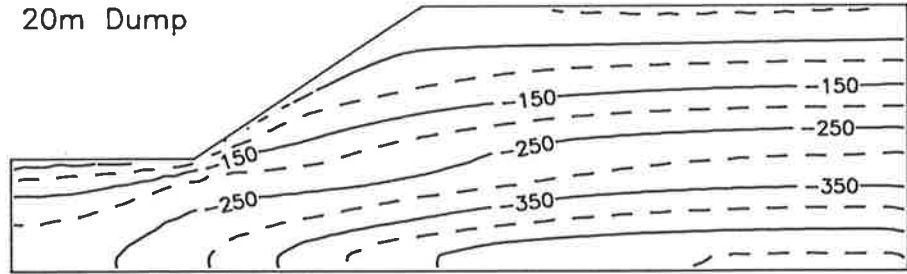


Figure 7-8 Horizontal Stresses for RM27A - main Run

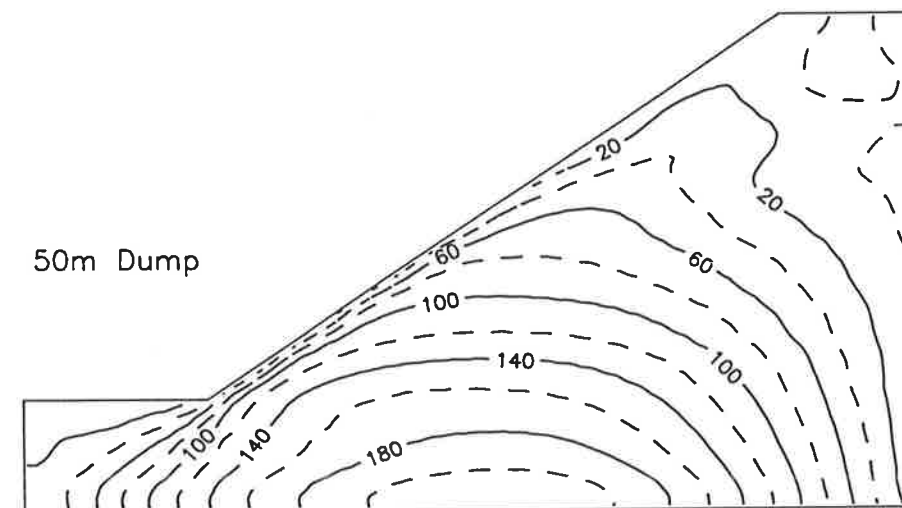
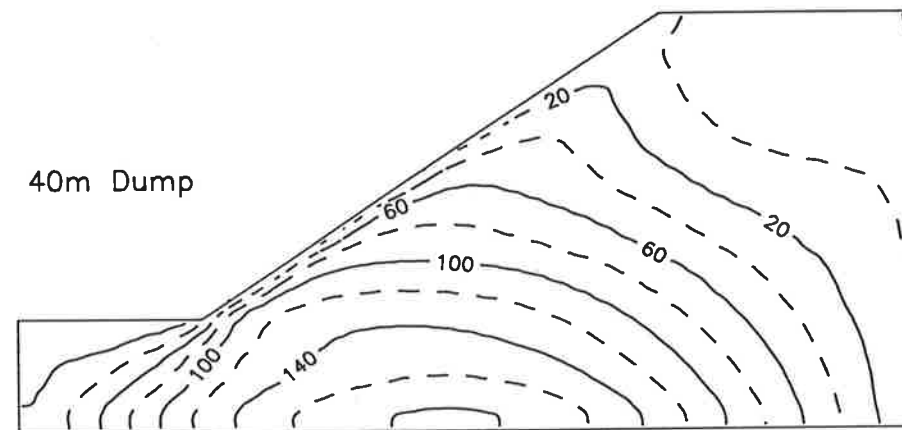
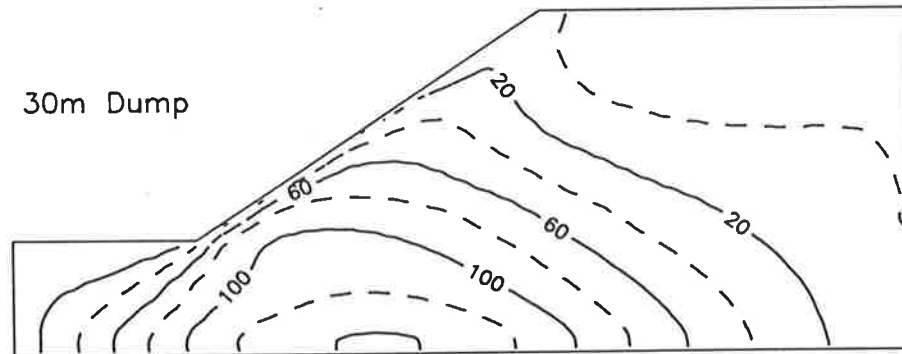
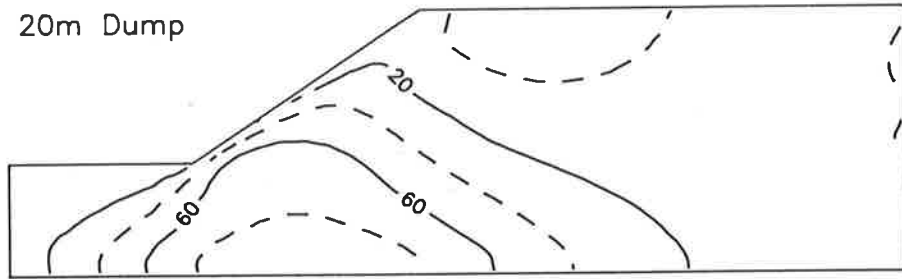


Figure 7-9 Shear Stresses for RM27A - main Run

Horizontal stress contours were somewhat more informative. In Figure 7-8, the kinks just above the base indicate outward horizontal thrust developing at that level. (For material JAB201, for which the dump was stronger than the base, these kinks were less pronounced and located in the row of elements immediately below the dump.) Minor zones of horizontal tension occurred along the top of the dump which sometimes extended a short way down the right boundary at the final lift, as if the mesh was trying to pull away at that corner. This suggested that the model was not large enough to contain the complete sliding mass. However this did not appear to significantly interfere with the lower part of the model and since the mesh was already near the size limit for the programme, the shortcoming was tolerated.

As seen from Figure 7-9, shear stress (along horizontal and vertical planes) was also concentrated at the toe. At each load increment contours tended to elongate slightly along a line somewhat steeper than the face, which might be envisaged as a surface of minimum stability for the dump at that height. This line appears to intersect the face at the top of the dump until the final lift when, as illustrated by the 20kPa contour, the higher shear stress propagates back into the dump. (There may be a connection with the extended zone of horizontal tension noted at this stage.) However, condition flags for the one run in this series which resulted in slope failure suggested a slip surface further from the face at that level. In summary, stress data produced by the analyses were plausible and consistent with static equilibrium (up to the occurrence of mass failure), but provided no clear indication of the development of slope instability.

In this *main* series most runs behaved in a similar manner, except the analysis incorporating material MG08, in which mass instability occurred when the final lift was applied. Up to 30m dump height element stresses were much the same as for other materials but at 40m some localised stress oscillations were noted, and at 50m failure was evident in the body of the dump and the top of the dump model became numerically unstable. The analysis was repeated with the final lift applied in two stages and despite the persistence of numerical inconsistencies, failure was controlled sufficiently for the condition flags to delineate the slip. Figure 7-10 indicates the failed mass as a broad arc daylighting in the toe, rising almost parallel to the face,

and intersecting the right mesh boundary in about the fourth lift. Such a failure is consistent with an embankment on a sound foundation.

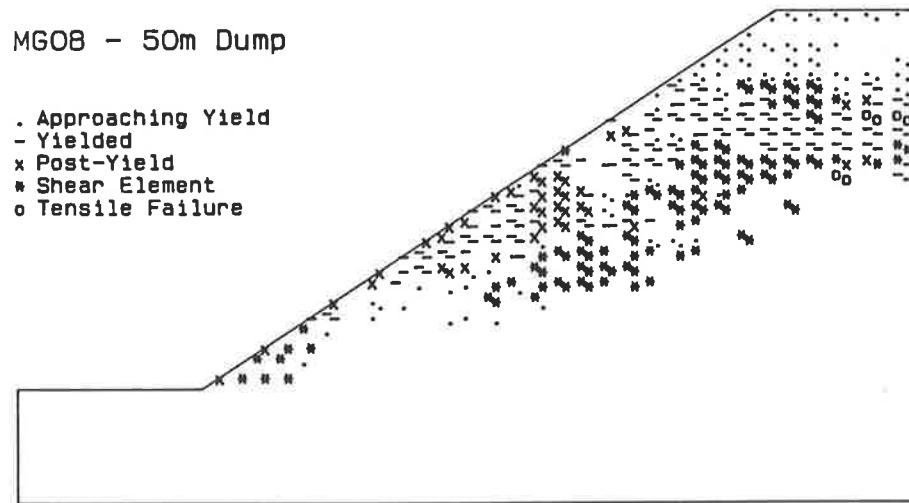


Figure 7-10 Condition Flags for MG08 - *main* Run

The hypothetical material Frag75 showed evidence of approaching instability at the final lift, with some elements in the toe region converted to shear elements and other limited zones of overstress, particularly extending from the right mesh boundary between 36m and 42m height. No other runs in this *main* series showed significant actual or numerical instability. Materials MG08 and Frag75 represented waste-rock after about 6-10 years exposure on the dump batters, a stage when both c and ϕ were reduced (relative to as-mined rock) by the decline of particle interference effects, but before there was sufficient clay to develop true cohesion.

The resultant trough in the value of shear intercept (refer Section 6.1.2 and Figure 6-4) is apparently the critical factor, since friction angle continues to decrease with degree of weathering but the older materials did not fail in 50m high dumps. The specific implication of a low value of shear intercept is lower shear strength at low normal stress, that is, when the friction contribution is not dominant. Consistent with this, the failure for MG08 was mainly initiated in the top of the dump (under low vertical stress) and propagated downwards. A suggested translation into the physical slope is that the weight of the new lift deforms the existing dump to an extent that the consequent strain induced in the new lift, keeping in mind the low confining

stresses, is sufficient to commence failure. The subsequent load redistribution and further deformation permit the slip to progress through the dump batter. It may be doubtful whether a real slope would fail extensively in such a manner, or whether the top lift would simply slump and repack. The (initially) independent local toe failure supports the former. At the least, it may be concluded that slopes comprising waste-rock in a condition represented by MG08 are significantly less stable than those consisting of fresher or more weathered material.

Figure 7-11, in which displacement vectors for MG08 are compared with those for RM27A, shows both the similarity of results at 40m height and the region of numerical instability when MG08 failed. This indeterminacy was at least exacerbated by the mathematical possibility for an element to suffer more than 100% compressive strain, which is of course physically not possible. Stability of the solution might be improved by programming against this, such as by increasing stiffness parameters again after 60% strain. However, the numerical difficulty is probably more fundamental, reflecting the fact that a massive slip destroys the material continuum and contravenes static equilibrium. Therefore, since most of the mesh remained solvable and was not greatly affected, it was not attempted to modify the programme and the results were accepted as produced.

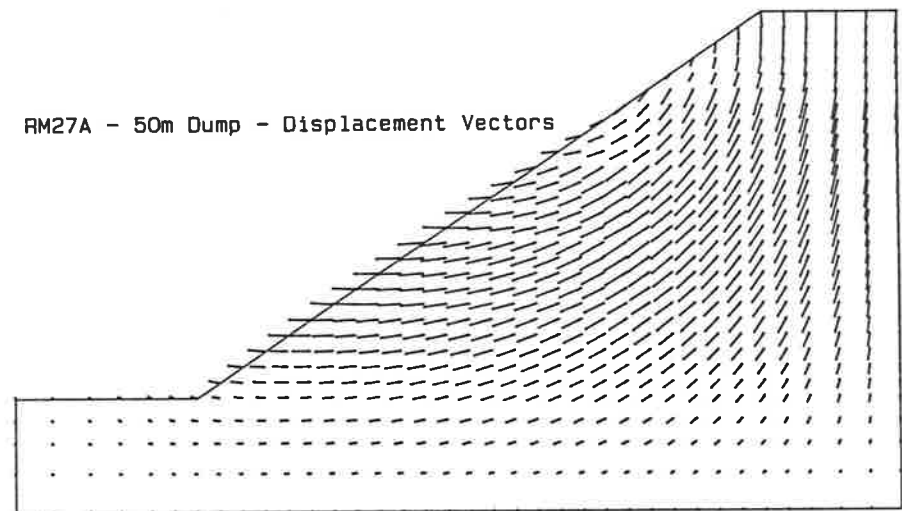
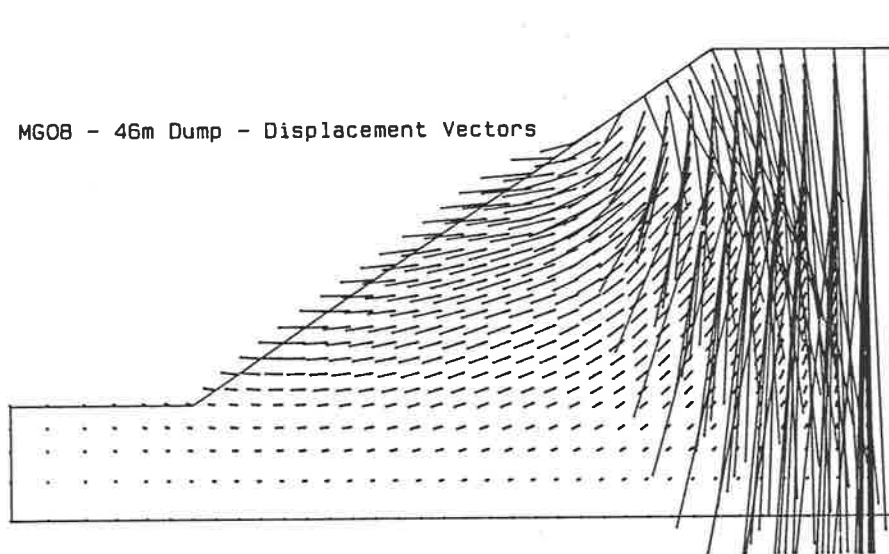
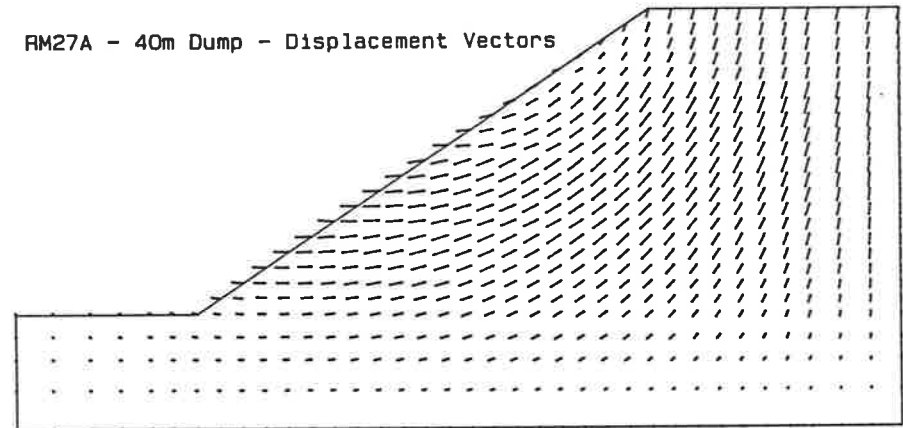
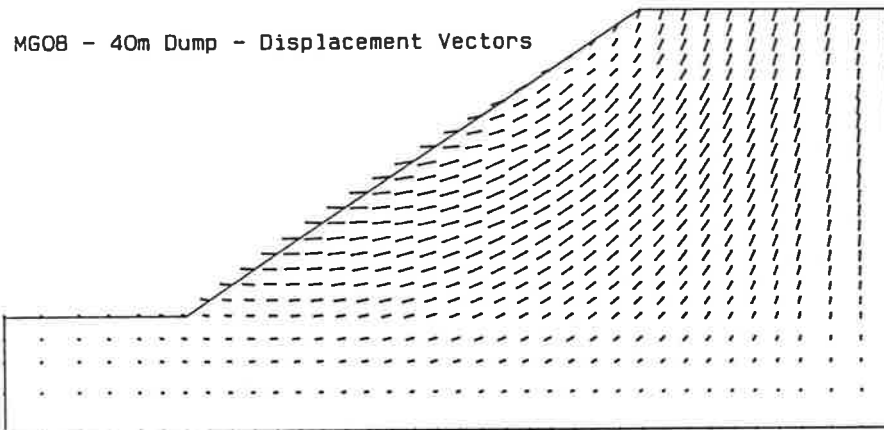


Figure 7-11 Displacement Vectors for MG08 and RM27A - *main* Runs

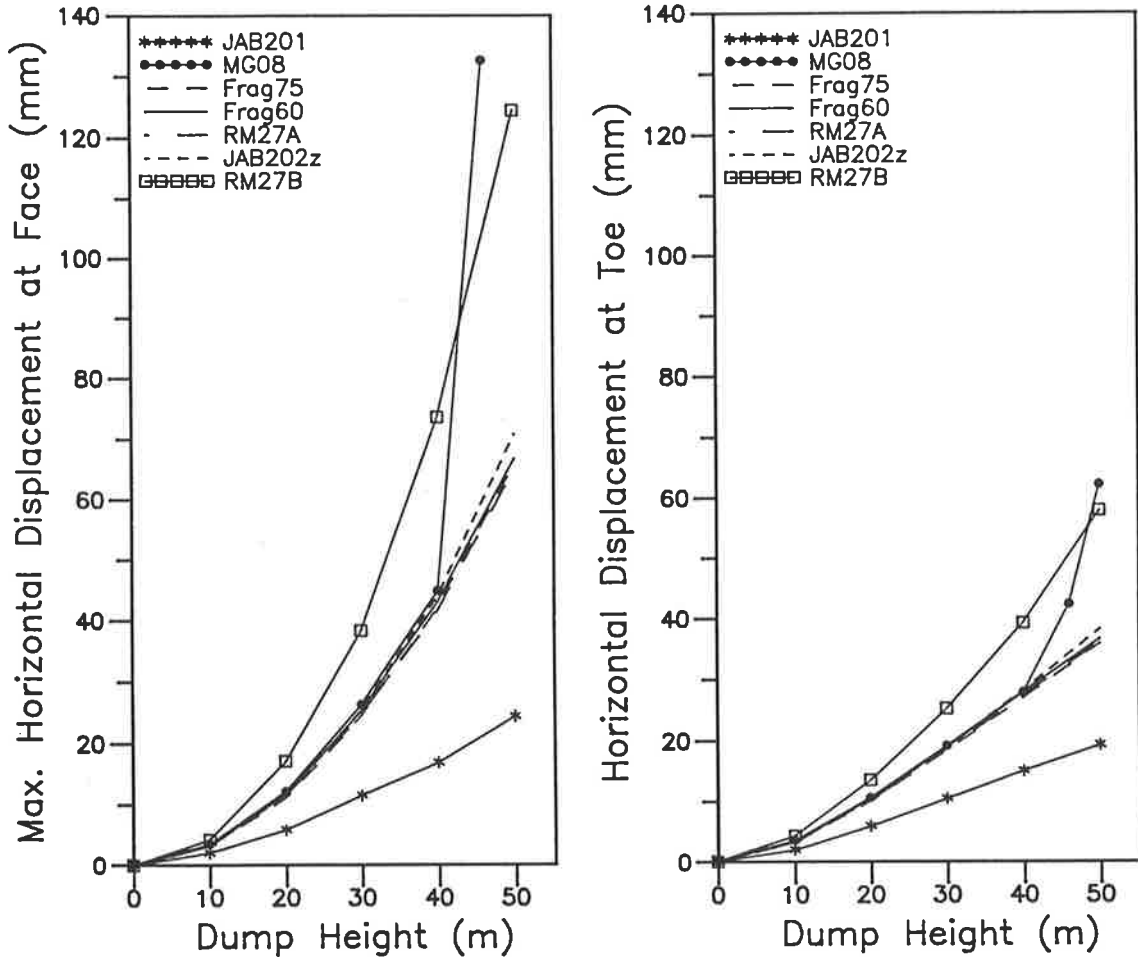


Figure 7-12 Characteristic Displacements at Slope Face - *main* Runs

Characteristic displacements at the dump face are presented in Figure 7-12 (refer Table 7-1 for material descriptions and properties). The freshest material, JAB201, produced the least deformation, and the approximately linear increase in displacement with dump height implies that it would be stable at 1:1.5 (33.7°) slope almost regardless of height. This result is reasonable, considering the high angle of internal friction (29.8°) and the significant shear intercept due to fragment interference. At the other extreme, material RM27B was markedly more deformable even at low dump heights, with increasing increments of displacement after each successive lift. The shape of the curve suggests a component plastic deformation, and the material might be susceptible to long-term creep. Consequently, despite the fact that this analysis showed only minor overstressing at the toe and in the fourth lift, it cannot be confidently predicted that this material will be stable indefinitely at 1:1.5 slope. However, RM27B was included in the *main* series mainly for comparison of materials, and it is unlikely

that the dumps will weather to this degree before they are flattened and reshaped into the final rehabilitated landform.

Results for the remaining five materials were remarkably similar, except that for MG08 horizontal displacements were much greater at the final lift. The curves for both characteristic displacements steepened slightly in the previous lift but not enough to be a clear warning of impending failure. Frag75, which at 50m appeared from localised stress concentrations to be at about the same stage as MG08 was at 40m, was not distinguishable from the other materials. The physical dumps are developed somewhat differently from the model, each lift as-constructed consisting of freshly mined waste-rock (JAB201) and then weathering, possibly non-uniformly, to the state represented by MG08. (Also, the current dump height is limited to 30m.) Furthermore, without calibration of the model against field prototypes at Ranger, the resultant displacements are only valid in a relative sense. However it may be concluded from this series of analyses that with respect to slope stability, the critical stage of waste-rock weathering is when shear intercept is minimised (for example, at 5-10 years exposure on batters). Any failure in such material is be expected to be of a rapid and massive nature.

7.3.3 Analyses Incorporating Soil Layers (*soil*)

The second series of finite element analyses (*soil*) modelled 1:1.5 dump slopes comprised mainly of uniform material except for 2m deep soil layers (material JAB202z) at the top of each of the first three lifts. This configuration reproduced conditions observed on some actual dumps (Fitzpatrick 1986), where lift terraces were at final height or had been left exposed for several years before constructing subsequent lifts.

Stress contours interpreted from the analysis for RM27A were almost identical to those from the corresponding *main* run, which is understandable considering the similar mechanical properties of RM27A and JAB202z. Material JAB201 showed small increases in horizontal stress at the soil layers, but in general the effects were minimal. MG08 again resulted in slope instability but, as shown in Figure 7-13, the slip was not as fully developed as in the main run (compare to Figure 7-10). By contrast, Frag75 showed a relative increase in

instability, which was however largely contained within the fourth and fifth lifts, as is apparent from the displacement vectors in Figure 7-14.

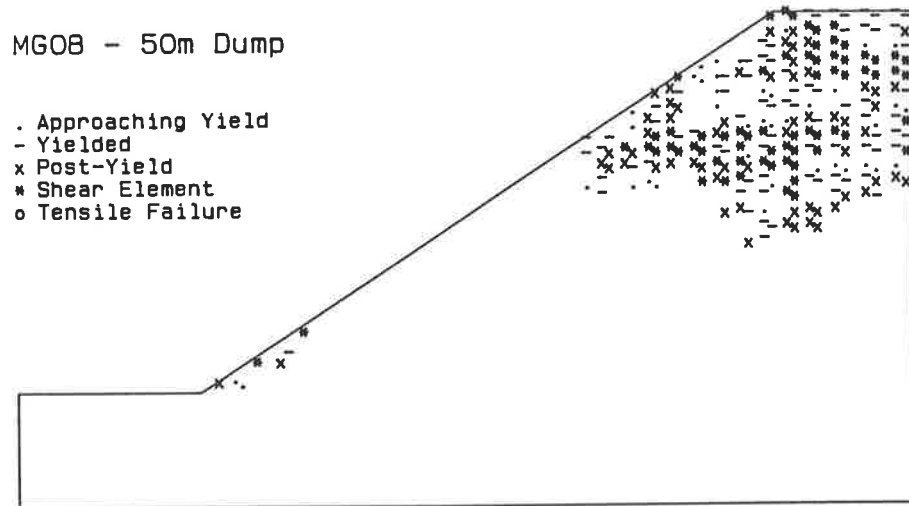


Figure 7-13 Condition Flags for MG08 - soil Run

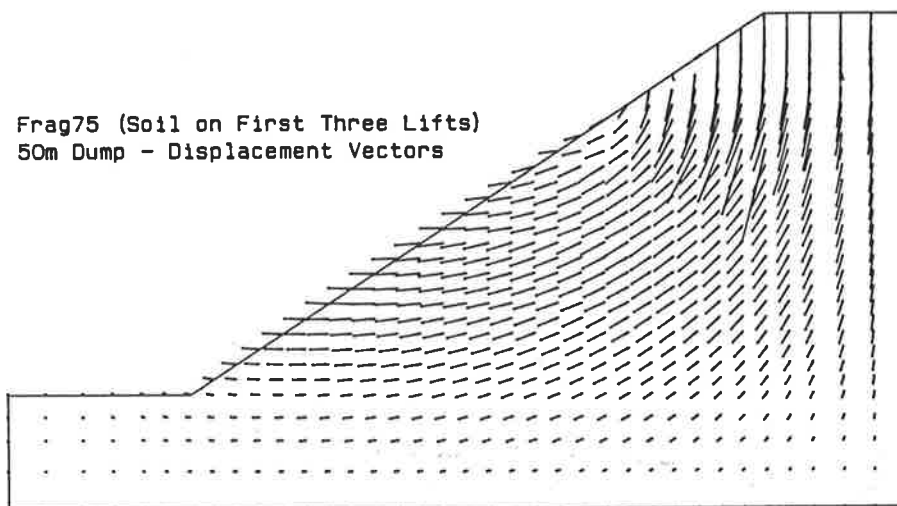


Figure 7-14 Displacement Vectors for Frag75 - soil Run

In comparison with Figure 7-12, the characteristic horizontal displacements in Figure 7-15 showed few significant differences between the two series of analyses. The slightly increased deformation for JAB201 was a simple consequence of inserting layers of weaker material, while the middle group of materials produced only marginally smaller displacements. However, despite the fact that for MG08 the top part of the model had again become numerically unstable, impending failure was not obvious from the slope face displacements for this analysis.

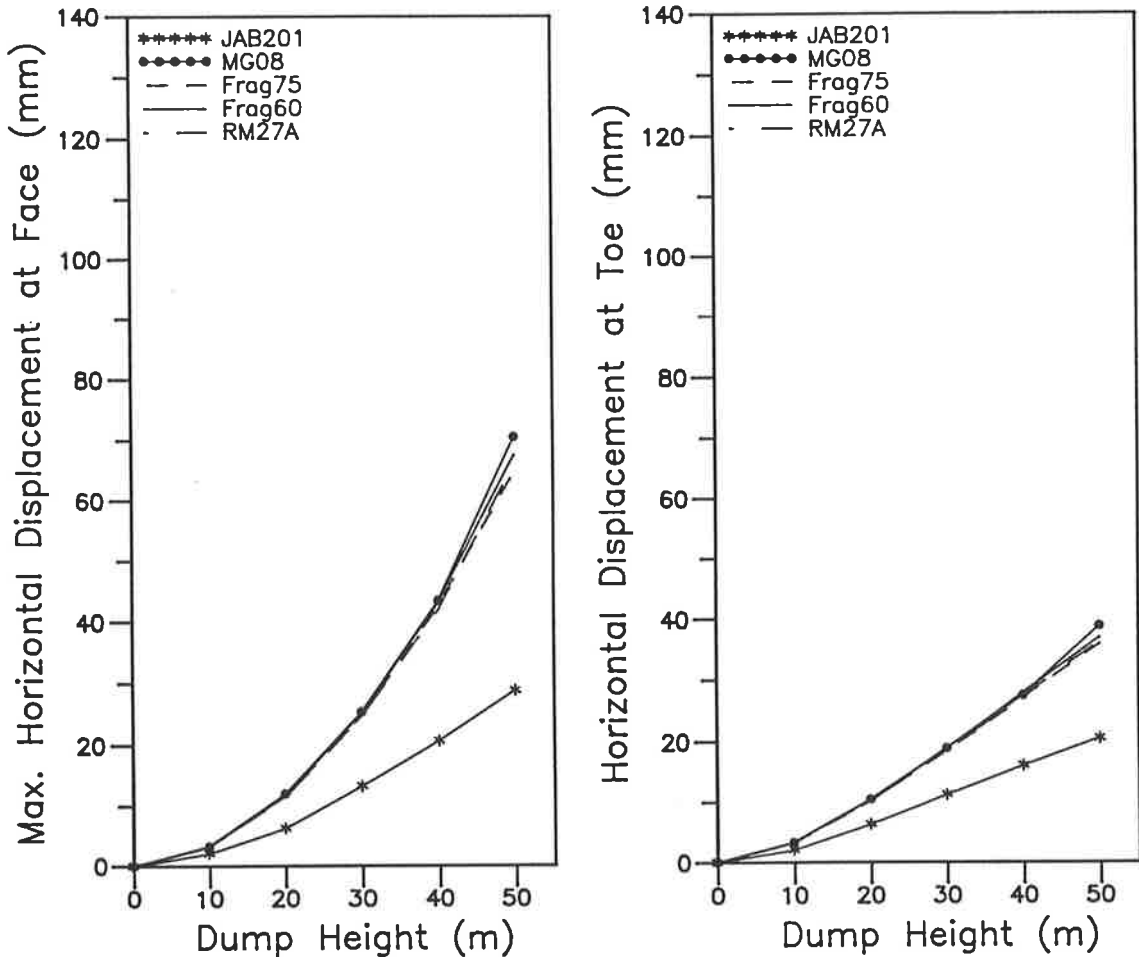
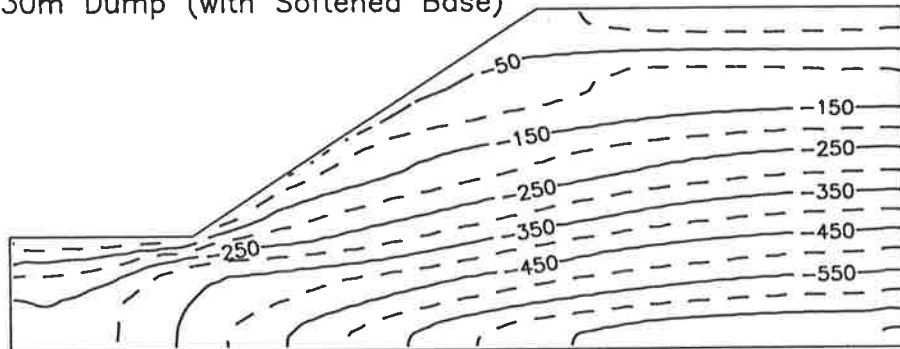


Figure 7-15 Characteristic Displacements at Slope Face -
soil Runs

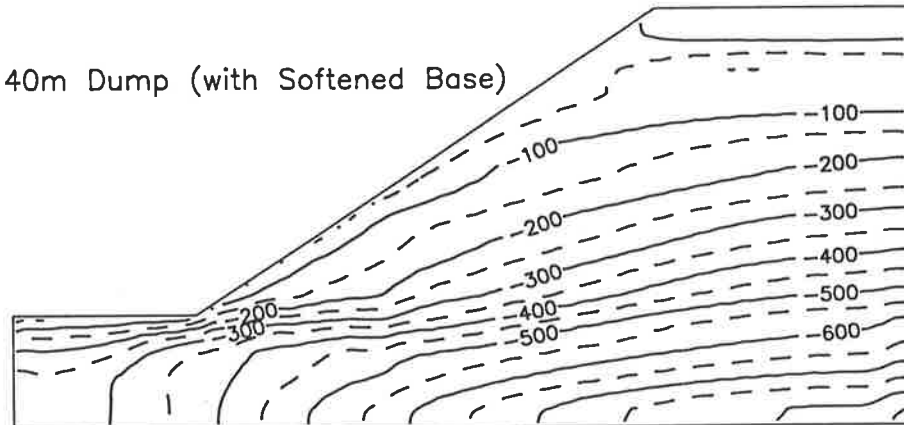
The basic conclusion from this series was that the inclusion of soil layers had only minor effects on finite element modelling of the dump slopes. Consequently, the simpler uniform material configuration was used in remaining analyses. However, it is noted in passing that dumps in which soil has been formed at lift terraces may be marginally more stable than those which were constructed in an effectively continuous operation from foundation to final height.

7.3.4 Analyses Incorporating Softening Under Dump (base)

30m Dump (with Softened Base)



40m Dump (with Softened Base)



50m Dump (with Softened Base)

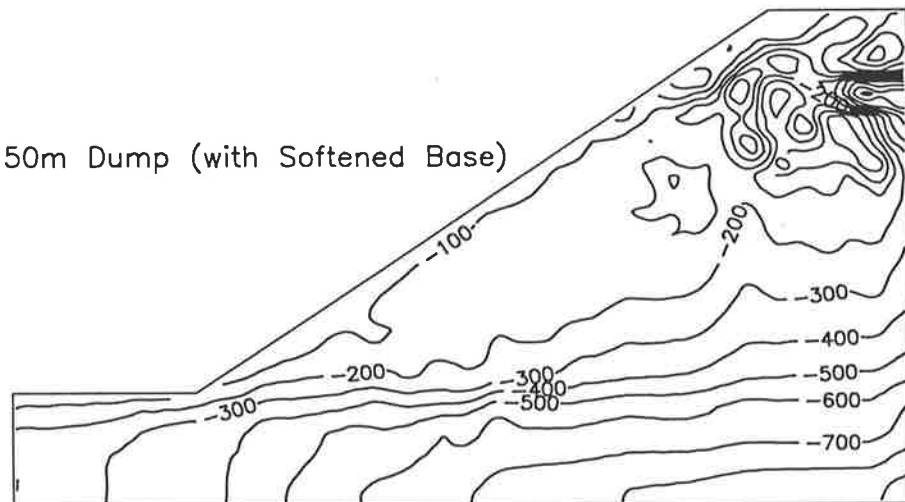


Figure 7-16 Horizontal Stresses for RM27A - base Run

As described in Section 7.2.3, it is feasible, even likely, for the foundation material immediately below the dump to become wet and

softened. The final series of programme runs (*base*) using the 1:1.5 slope mesh investigated this possibility. In all analyses, slope instability was observed developing after the third lift was placed (the base was softened after the second lift). Comparing Figure 7-16 with Figure 7-8, at 30m dump height there is apparent a much higher horizontal thrust directly below the toe and extending beyond the toe (for example, consider the 250kPa contour). The imminence of slip is more evident after the fourth lift, with contours below the toe being closely spaced and tending to align horizontally. At 50m the slope had failed and, despite obvious numerical instability in the top of the mesh, the large region of relatively constant horizontal stress bounded by the 200kPa contour can be envisaged as a block sliding out horizontally.

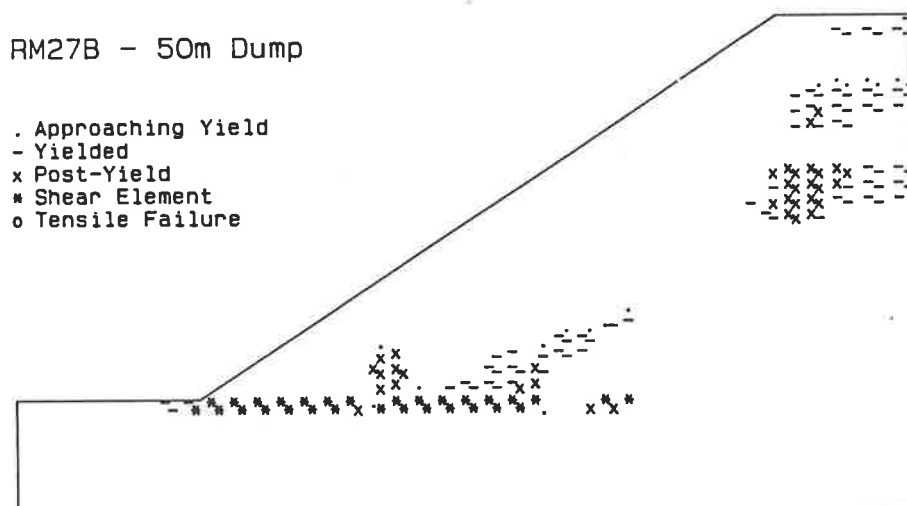
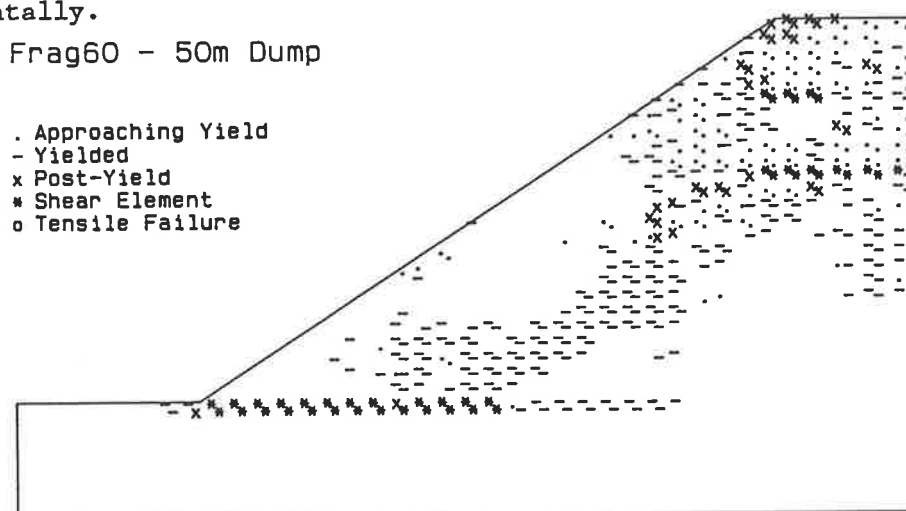


Figure 7-17 Condition Flags for Frag60 and RM27B - *base* Runs

Stress condition flags for MG08, which was once again the most unstable material, showed elements at or beyond shear failure in extensive regions of the final dump, while for JAB201 slope failure was just commencing and predominantly contained in the final lift. Between these limits, condition flag plots for other materials provided clearer illustration of the mode of failure. In the first example given in Figure 7-17, Frag60 showed the horizontal shear zone through the base met by a linear slip surface approximately parallel to the slope face. The top of the dump was somewhat confused, reflecting numerical instability, but below this most of the slope in front of the slip surface was essentially unfailed. The more restricted overstress from RM27B highlights the zones from which failure was propagated, namely, below the toe, an area at the bottom of the first lift, and at the top of the third lift. From interpretation of the results in overview, a simple two-wedge failure mode may be postulated, similar to that described by Blight (1985) for first time dump failure on a thin cohesive foundation.

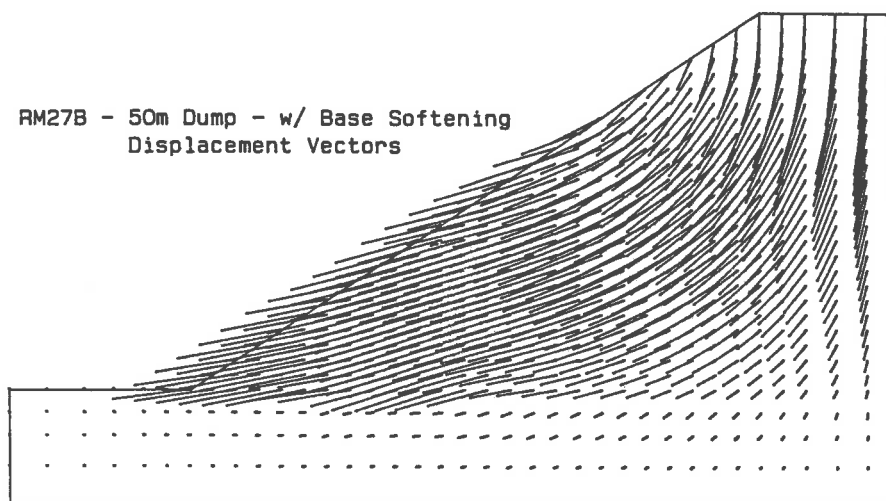


Figure 7-18 Displacement Vectors for RM27B - *base Run*

The displacement vectors for RM27B (Figure 7-18) are also illustrative. In particular, displacement along the base/dump interface suggests two centres of thrust, which further supports a two wedge mechanism. Figure 7-19, summarising horizontal displacement at the toe, reproduces the previous relations between materials (note the reduced scale relative to previous similar graphs). JAB201 again produced a much stiffer response, although slope instability was apparent after the fourth

lift. Results for the next five materials were clustered as usual up to 40m dump height, with increased displacements between 30m and 40m warning of the impending slope failures. The important feature after the final lift is that slips had obviously occurred: it would be difficult to draw a firm conclusion from actual values of final toe displacement, although it may be significant that those for MG08 and Frag75 were largest. Characteristically, RM27B showed greater deformation at the lower lifts, less evidence of shear failure at the final lifts, and no distinct transition from stable to unstable dump.

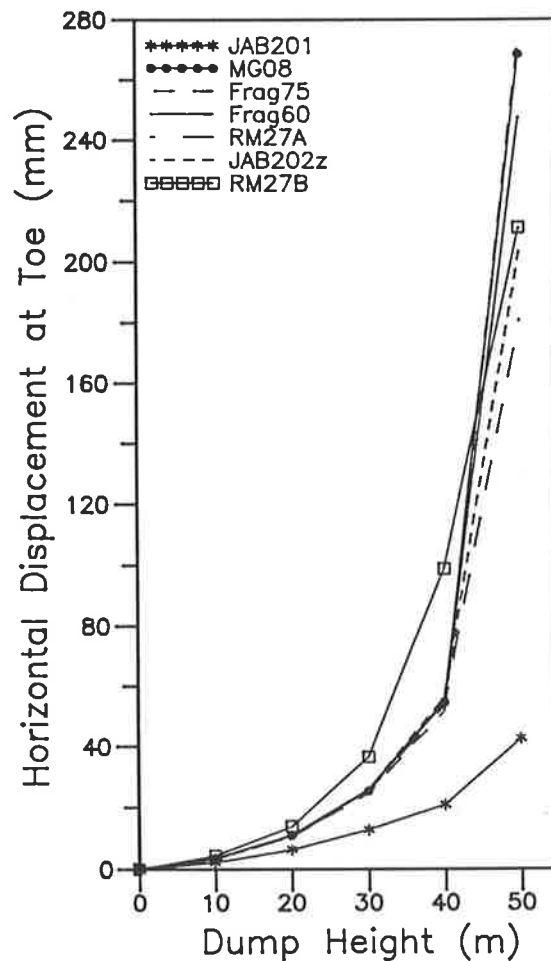


Figure 7-19 Characteristic Displacement at Toe - *base* Runs

Although, as stated in Section 7.2.3, the material properties modelling a softened base were only guessed reasonable values, the preceding analyses have shown that failure through a softened base is the most likely mode of dump failure. No instability was observed up to 30m, which is the height at which actual dumps are currently stable. In fact, the modelling suggested that dumps might be generally stable to 40m height, although a more extensive analysis of the sensitivity to

material properties would be advisable before adopting this limit for design. However, in summary it may be concluded that there is no cause to doubt the stability of the present dump geometry over the planned life of the mine, but that higher dumps should not be constructed without thorough geotechnical investigation with emphasis on the potential for foundation failure.

7.3.5 Assessment of Stability over the Long-Term

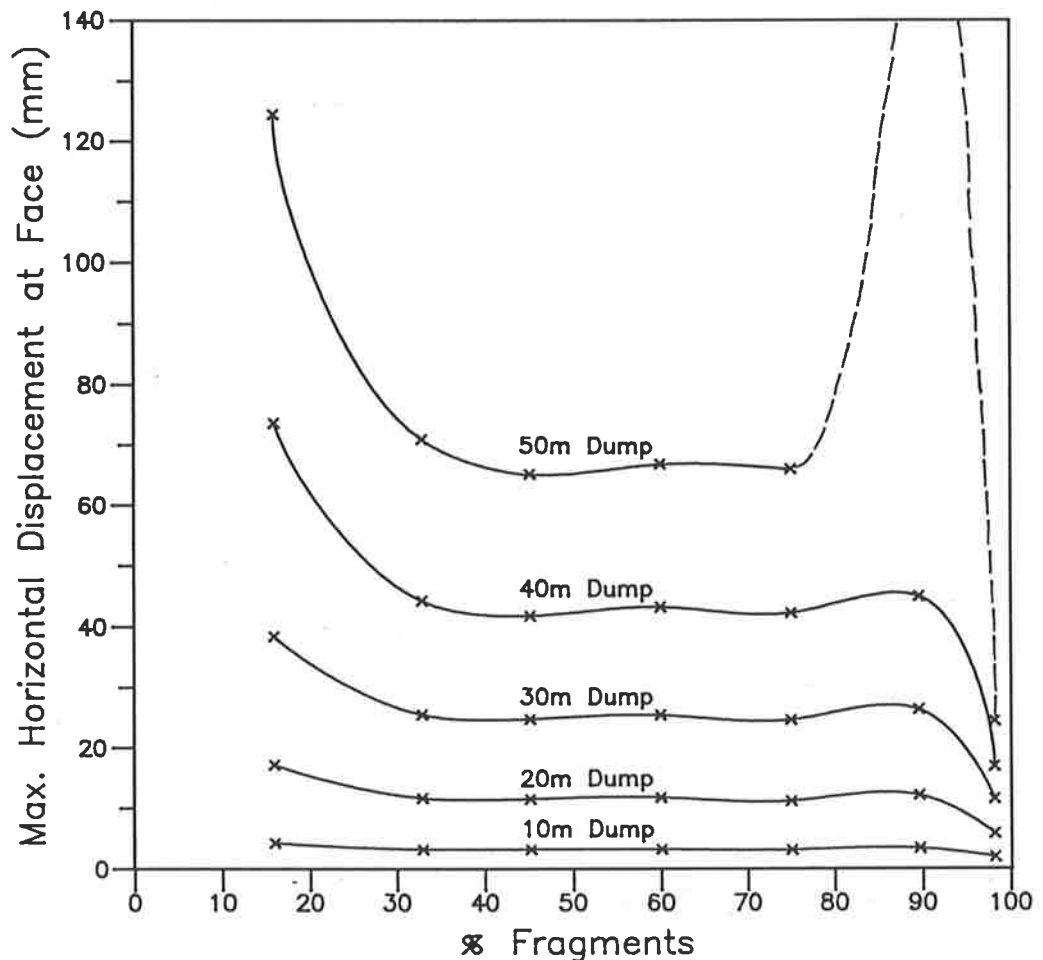


Figure 7-20 Correlation between Toe Displacement and Proportion of Coarse Fragments

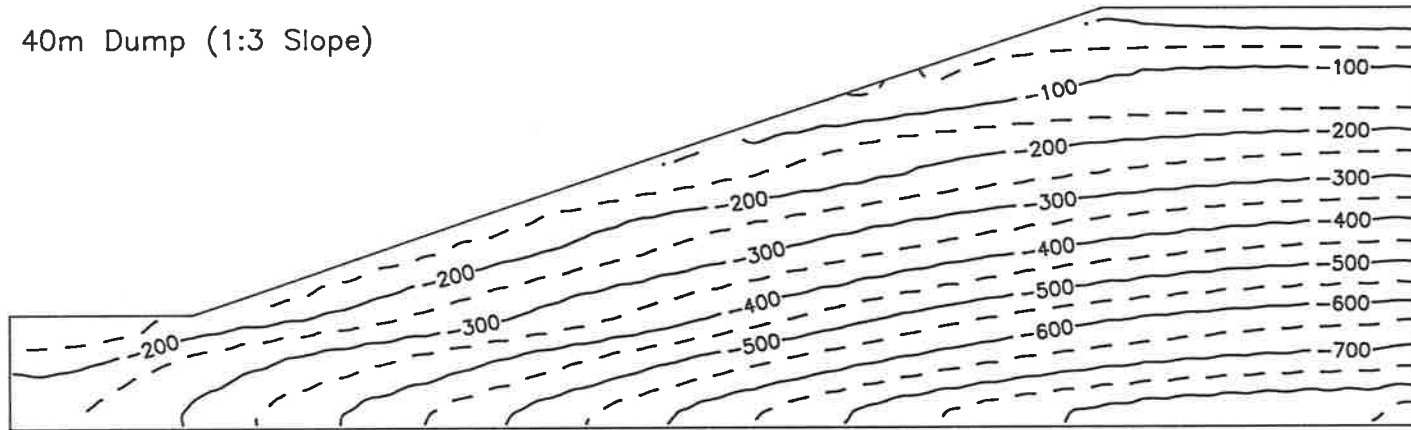
The relationship between material weathering and dump stability is better illustrated in Figure 7-20, in which characteristic horizontal displacements are plotted against %Fragments. There is a critical range as fresh waste-rock disintegrates to 80-90% coarse fragments, when the material is cohesionless, possibly highly voided, but not strongly interlocking. With further disintegration and the start of decomposition a more coherent grading is produced, after which there is

little effective further change in stability until less than about 40% coarse fragments remain. It is suspected that after this stage, the clay starts to become a significant component in the fine matrix (previously dominated by the sand fractions), which leads to increased deformability, although not automatically to decreased slope stability. This marks a significant change in the character of the material and the possibility of different types of failure, such as creep-related, becoming important. However, this phase of weathering may be more relevant to final rehabilitated landforms.

Regarding later dump shapes, a further series of analyses was performed for a 1:3 batter slope (refer Figure 7-6) and foundation softening as previously considered. Comparing Figure 7-21 of horizontal stress contours at 40m dump height with those for the corresponding base run (Figure 7-16), there was, predictably, much less thrust developed at the toe. Shear stresses were similarly less intense. There were no more than occasional isolated zones flagged as near or at shear failure for any material.

Characteristic horizontal displacements in Figure 7-22 show the same relationship between materials as in previous series. However, unlike the 1:1.5 dump slope, the incremental displacements from successive lifts did not continue to increase, so that the curves (which show cumulative displacement), tend to be linear or levelling out, rather than becoming steeper for the later lifts. In addition, total displacements were less than half the magnitude of the corresponding results from base runs. From these two attributes it is inferred that 1:3 dump slopes could be stable against mass sliding under long-term conditions throughout the potential phase of accelerated weathering. The current proposal is understood to be for 1:5 slopes and on the results of these analyses, excepting construction over a steeply sloping base, mass structural stability will not be the limiting factor. Another mechanism, such as surface erosion, is likely to control landform design.

40m Dump (1:3 Slope)



50m Dump (1:3 Slope)

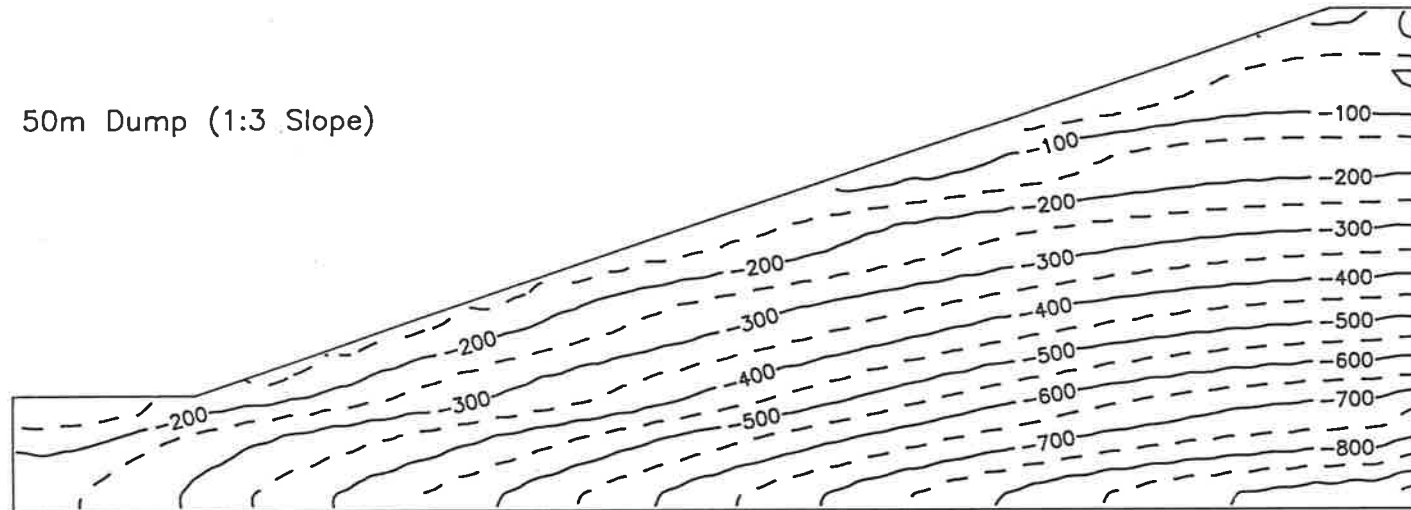


Figure 7-21 Horizontal Stresses for RM27A - 1:3 Slope

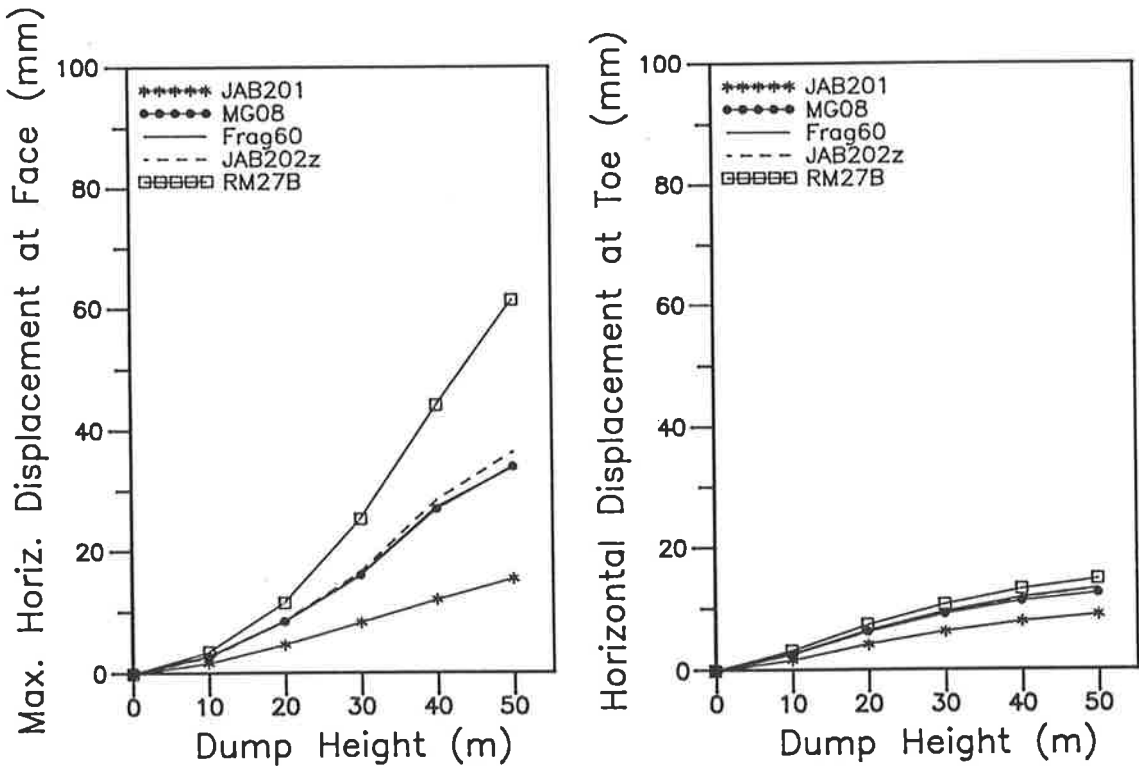


Figure 7-22 Characteristic Displacements at Slope Face - *1 in 3* Slope

To summarise, without confirmation of actual material conditions and moisture regimes inside the waste-rock dumps, results of the finite element analyses must be treated as indicative rather than as absolute predictions. However, it has been made apparent that failure through a softened foundation is the most critical mode of slope instability in the present waste-rock dumps, for which a wedge analysis would be suitable. The crucial stage of weathering occurs after 5-10 years exposure on the batters (or an equivalent degree of weathering within the dump), when shear strength under low normal stress is at a minimum. Finally, mass instability is unlikely to impact on the design of final rehabilitated landforms.

CHAPTER EIGHT

8. SUMMARY AND CONCLUSIONS

8.1 Techniques for Investigation

The stability of slopes constructed from mine spoil is a matter of growing importance both to the general community, which wishes to recover the use of areas after mining, and to the mining industry, which has to meet that wish. Although the primary objective of this thesis was to explore the link between degradation of waste-rock and dump slope stability (specifically at Ranger Uranium Mine), in the course of the work techniques were developed and extended to suit the particular constraints of these types of materials and constructions.

The main such technique was the photo-sieving procedure, devised to obtain complete particle size distributions for waste-rock containing fragments which are too large to sieve in reality. To achieve compatibility with the results of normal mechanical sieving, a theoretical approach was adopted. This included statistical simulation of the relationship between intermediate axis (sieve size) of actual particles and linear measures of their outlines on an image plane. Consequently, the following decisions were taken for the procedure:

- a) All particles in the photograph to be selected for analysis;
- b) Particle size to be designated by geometric average of the horizontal and vertical axes of the particle image outline (refer Figure 3-8); and
- c) In the resultant particle size distribution, each particle to be valued (weighted) according to the area of its image as a proportion of its total image area.

Key activities in the procedure subsequently developed to "photo-sieve" dump batters at Ranger were:

1. Four scale markers were placed on the batter to be photographed (two lying upslope and two lying across slope);
2. Several photographs were taken of the batter, ranging from close to long distance;
3. A subsample of waste-rock, containing particles not larger than gravel size, was collected from the batter;

4. The photographs were developed as slides, from which paper copies of the particle outlines were traced using a stereo microscope;
5. Each outline trace was entered into computer via a video digitiser, and particle sizes and areas were measured using image analysis software developed for the purpose;
6. A particle size distribution for each photograph was calculated from the data for individual particles; and
7. Particle size distributions for photographs of the same batter, and results from mechanical sieving of the collected subsample, were collated into a complete grading curve for that dump site.

An important feature of the technique was the adoption of linear approximations for tilt distortion, based on a study of tilted photographs of brickwork. This permitted use of scale markers instead of surveyed points, and of simple rectification algorithms in the image analysis programme. It appeared that this simplification might have introduced, or contributed to, a systematic error in axis estimation, but resultant particle distributions were not recognisably affected.

As used, the technique demonstrated the feasibility of photo-sieving to quantify physical description of waste-rock and similar material. However, the tracing and particle analysis steps, in particular, were time consuming and would not be suitable for routine use. A summary of procedures and possible improvements was provided in Table 3-7.

No special techniques were developed for mineralogical characterisation of the dump materials, other than that of focussing on different size fractions to infer data on initial composition and current alteration. Laboratory strength testing required the adaptation of previous work by others to scale waste-rock grading curves down to 20mm maximum particle size. The approach taken was to maintain the relative proportions of silt, clay, sand, and coarser-than-sand. In practice, this resulted in replacement of the proportion larger than 20mm with the same percentage in the range 2.4-20mm. Although research into the effects of scaling on strength has been inconclusive, when prepared for testing the laboratory samples had water contents and percentages of air voids which appeared reasonable in comparison to similar investigations of rockfill.

The method used for slope stability analysis was an existing finite element procedure with wide application to geotechnical engineering. One of the main advantages of finite elements over more traditional methods of stability analysis was that the mode of slope failure was not predetermined. Because of the nature (and scatter) of results correlating weathering and material strength, it was not attempted to integrate the effect of weathering into the analytical model. Instead, discrete analyses were performed covering a range of weathering states from as-dumped to soil. Results of this finite element modelling permitted clear comparison of changes in slope stability as the waste-rock degrades. Unfortunately however, there is no established method to quantify slope stability from the output of a specific finite element analysis.

8.2 Description of Dump Materials

8.2.1 Weathering

From field observations, physical description, and mineral characterisation, a description was formulated of the mechanisms and progress of weathering on the batters of the waste-rock dumps at Ranger Uranium Mine.

As dumped, waste-rock is a coarse material - more than 95% by weight larger than 2mm particle size - and the fine particles that are present initially are removed from the surface within one year of dumping. The batters are thus open and free-draining, and in the first phase of weathering (0-5 years), decomposition is highly localised at grain boundaries and other similar flaws. Because of the volume increase associated with, especially, the decomposition of chlorite to smectite, such limited chemical alteration results in the breaking down of larger rock fragments into successively smaller particles. This is manifest as an increase in the sand size fraction, from less than 1% to about 10%, in the first half decade of exposure. The amount of weathering product instigating this disintegration was almost undetectable in the batter samples analysed.

Silt and clay size particles follow the increase in sand content after a couple of years, and it appears that the sand fraction may govern the emergence of decomposition as a process evident in its own right. Based on previous investigation of soils formed on the tops of the dumps, it is suggested that when the proportion of sand becomes sufficient to slow the passage of moisture out of the batters, the weathering reactions are accelerated: not only is the retention of water necessary for chemical alteration, it also permits the establishment of sparse vegetation, the litter of which is required by soil bacteria in their own soil decomposition activities. The oldest dump batters have reached this stage, when disintegration is still dominant, but the waste-rock has developed a coarse sandy gravel texture, and the products of alteration are identifiable in the (small) clay fraction.

Examination of naturally weathered materials from the minesite indicated that disintegration of larger fragments will continue as decomposition becomes more significant, with the major weathering

products being smectite (from chlorite), probable illite (from muscovite), and kaolinite (from smectite and illite). A sample of soil from the top of a dump (exposed less than 10 years) showed chemical alteration consistent with that of unmined extremely weathered rock, emphasising the greatly accelerated weathering occurring on the lift terraces. However, even in the most extensively decomposed in-situ samples, only about 40% of weatherable primary mineral has been altered. As degradation on the dumps proceeds and waste-rock approaches the character of natural residual minesoil, the factors promoting more rapid weathering will decline. Consequently, current minesoil may be considered the limiting material generated from waste-rock due to exposure on the dumps. Further decomposition, leading to eventual depletion of smectite and illite in favour of kaolinite, should then proceed at a similar rate as in undisturbed landforms.

8.2.2 Strength

The shear strength of waste-rock was investigated within the framework of continuum soil mechanics theory. Initially the characteristics are essentially frictional and non-cohesive. Triaxial compression tests gave angles of internal friction in the range 30-35° for dump batter materials exposed for up to about 6 years, with a trend of ϕ decreasing with batter age. As described in the previous section, negligible mineralogical change occurs in this period, and the loss in frictional strength is apparently due to the disintegration of large fragments reducing the effect of particle interlock during shearing. Non-zero shear intercepts (40-70kPa) obtained for these cohesionless materials were also attributed to particle interference, and also decreased with increasing duration of exposure.

Changes in strength parameters correlated well with the proportion of coarse fragments (gravel + cobble + boulder) for batter samples. Some correlation persisted in the more weathered materials but, consistent with the increasing importance of decomposition as a weathering process, the simple physical descriptor become less discriminating of variation in material strength. At this stage of weathering mechanical behaviour is governed by the matrix of fine particles. Correlation was found between strength and percentage of clay with a 2:1 layer structure, although it is thought that at least part of the dependence

is due to the fact that the abundance of these minerals (illite and smectite) also reflects the proportion of platy chlorite and muscovite particles in the sand and silt size fractions.

Among these weathered samples, friction angle decreased from 26° to 12° as percentage 2:1 layer clays increased from about 1-10%, and shear intercept increased less definitely from about 60-100kPa for the same range. With particle interference no longer effective, reduction in the frictional component of shear strength is probably due to both continuing changes in particle size distribution and production of the weak clay minerals. Shear intercept is due to normal clay cohesion, and understandably increases with increasing clay fraction. From one sample which contained little smectite and illite but significant kaolinite, it is possible that waste-rock will have least strength when the proportion of 2:1 clay minerals is greatest: as these are altered to the more stable (less plastic) kaolinite, friction angle may increase again. (However, weathering has not commonly progressed to this extent even in the natural profile.)

Mechanical behaviour of the waste-rock and other mine materials examined was not differentiable on the basis of either initial mineral composition or natural rock fabric. Results of investigation into the relationship between weathering and material strength were summarised in Figure 6-14.

8.3 Slope Stability at Ranger Uranium Mine

Following a brief review of available analytical procedures, a non-linear finite element model was selected to investigate dump stability against mass sliding. Stress-dependent material properties were estimated from back-analysis of triaxial compression tests. Subsequent dump slope analyses considered discrete stages of weathering (each represented by a specific sampled material), feasible long-term moisture conditions, and dumps constructed in 10m lifts. The following conclusions were drawn from the results:

1. Slopes at current batter angles (about 1:1.5) will be stable at 30m height under typical conditions throughout the intended life of the dumps;
2. Dumps up to 40m height might also be generally stable but further investigation would be required to confirm this as a design limit;
3. Batters are least stable in the period about 5-10 years after dumping, due to waste-rock at this stage of degradation having low shear strength at low normal stress;
4. The critical mode of failure is sliding along a softened base. (Softening of an initially competent base is feasible, even likely, because of the sink created in the natural surface by the weight of the overlying dump.) Of the traditional static equilibrium methods of stability analysis, a multiple wedge method is most appropriate to the failures observed in the finite element models; and
5. With regard to landforms in the rehabilitated site, slopes of 1:3 would be stable against mass sliding under long-term conditions.

These analyses were based on conditions considered reasonable for the dumps for sustained periods. Before incorporating any of the findings into design changes for the dumps or final landscape, specific consideration should be given to extreme conditions, such as those related to moisture regimes and water flow in severe wet seasons.

8.4 Further Research

As observed throughout this thesis, materials such as waste-rock have physical characteristics which place them at the limits of current soil mechanics theories. However, it is unlikely that the growing need for better design and management of spoil heaps is alone sufficient to generate development at a fundamental level. Consequently, it is important to extend techniques and methods so that waste-rock/rockfill is more rationally accommodated within the existing framework of understanding and practice. Areas with potential for such development include:

a) Virtual Sampling (photo-sieving) -

The power of this approach has been demonstrated in this project, where comprehensive physical characterisation was achieved beyond the practical limits of normal laboratory methods. Currently the method is restricted by the lack of strong validation of the attempted equivalence between photo-sieving and mechanical grading. If this deficiency was redressed, it is likely that wide acceptance, and development of more convenient analytical procedures would follow.

b) Measurement of Field Conditions -

One of the difficulties in the laboratory strength testing programme was deciding the conditions at which to prepare specimens for triaxial compression tests. Improvement of techniques to measure in-situ properties such as density, water content, and void ratio would greatly improve laboratory modelling of these materials; as input both to testing programmes and to research into aspects such as the effect of maximum particle size.

c) Characterisation of Material Variability -

There are two aspects to this issue, namely spatial variability of materials in the dump structure, and random variation of properties within a particular material. Because of the comparative nature of the stability analyses undertaken, the use of 'average' or 'typical' attributes was adequate in this project. However, in the context of detailed geotechnical design, there is great scope for both the accumulation of relevant data and the extension of analytical techniques to utilise non-deterministic parameters.

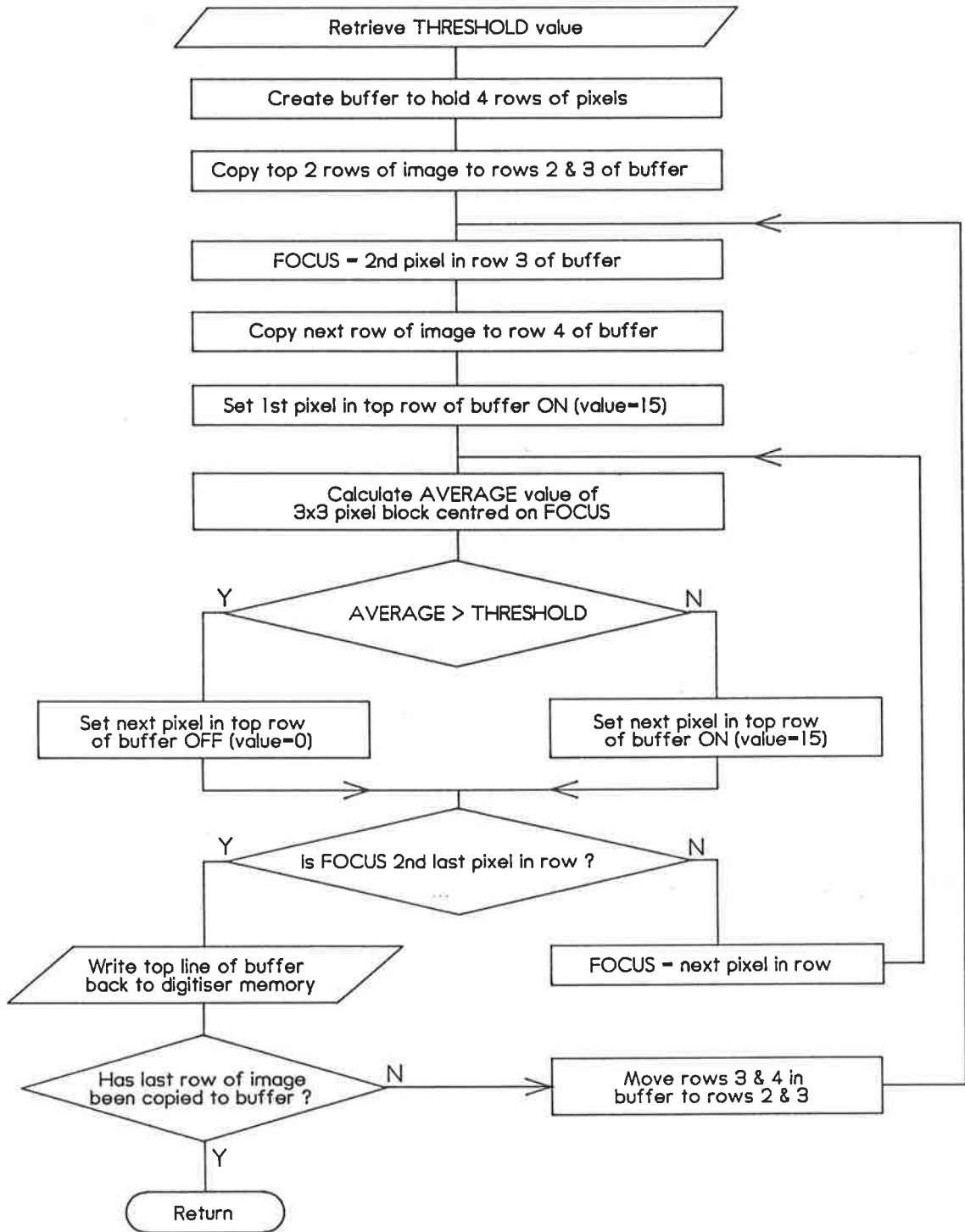
Specific to the dumps at Ranger Uranium Mine, there are also areas warranting further investigation. With regard to the relationship between weathering and strength, there was a significant gap between the oldest batter samples and the least decomposed naturally weathered sample. Future examination of dump materials (for example, about ten years hence) would improve understanding of the correlation between mechanisms of weathering and strength. As noted in Section 8.3, there is also a need to investigate and develop models for moisture conditions and water flow through the dumps. Such research is relevant to dump stability in the broadest sense, not just safety against sliding failure, but also to surface erosion and to movement of contaminants.

The particular research difficulties encountered in this project highlighted the importance of gathering data from a range of sources. No approach or analysis in isolation could specify the effect of weathering on the shear strength of waste-rock and, subsequently, on dump stability. However by collating evidence from field observation, laboratory analysis and theoretical modelling, understanding was developed both of the effects of weathering and the mechanisms producing those effects. It is worth noting that in the experience of this project, observation provided much of the central evidence.

APPENDICES

A. COMPUTER SUBROUTINES FOR IMAGE ANALYSIS

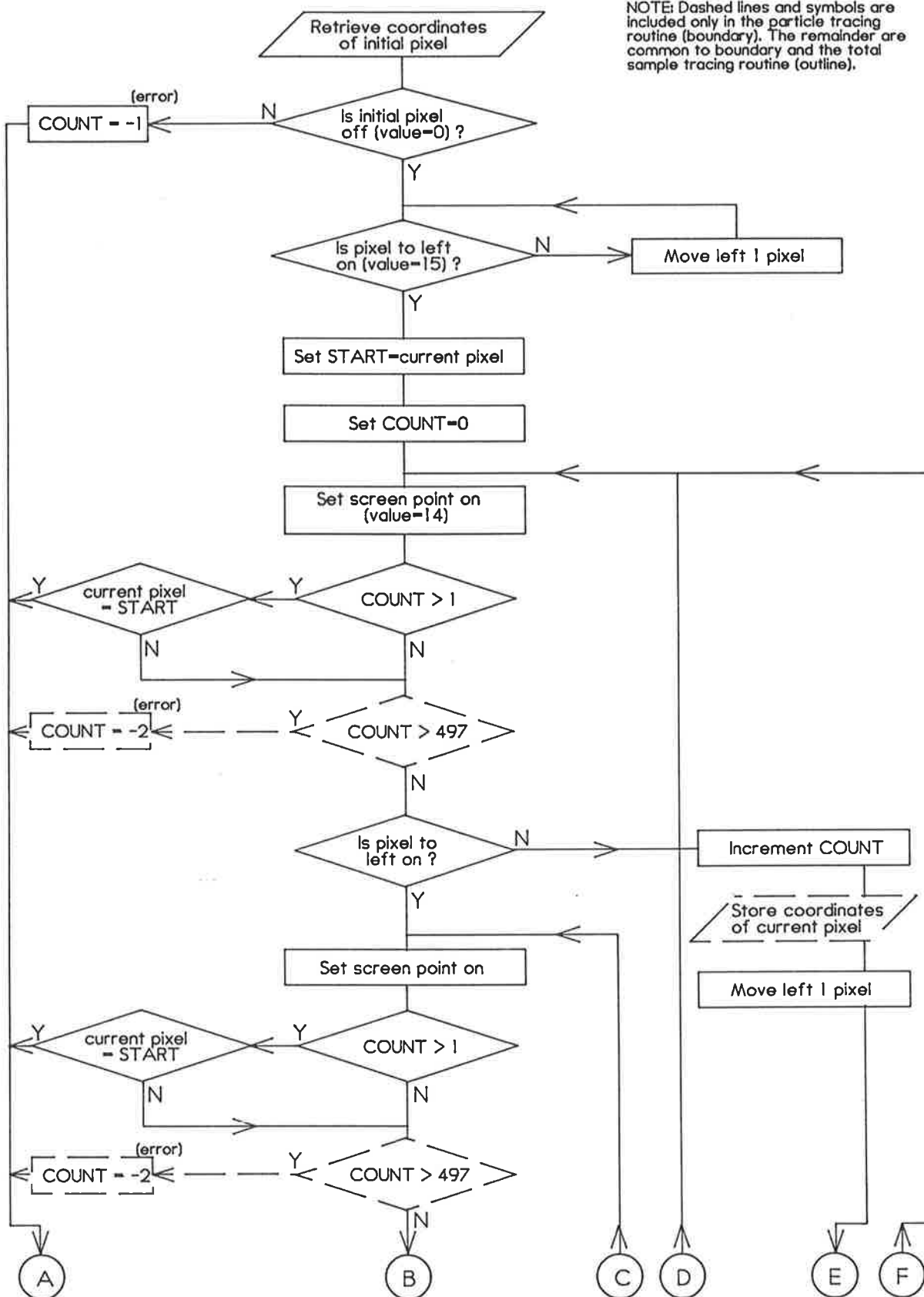
line_detect

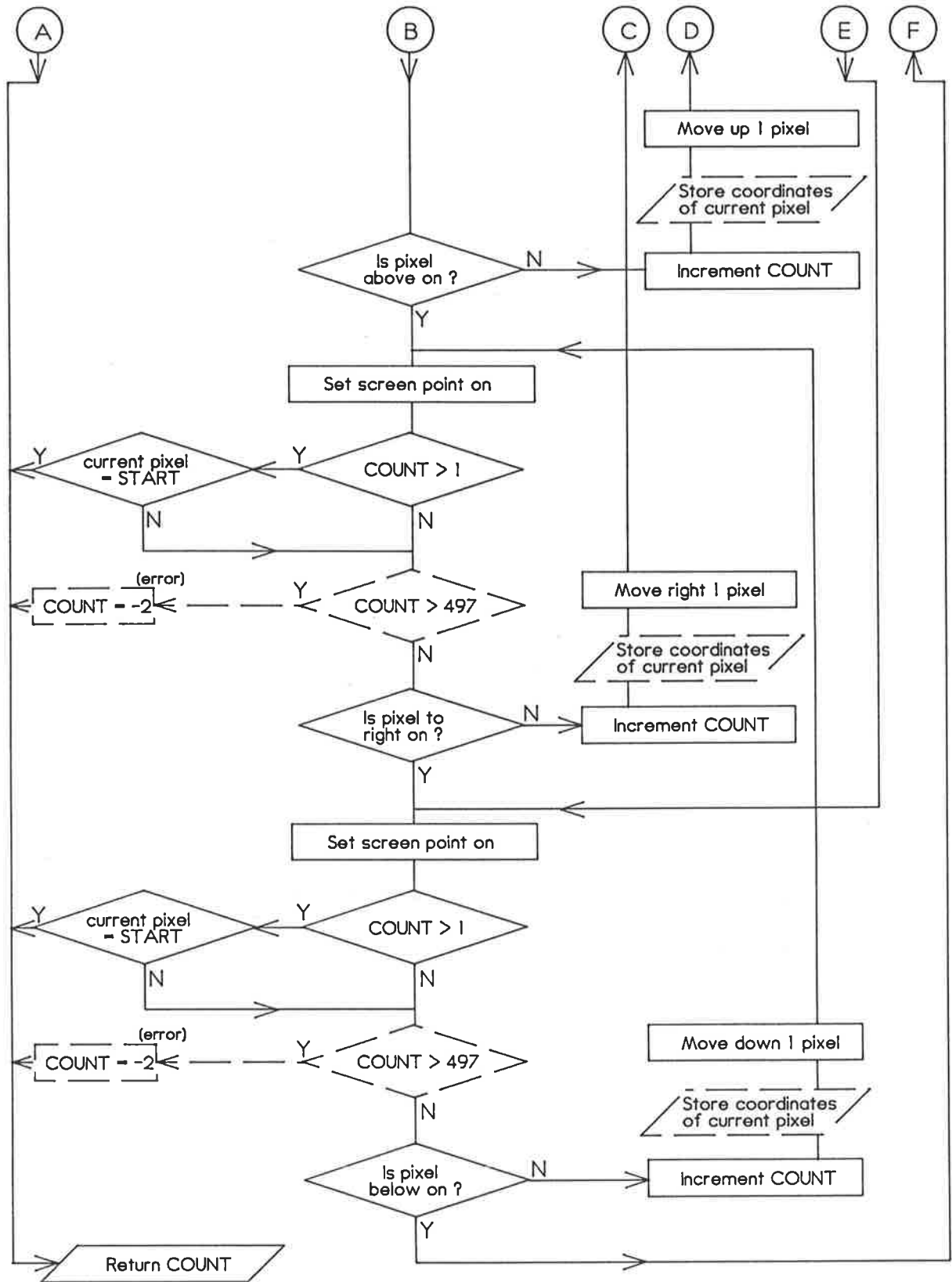


A1 - Function to Produce On/Off Pixel Image of Outlines

A2 - Boundary Tracing Routines for Total Sample and Individual Particles

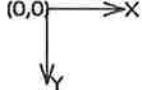
outline/boundary

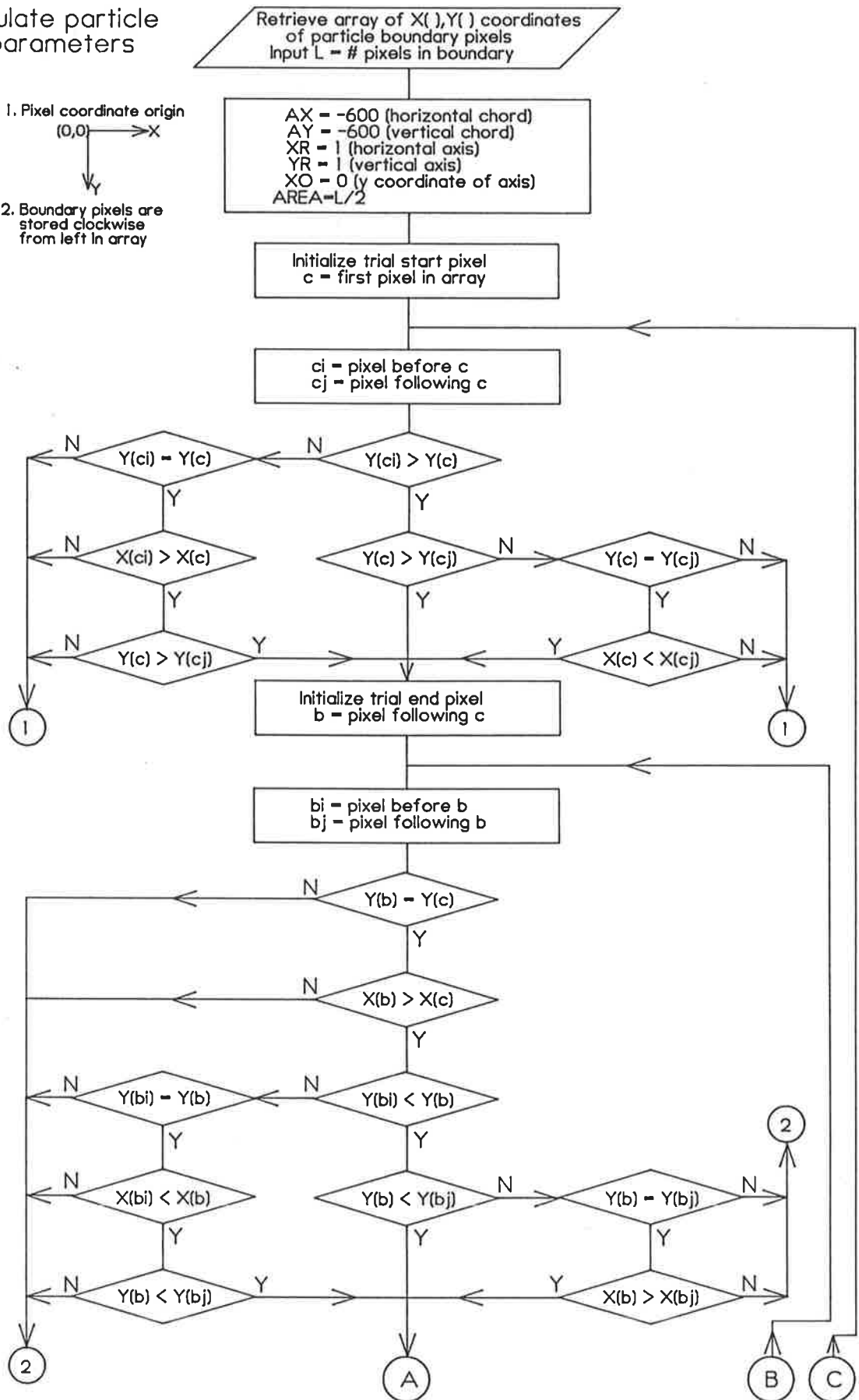




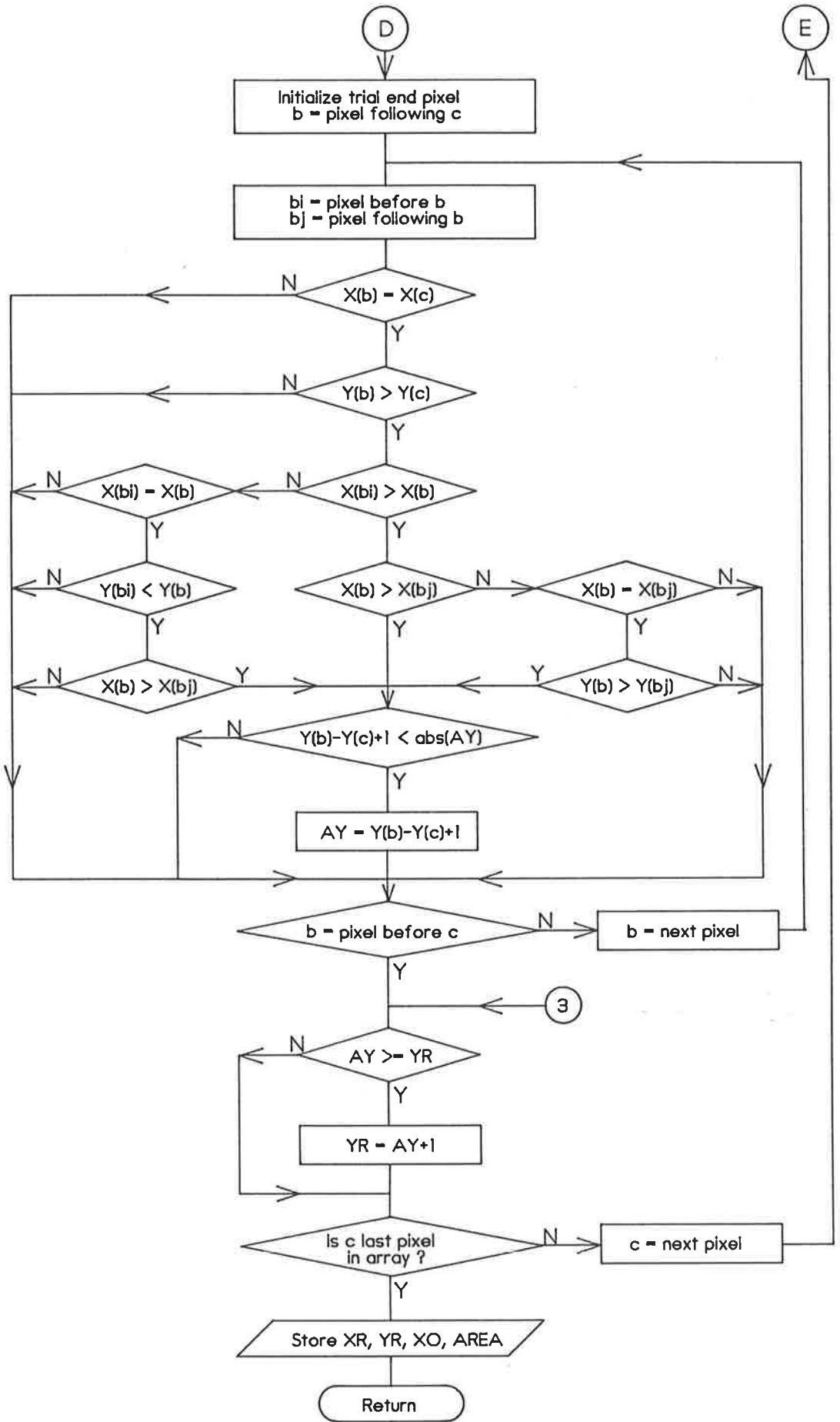
A3 - Routine to Calculate Particle Axes and Area

calculate particle parameters

- NOTES: 1. Pixel coordinate origin (0,0) 
2. Boundary pixels are stored clockwise from left in array



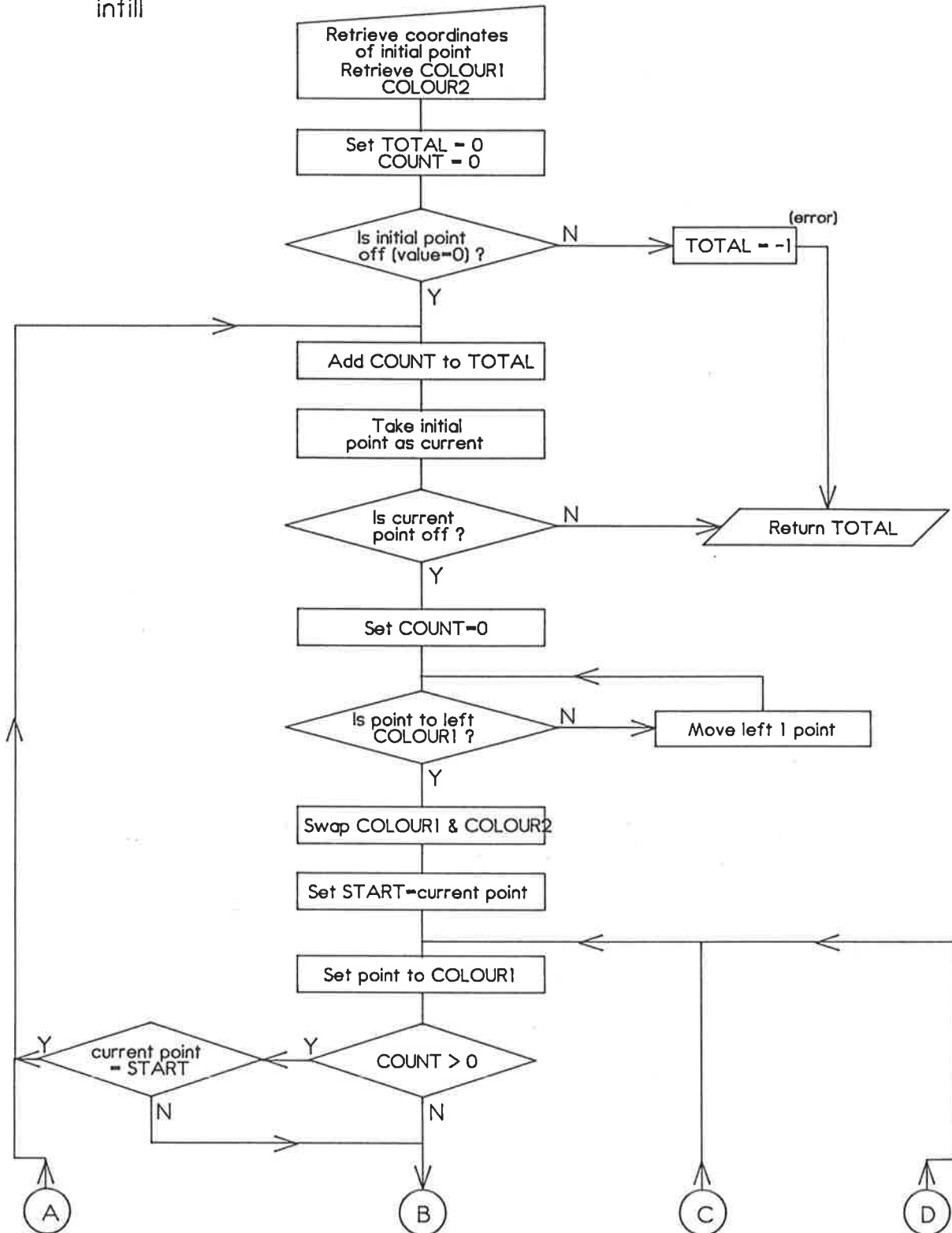
AX = -600 (horizontal chord)
 AY = -600 (vertical chord)
 XR = 1 (horizontal axis)
 YR = 1 (vertical axis)
 XO = 0 (y coordinate of axis)
 AREA=L/2

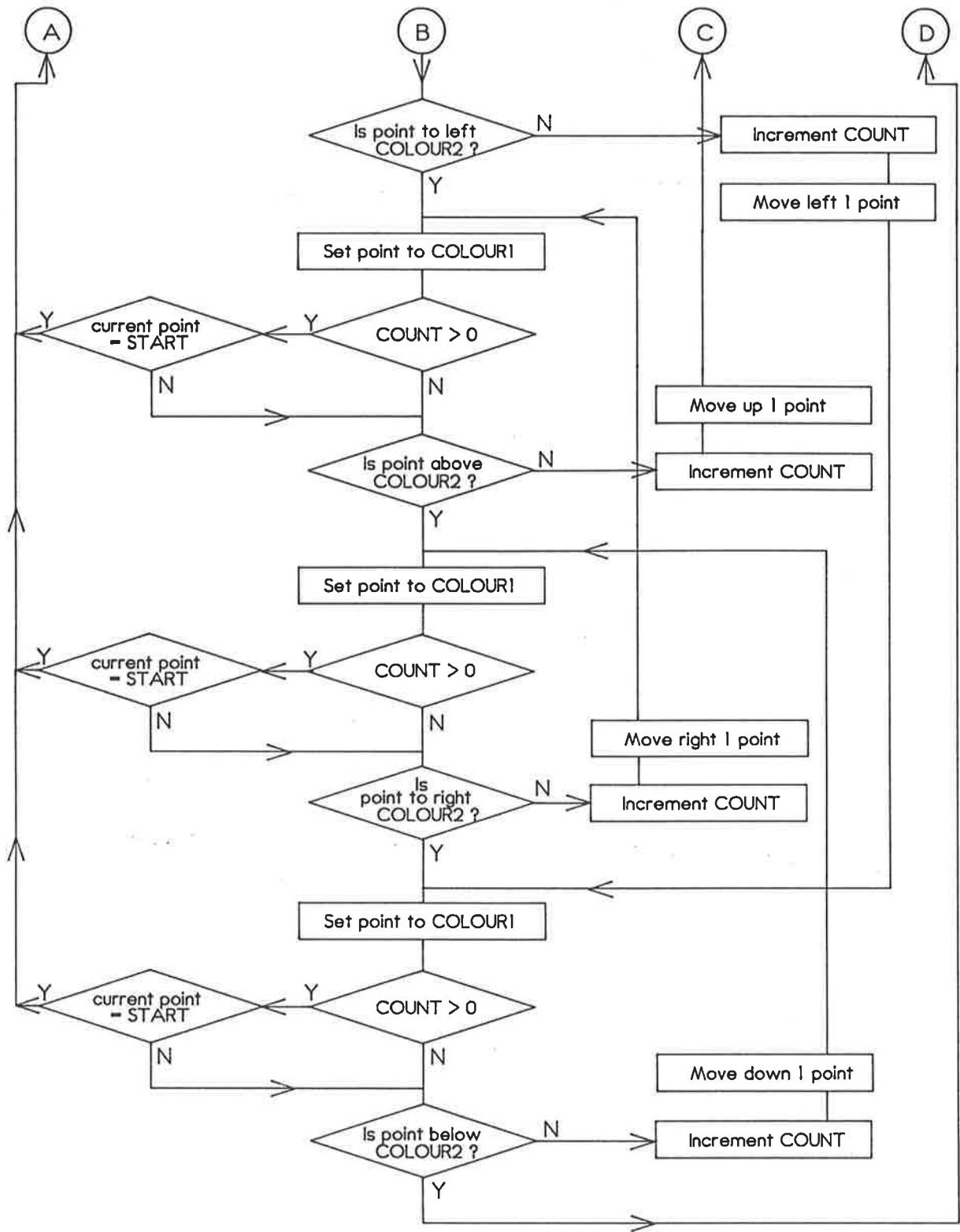


A3 - calculate particle parameters (continued)

A4 - Function to Count Pixels Filling an Area

infill

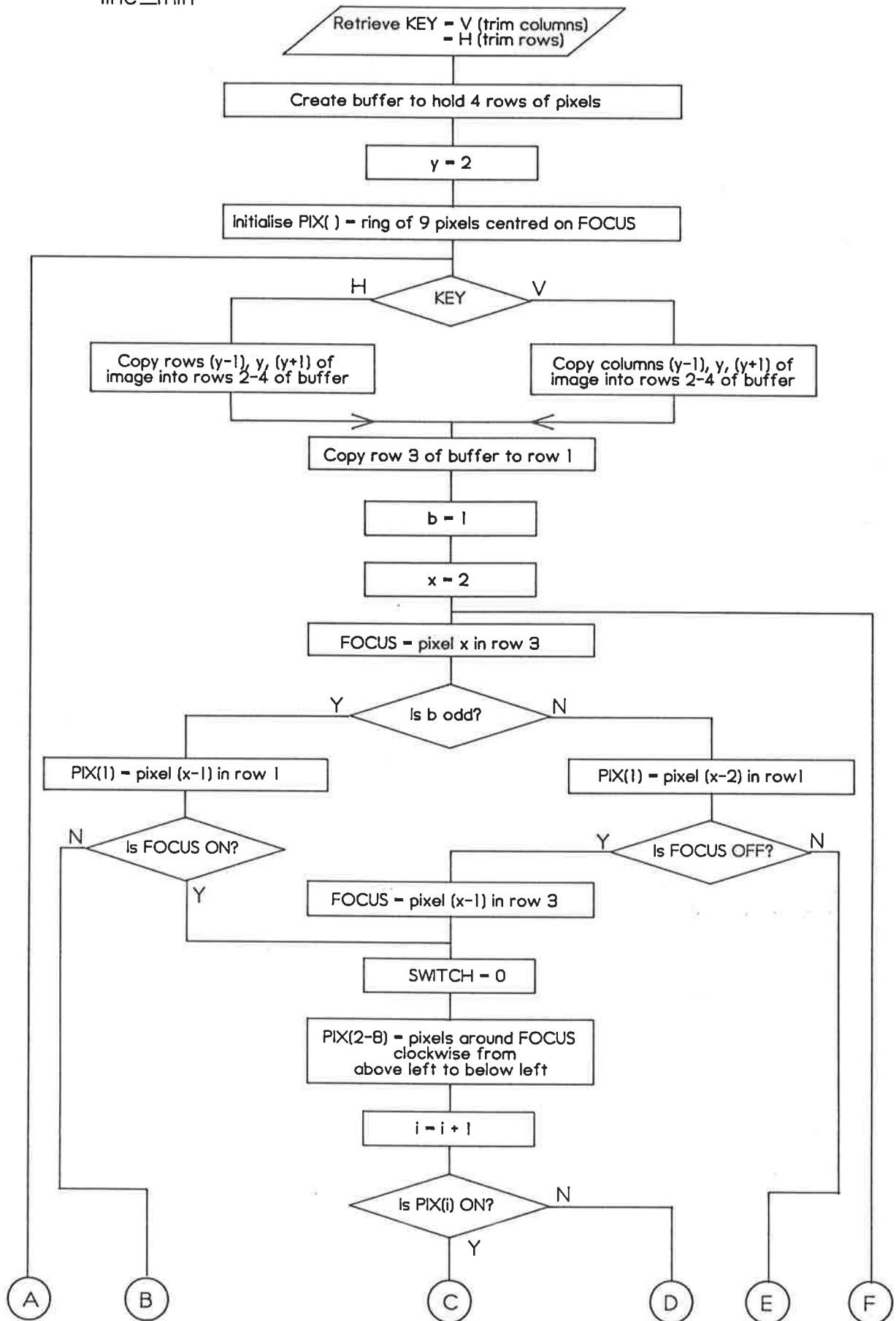


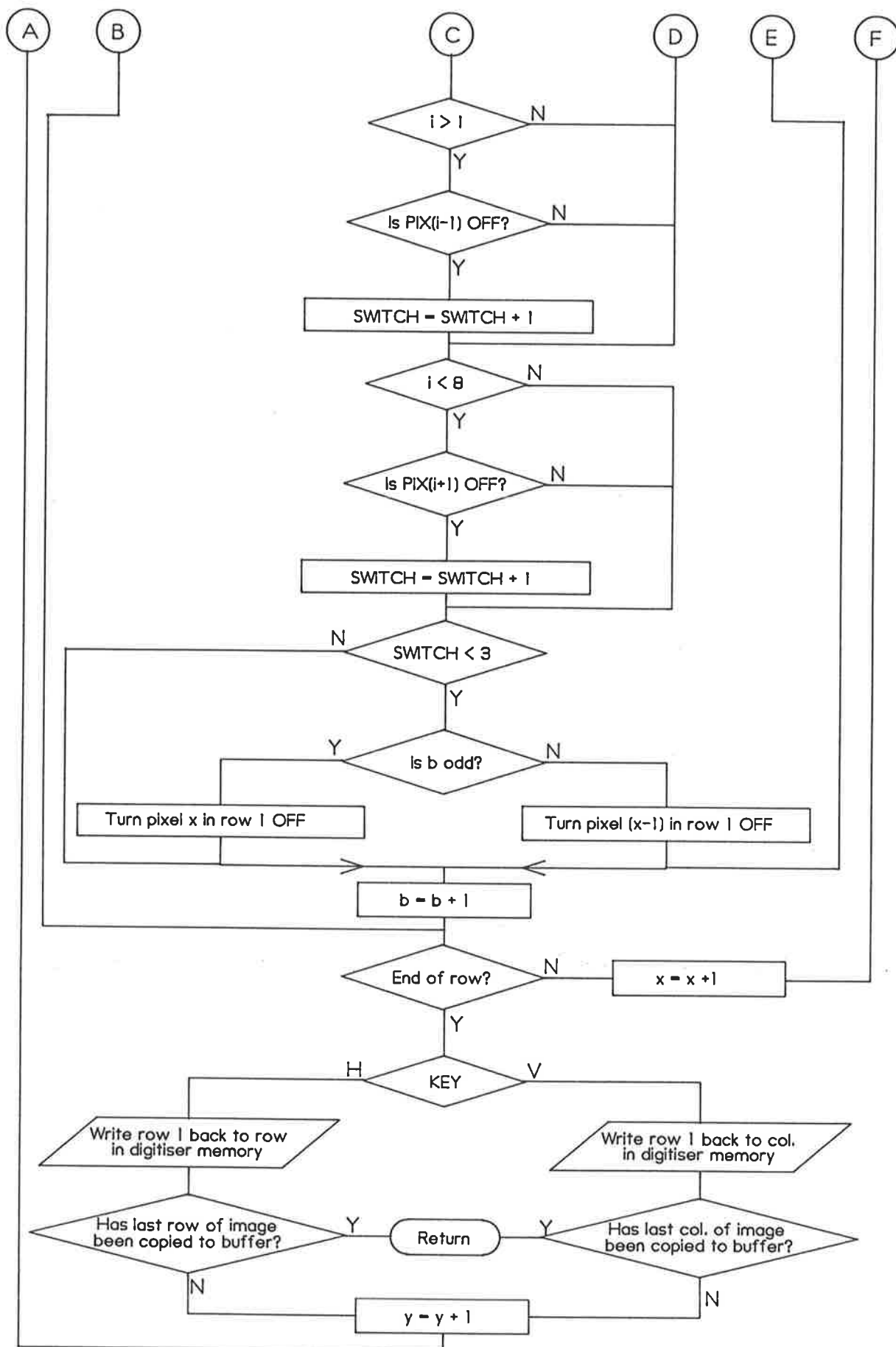


A4 - infill (continued)

A5 - Function to Thin Outlines

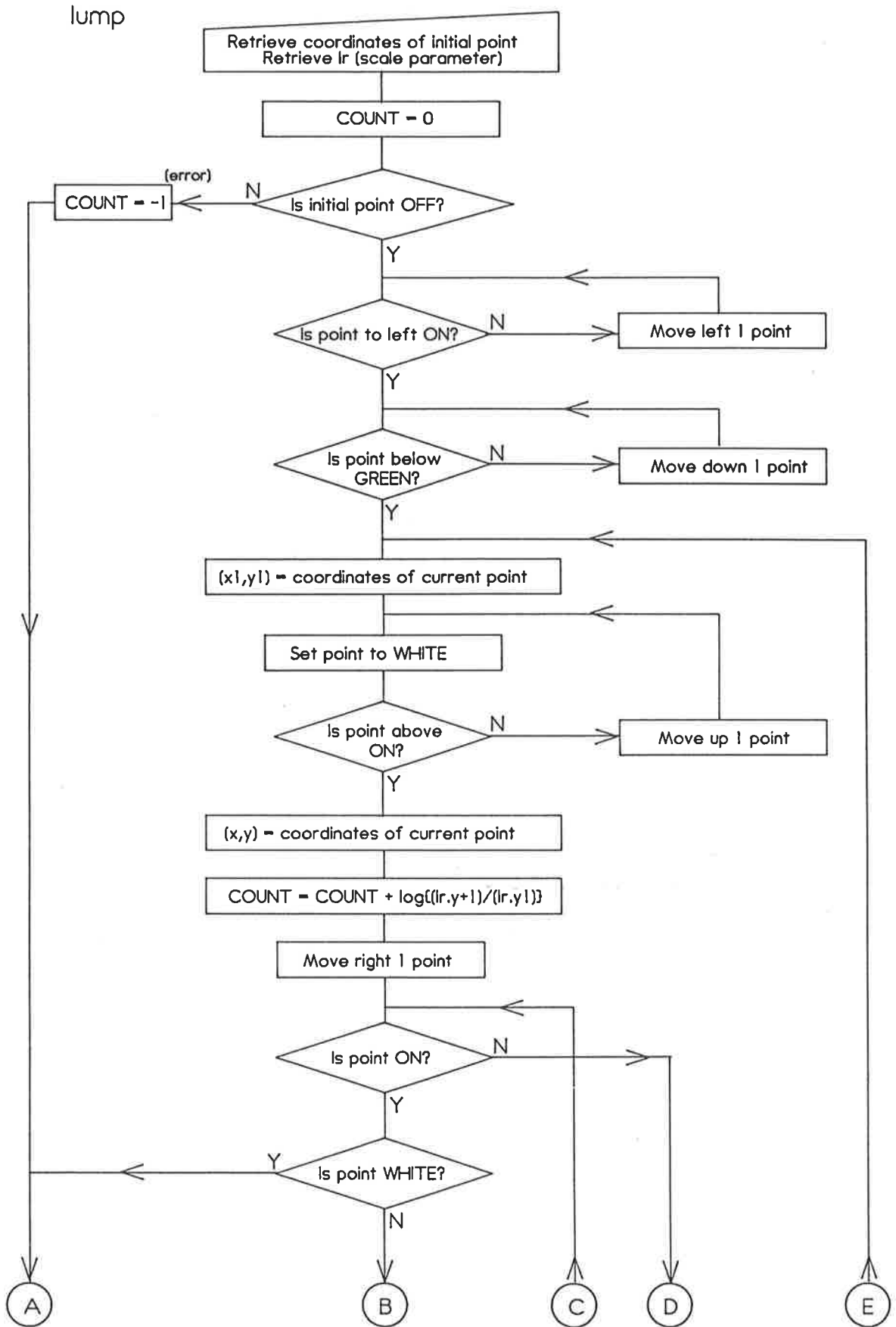
line_thin

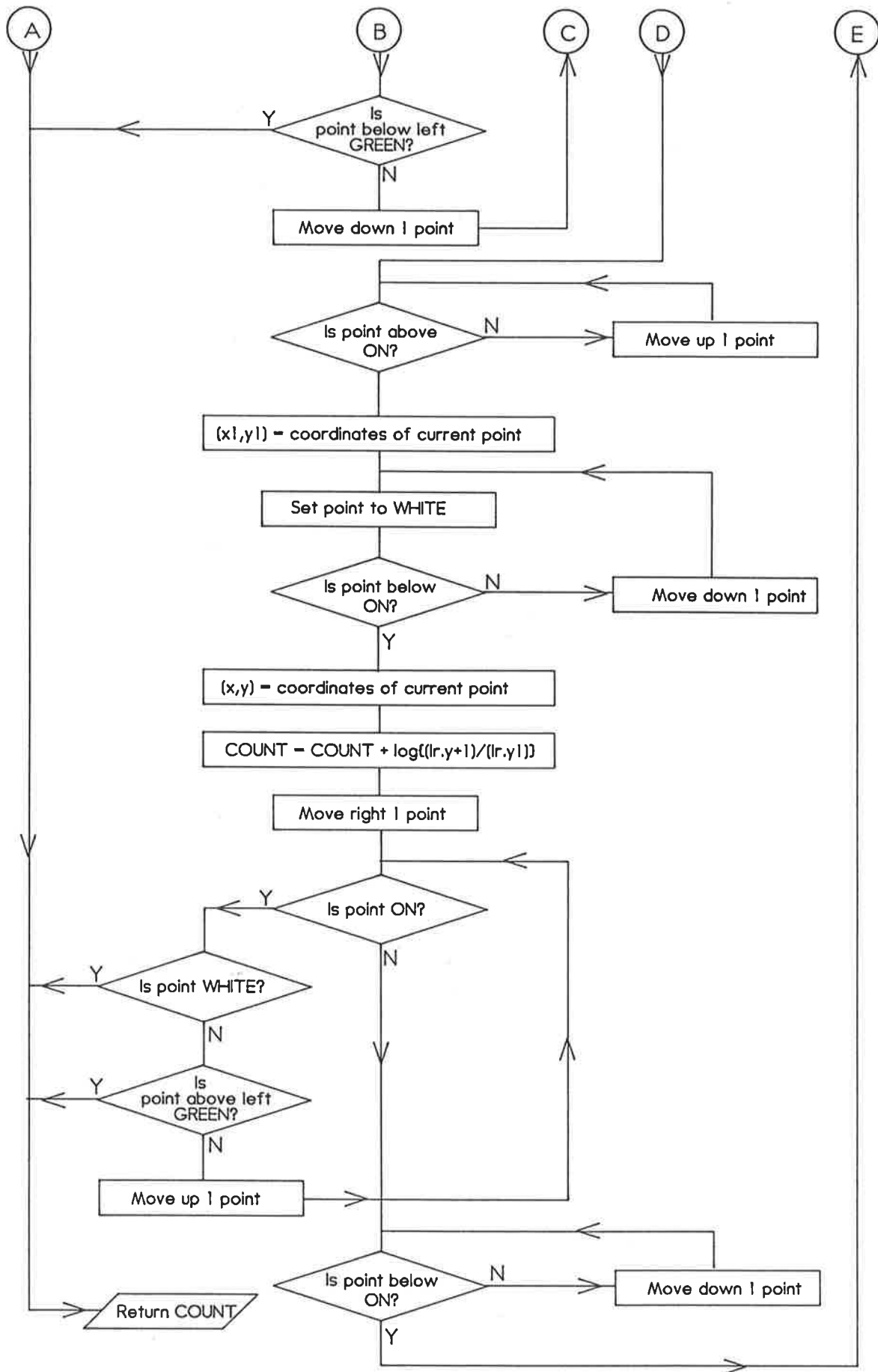




A5 - line_thin (continued)

A6 - Function to Measure 'Lumped' Areas



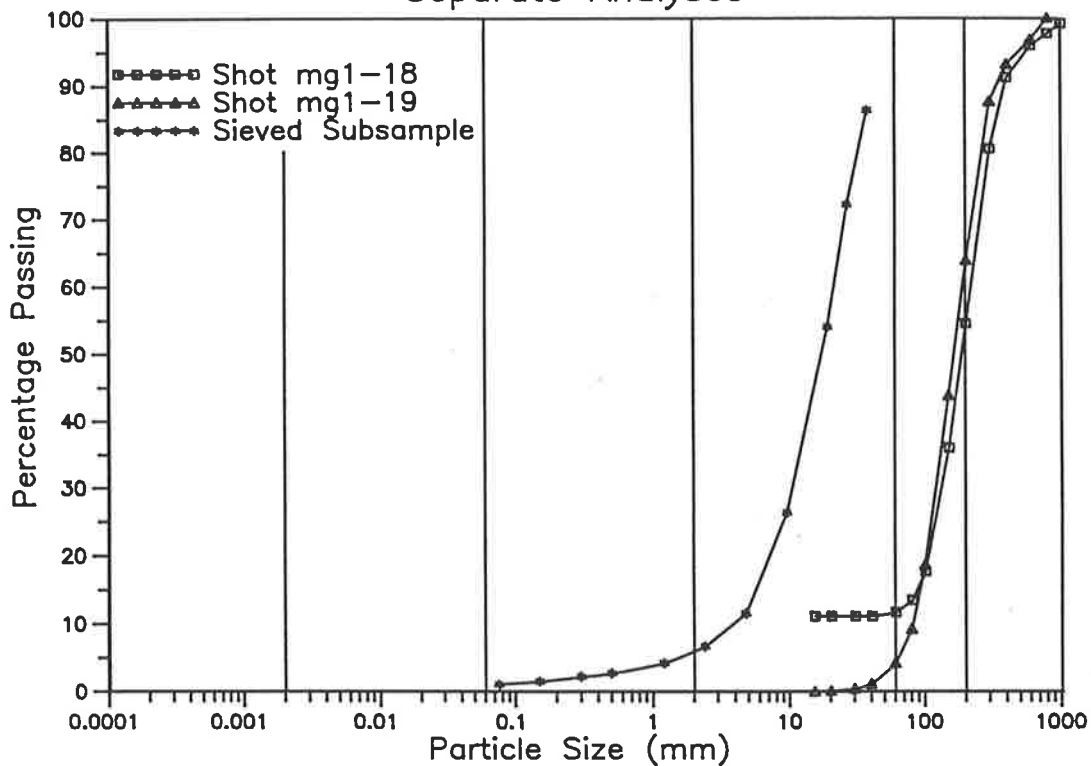


A6 - lump (continued)

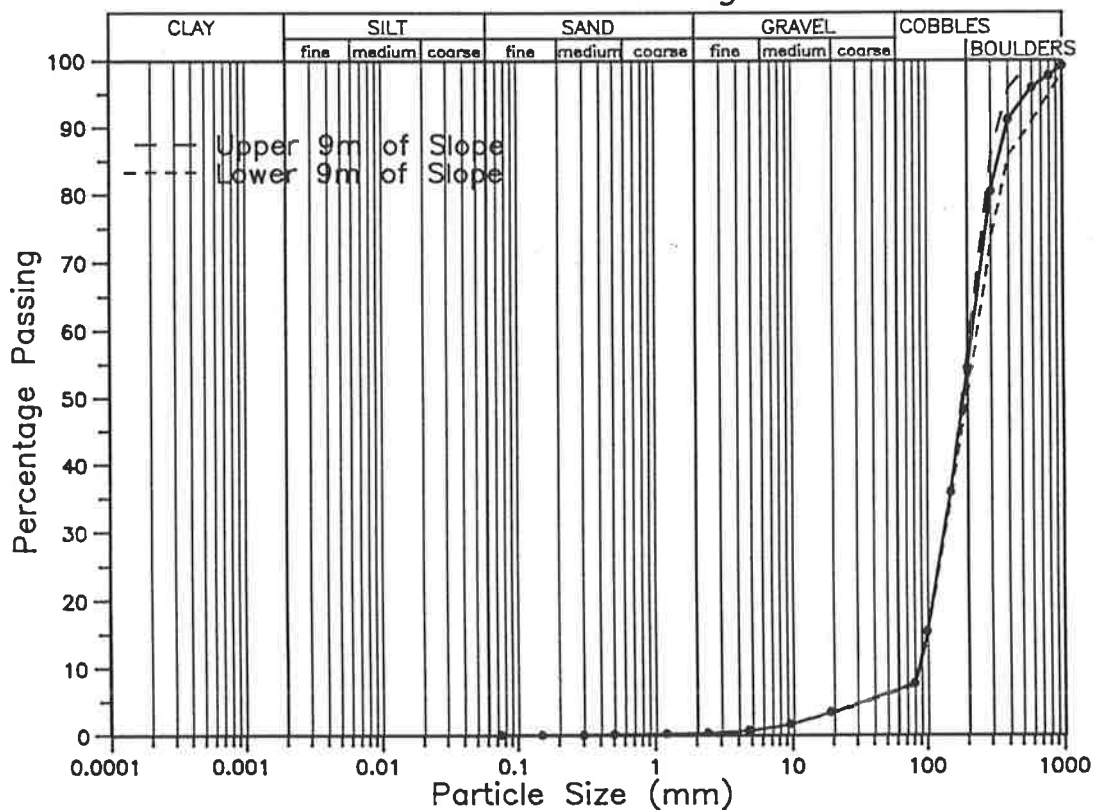
B. DUMP SLOPE GRADING CURVES

SITE 4

Separate Analyses

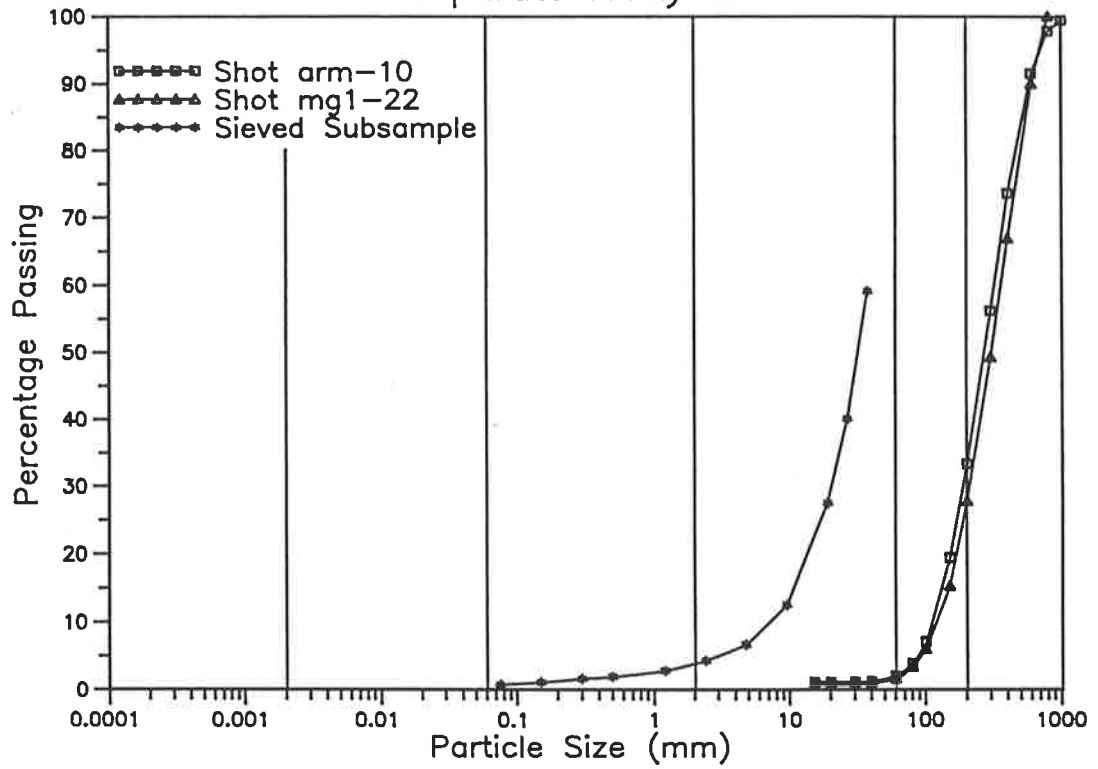


Site Grading

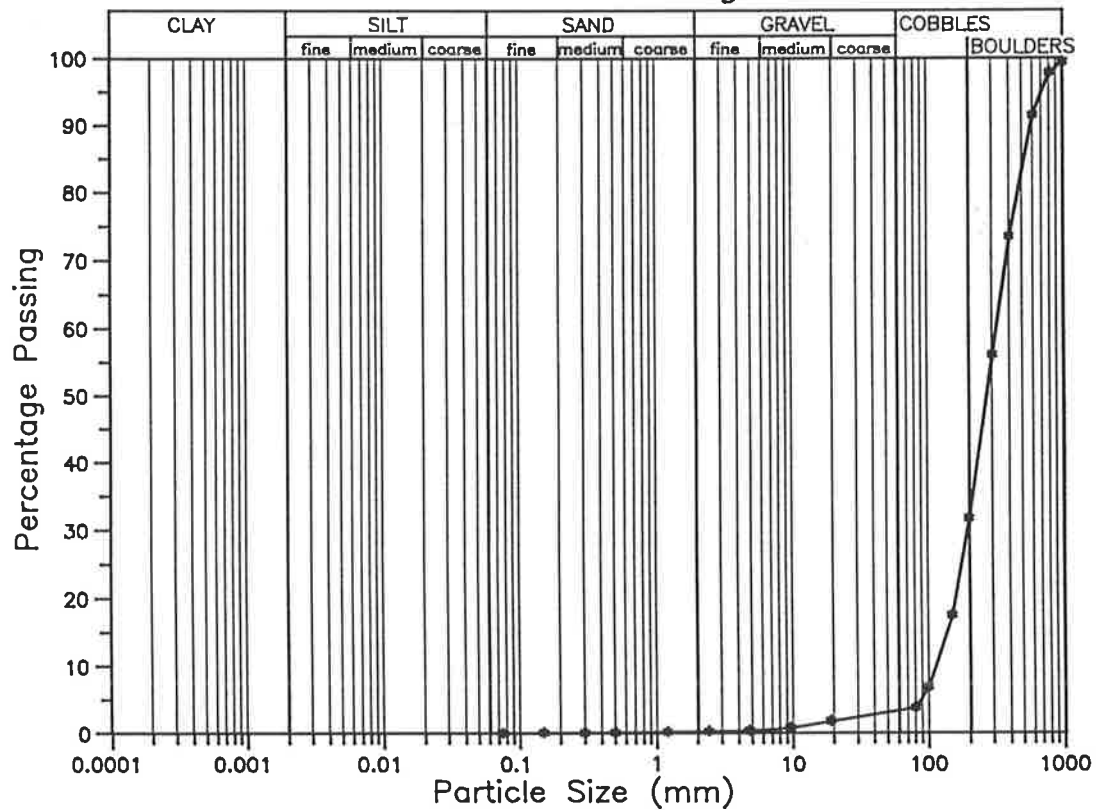


SITE 5

Separate Analyses

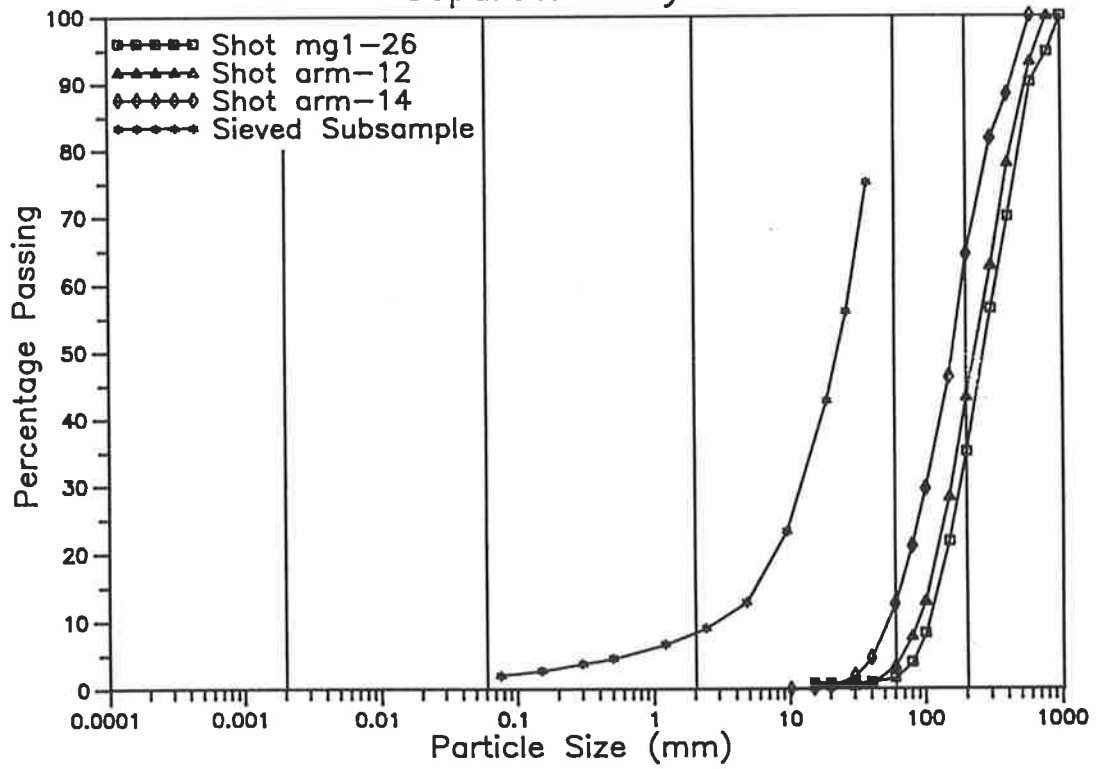


Site Grading

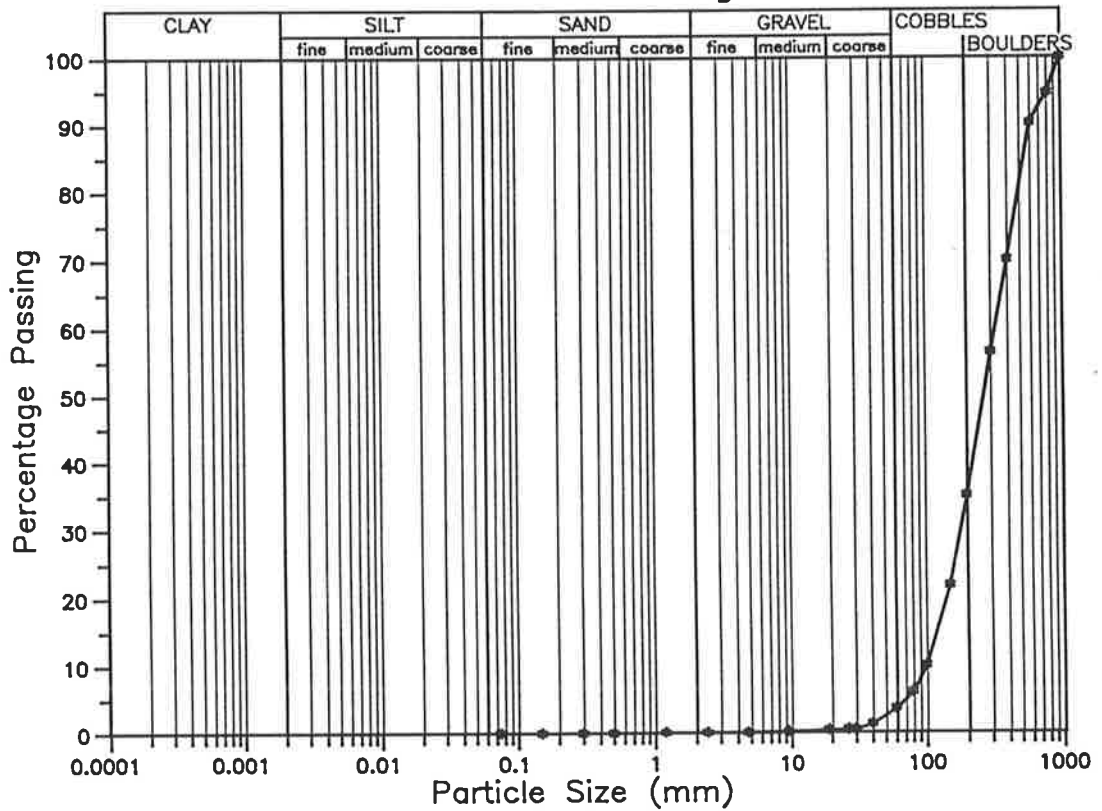


SITE 6

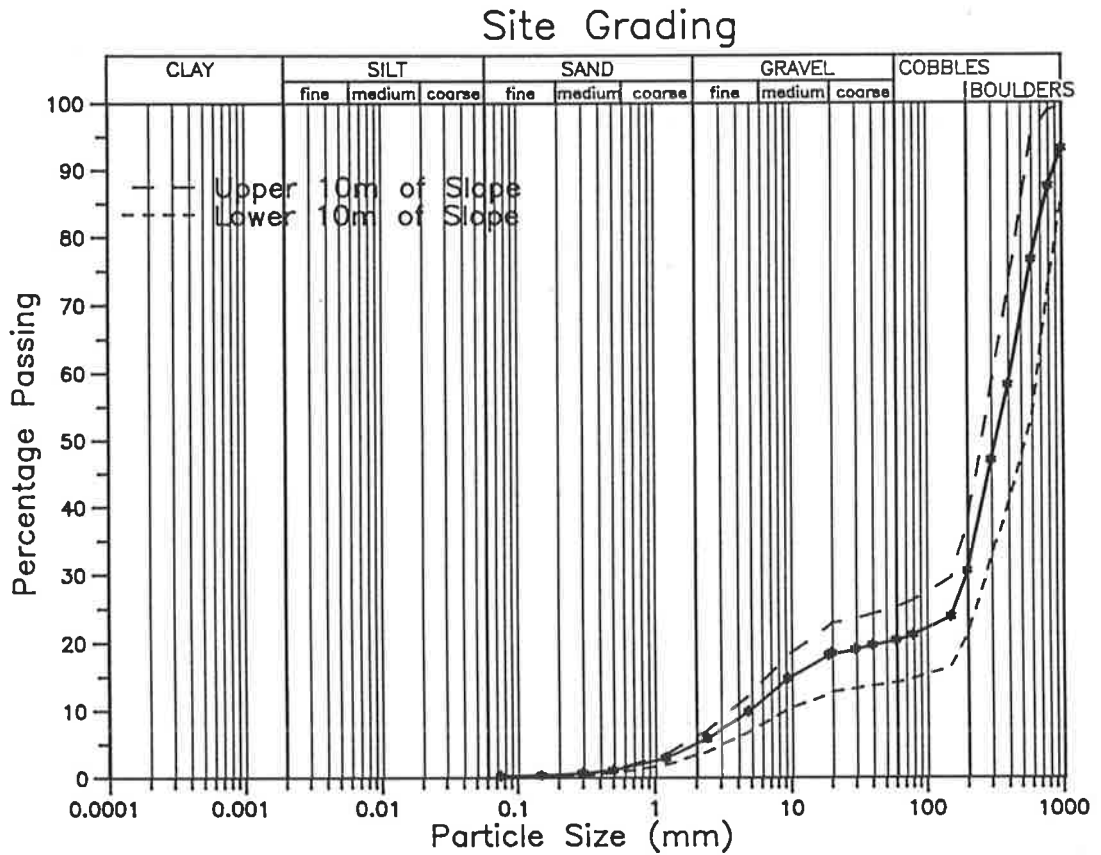
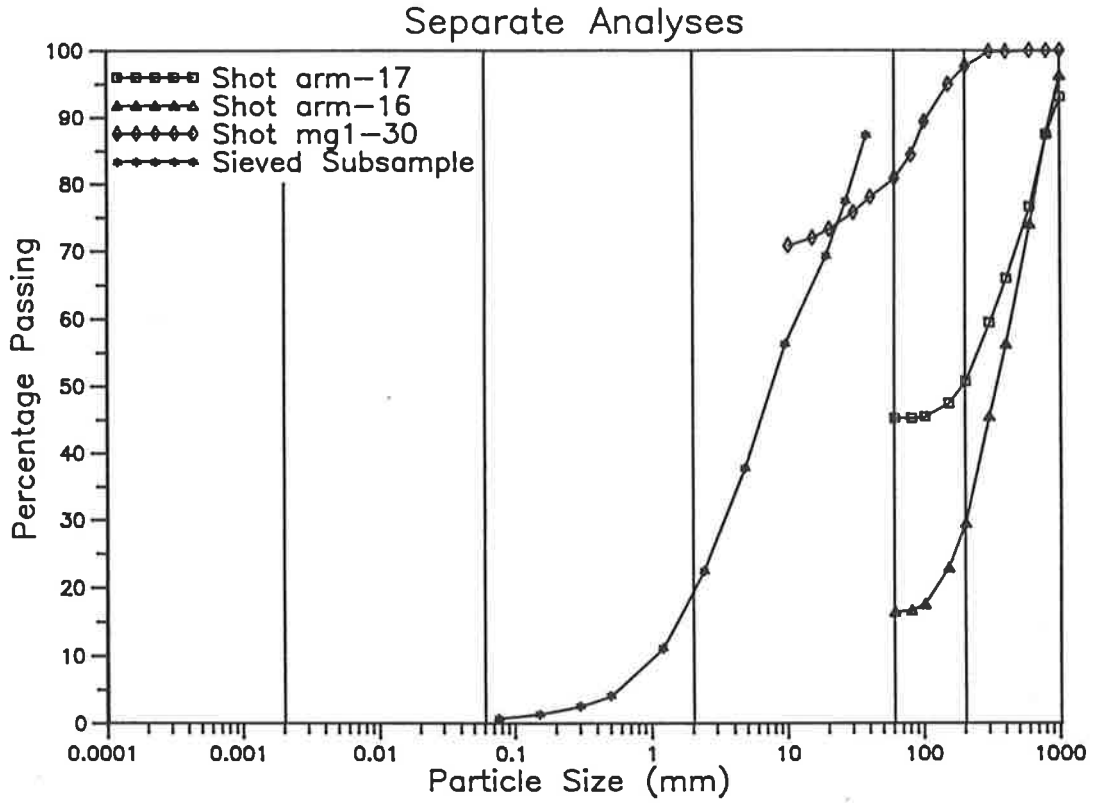
Separate Analyses



Site Grading

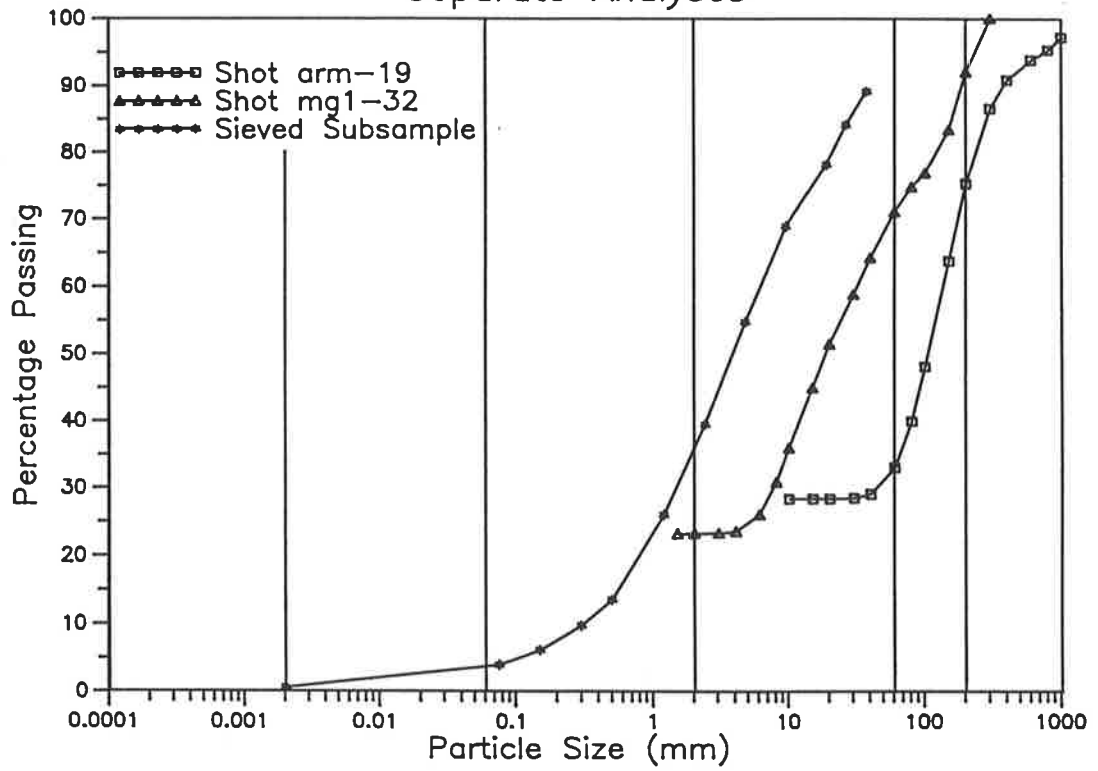


SITE 7

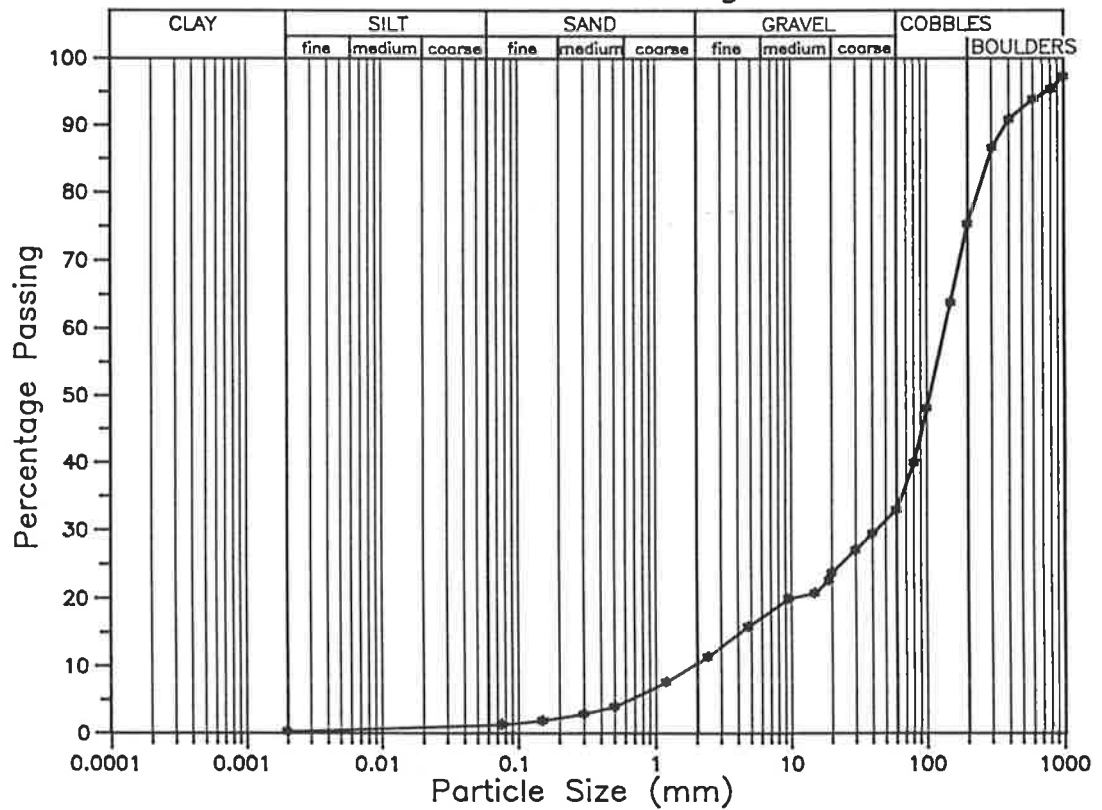


SITE 8

Separate Analyses

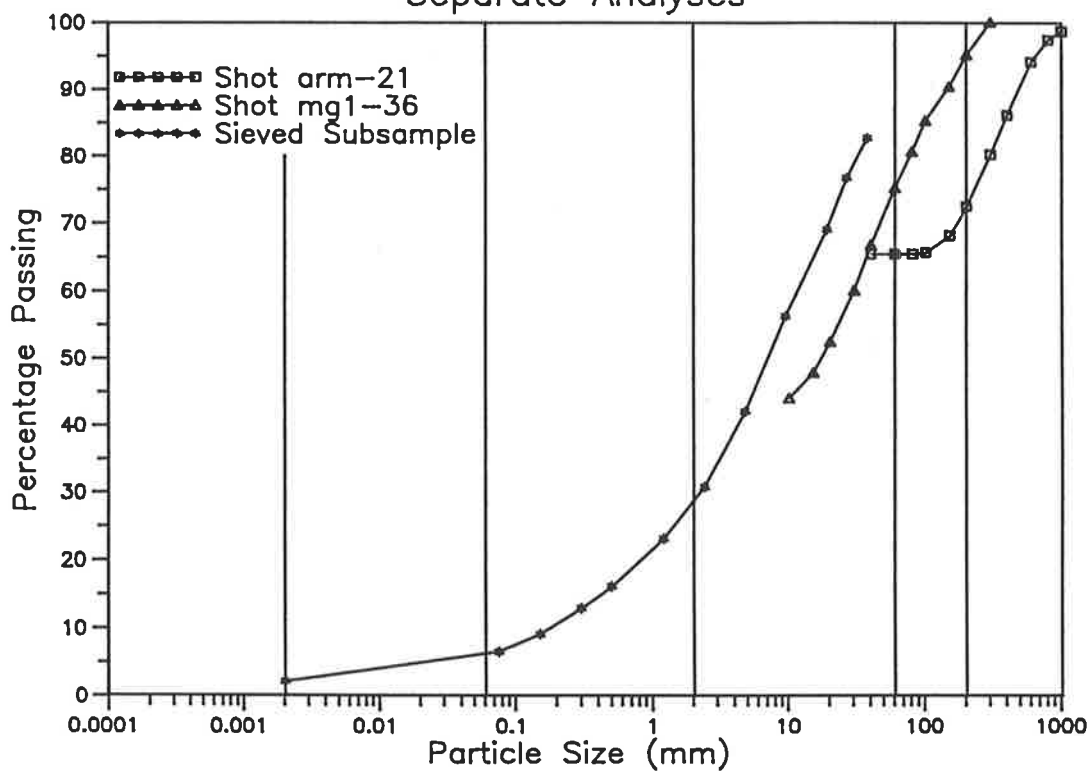


Site Grading

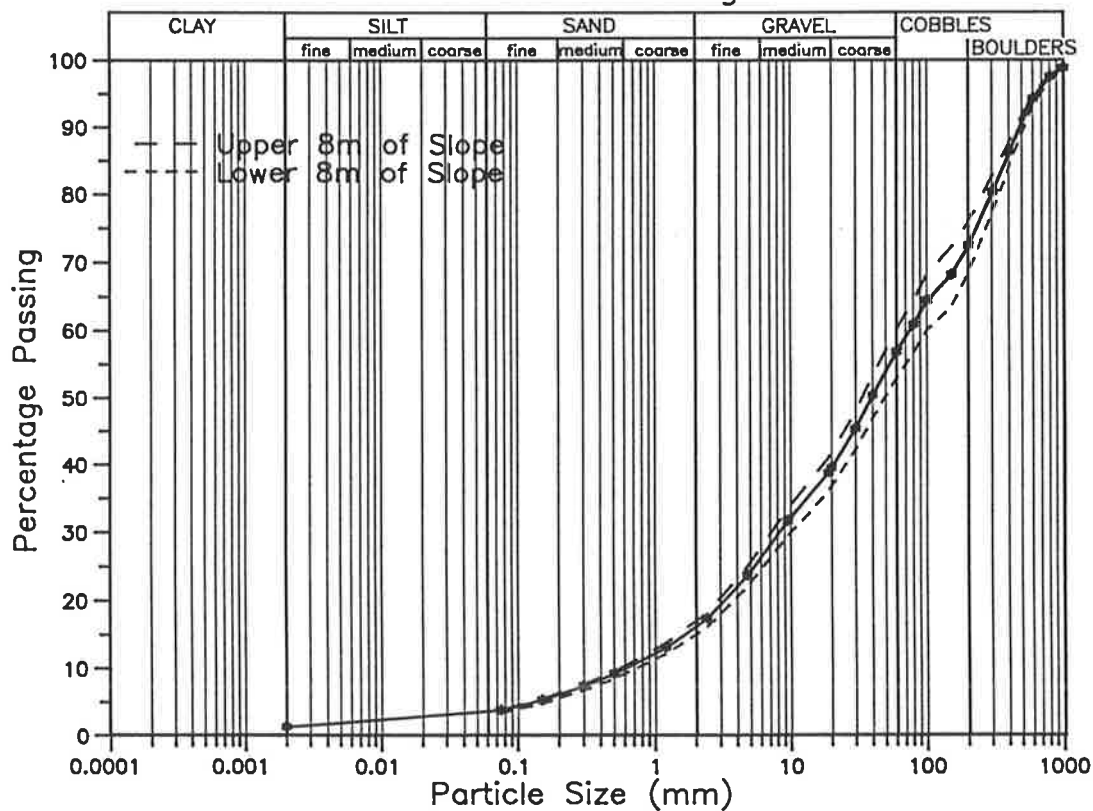


SITE 9

Separate Analyses

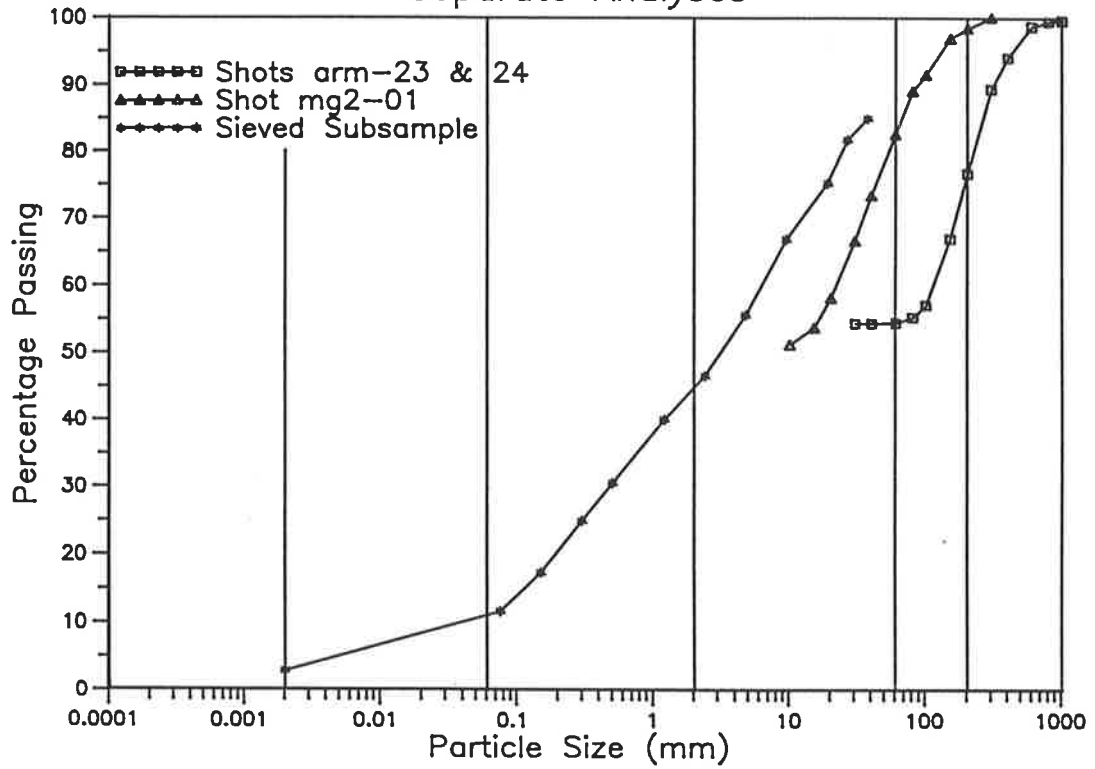


Site Grading

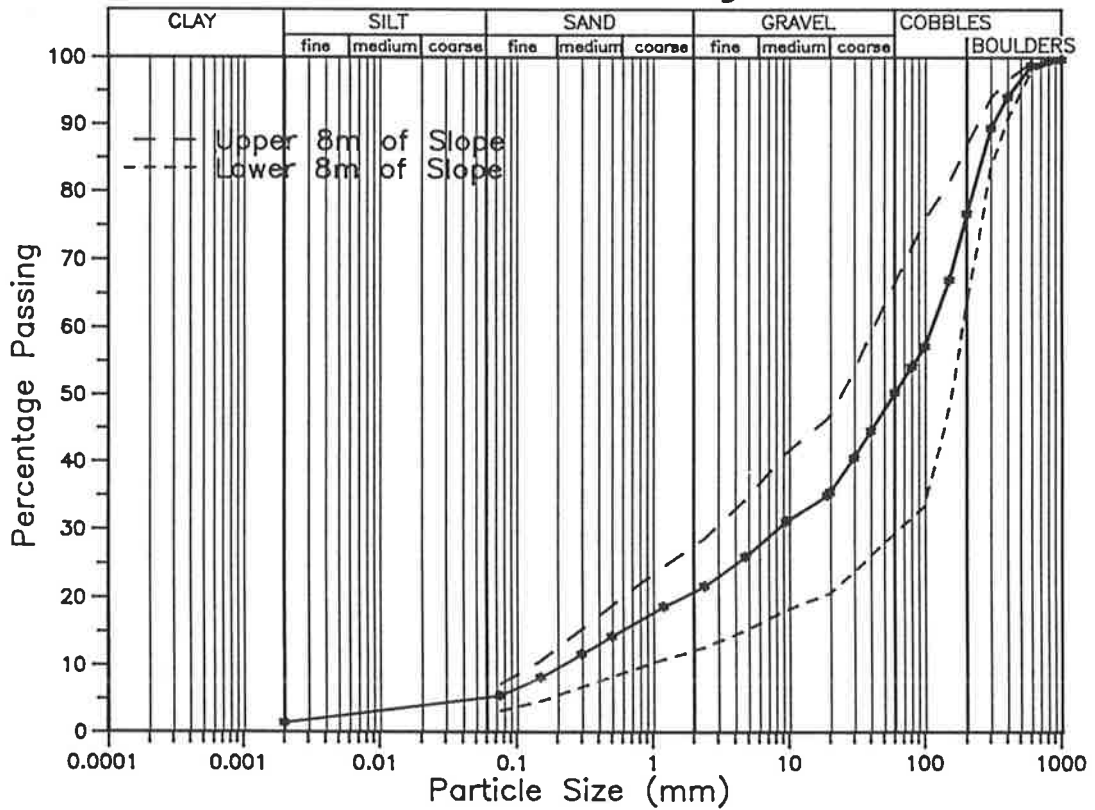


SITE 10

Separate Analyses

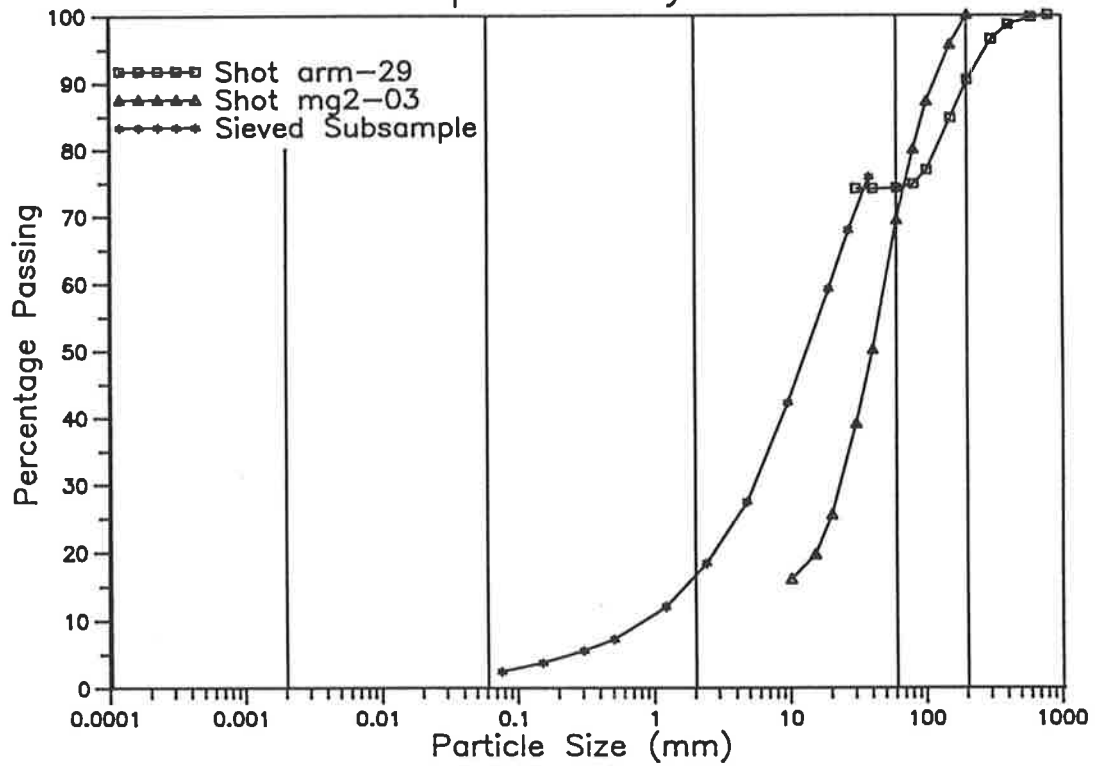


Site Grading

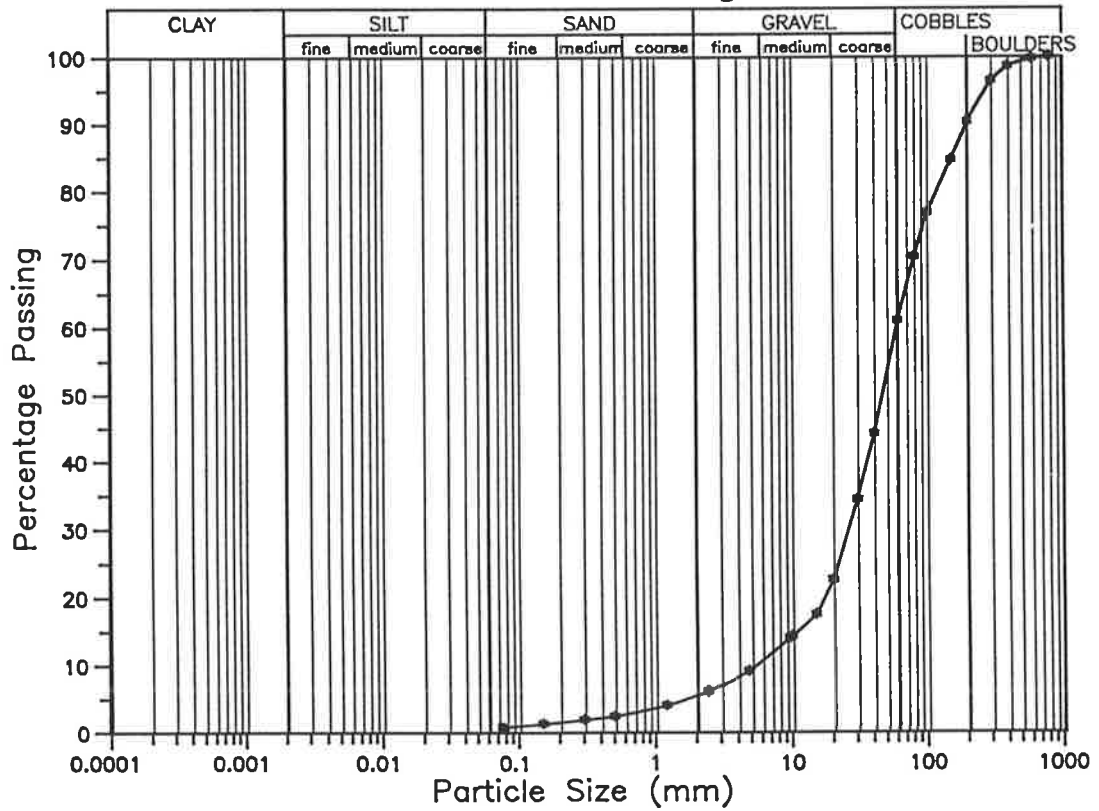


SITE 11

Separate Analyses

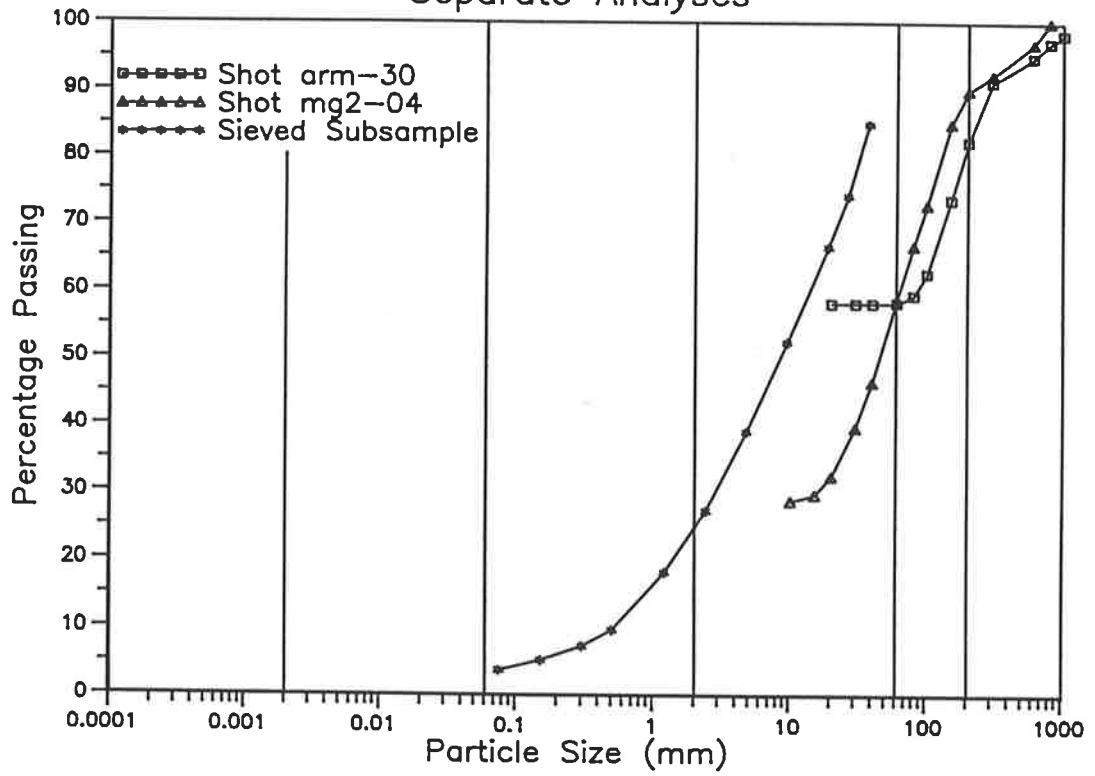


Site Grading

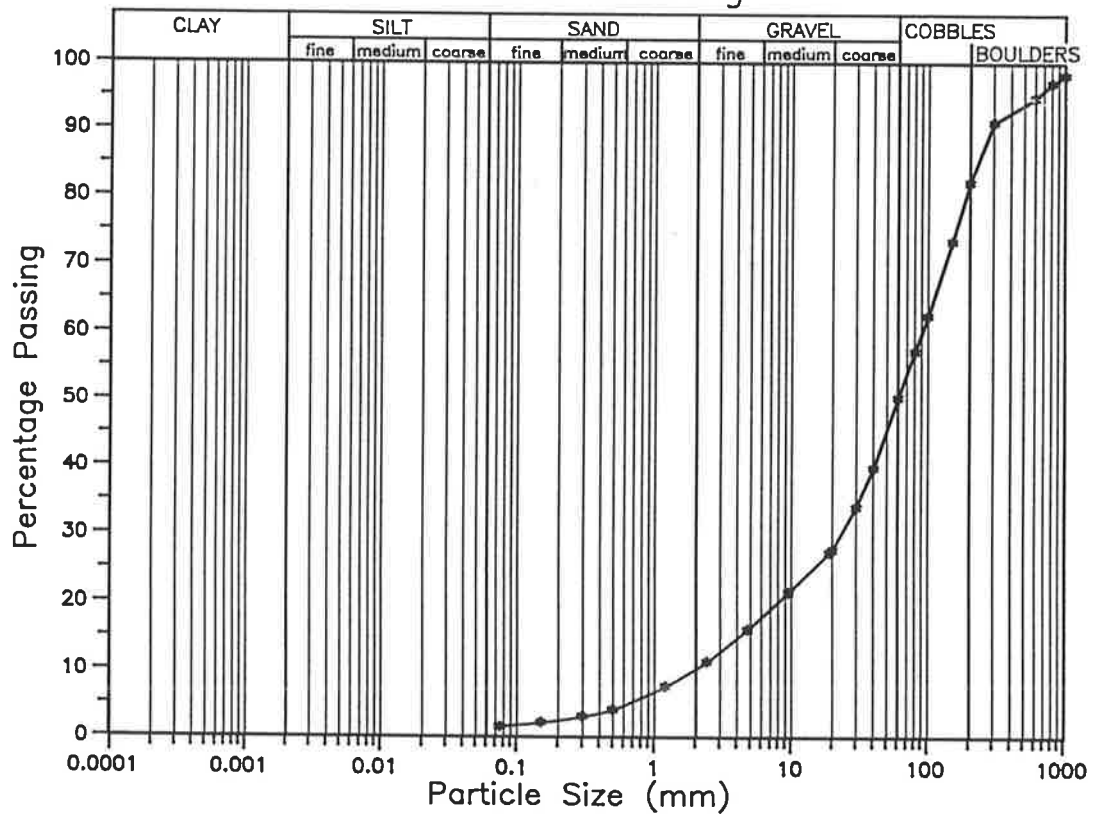


SITE 12

Separate Analyses

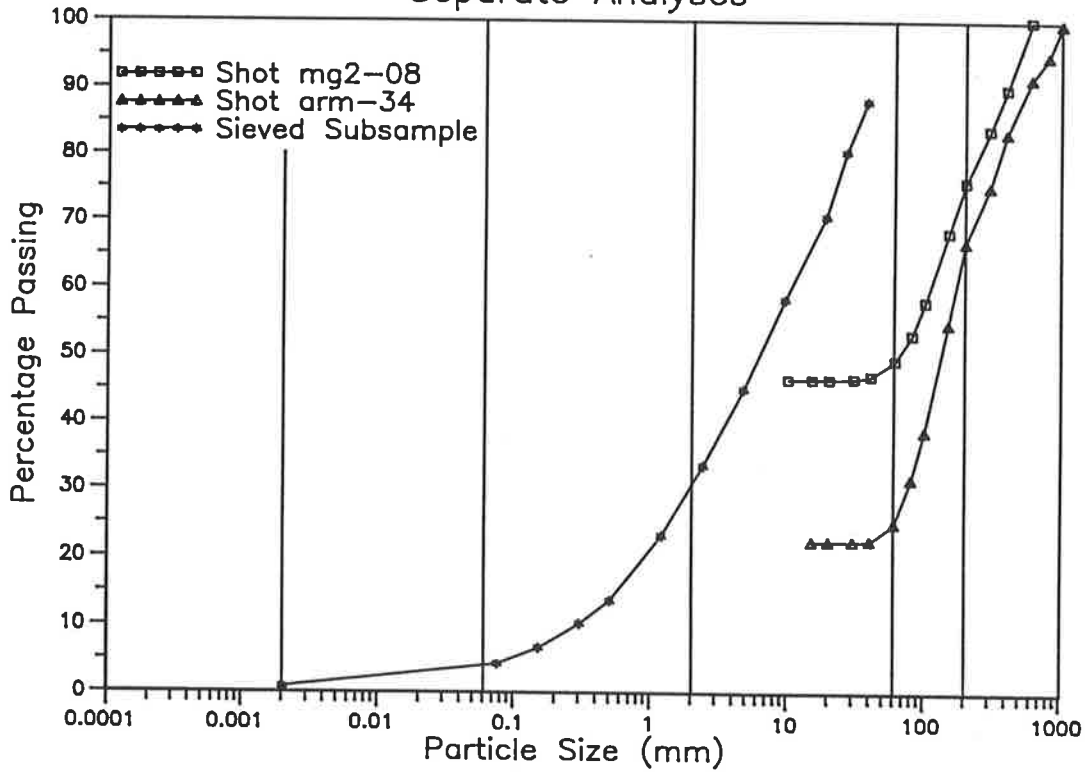


Site Grading

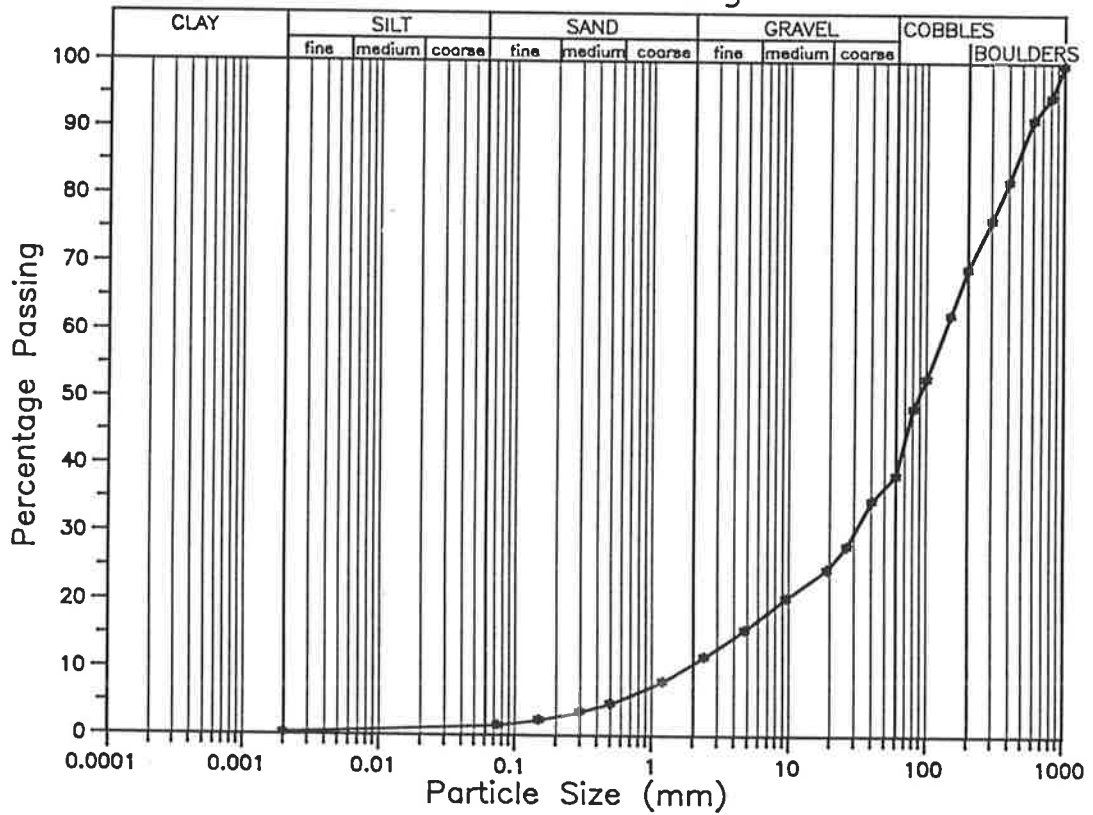


SITE 14

Separate Analyses

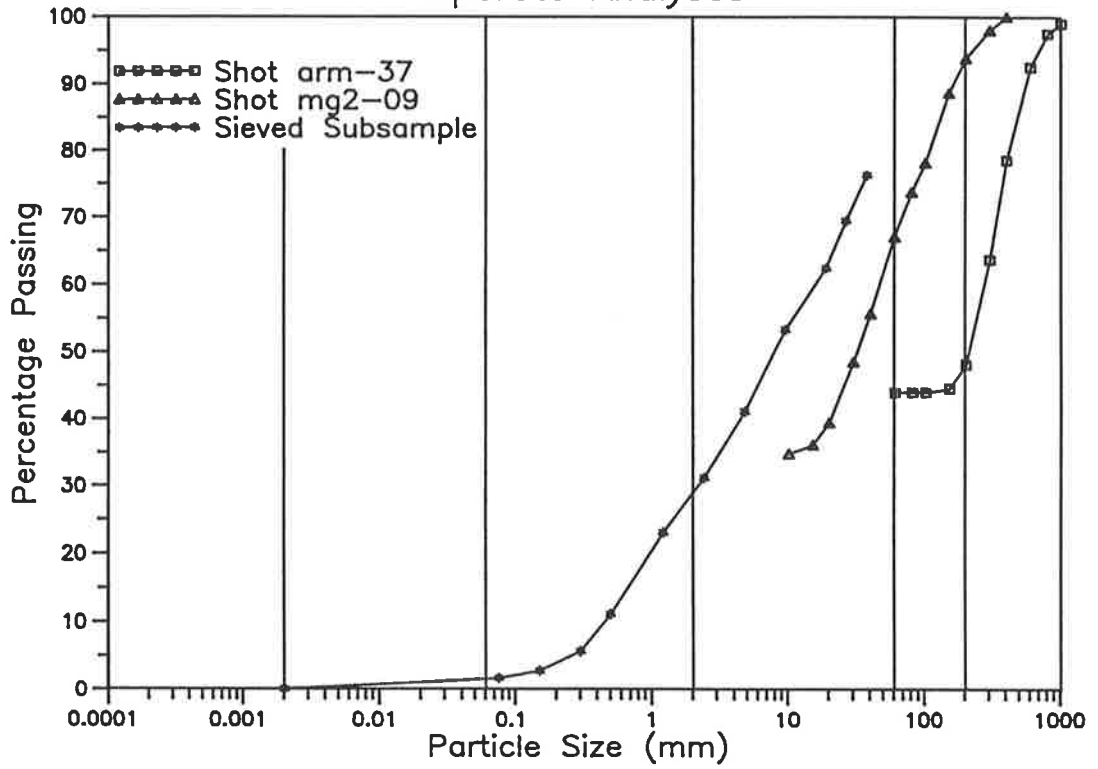


Site Grading

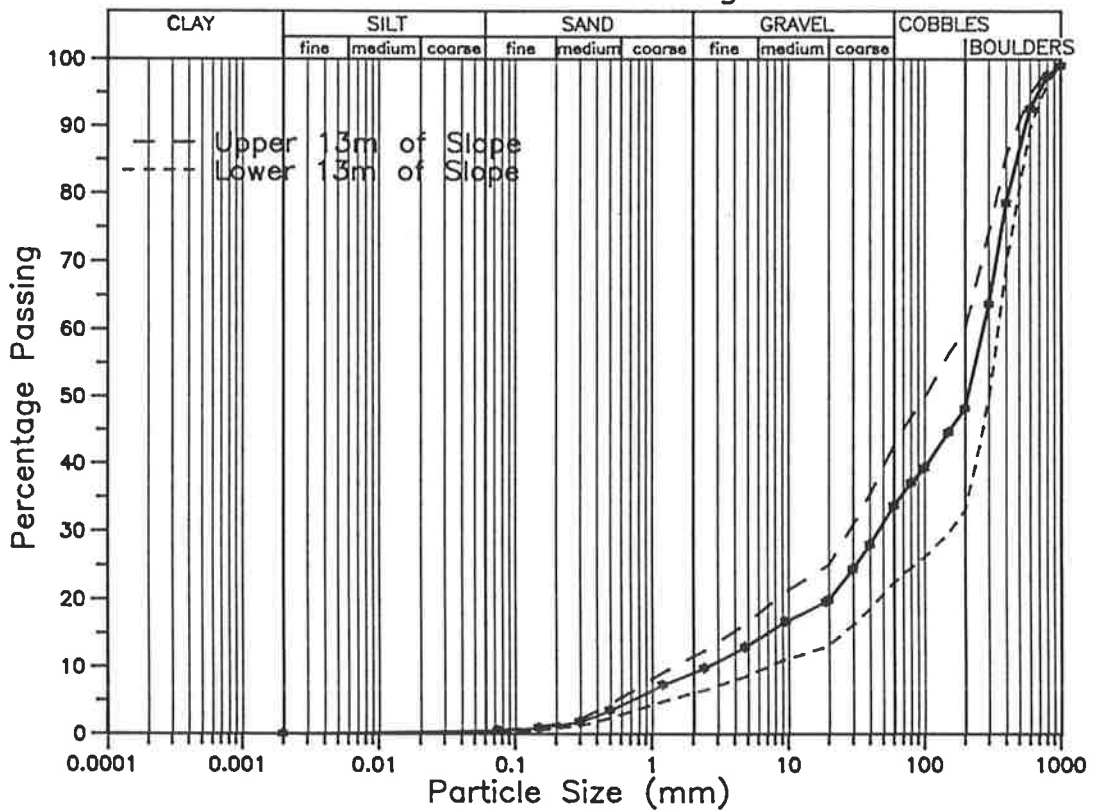


SITE 15

Separate Analyses

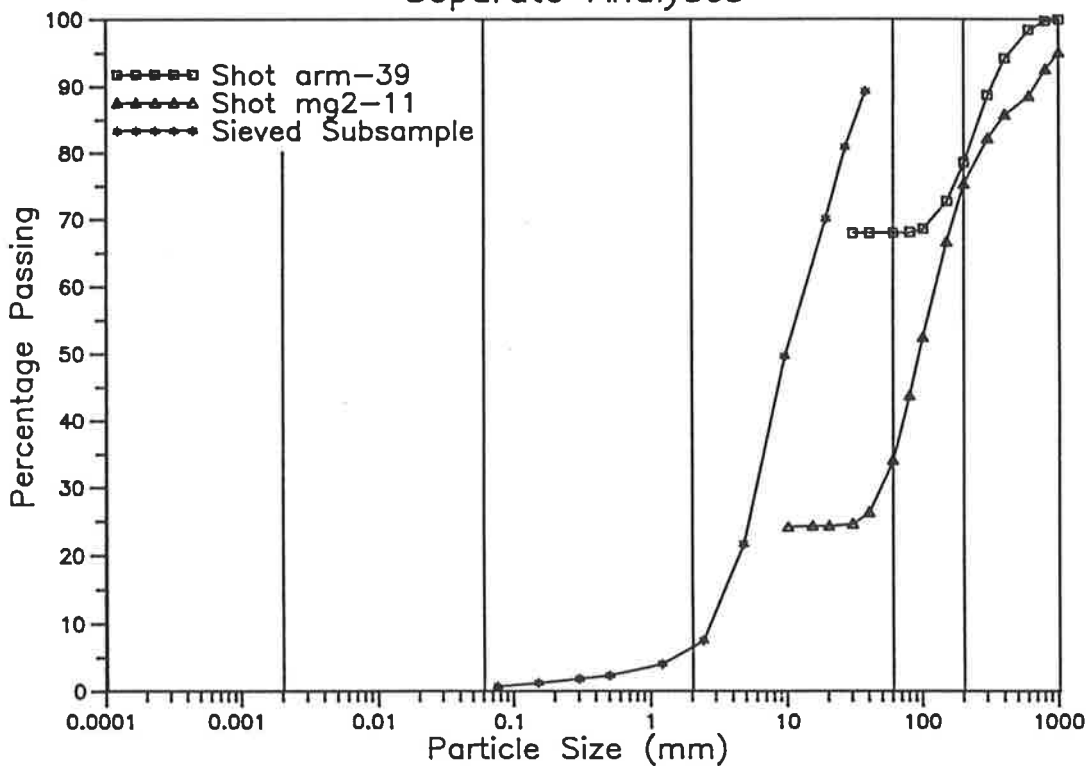


Site Grading

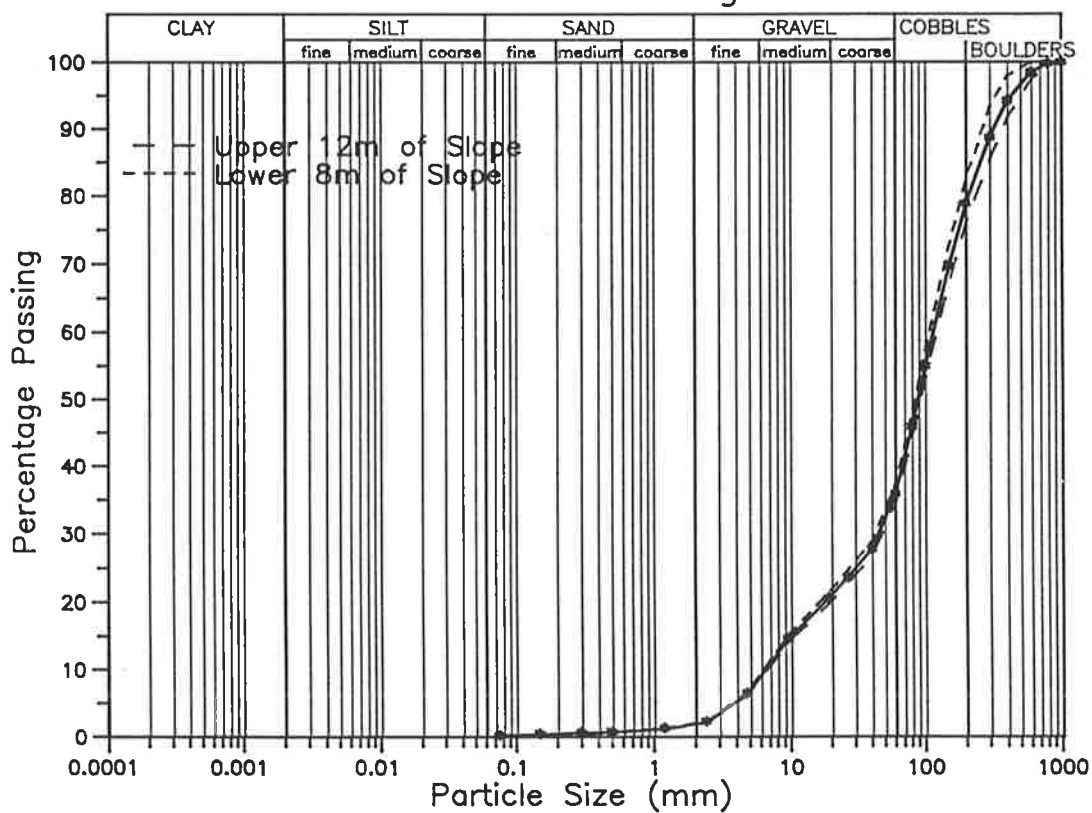


SITE 16

Separate Analyses

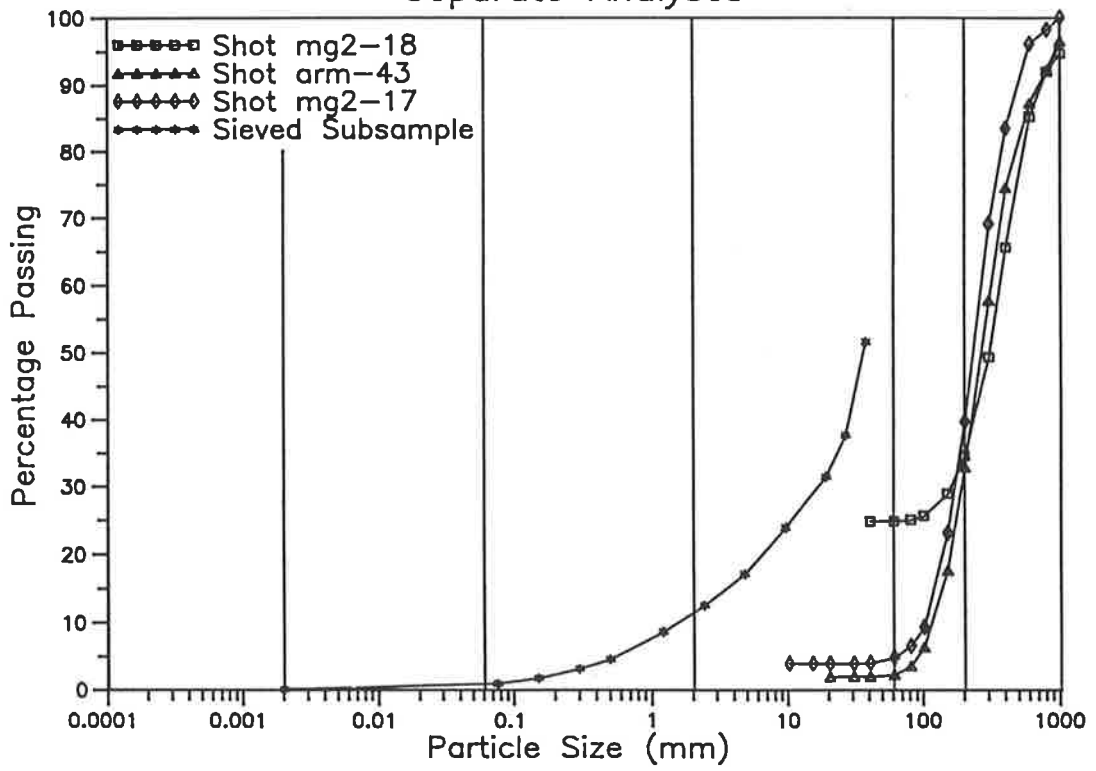


Site Grading



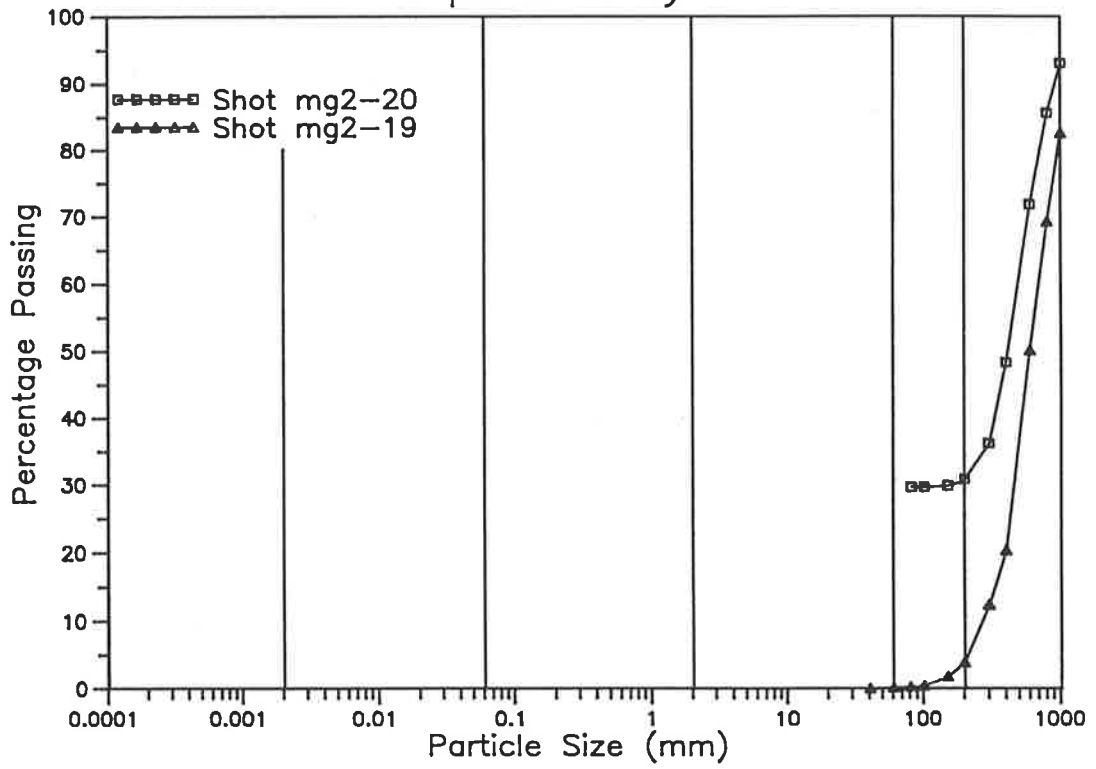
SITE 17b

Separate Analyses

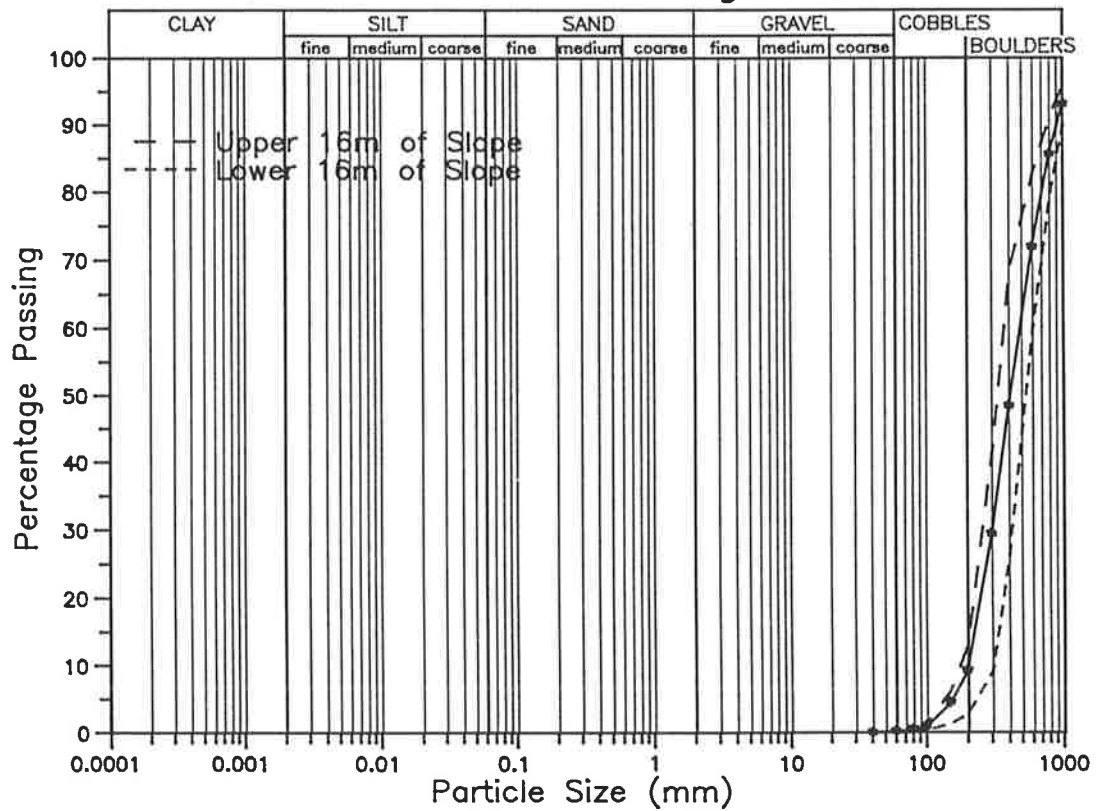


SITE 18

Separate Analyses

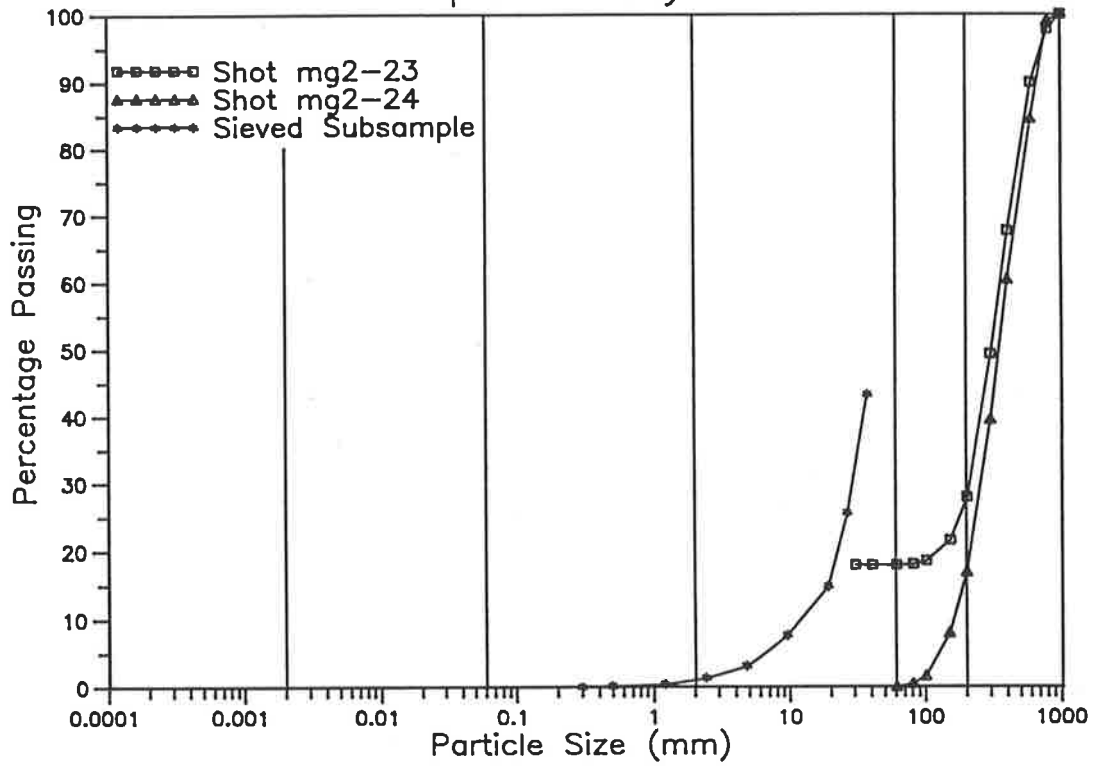


Site Grading

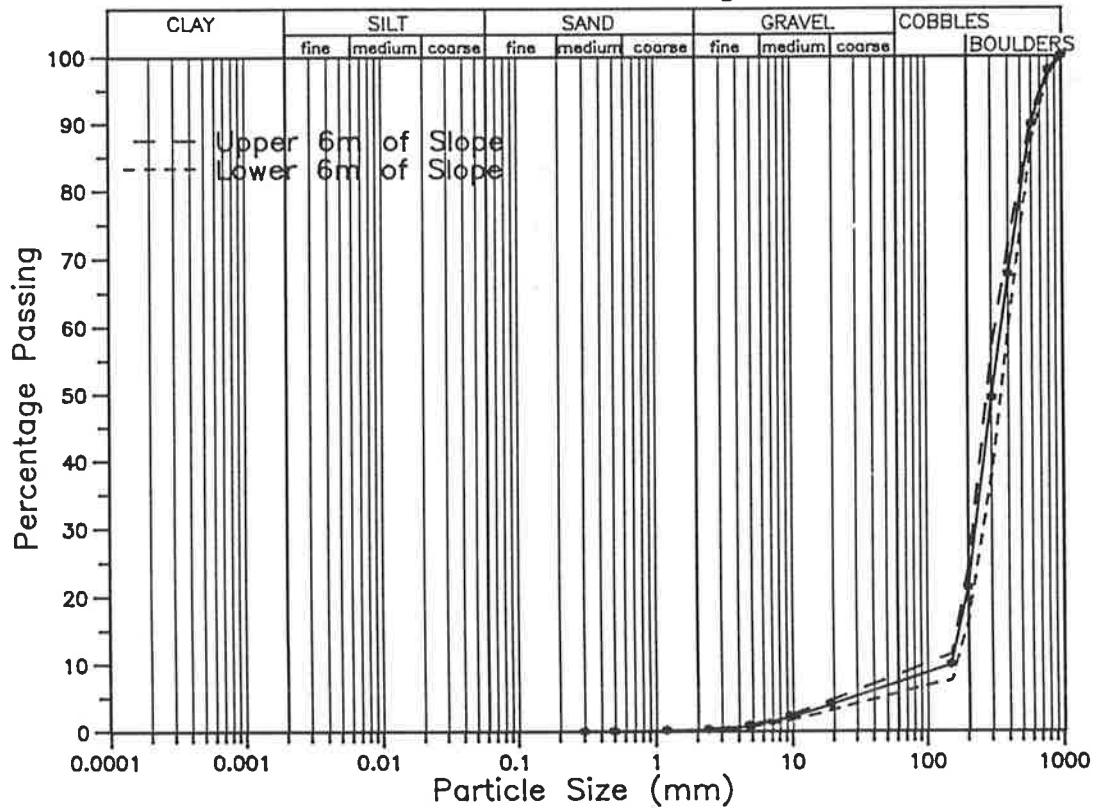


SITE 19

Separate Analyses

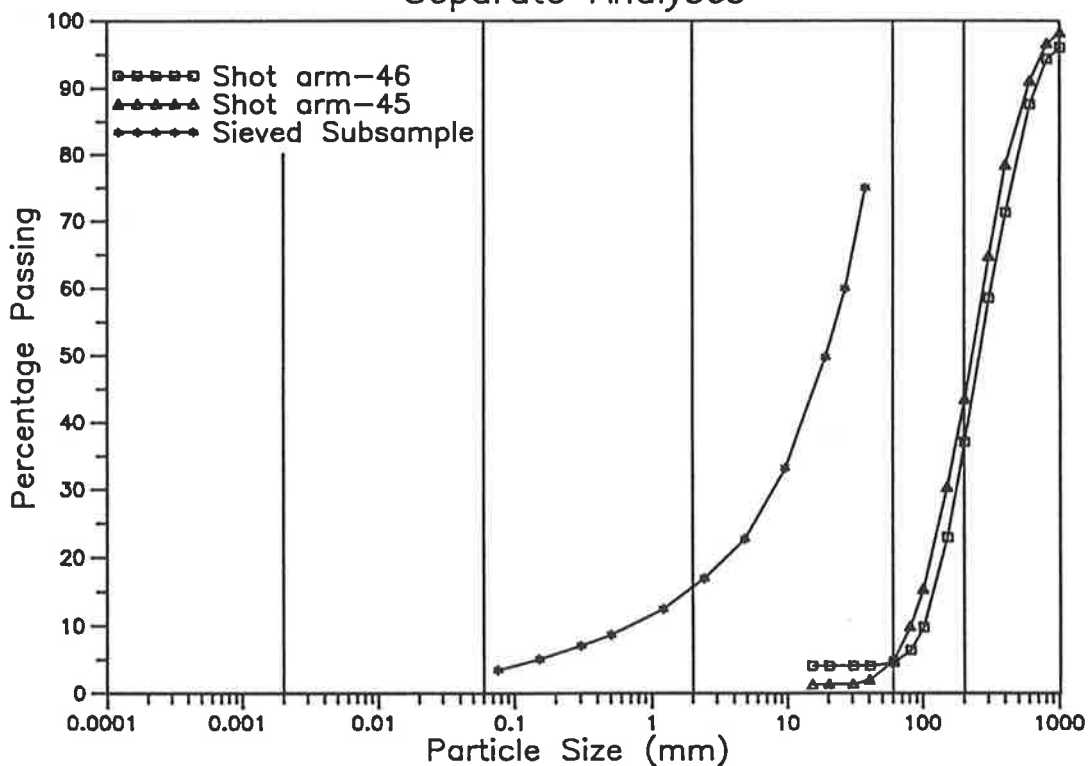


Site Grading

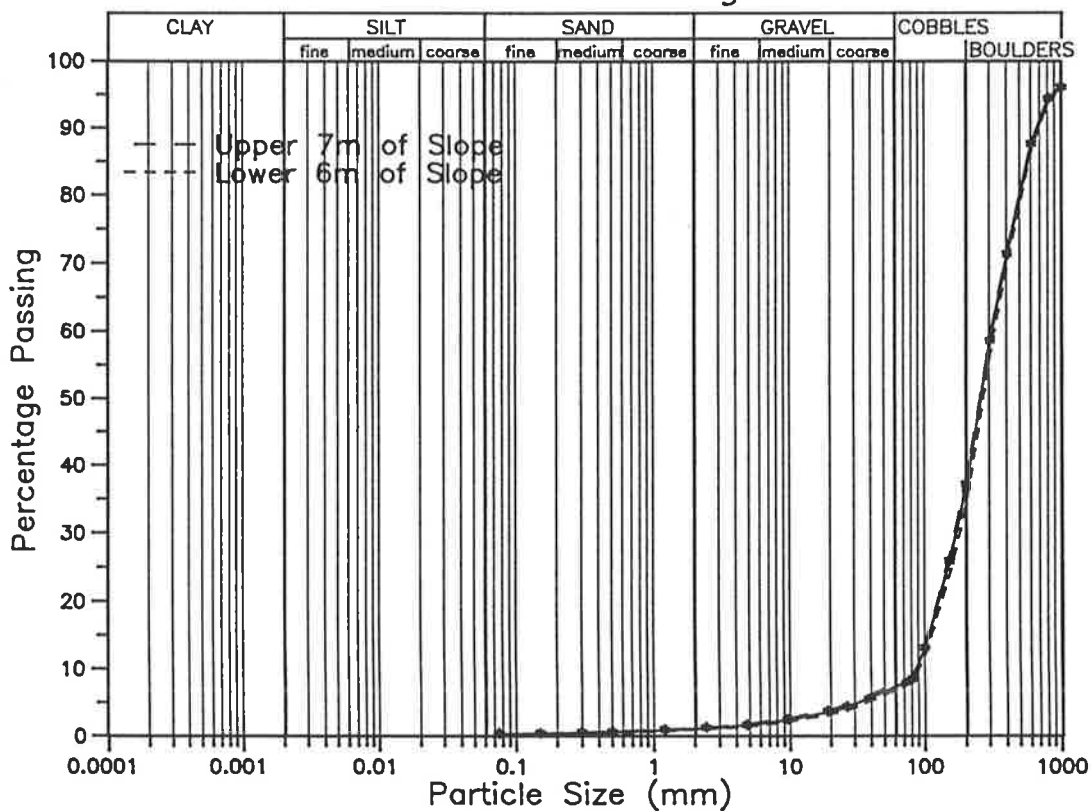


SITE 20

Separate Analyses

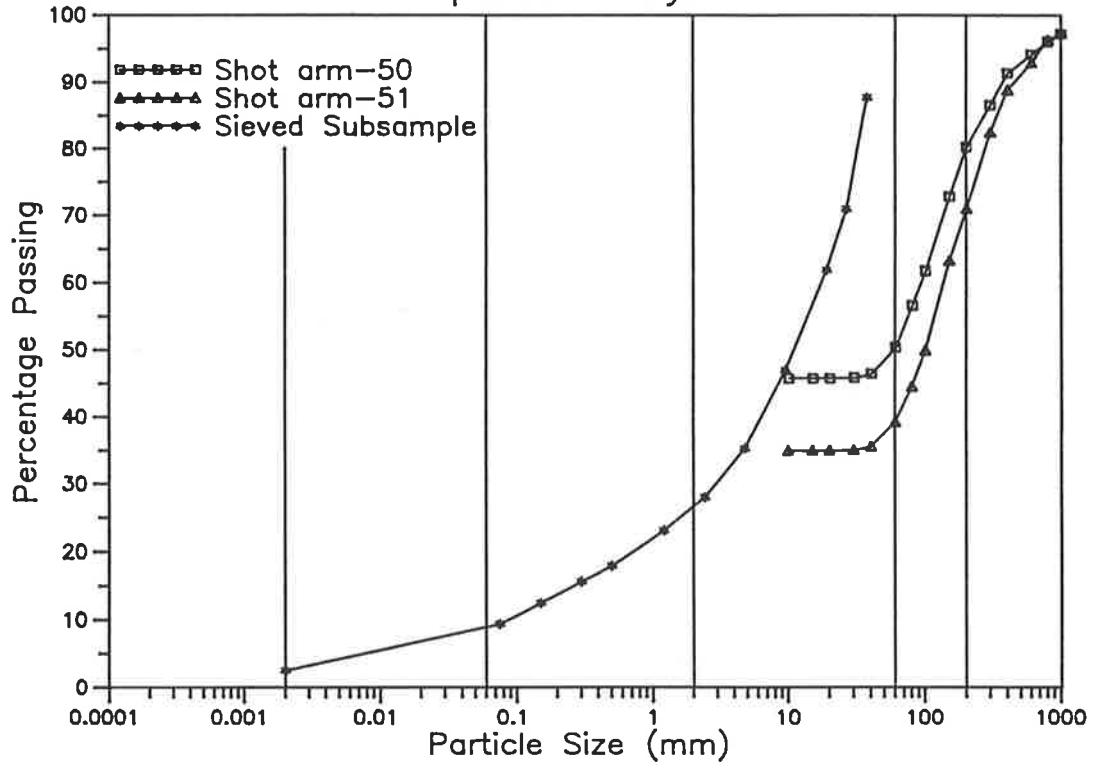


Site Grading

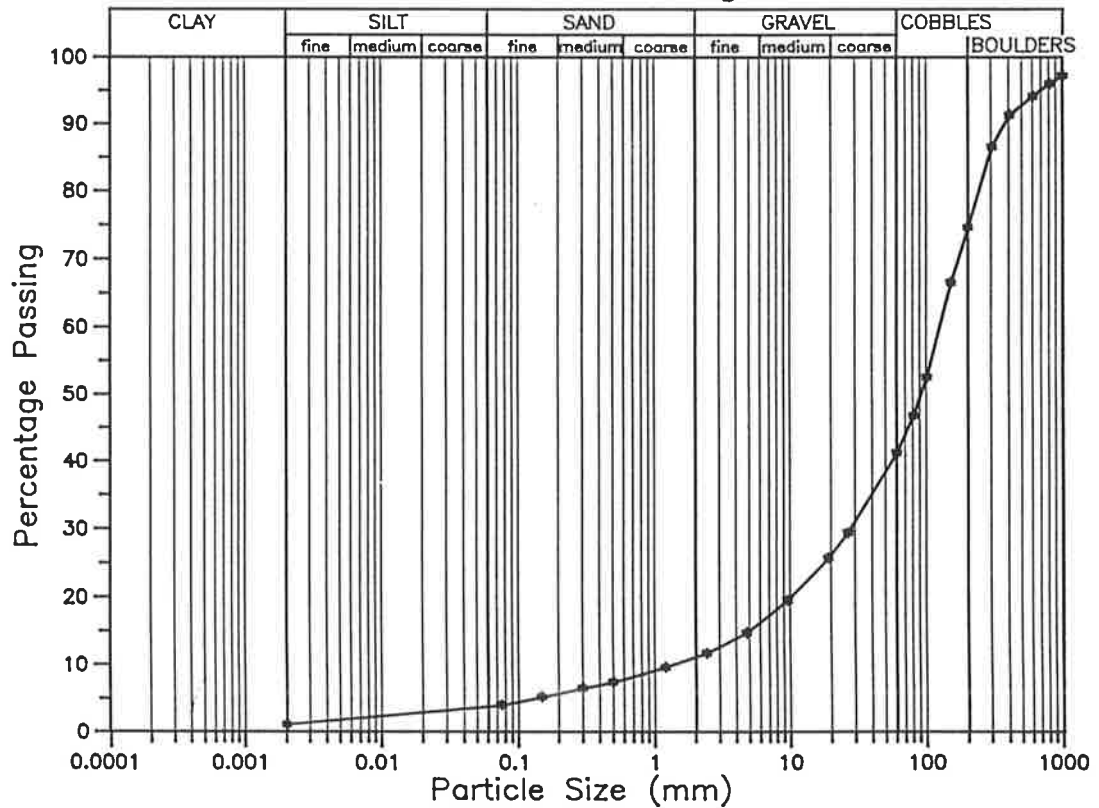


SITE 22

Separate Analyses

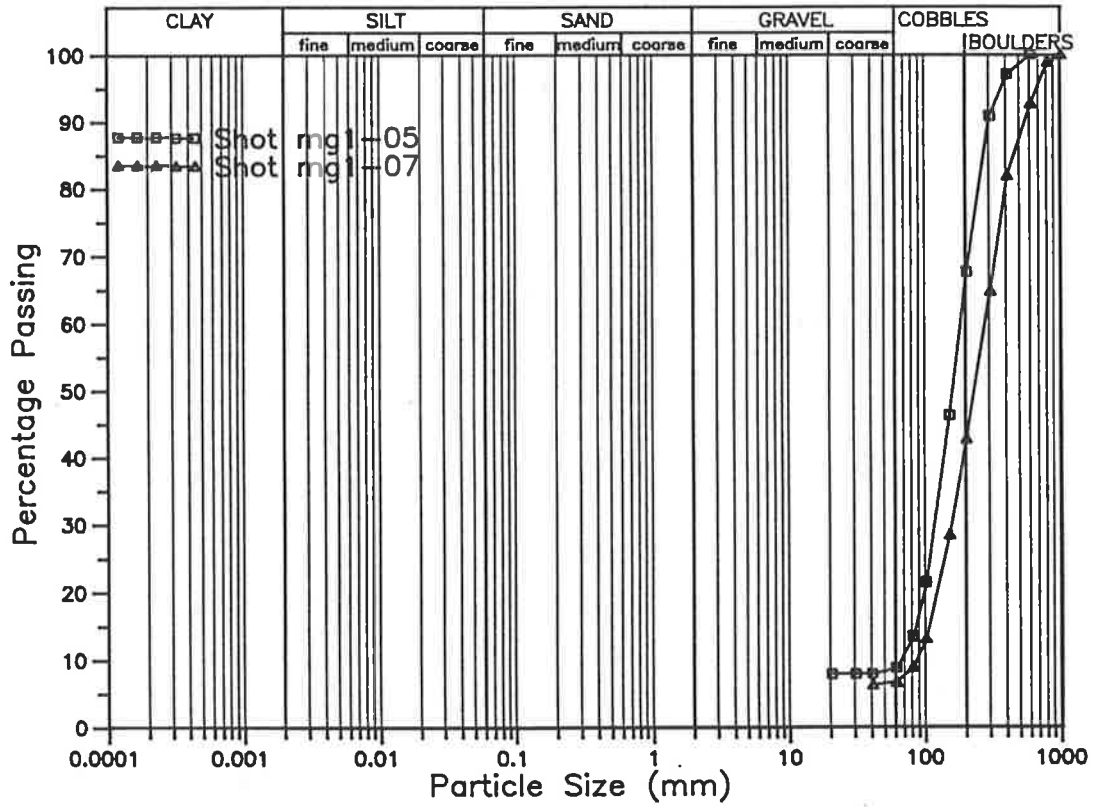


Site Grading

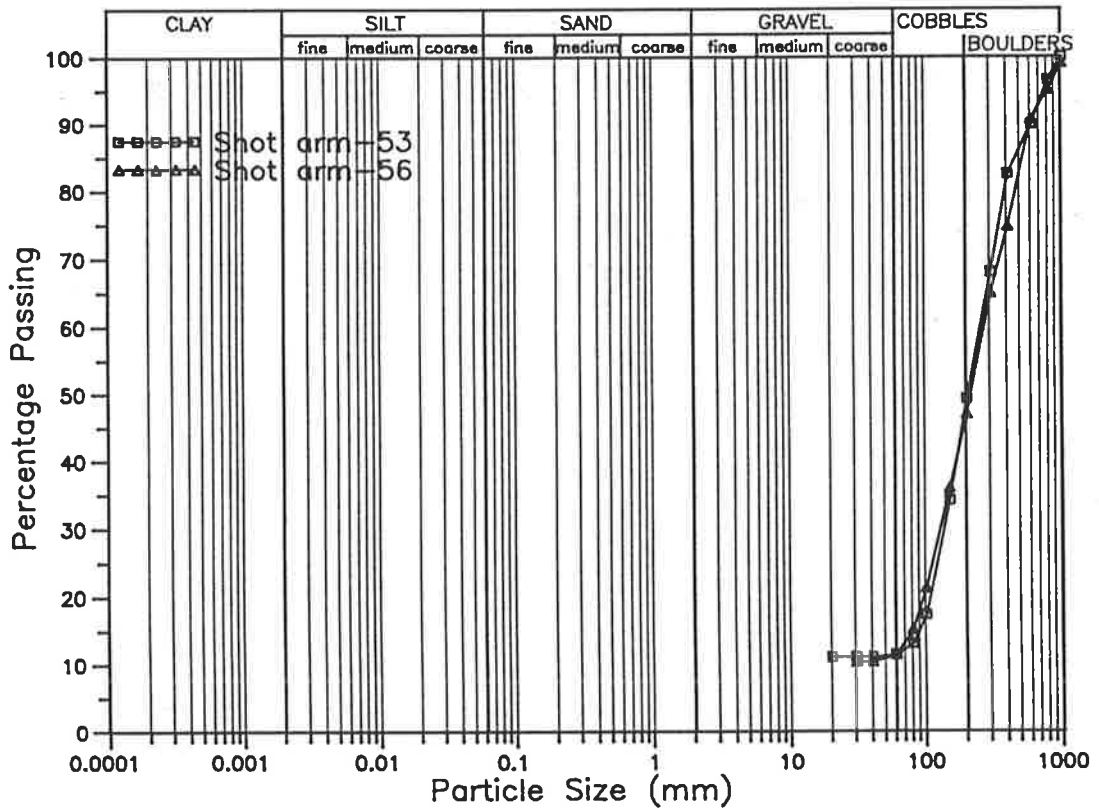


TRUCK TRAYS

June 1989

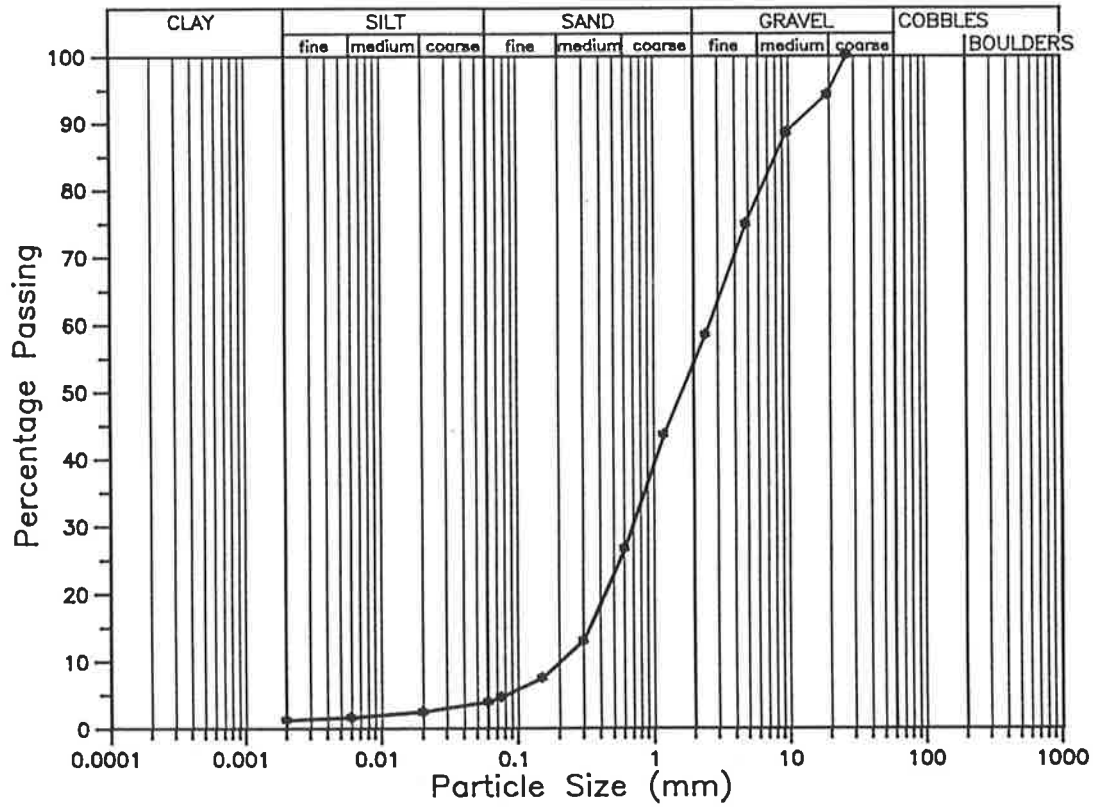


Later site visit

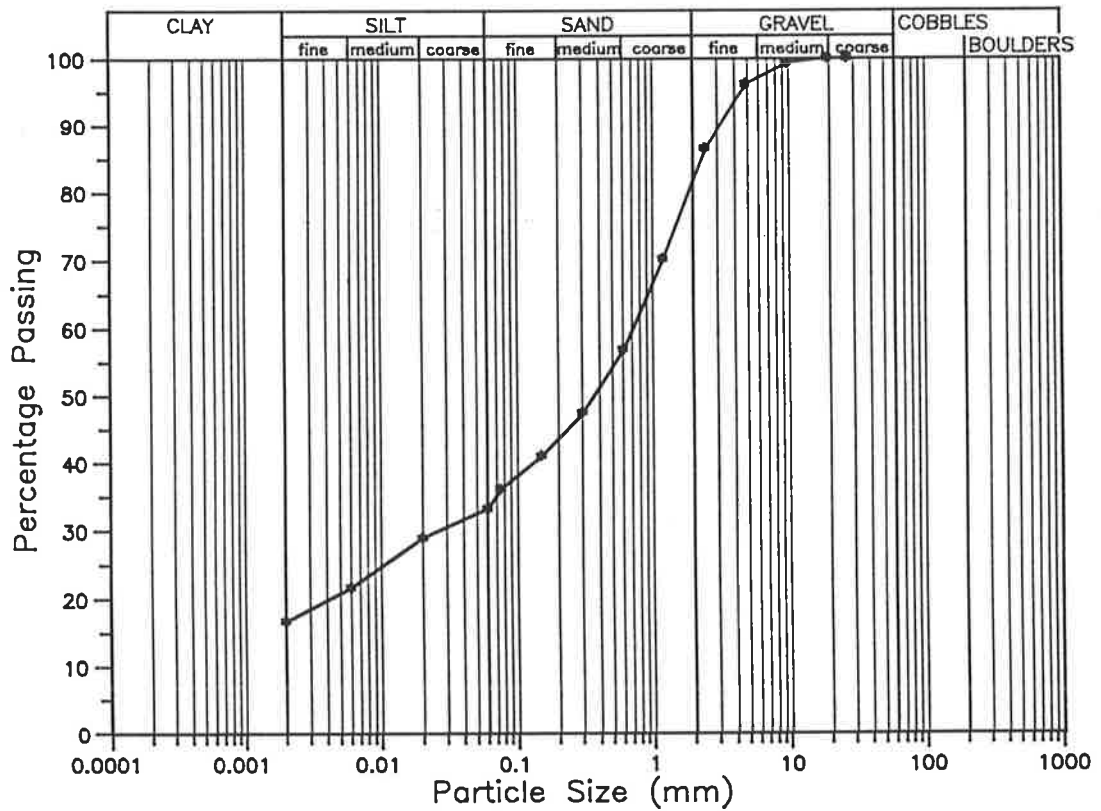


PIT/SOIL SAMPLES

RM27A

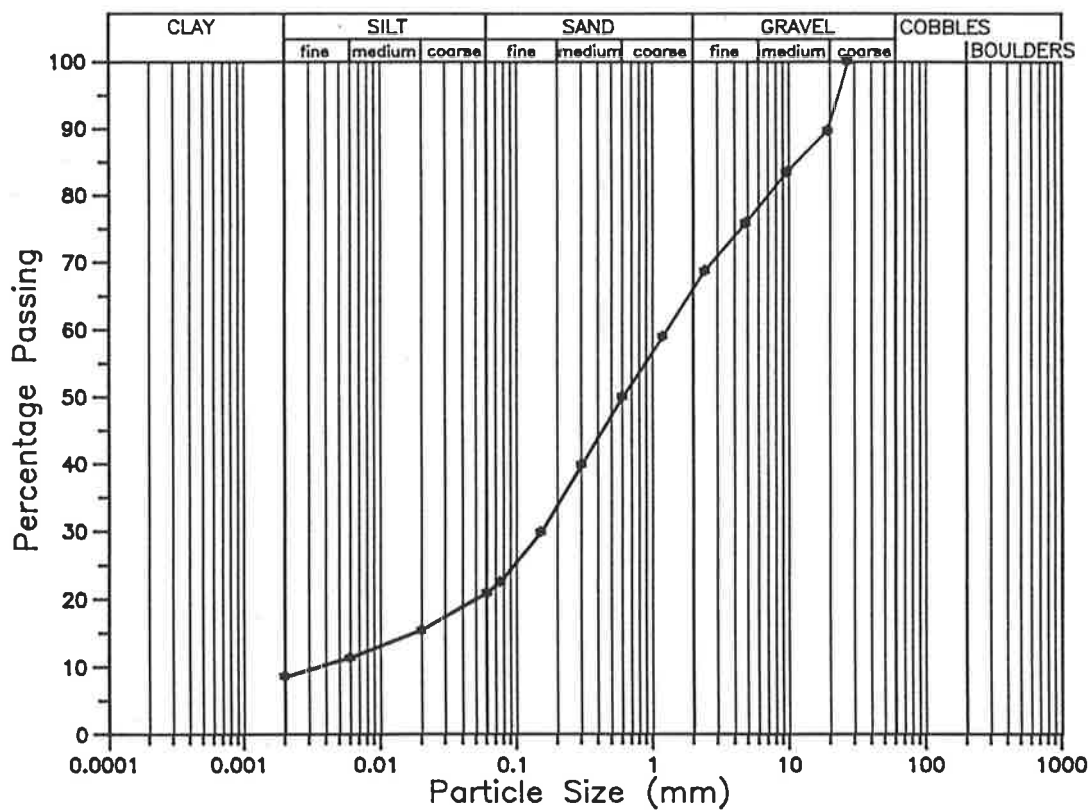


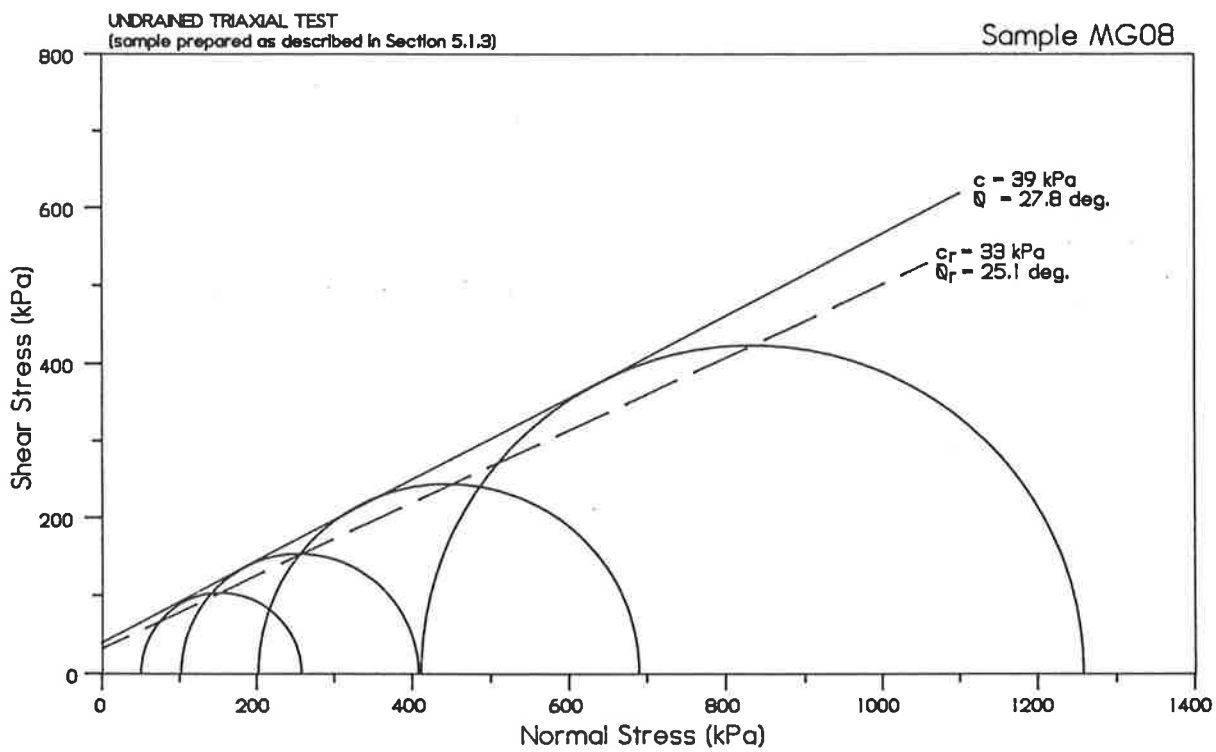
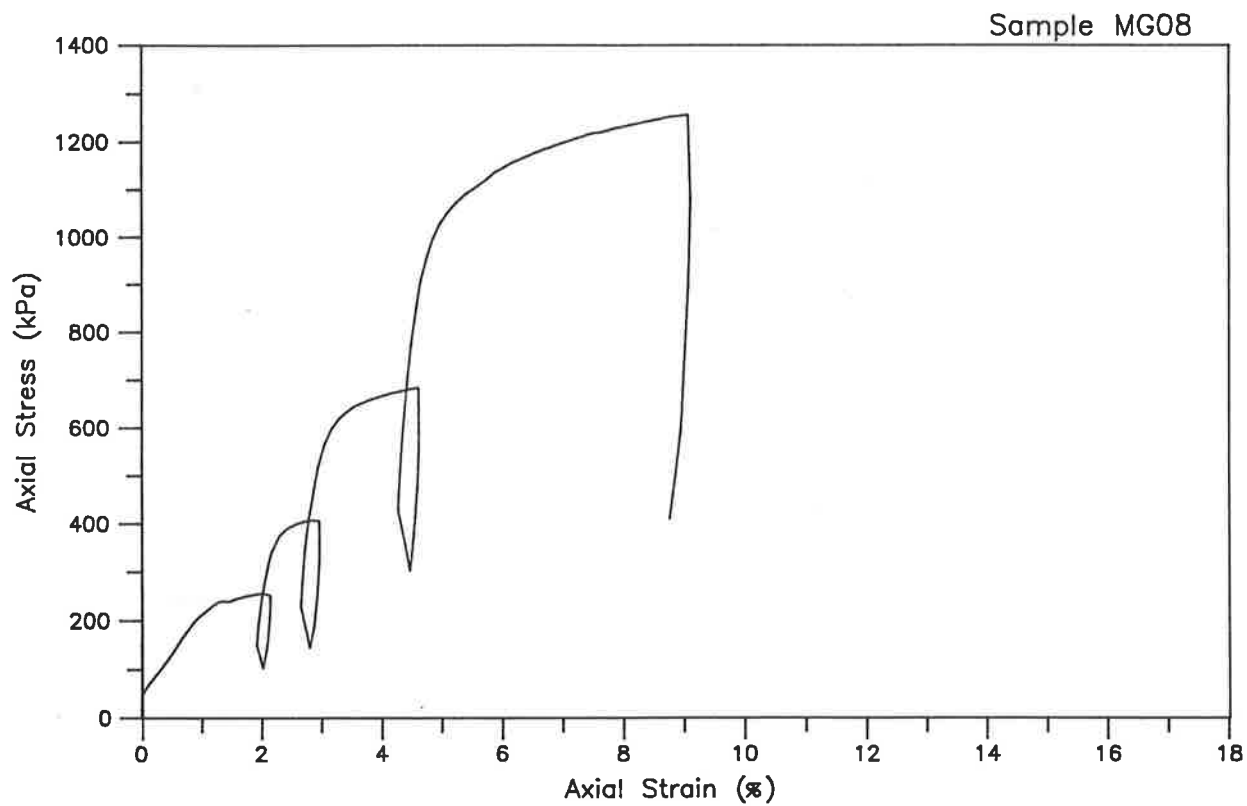
RM27B

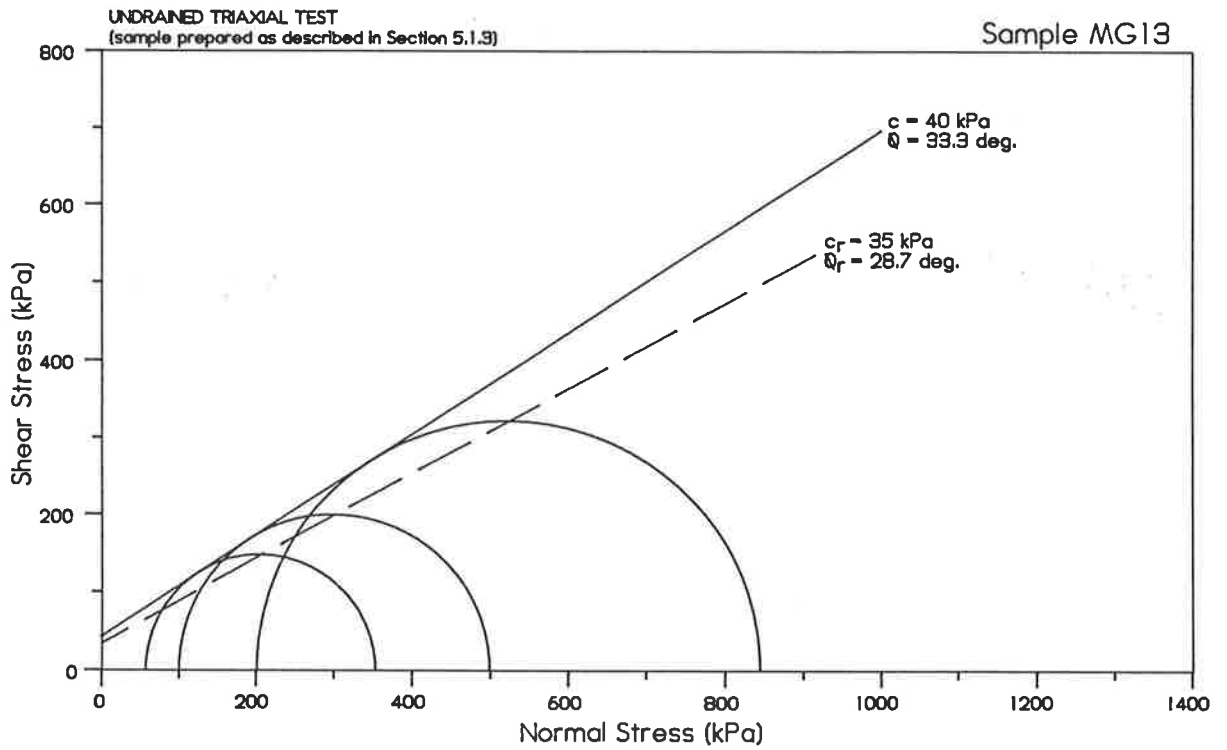
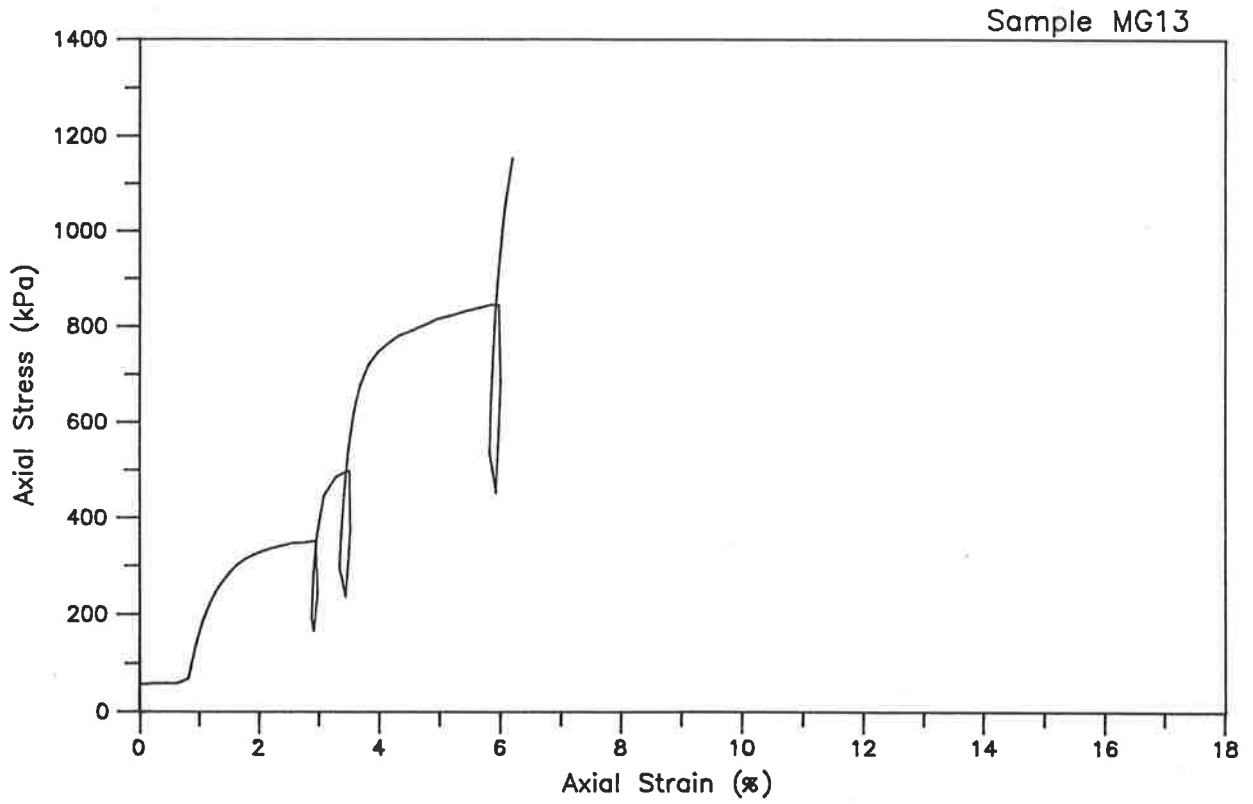


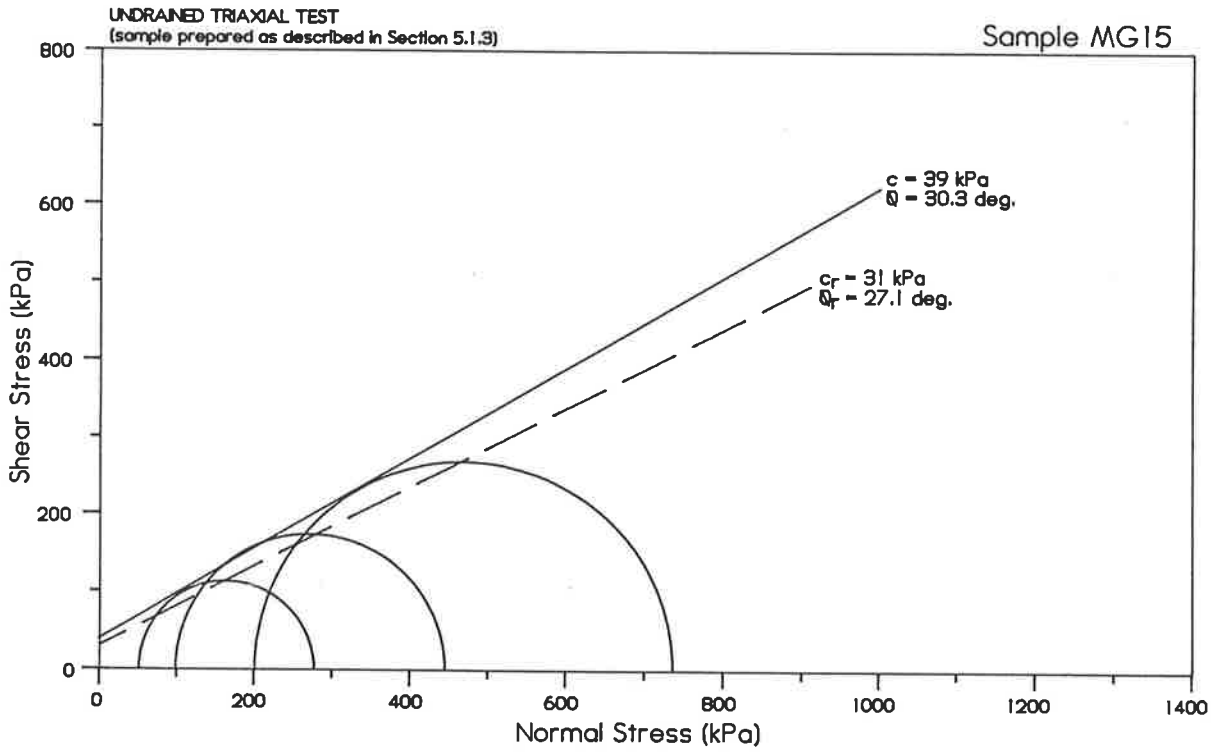
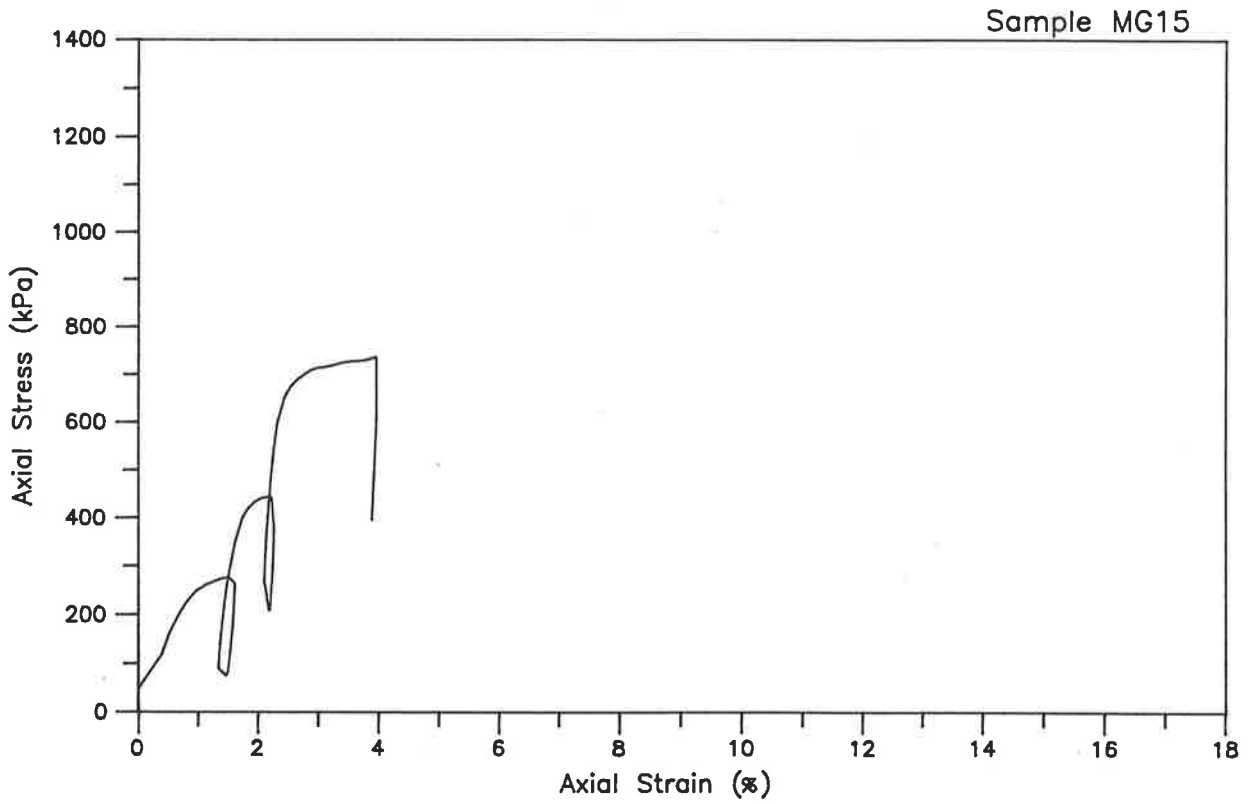
PIT/SOIL SAMPLES

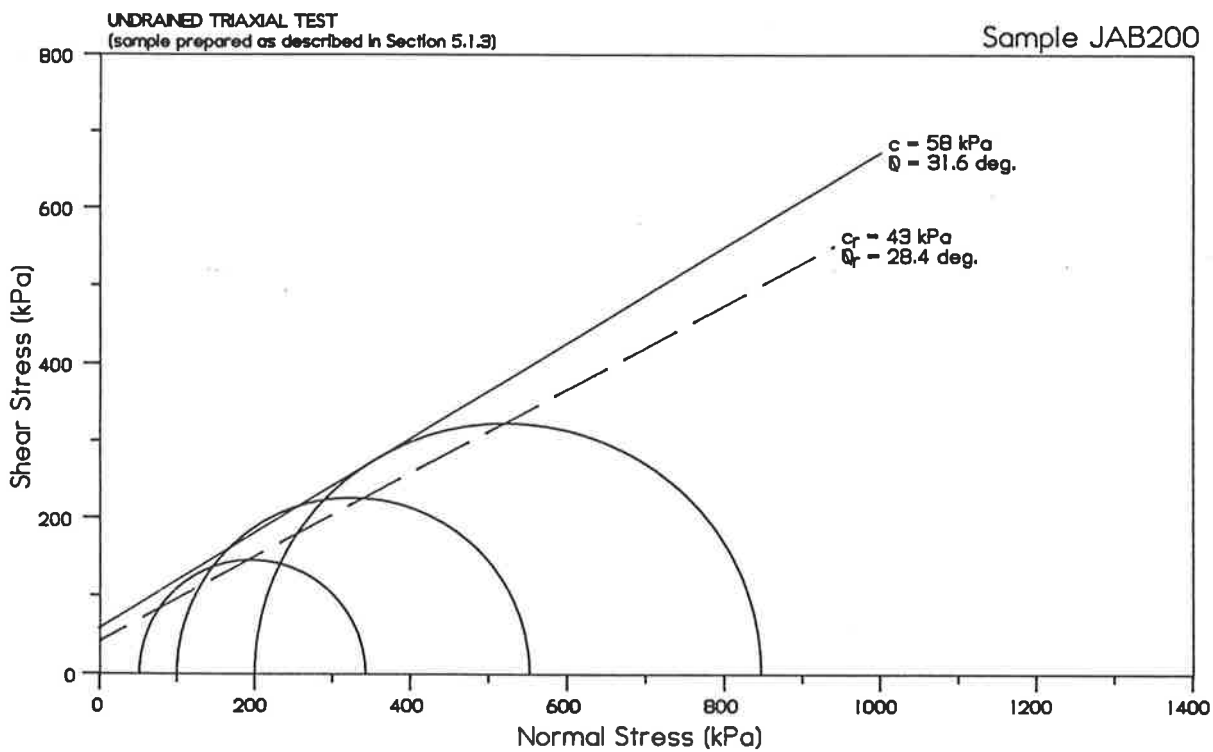
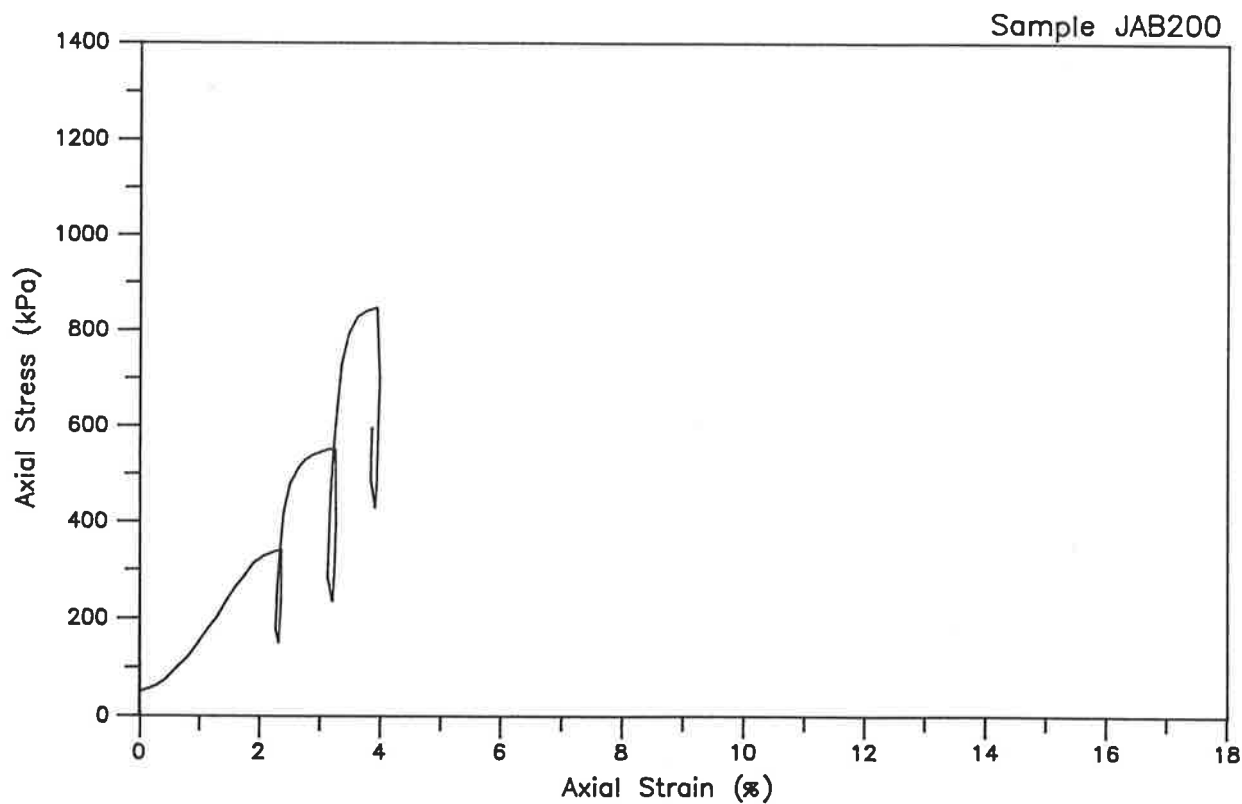
JAB202z

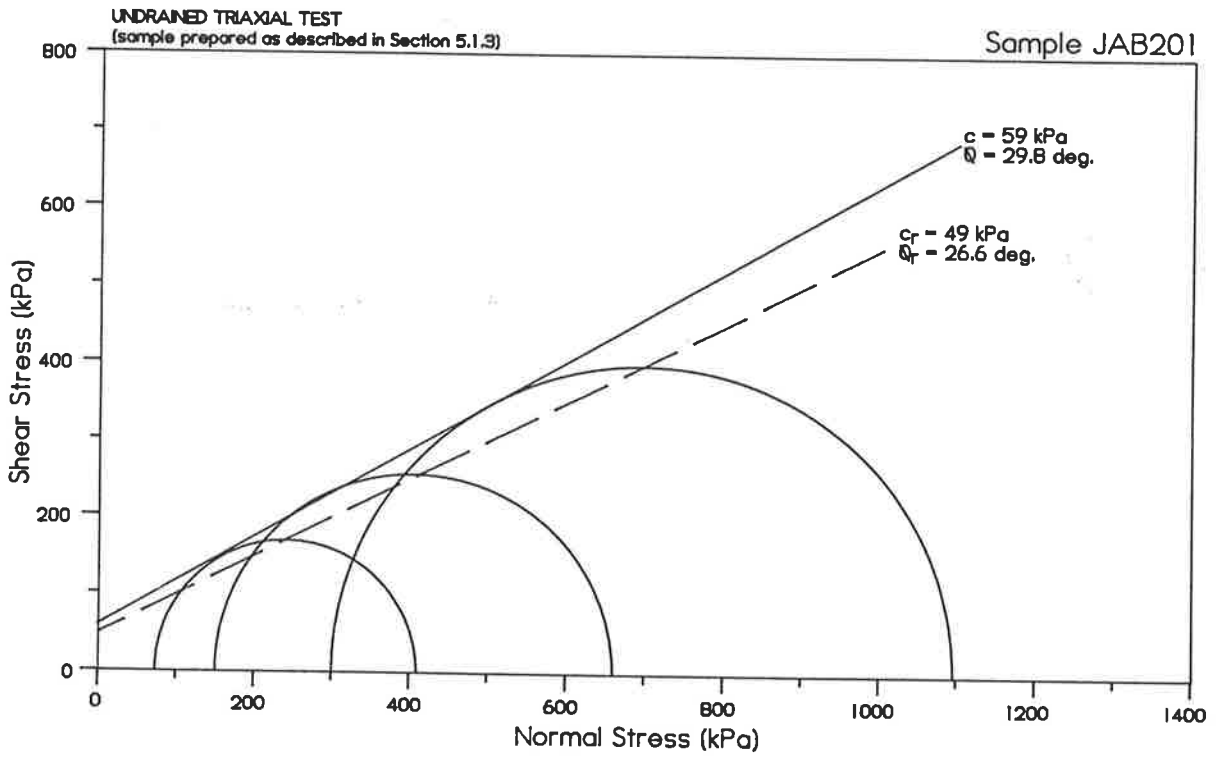
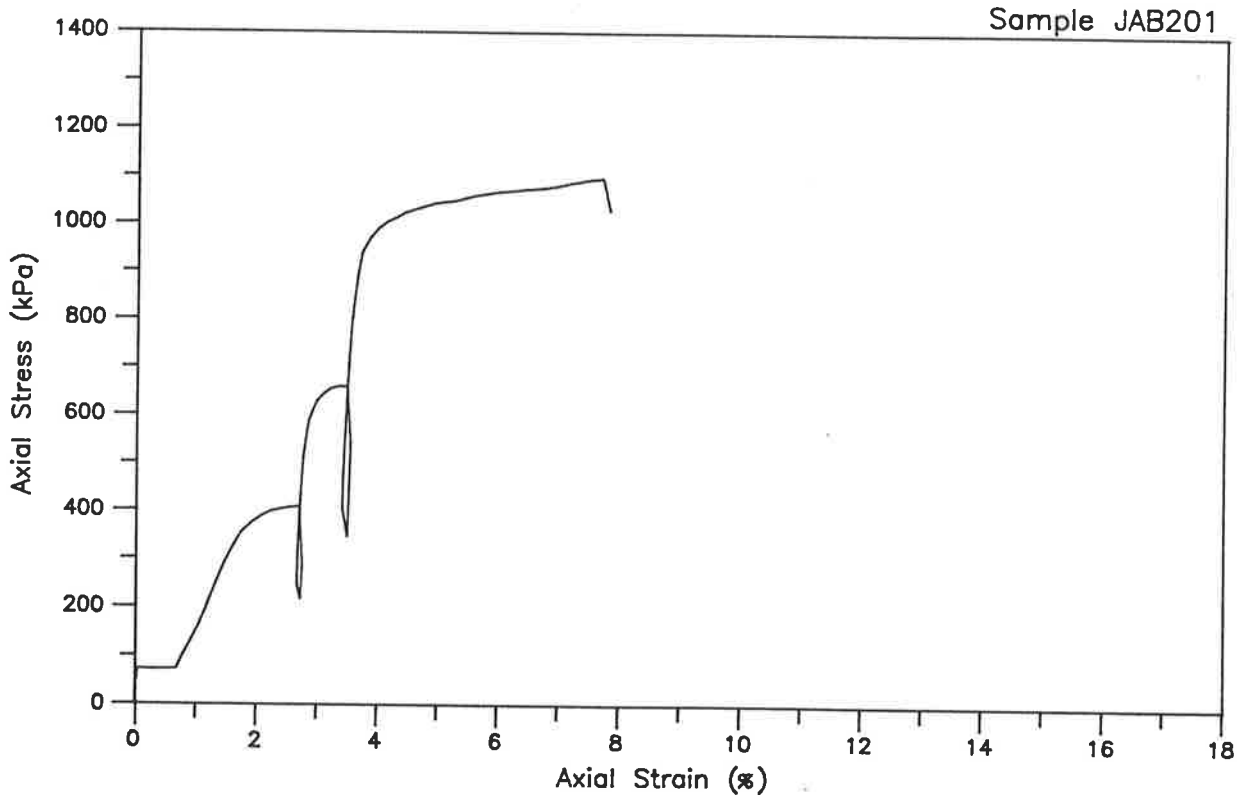


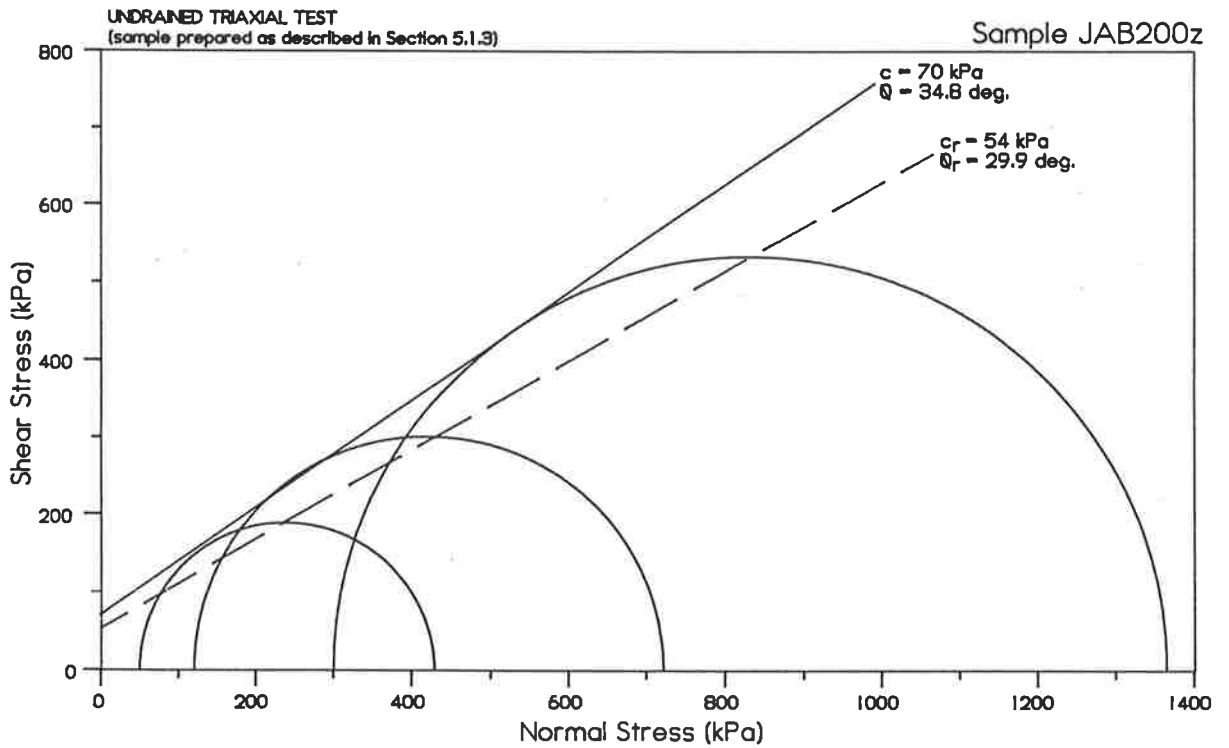
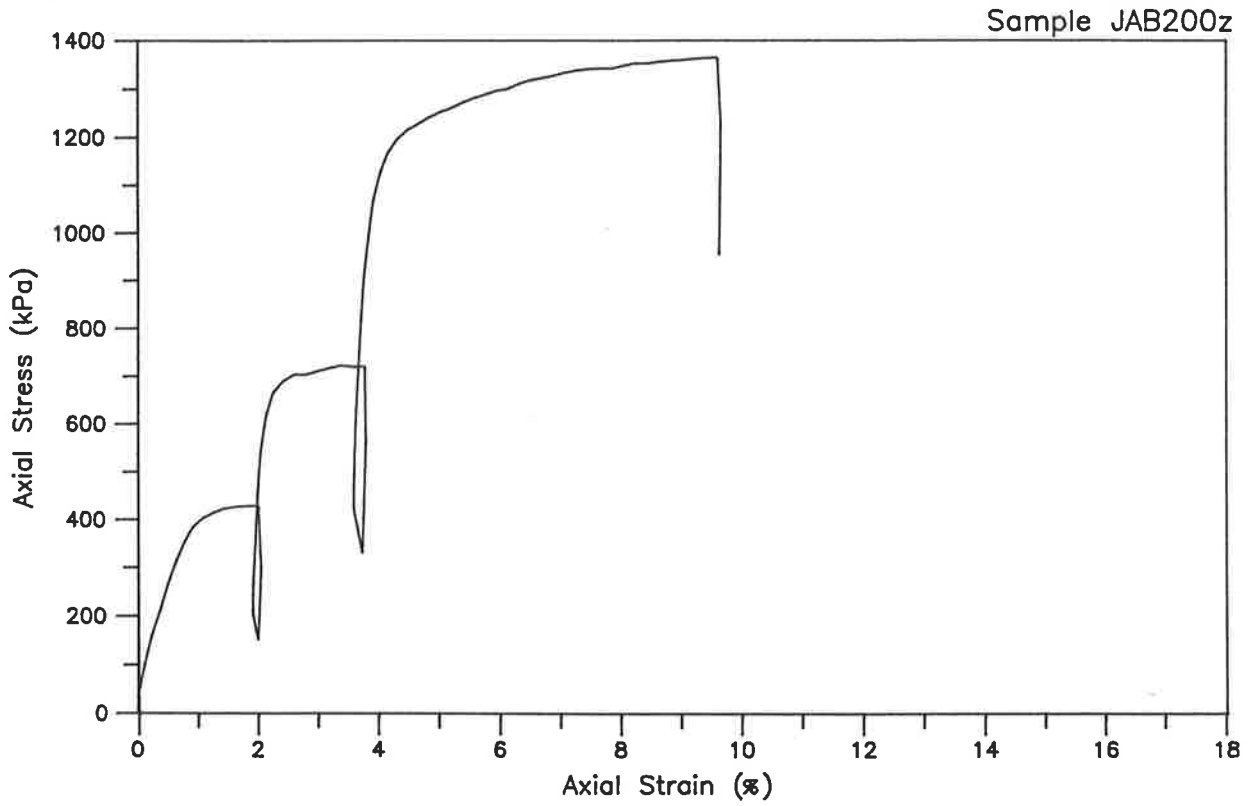


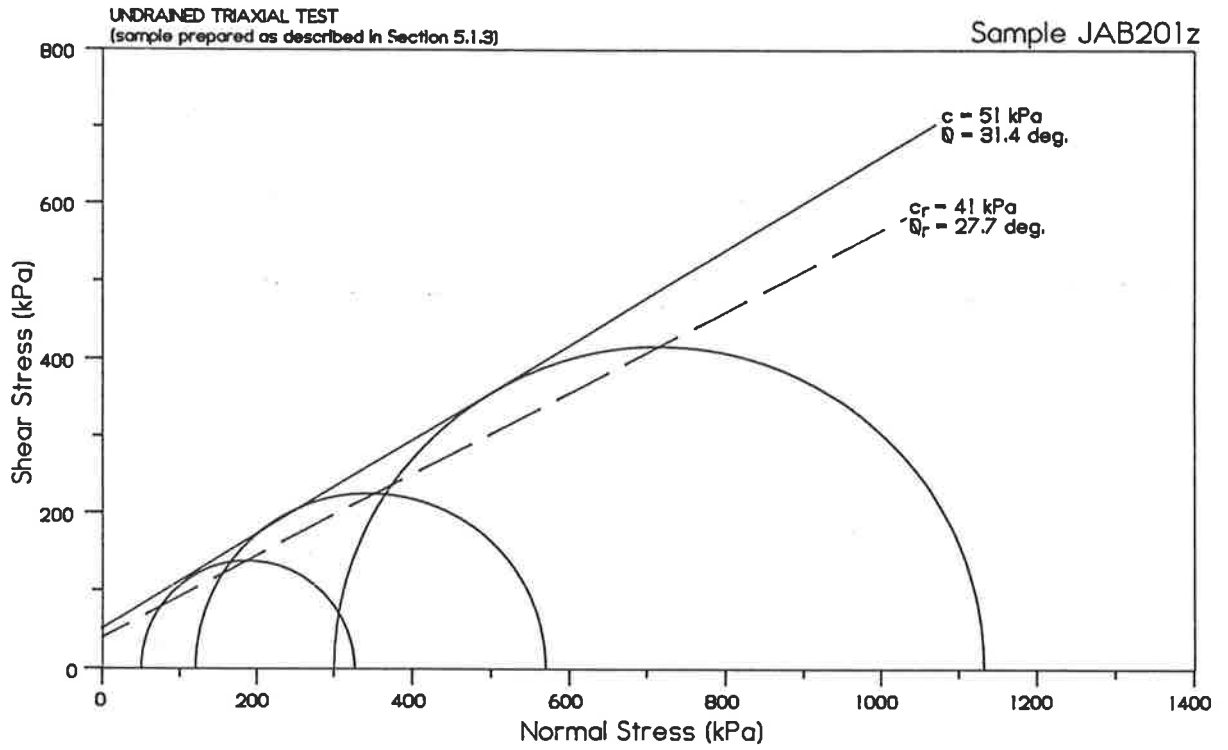
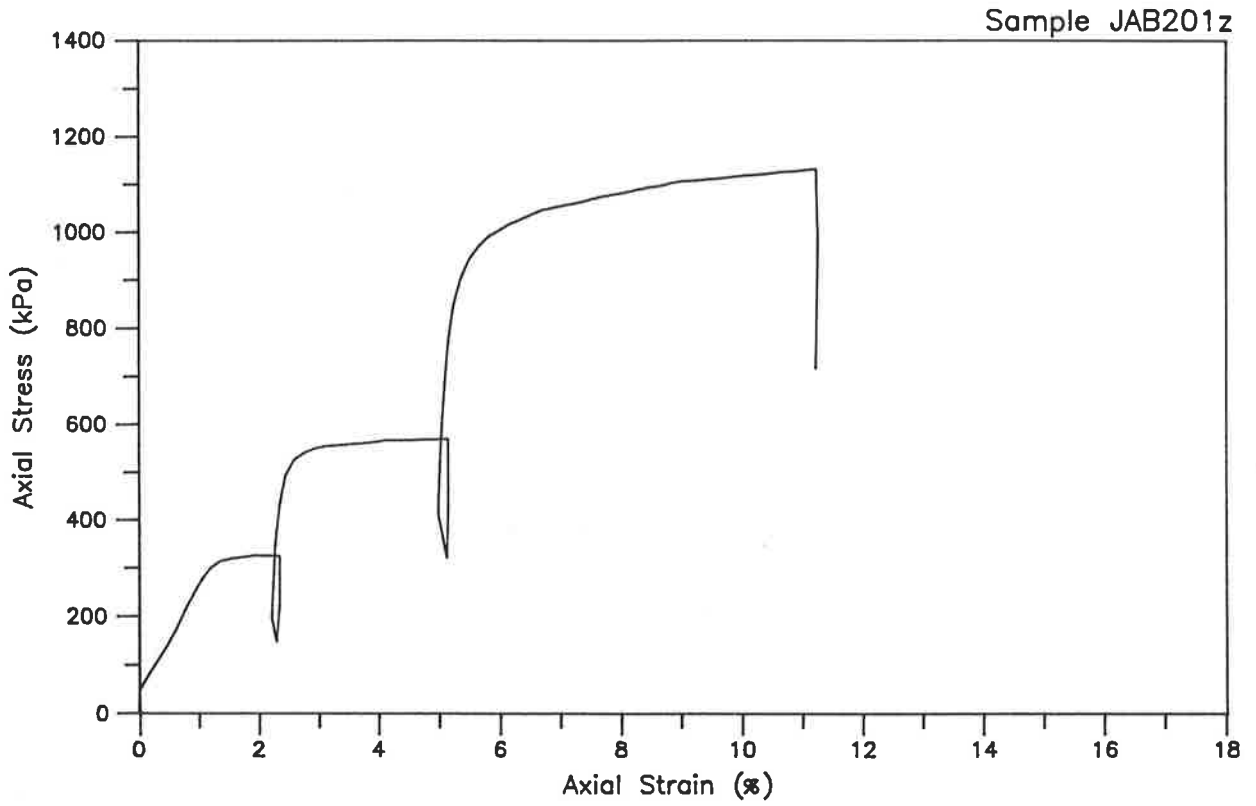








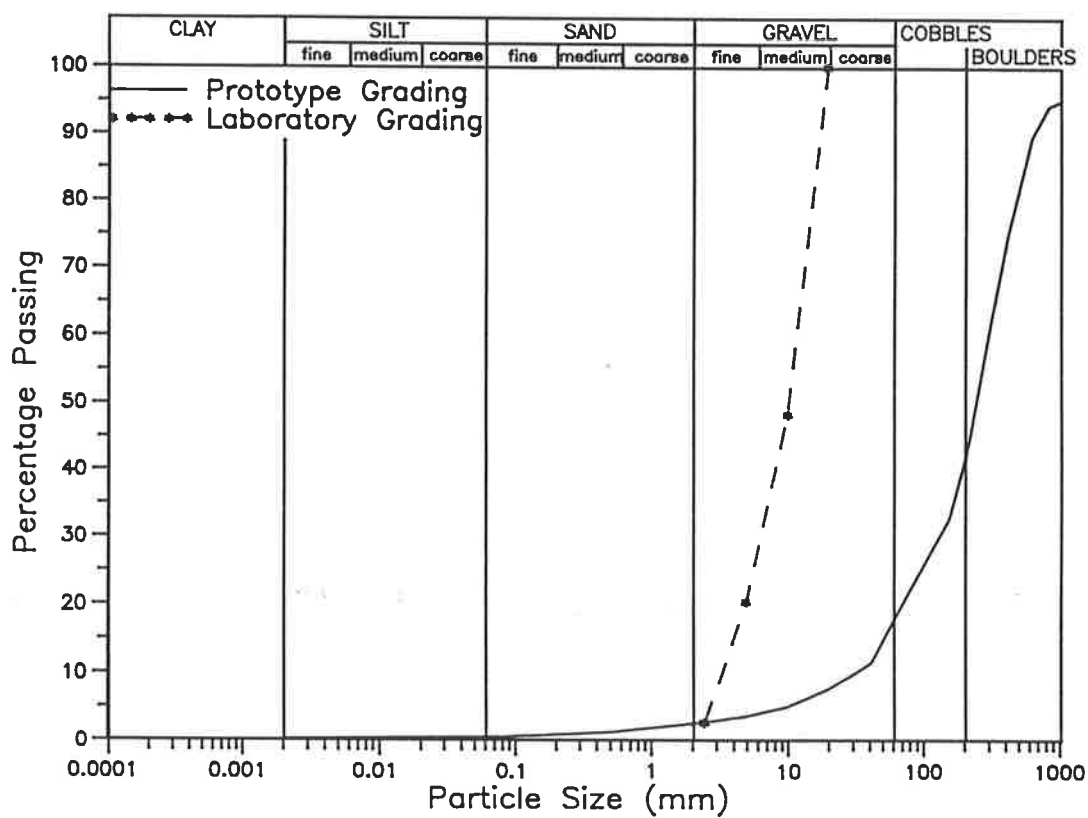


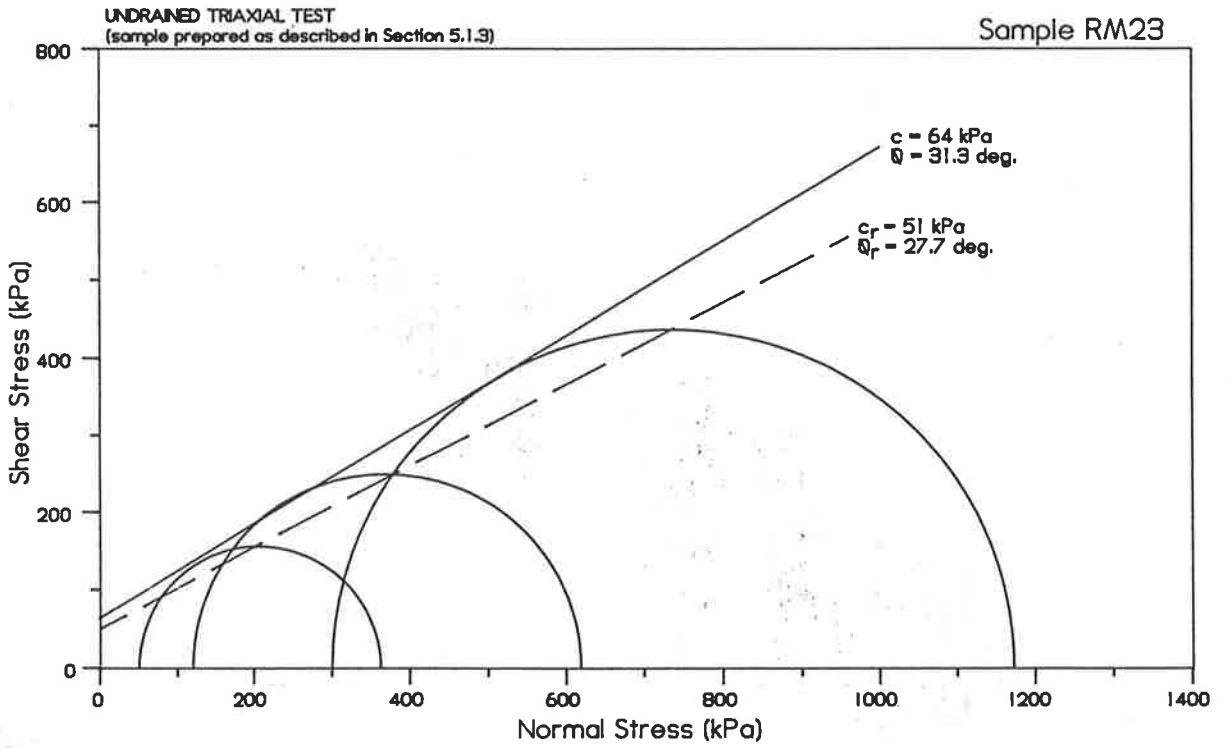
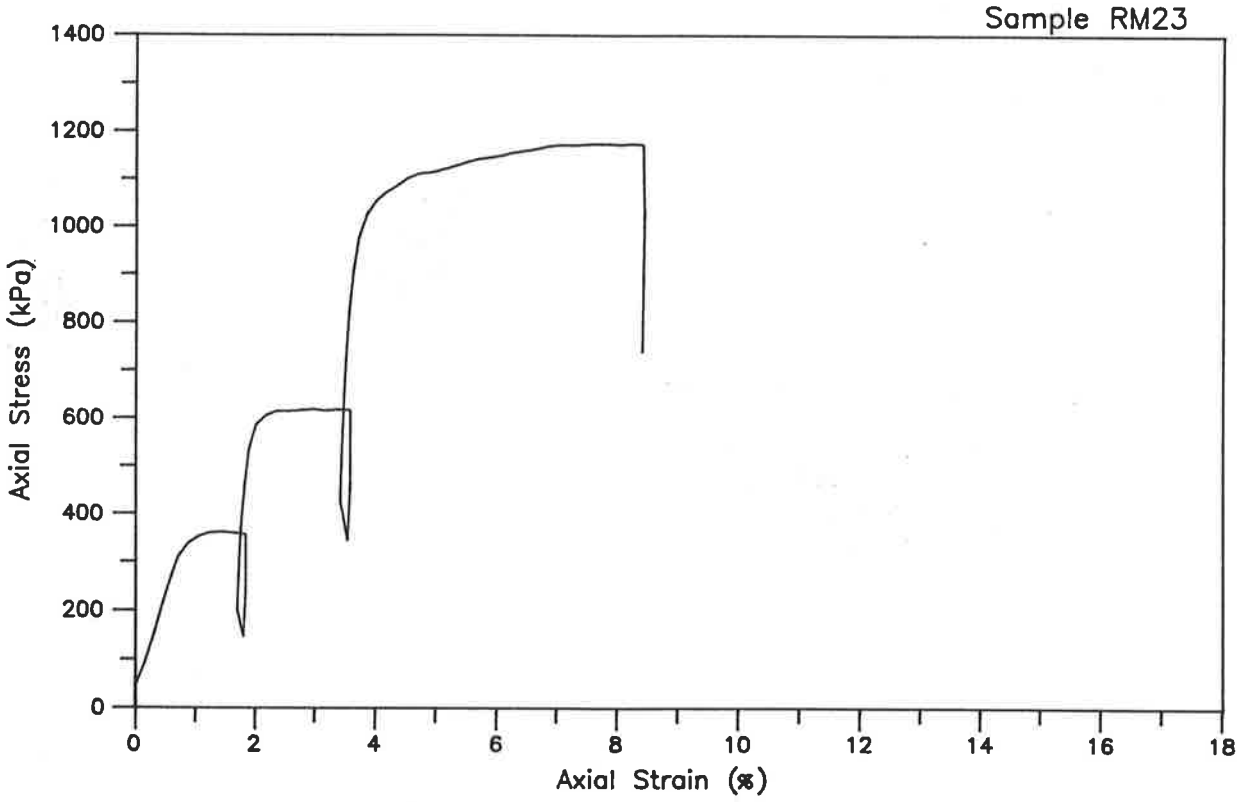


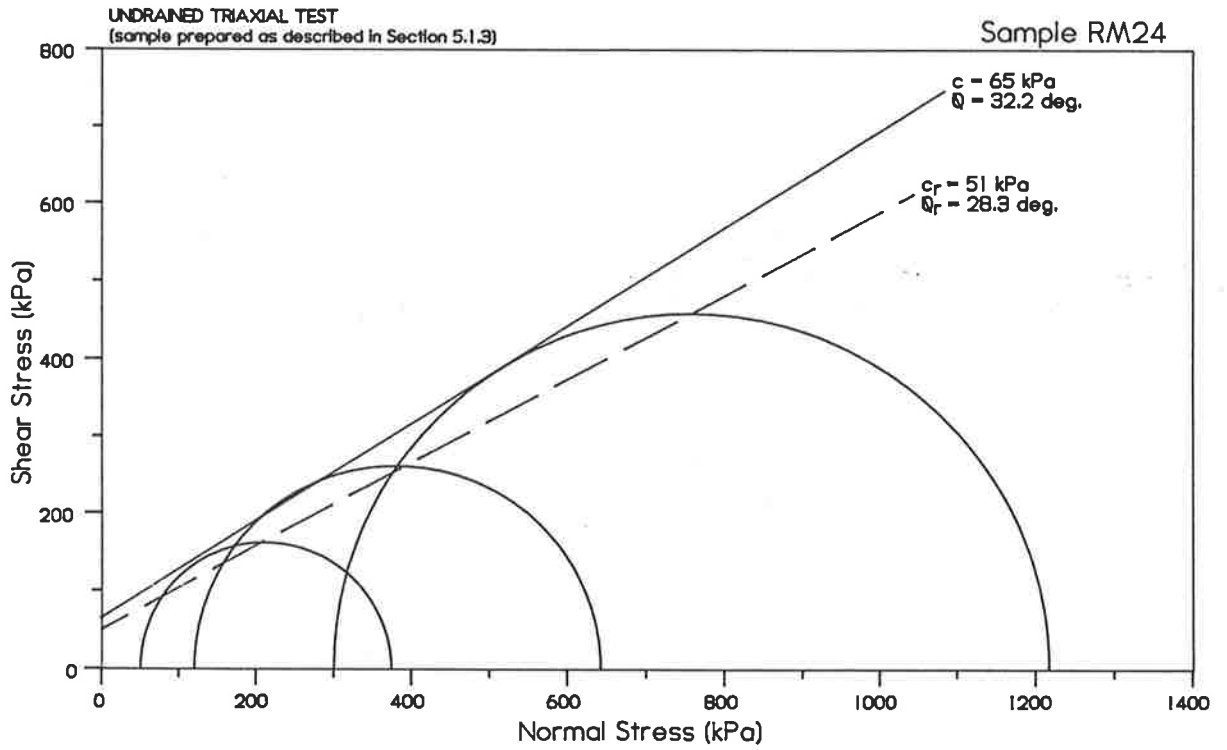
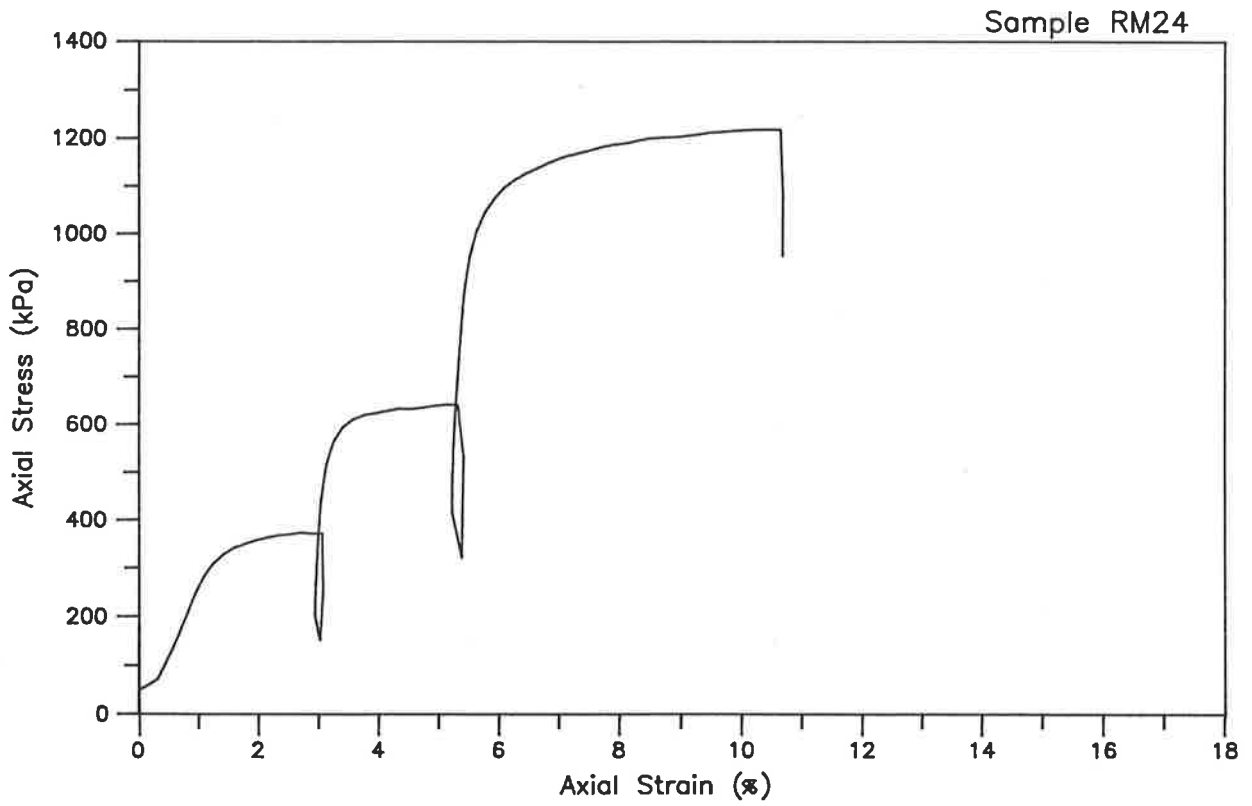
Sample: RM23 Date Tested: 28-7-91
 Description: Pegmatite (fresh)
 Test: Unsaturated Undrained Triaxial Compression

Prepared to: $mc = 2.4 \%$ After Test: $mc = 2.2 \%$
 $\rho_d = 1.89 \text{ t/m}^3$ $\rho_d = 1.96 \text{ t/m}^3$

Comments:



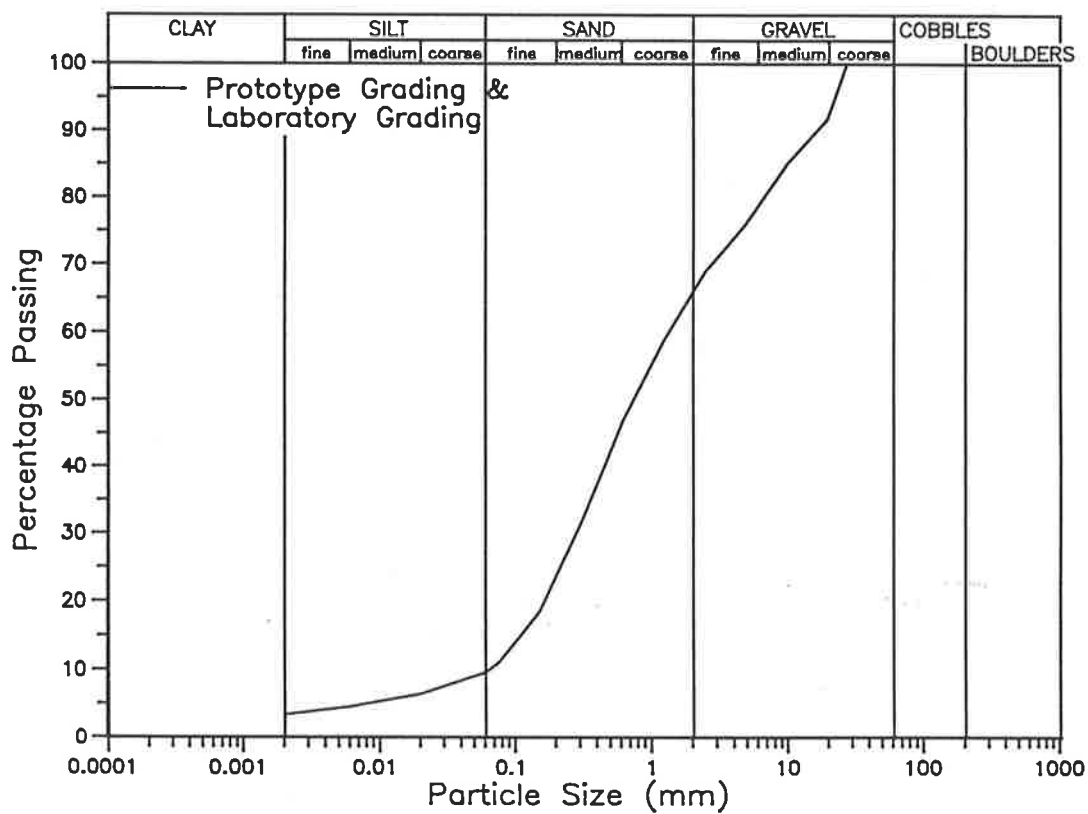


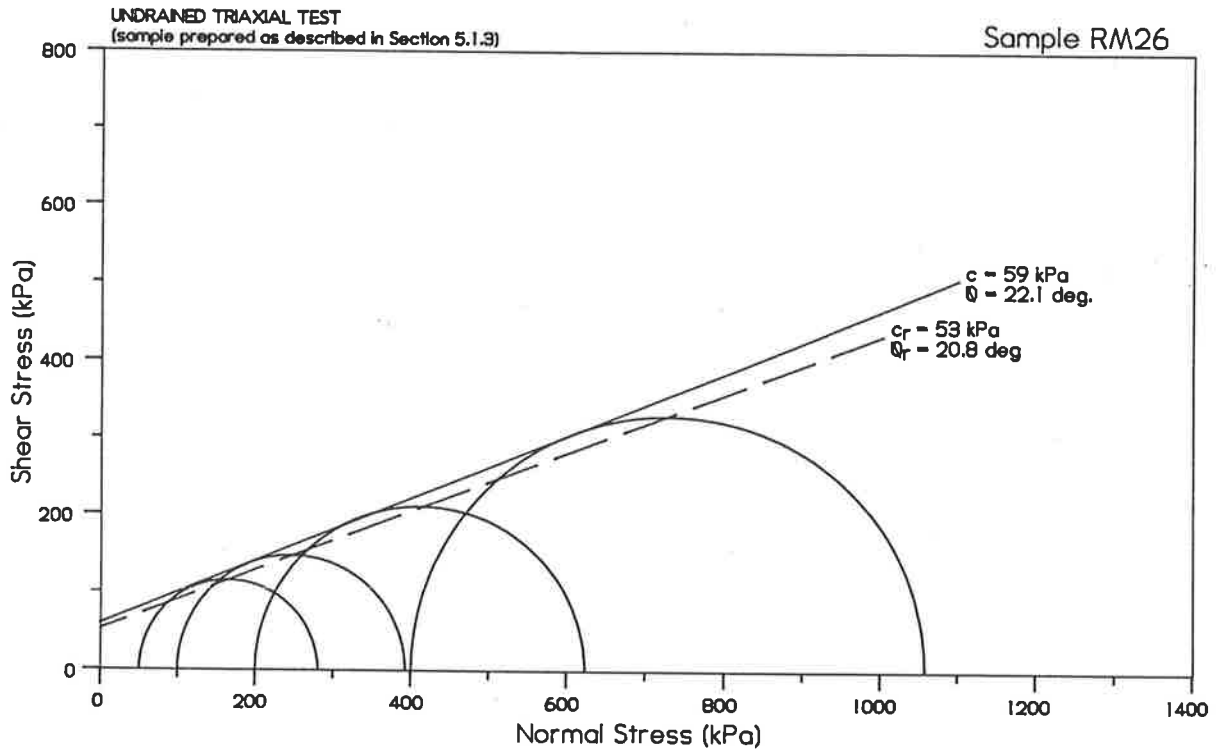
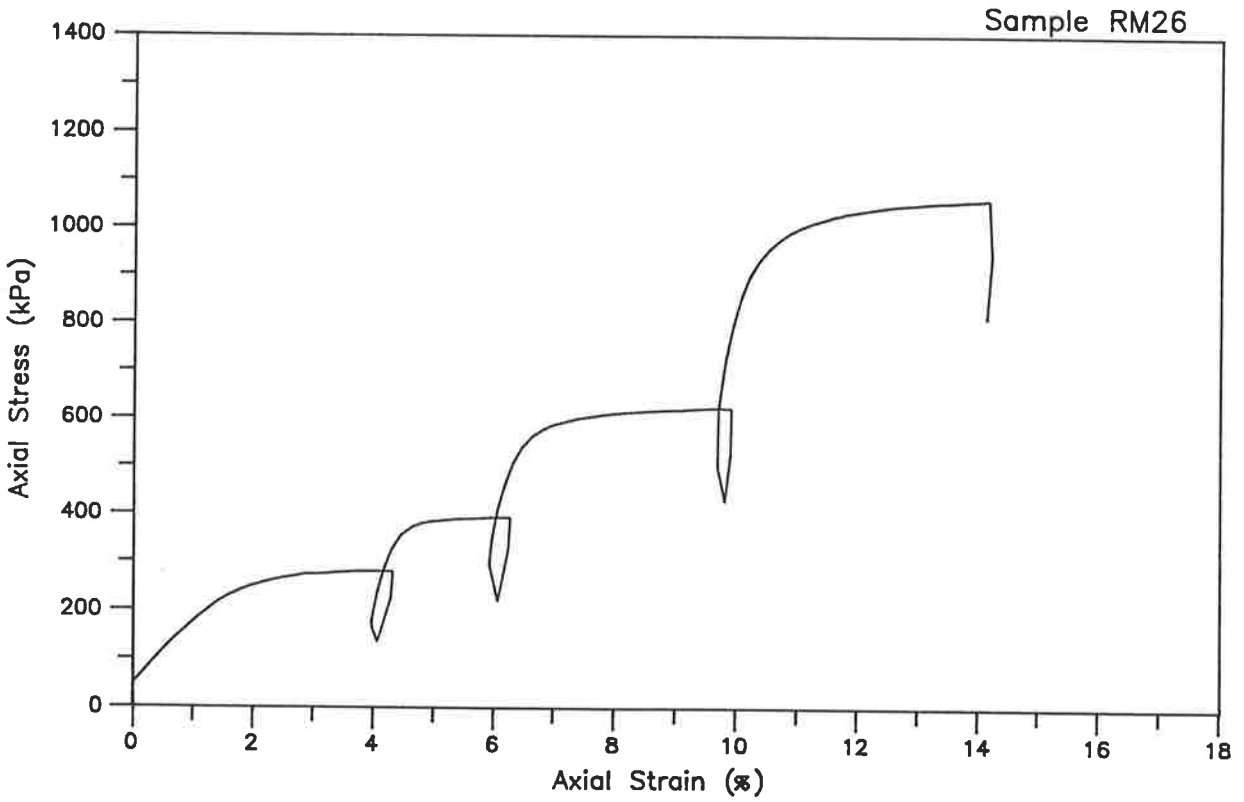


Sample: RM26 Date Tested: 5-7-91
 Description: Extremely weathered Schist
 Test: Unsaturated Undrained Triaxial Compression

Prepared to: $mc = 12.2 \%$ After Test: $mc = 11.9 \%$
 $\rho_d = 1.94 \text{ t/m}^3$ $\rho_d = 1.98 \text{ t/m}^3$

Comments:

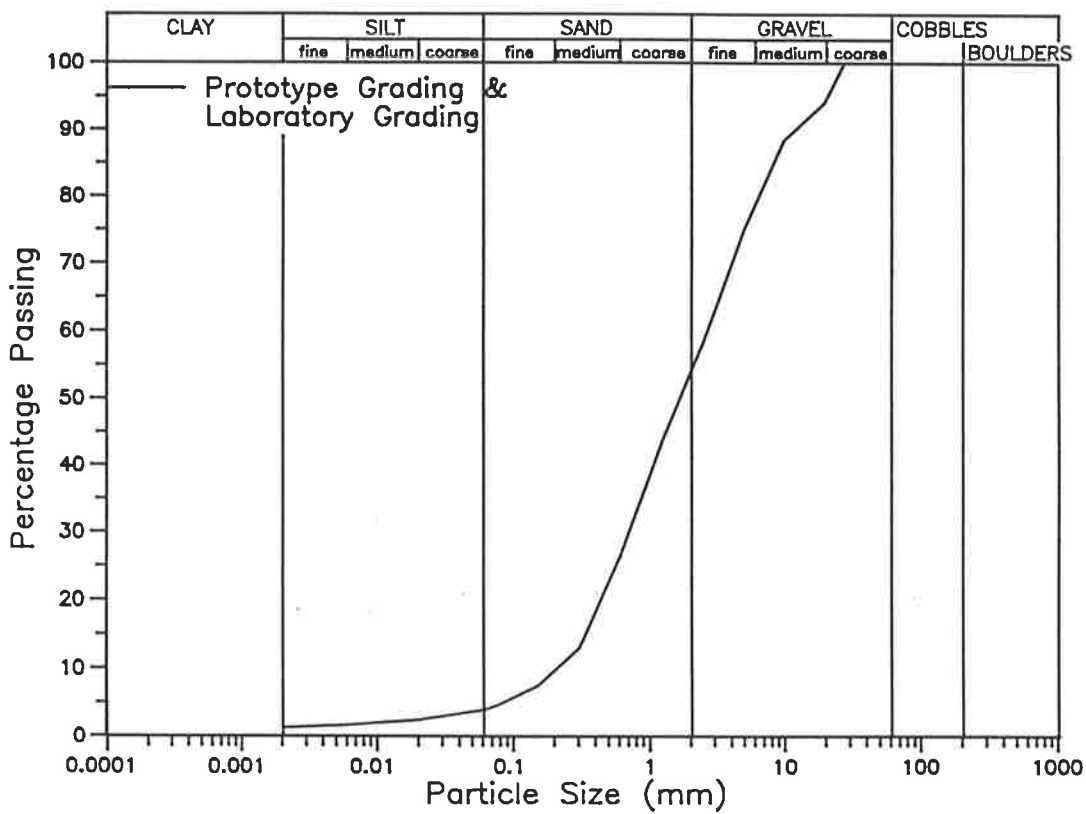


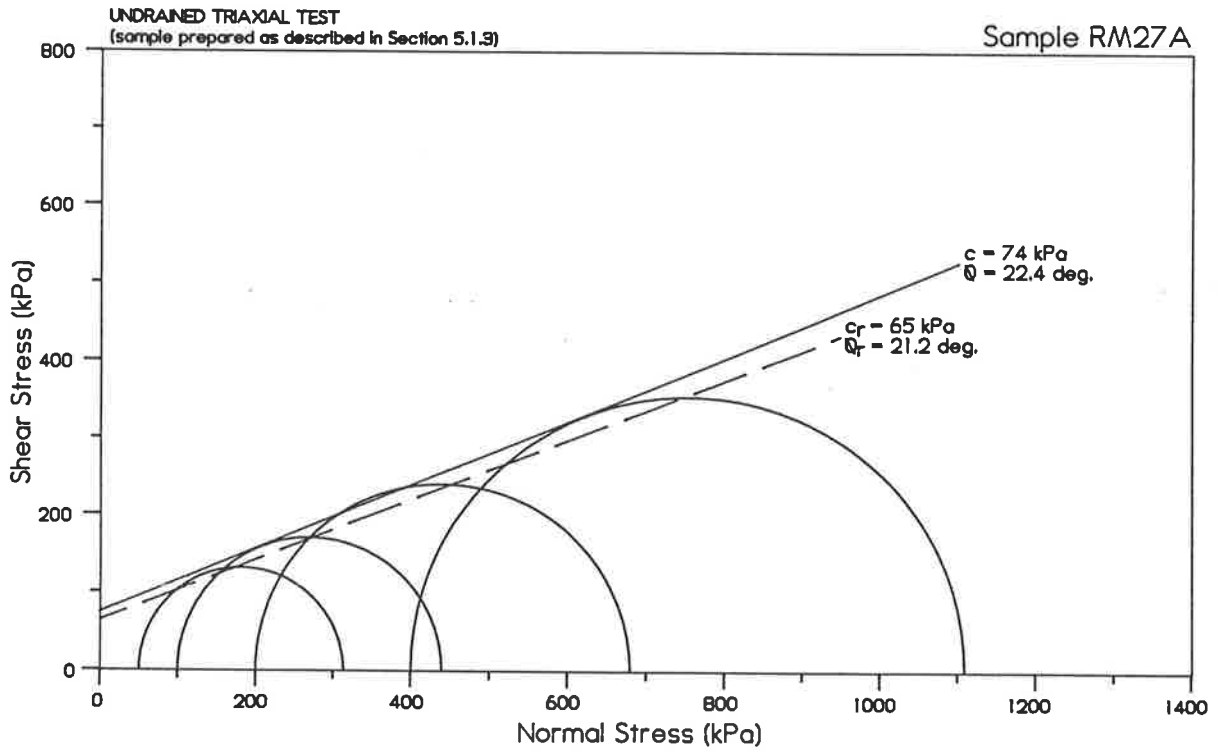
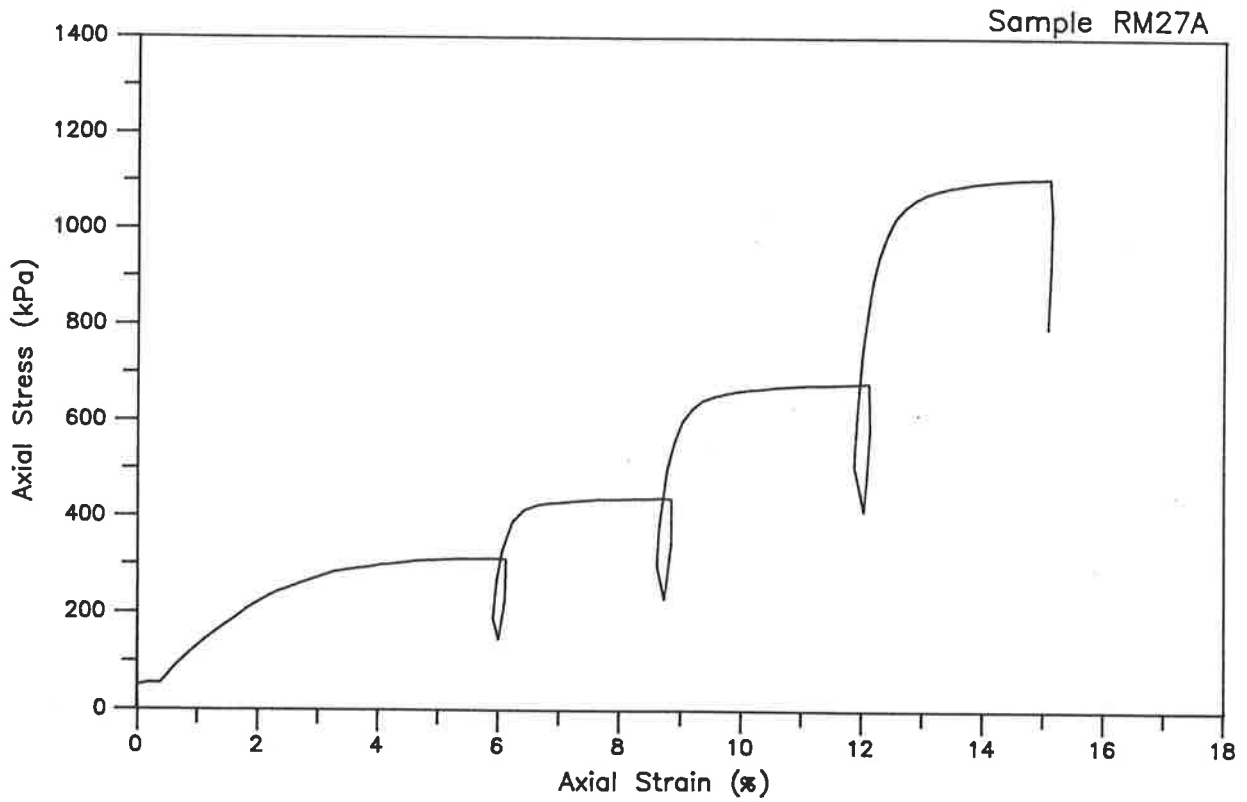


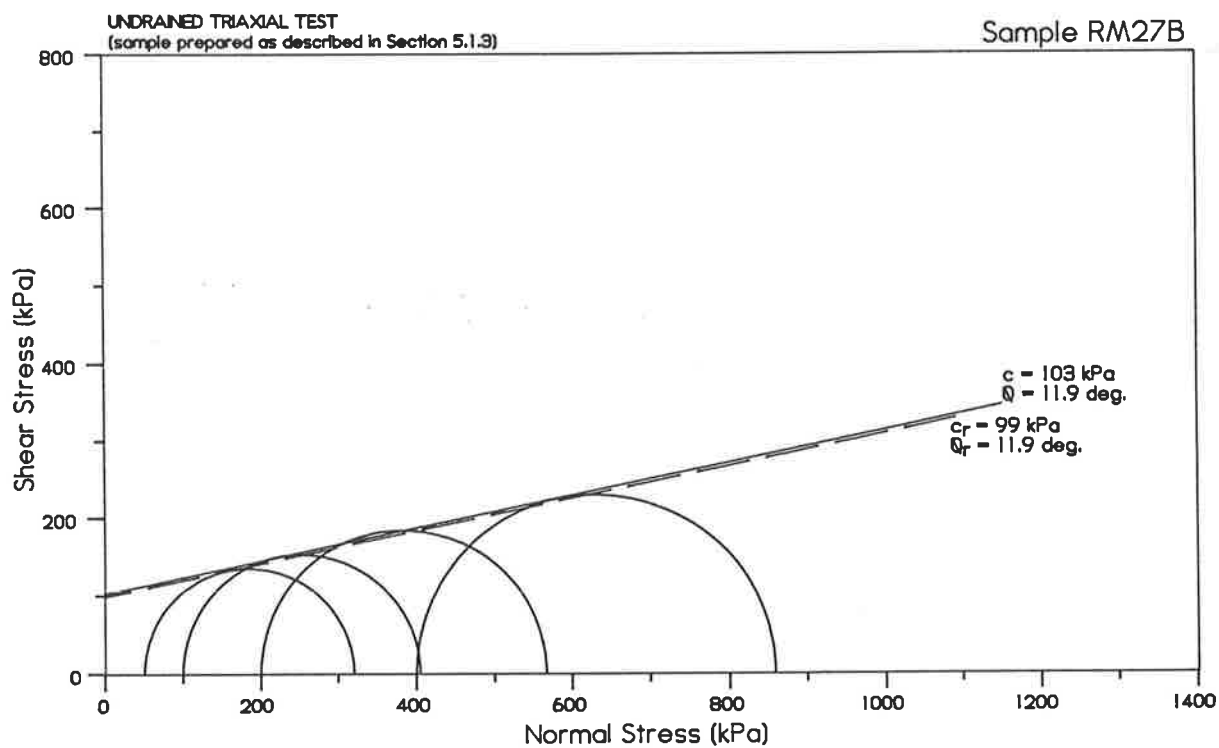
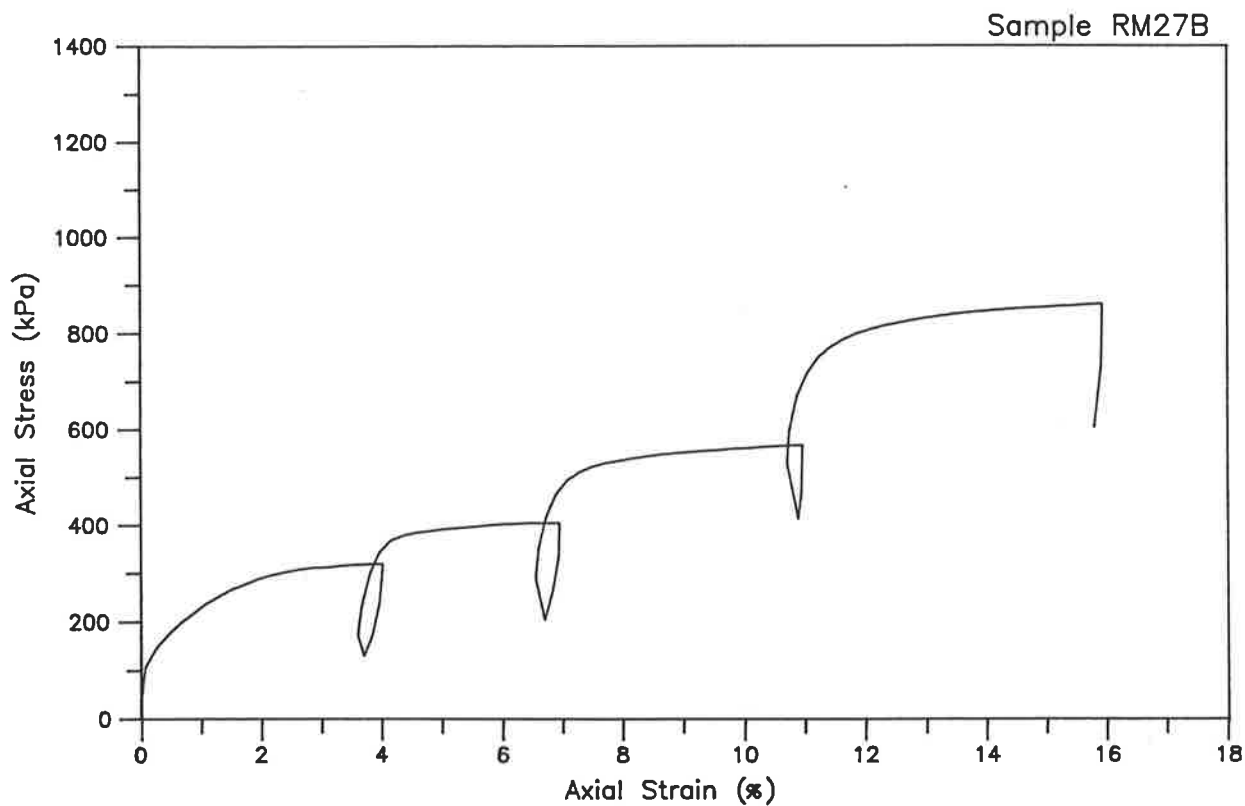
Sample: RM27A Date Tested: 9-7-91
 Description: Extremely weathered Pegmatite
 Test: Unsaturated Undrained Triaxial Compression

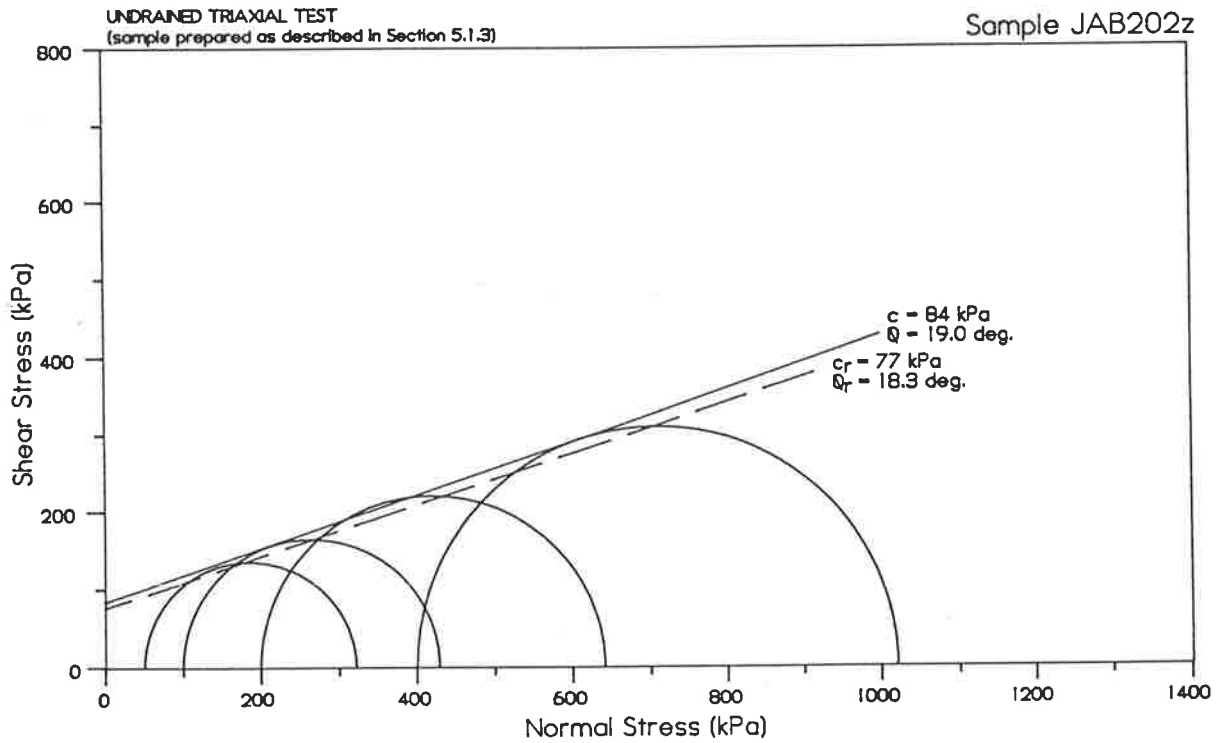
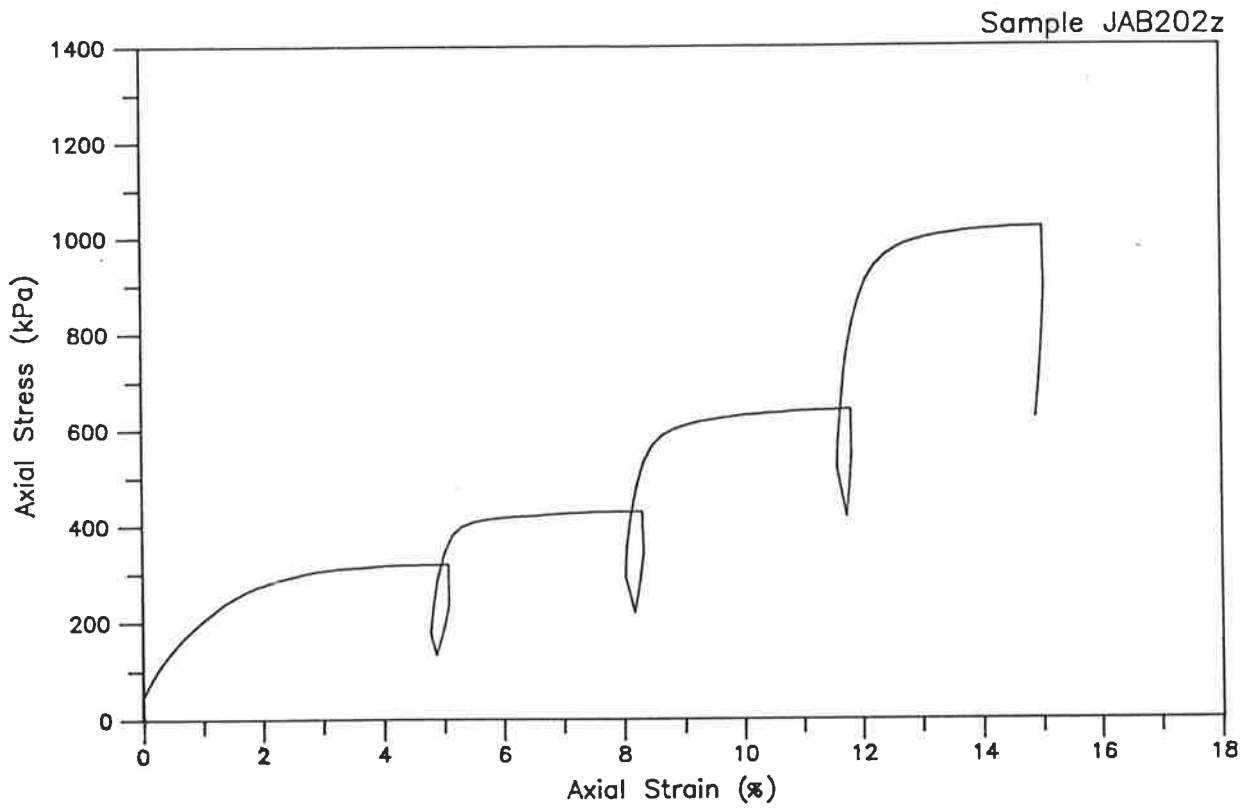
Prepared to: $mc = 10.8 \%$ After Test: $mc = 10.1 \%$
 $\rho_d = 2.02 \text{ t/m}^3$ $\rho_d = 2.13 \text{ t/m}^3$

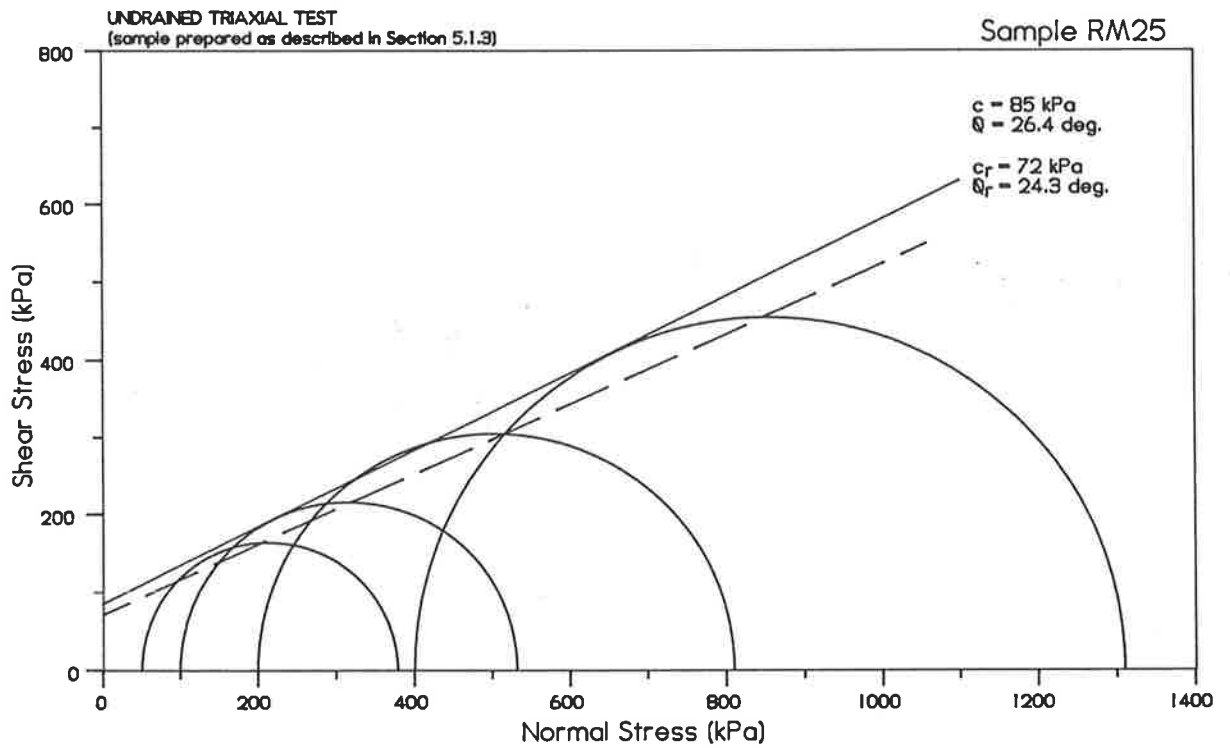
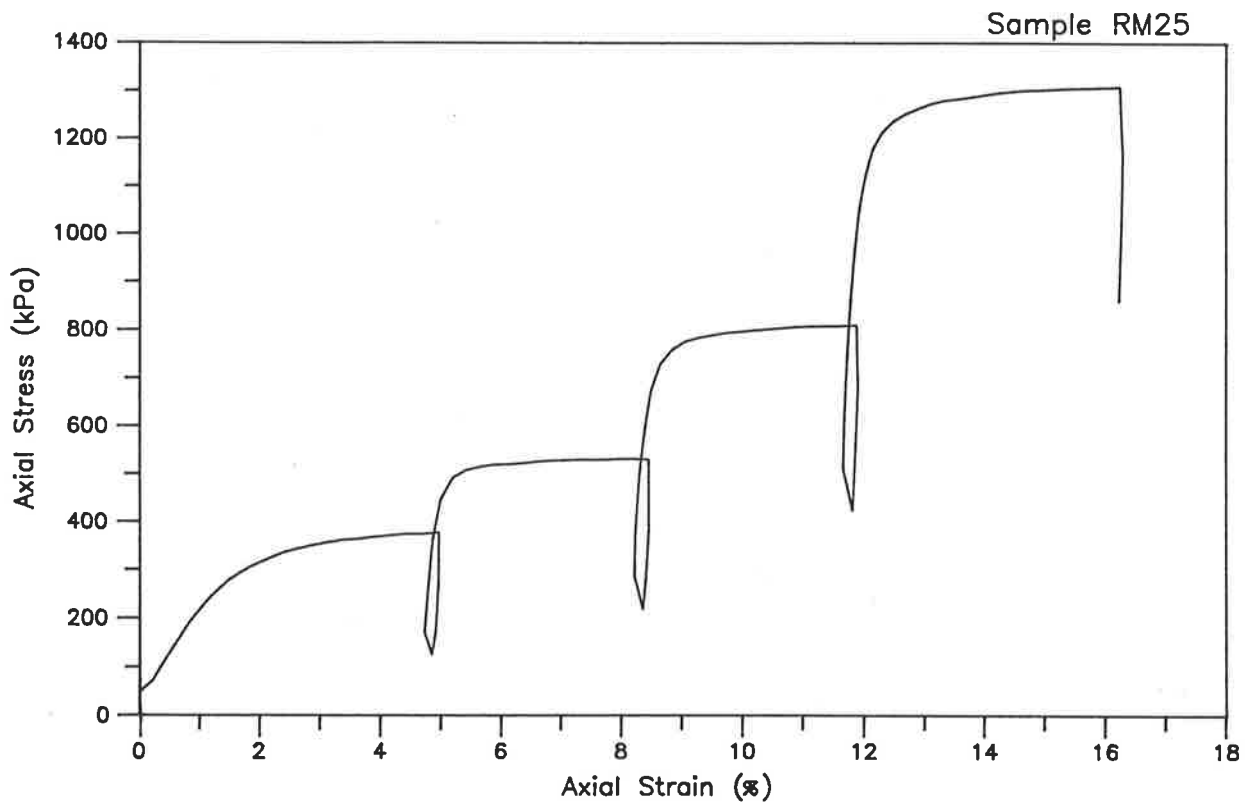
Comments:

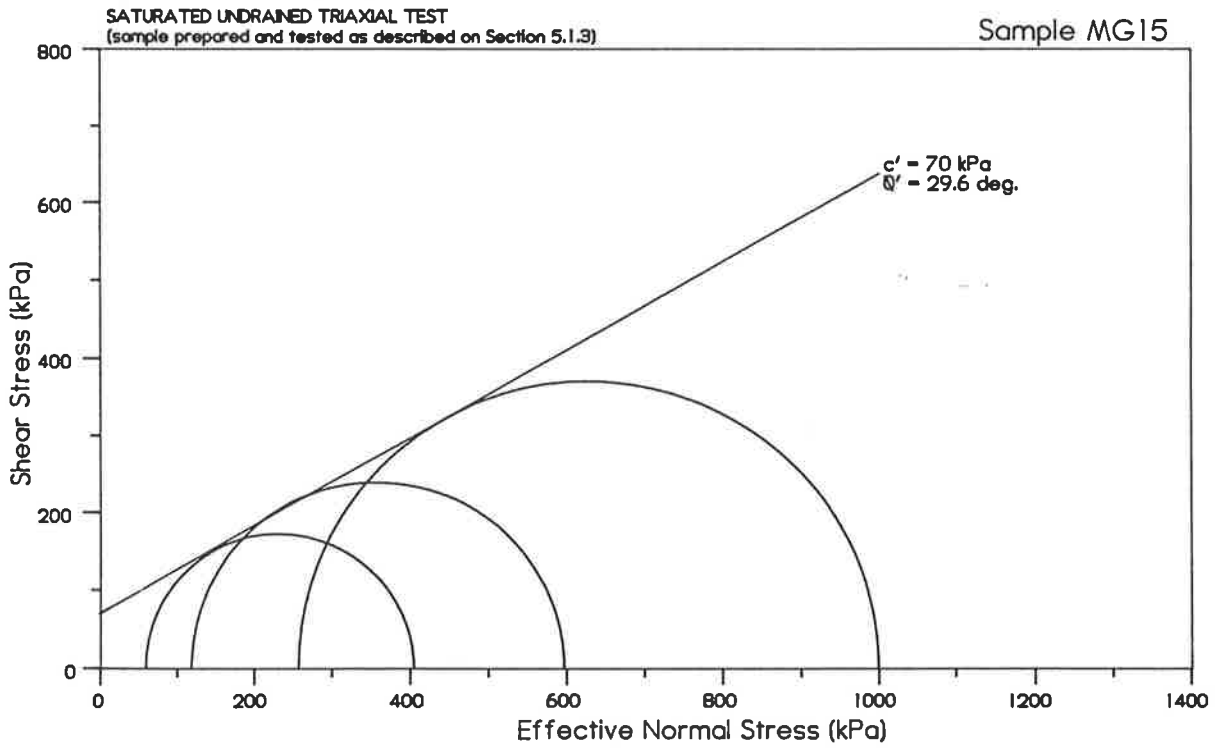
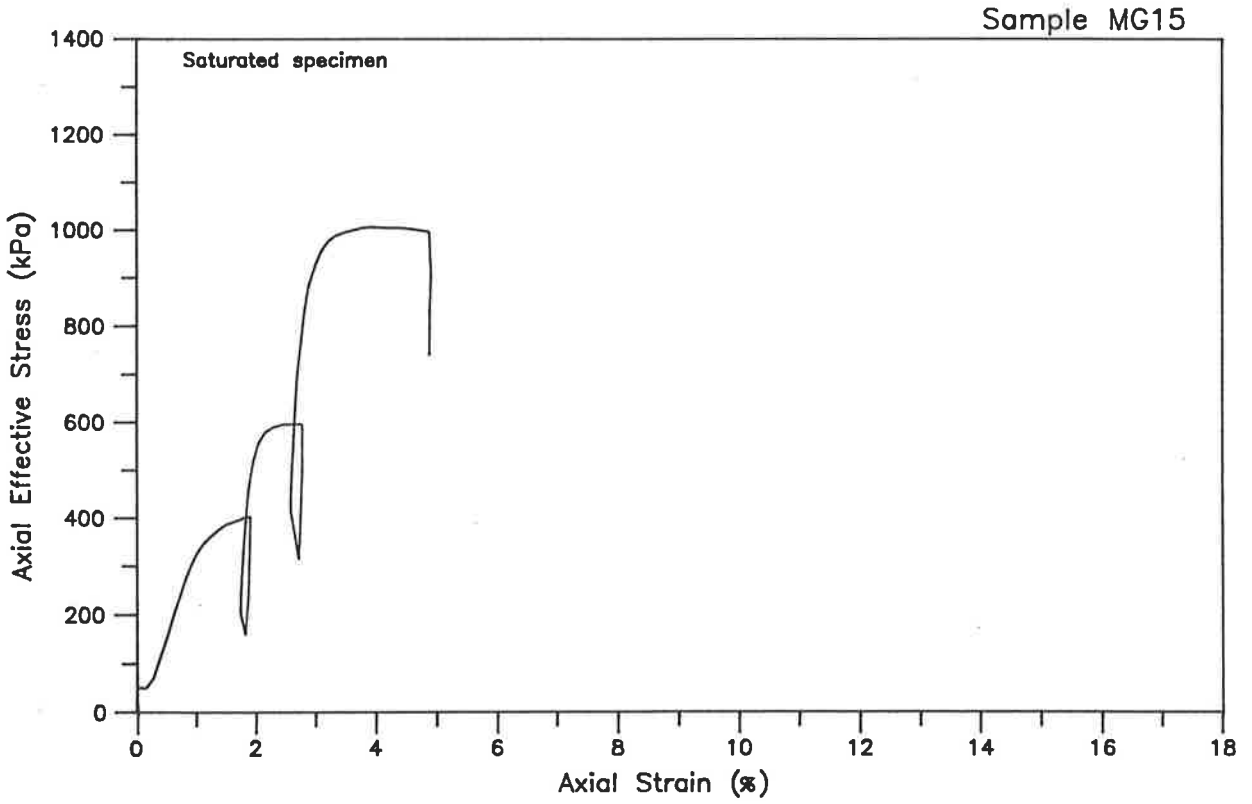


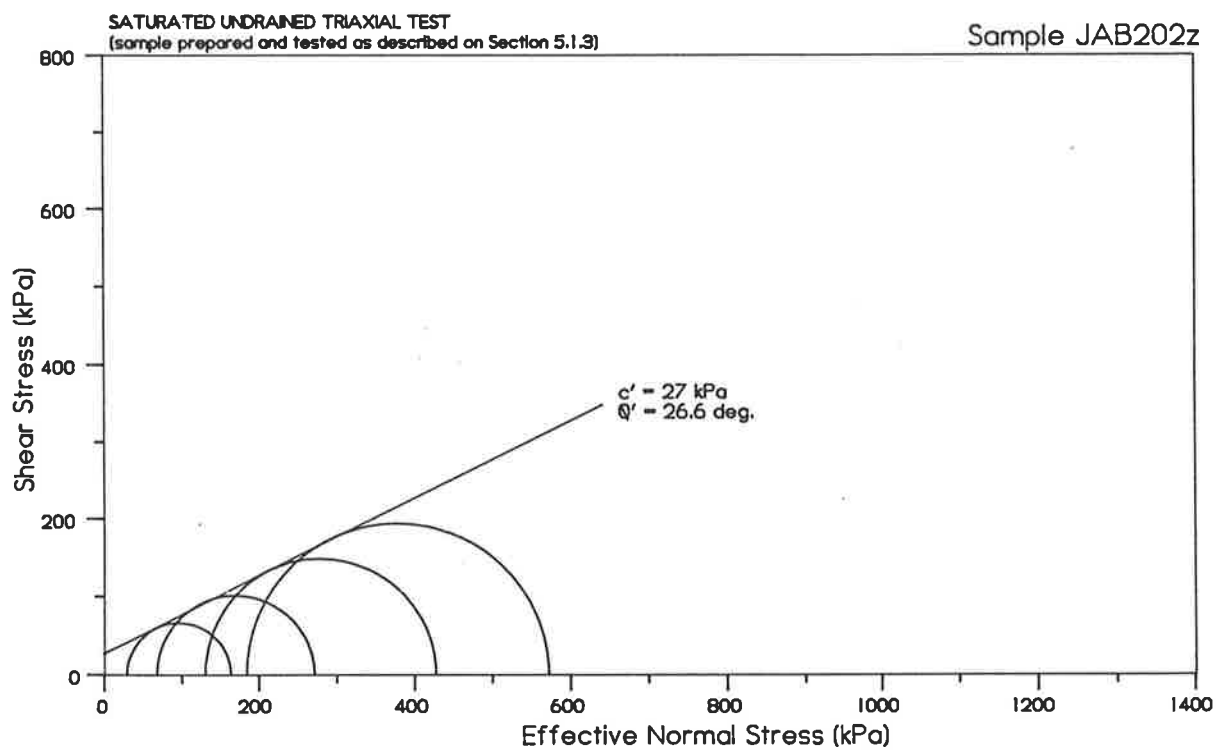
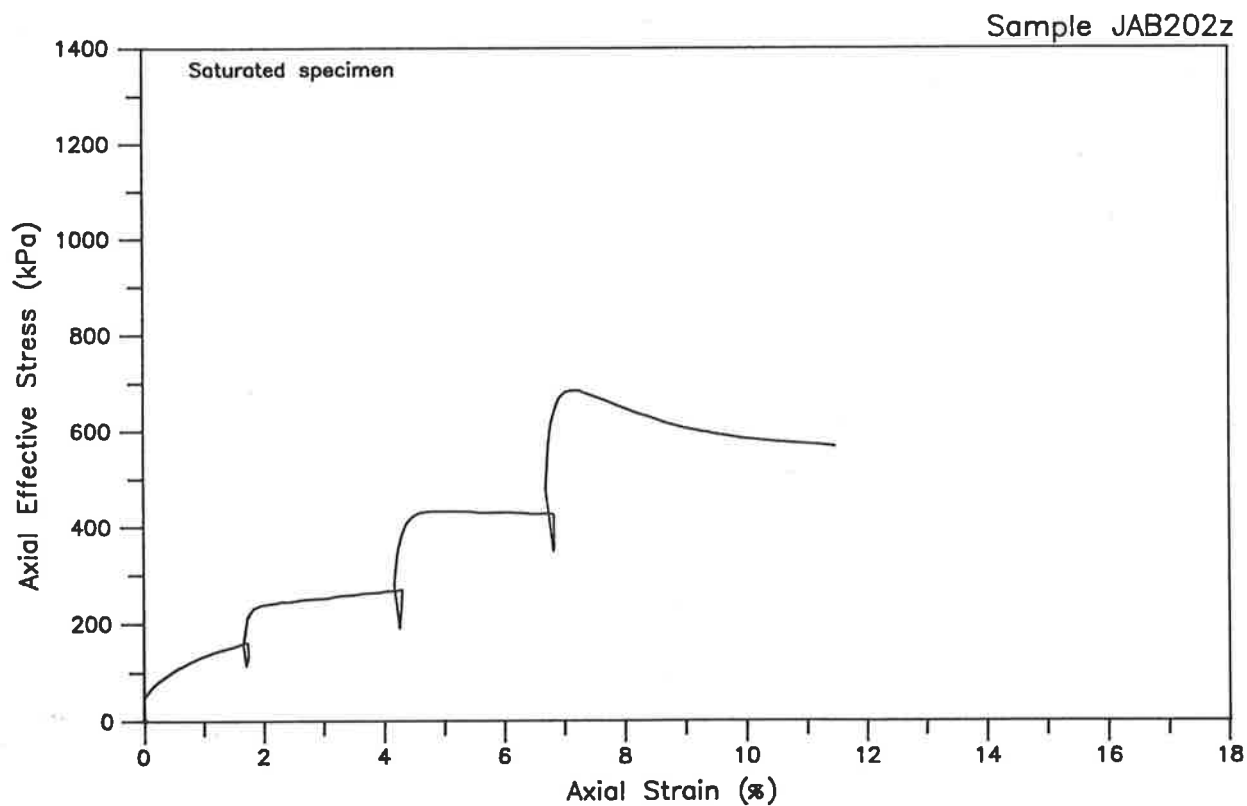




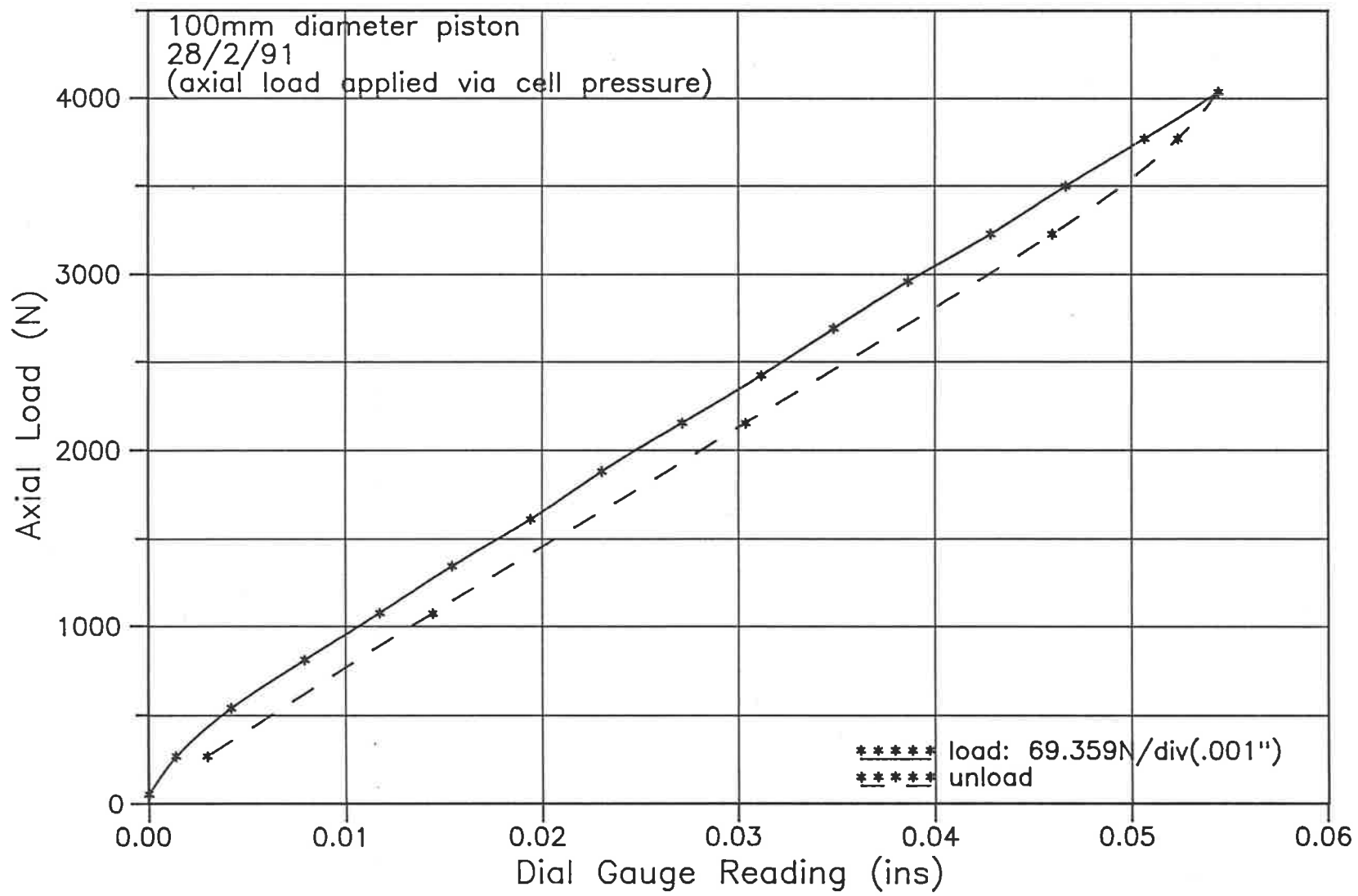




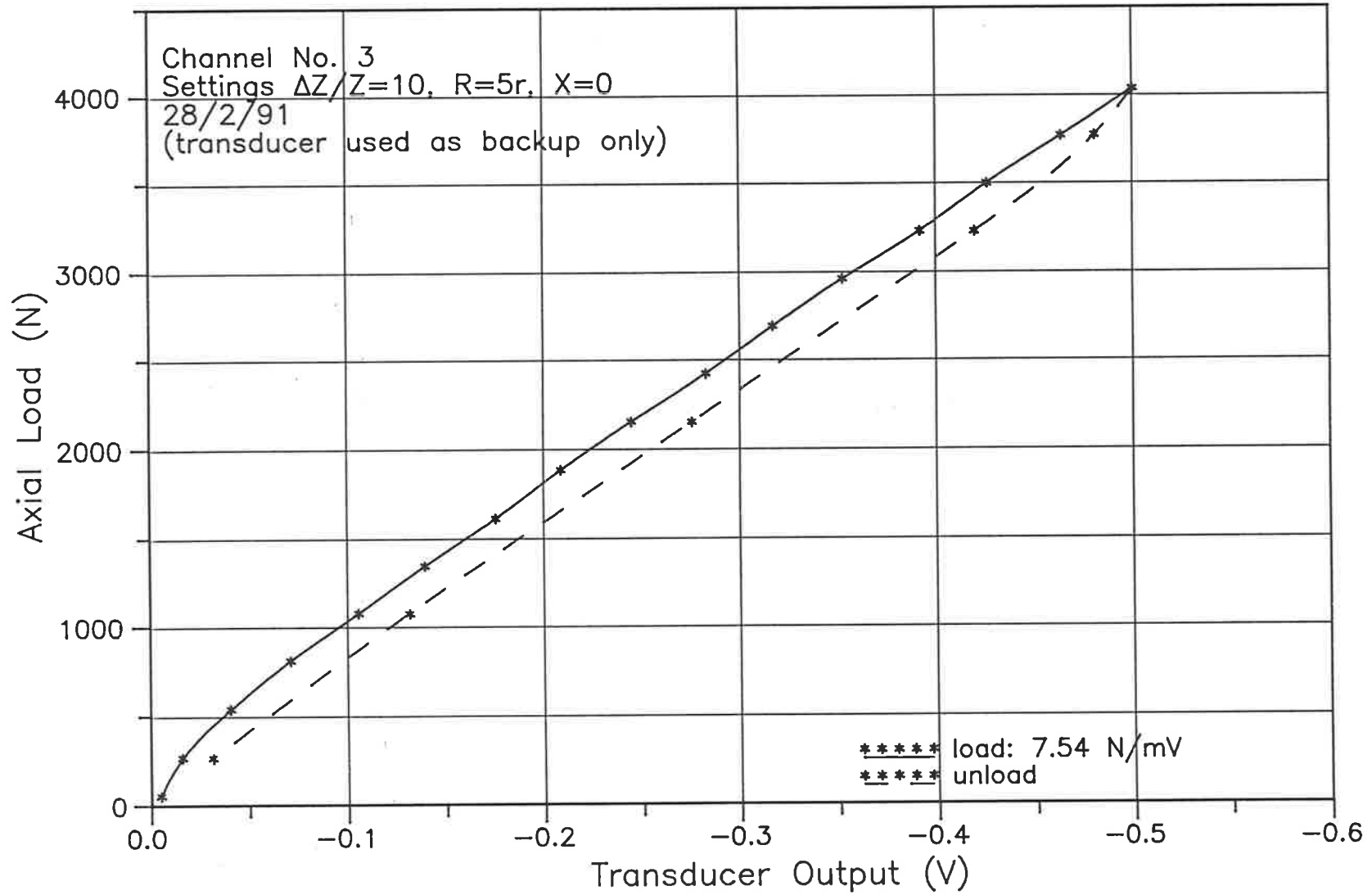




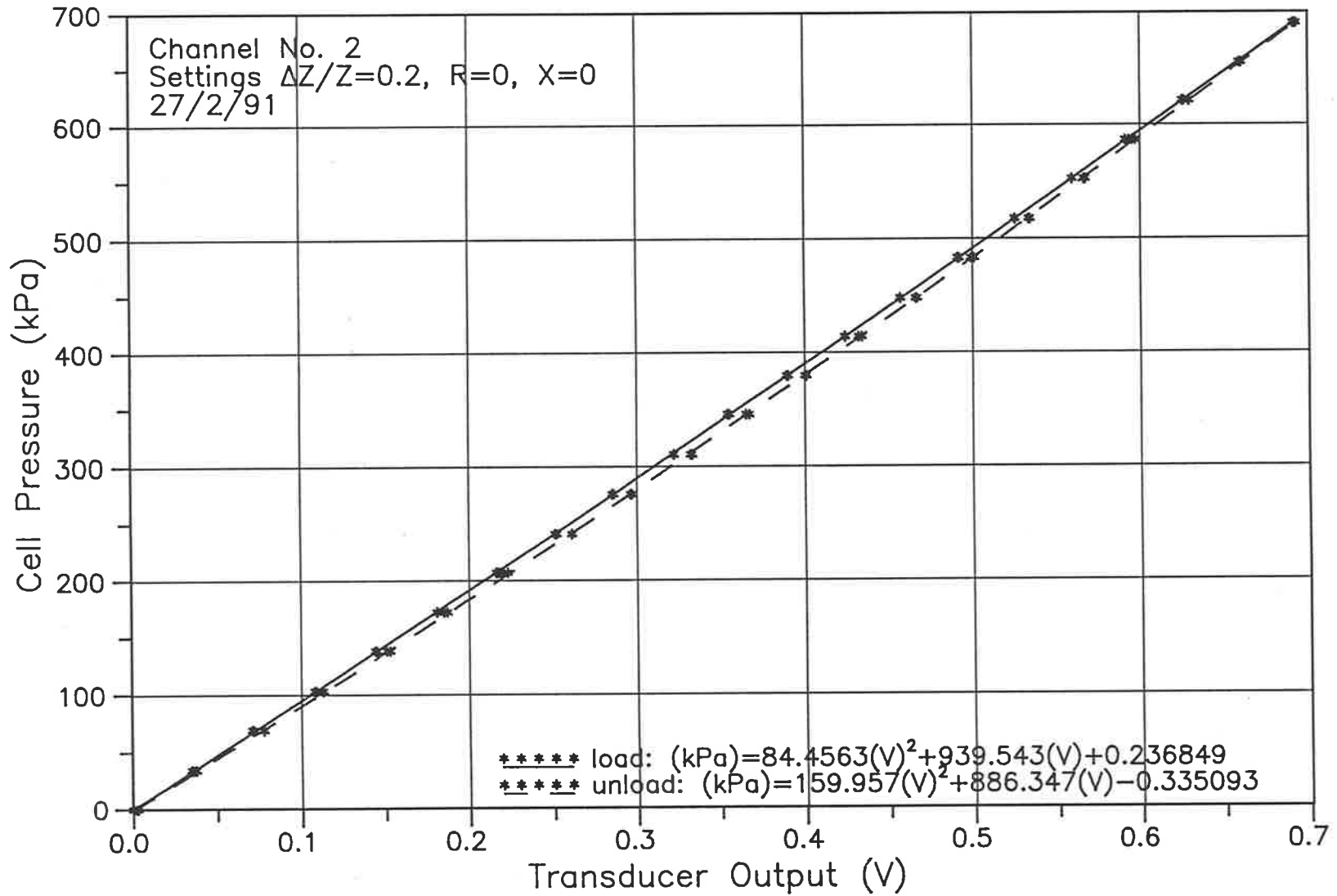
Axial Load Calibration – Dial Gauge



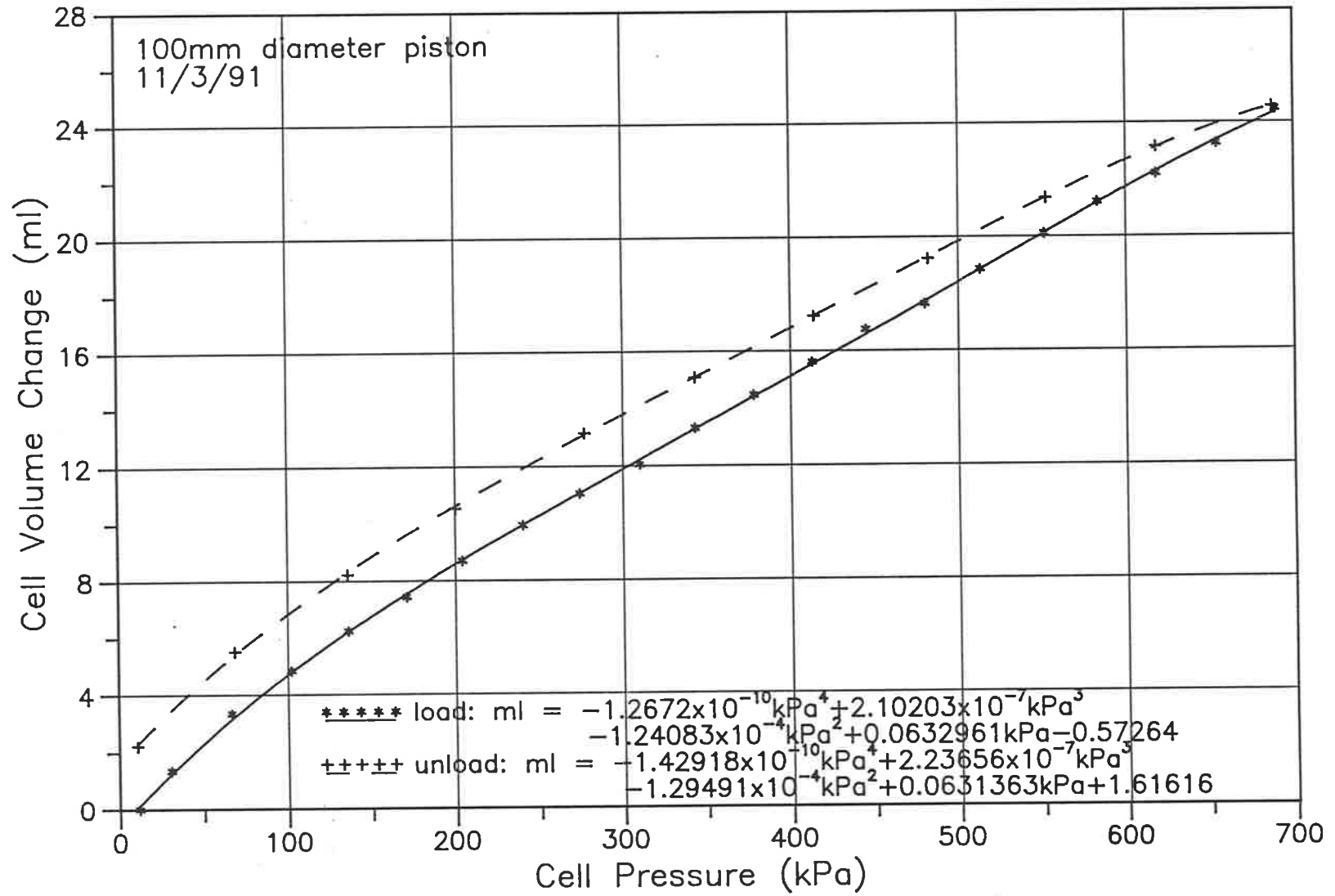
Axial Load Transducer Calibration



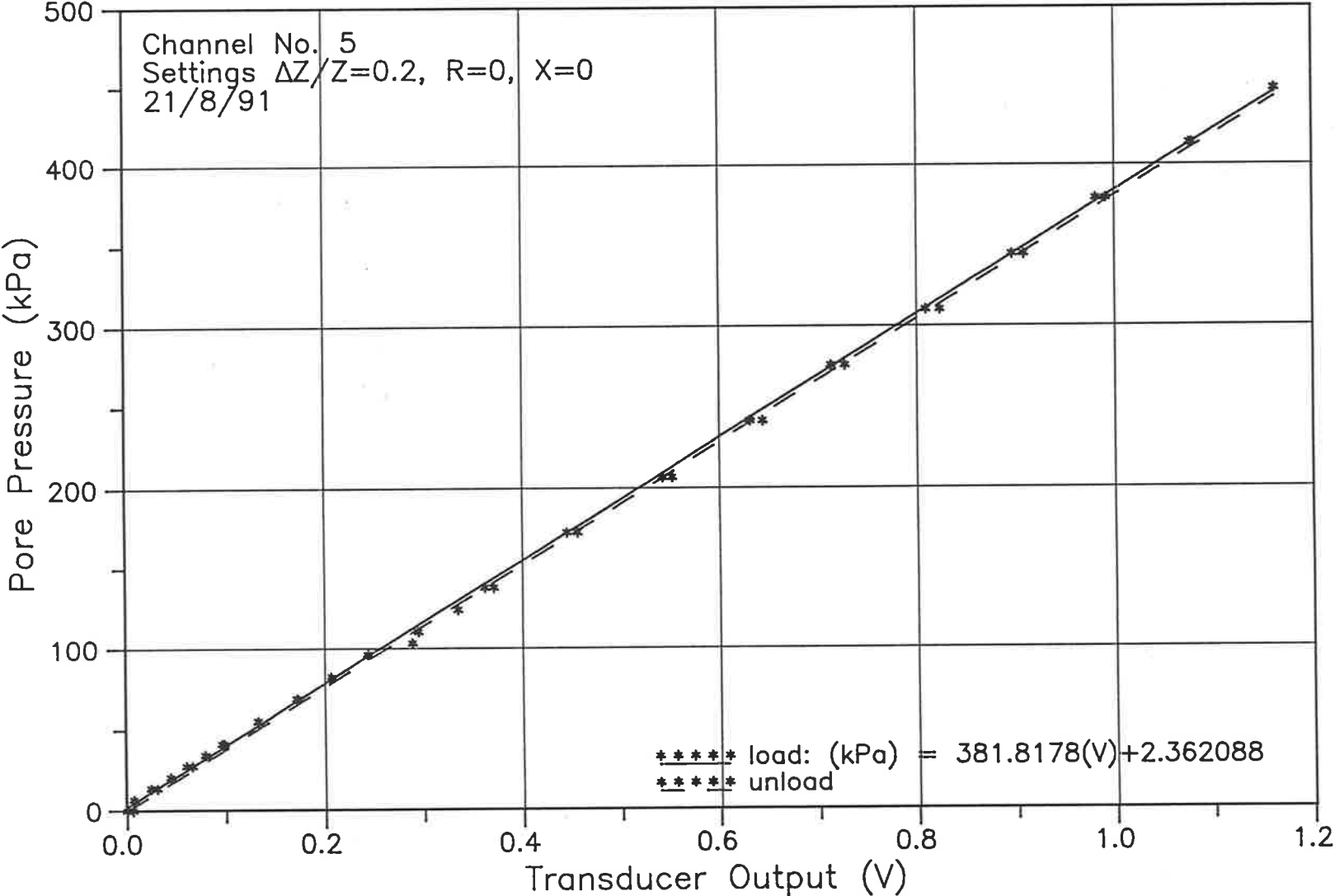
Cell Pressure Transducer Calibration



Cell Volume Change Correction



Pore Pressure Transducer Calibration



E. OPERATION SUMMARY OF THE FINITE ELEMENT MODEL

- MAIN
- initialise
 - call FEDAT
 - open temporary data files
 - call FEANAL
 - stop
- FEDAT
- open input file
 - read in node & element specifications or call NODES
 - generates node & element specifications according to a rectangular grid, numbered from top left
 - read in material specifications
 - call BOUNDB - (if invoked) generates roller boundary conditions along specified horizontal and vertical coordinates
 - read in any additional boundary specifications
 - read in any nodal load specifications
 - read in increment specifications: stresses; effective materials; displacements
 - read in any pore pressure specifications
 - read in initial stresses and strains
 - read in any specifications for changes in material types during the run
 - assemble geometric, load, & boundary data into element-based arrays
 - generate lists of node & element numbers, sorted along rows from top left (required for output file)
 - return
- FEANAL
- set programme control flags: analysis type; failure criterion; constitutive equations; etc.
 - set increment and iteration counters
 - * - determine matrix bandwidth; set counters for block matrix solution

- block by block:
 - element by element, if element is included in current block
 - assign any new gravity loads (eg. from materials just becoming effective) and nodal loads applied this increment into global array
 - if element is just becoming effective calculate gravity stresses as current stresses
 - test current stress against failure criterion and update condition flag
 - calculate element stiffness parameters according to current stresses, constitutive equation flag, and stress condition flag
 - call FEM - calculates and assembles element elastic matrix [D], strain displacement matrix [B], and element stiffness matrix [K^e]. [D] and [B] are written to a temporary storage file and [K^e] is returned.
 - if element is currently overstressed, assign redistributed loads into global array.
 - if element is effective, modify element stiffness matrix and global load array to include any boundary conditions.
 - if element is not effective, divide stiffness matrix by 1000.
 - add element element stiffness entries into global stiffness matrix.
- update programme control flags and increment and iteration counters.
- call BANSOL - performs the matrix inversion and solution. Incremental nodal displacement array is returned.
- call STRESS
- if last iteration of current increment, call FEPRT - writes failure condition flags, stresses, displacements, etc. (as requested) to ASCII output file.
- if not last iteration of last increment, repeat from *
- return.

- STRESS - element by element, if element is effective in current increment
- add incremental nodal displacements into working array of current nodal coordinates
 - if last iteration, update stored array of current nodal coordinates
 - read element matrices [D] and [B] from temporary storage file
 - calculate incremental strains $\{\epsilon\} = [B]\{\delta\}$ and incremental stresses $\{\sigma\} = [D]\{\epsilon\}$
 - assign stresses and strains to incremental global arrays
 - average stresses and strains for pairs of adjacent elements
 - add incremental stresses and strains into working arrays of current stresses and strains
 - if last iteration of current increment, update stored arrays of current stresses and strains
 - calculate current total displacements
 - return.

REFERENCES

REFERENCES

- ADAMS, J. 1979, 'Gravel size analysis from photographs', Journal of the Hydraulics Division, Proceedings, ASCE, vol. 105, pp. 1247-1255.
- AS1289.A1-1983 'Scope and general', in AS1289 Methods of Testing Soils for Engineering Purposes, Standards Association of Australia, North Sydney.
- AS1289.A2-1977 'Preparation of Disturbed Soil Samples for Testing', in AS1289 Methods of Testing Soils for Engineering Purposes, Standards Association of Australia, North Sydney.
- AS1289.C6.1-1977 'Determination of the particle size distribution of a soil - Standard method of analysis by sieving', in AS1289 Methods of Testing Soils for Engineering Purposes, Standards Association of Australia, North Sydney.
- AS1289.C6.2-1977 'Determination of the particle size distribution of a soil - Analysis by sieving in combination with hydrometer analysis (subsidiary method)', in AS1289 Methods of Testing Soils for Engineering Purposes, Standards Association of Australia, North Sydney.
- AS1289.E1.1-1977 'Determination of the dry density/moisture content relation of a soil using standard compaction - standard method', in AS1289 Methods of Testing Soils for Engineering Purposes, Standards Association of Australia, North Sydney.
- BECKER, E., CHAN, C.K., and SEED, H.B. 1972, Strength and Deformation Characteristics of Rockfill Materials in Plane Strain and Triaxial Compression Tests, Report TE-72-3, Department of Civil Engineering, University of California, Berkeley.
- BISHOP, A.W. 1973, 'The stability of tips and spoil heaps', Quarterly Journal of Engineering Geology, vol. 6, Nos. 3&4, pp. 335-376.
- BISHOP, A.W. and HENKEL, D.J. 1962, The Measurement of Soil Properties in the Triaxial Test, 2nd edn, Edward Arnold (Publishers) Ltd, London.

BJERRUM, L. 1967, 'Progressive failure in slopes of overconsolidated plastic clay and clay shales (3rd Terzaghi lecture)', Journal of the Soil Mechanics and Foundations Division, Proceedings, ASCE, vol. 93, SM5, pp. 3-49.

BLIGHT, G.E. 1969, 'Foundation failures of four rockfill slopes.', Journal of the Soil Mechanics and Foundations Division, Proceedings, ASCE, vol. 95, SM3, pp. 743-767.

BLIGHT, G.E. 1985, 'Failure mode', in Design of Non-impounding Mine Waste Dumps, M.K. McCarter (ed), Society of Mining Engineers, New York.

CALDWELL, J.A. and MOSS, A.S.E. 1985, 'Simplified stability analysis', in Design of Non-impounding Mine Waste Dumps, M.K. McCarter (ed), Society of Mining Engineers, New York.

CAMPBELL, D.B. and SHAW, W.H. 1978, 'Performance of a waste rock dump on moderately to steeply sloping foundations', Proceedings, 1st International Symposium on Stability in Coal Mining, Vancouver (Miller Freeman Publications), pp. 395-405.

DAVIS, E.H. 1968, 'Theories of plasticity and the failure of soil masses', in Soil Mechanics Selected Topics, I.K. Lee (ed), Butterworth & Co. (Publishers) Ltd, Sydney.

FITZPATRICK, R.W. 1986, 'Morphology, classification and genesis of "mine soils" on the rock dumps', in Rehabilitation of Waste-rock Dumps, Ranger No.1 Mine, N.T., Confidential Report to Ranger Uranium Mines Pty Ltd, CSIRO Division of Soils, Adelaide.

FITZPATRICK, R.W., BEECH, T.A., RILEY, G.G., FAZEY, P.G., and MILNES, A.R. 1989, 'Profile descriptions and tables of soil analytical data', in Comparison of Minesoils with Stockpiled and Undisturbed Natural Soils: Physical, Chemical, Microbiological and Vegetation Characteristics, A.R. Milnes (ed), Confidential Report to Ranger Uranium Mines Pty Ltd, CSIRO Division of Soils, Adelaide.

FREDLUND, D.G. and KRAHN, J. 1977, 'Comparison of slope stability methods of analysis', Canadian Geotechnical Journal, vol. 14, No. 3, pp. 429-439.

- FUMAGALLI, E. 1969, 'Tests on cohesionless materials for rockfill dams', Journal of the Soil Mechanics and Foundations Division, Proceedings, ASCE, vol. 95, SM1, pp. 313-332.
- GONANO, L.P., KIRKBY, R.W., and DIGHT, P.M. 1978, 'Triaxial Testing of Cemented Rockfill', Technical Report No. TR72, CSIRO Division of Applied Geomechanics, pp. 60.
- GRIFFITHS, J.C. 1967, Scientific Methods in Analysis of Sediments, McGraw-Hill Book Company, Inc. USA, New York.
- GUY, H.P. 1969, 'Laboratory theory and methods for sediment analysis', in Techniques of Water-Resources Investigations, United States Geological Survey.
- HAHN, G.H. and SHAPIRO, S.S. 1967, 'Drawing conclusions about system performance from component data', in Statistical Models in Engineering, John Wiley & Sons, Inc., New York.
- IBBEKEN, H. and SCHLEYER, R. 1986, 'Photo-sieving: A method for grain size analysis of coarse grained, unconsolidated bedding surfaces', Earth Surface Processes and Landforms, vol. 11, No. 1, pp. 59-78.
- IRIONDO, M.H. 1972, 'A rapid method for size analysis of coarse sediments.', Journal of Sedimentary Petrology, vol. 42, pp. 985-986.
- JAEGER, J.C. 1971, 'Friction of rocks and stability of rock slopes (11th Rankine lecture) ', Geotechnique, vol. 21, No. 2, pp. 97-134.
- KELLERHALS, R. and BRAY, D.I. 1971, 'Sampling procedures for coarse fluvial sediments', Journal of the Hydraulics Division, Proceedings, ASCE, vol. 97, HY8, pp. 1165-1180.
- KORN, G.A. and KORN, T.M. 1961, Mathematical Handbook for Scientists and Engineers, McGraw-Hill Book Company Inc., New York.
- LAMBE, T.W. and WHITMAN, R.V. 1969, Soil Mechanics, John Wiley & Sons, Inc., New York.
- LEPS, T.M. 1970, 'Review of shearing strength of rockfill', Journal of the Soil Mechanics and Foundations Division, Proceedings, ASCE, vol. 96, SM4, pp. 1159-1170.

LOWE, J. 1964, 'Shear strength of coarse embankment dam materials', Proceedings, 8th Congress on Large Dams, pp. 745-761.

MARACHI, N.D., CHAN, C.K., and SEED, H.B. 1972, 'Evaluation of properties of rockfill materials', Journal of the Soil Mechanics and Foundations Division, Proceedings, ASCE, vol. 98, SM1, pp. 95-114.

MARSAL, R.J., GOMEZ, E., NUNEZ, A., CUELLAR, R., and RAMOS, R.M. 1965, Research on the Behaviour of Granular Materials and Rockfill Samples, Report Comision Federal de Electricidad, Mexico.

McANALLY, P.A. and BOYCE, B.T. 1980, Geomechanics Design, Queensland Institute of Technology, Brisbane.

McKEAN, R.M. 1980, 'Engineering geology related to pit wall stability at Goonyella mine', in Stability Problems in Open Strip Excavations and Spoil Piles - Final Report, P.G. Fuller (ed), CSIRO Division of Geomechanics.

McMAHON, B.K. 1982, 'Probabilistic methods in slope design', Proceedings of the Symposium on Risk Assessment in Geomechanics, The Institution of Engineers, Australia (Qld Division), Brisbane.

McSAVENY, E.R. 1972, 'The surficial fabric of rockfill talus', in Quantitative Geomorphology: Some Aspects and Applications, M.E. Morisawa (ed), Publications in Geomorphology, Binghamton, N.Y.

MILNES, A.R. and FAZEY, P.G. 1988, 'Acid Leaching of Uranium from Ore Stockpiles and Waste-rock Dumps in the Ranger Project Area, East Jabiru', Confidential Technical Paper No. 2 to Ranger Uranium Mines Pty Ltd.

MILNES, A.R., FITZPATRICK, R.W., SELF, P.G., FORDHAM, A.W., and McCLURE, S.M. 1991, 'Natural iron precipitates in a mine retention pond near Jabiru, Northern Territory, Australia', Catena (Special Issue), in press.

MILNES, A.R., RILEY, G.G., and RAVEN, M.D. 1986, 'Rock weathering, landscape development and the fate of uranium in waste-rock dumps and the low grade ore stockpile', in Rehabilitation of Waste-rock Dumps, Ranger No.1 Mine, N.T., Confidential Report to Ranger Uranium Mines Pty Ltd, CSIRO Division of Soils, Adelaide.

MITCHELL, J.K. 1976, Fundamentals of Soil Behaviour, John Wiley & Sons, Inc., New York.

NEEDHAM, R.S. 1982, 1:100 000 Geological Map Commentary - Cahill, Northern Territory, Commonwealth of Australia, Canberra.

OLLIER, C. 1969, Weathering, Geomorphology Text 2, Oliver & Boyd, Edinburgh.

OLSEN, R.W. and ALTENHOFEN, R.E., 1980, 'Rectification', in Manual of Photogrammetry, 4th edn, C.C. Slama, C. Theurer, and S.W. Henriksen (eds), American Society of Photogrammetry, Falls Church.

ORD, A. 1989, 'Real-time image analysis of size and shape distributions of rock fragments', Australian Institute of Mining and Metallurgy Bulletin and Proceedings, vol. 294, No. 1, pp. 28-31.

PRIEST, S.D. 1988, Approaches to Rock Slope Design, lecture notes for undergraduate civil engineering.

RANGER URANIUM MINES 1984, Ranger Uranium Mine - Geology and Mining, Ranger Uranium Mines Pty Ltd.

RICHARDS, B.G. 1978, 'Application of an experimentally-based non-linear constitutive model to soils in laboratory and field tests', Australian Geomechanics Journal, vol. G8, pp. 20-30.

_____ 1980a, 'Automatic joint element generation to simulate strain softening yield behaviour in earthen materials', Proceedings, 3rd Australia-New Zealand Conference on Geomechanics, vol. 2, pp. 233-239.

_____ 1980b, 'The analysis of the total load-deformation response of an expansive clay subgrade at Macalister, Qld', Proceedings, 10th Australian Road Research Board Conference, Sydney, vol. 10, No. 2, pp. 1-8.

_____ 1982, 'The finite element analysis of mine spoil slopes using slip elements to simulate strain softening yield behaviour', Transactions of the Institution of Engineers, Australia, vol. CE24, No. 1, pp. 69-76.

_____ 1984, 'Finite element analysis of volume change in expansive soils', Proceedings, 5th International Conference on Expansive Soils, Adelaide, pp. 141- 148.

_____ 1986, Printout of finite element analyses of slope stability of waste-rock dumps at Ranger uranium mine, Jabiru, in possession of B.G. Richards.

_____ 1987, Settlement Under Rock Dumps, Confidential Focus Report No.1 to Ranger Uranium Mines Pty Ltd, CSIRO Division fo Soils.

_____ 1991, 'Modelling interactive load-deformation and flow processes in soils, including unsaturated and swelling soils', Preprint of paper to be presented at 6th ANZ Conference on Geomechanics, February 1992.

_____, COULTHARD, M.A., and TOH, C.T. 1981, 'Analysis of slope stability at Goonyella mine', Canadian Geotechnical Journal, vol. 18, No. 2, pp. 179-194.

_____, PETER, P., and LUCAS, E.A. 1986, 'Measurement of the shear strength of the waste rock and the analysis of the slope stability of the waste-rock dumps', in Rehabilitation of Waste-rock Dumps, Ranger No.1 Mine, N.T., Confidential Report to Ranger Uranium Mines Pty Ltd, CSIRO Division of Soils, Adelaide.

RILEY, G.G. 1991, 'Mineralogy of clay fractions extracted from Ranger waste rocks', CSIRO Division of Soils Technical Memorandum 61/1991, private communication.

ROCKEY, K.C., EVANS, H.R., GRIFFITHS, D.W., and NETHERCOT, D.A. 1983, The Finite Element Method, 2nd edn, Granada Publishing Limited, Frogmore.

SCOTT, C.R. 1980, Soil Mechanics and Foundations, 3rd edn, Applied Science Publishers Ltd, London.

SKEMPTON, A.W. 1964, 'Long term stability of clay slopes', Geotechnique, vol. 14, No. 2, pp. 77-101.

STATHAM, I. 1973, 'Scree slope development under conditions of surface particle movement', Transactions of the Institute of British Geographers, vol. 59, pp. 41-53.

YOUNG, A. 1972, Slopes, Geomorphology Text 3, Longman Group Ltd.

ZELLER, J. and WULLIMAN, R. 1957, 'The shear strength of the shell materials for the Goschenalp Dam, Switzerland', Proceedings, Fourth International Conference Soil Mechanics and Foundation Engineering, vol. 2, pp. 399-404.

ZIENKIEWICZ, O.C. 1971, The Finite Element Method in Engineering Science, McGraw-Hill Publishing Co. Ltd, Maidenhead.

ZUSSMAN, J. 1967, 'X-ray diffraction', in Physical Methods in Determinative Mineralogy, J. Zussman (ed), Academic Press Inc., London.